PERFORMANCE BASED DESIGN OF COUPLED WALL STRUCTURES

by

Abdelatee Abdalla Eljadei

Bachelor of Science, AL-Fateh University, 1998

Master of Science, AL-Fateh University, 2003

Master of Science, Oklahoma State University, 2010

Submitted to the Graduate Faculty of

Swanson School of Engineering in partial fulfillment

of the requirements for the degree of

Doctor of Philosophy

University of Pittsburgh

2012

UNIVERSITY OF PITTSBURGH

SWANSON SCHOOL OF ENGINEERING

This dissertation was presented

by

Abdelatee Abdalla Eljadei

It was defended on

July 13, 2012

and approved by

Bahram M. Shahrooz, Ph.D., Professor, Department of Civil and Environmental Engineering, University of Cincinnati

Steven P. Levitan, Ph.D., Professor, Department of Electrical and Computer Engineering

Morteza A. Torkamani, Ph.D., Associate Professor, Department of Civil and Environmental Engineering

John C. Brigham, Ph.D., Assistant Professor, Department of Civil and Environmental Engineering

Dissertation Director: Kent A. Harries, Ph.D., Associate Professor, Department of Civil and Environmental Engineering

PERFORMANCE BASED DESIGN OF COUPLED WALL STRUCTURES

Abdelatee A. Eljadei, PhD

University of Pittsburgh, 2012

Coupled wall structures are outstanding lateral load resisting systems that not only reduce the deformation demands on the building, but also distribute the inelastic deformation both vertically and in plan, between the coupling beams and the wall piers. Coupled core walls (CCW's) result from the need to provide openings in elevator or stairwell shafts and often take C, L or H shapes. They provide inherent strength and stiffness, and in many cases they result in a compact plan, which results in more available rentable space on a floor plate. In addition, coupled core walls result in a relatively force-hardened and fire resistant structural system.

The research in this work considered a prototype 12-storey reinforced concrete coupled core wall (CCW) building located in Seattle, Washington. Five CCW prototype structures, having varying degrees of coupling and the same wall piers were designed allowing the study of the effects of decayed coupling action to be carried out. Elastic analyses using the equivalent lateral force (ELF) procedure and the continuous medium method (CMM) were utilized to establish initial proportions for the CCW system, and to determine the design forces and moments. Nonlinear static and dynamic analyses were conducted to investigate the CCW structural behavior, adequacy of the design, and the evolution of the structural form from CCW system to a collection of linked wall piers (LWP). An additional unique aspect of this work was that the wall piers in the CCW were significantly different in

terms of their dynamic and geometric properties: the moments of inertia of the two wall piers differed by almost an order of magnitude.

The results of this study indicate that the dual systems, consisting of reinforced concrete wall piers and steel coupling beams, performed very well and as what would be expected. The dual system provided superior lateral stiffness as a CCW in the elastic range, and maintained a good stiffness during the evolution toward a collection of linked wall piers (LWP). When the CCW structure (dual system) was subjected to lateral demand, the system first resisted the lateral loads by a combination of actions: frame action generated by shear in the coupling beams and flexural behavior of the individual wall piers. During the evolution process, the frame action degraded as the steel coupling beams yielded and formed hinges at their ends and the moment resistance was redistributed to the walls piers.

TABLE OF CONTENTS

LIST OF TABLES

LIST OF FIGURES

NOMENCLATURE

The following abbreviations and notation are used in this work:

Abbreviations

ACI	=	American Concrete Institute.
AISC	=	American Institute of Steel Construction.
ASCE	=	American Society of Civil Engineers.
ATC	=	Applied Technology Council.
CCW	=	Coupled Core Wall.
CMM	=	Continuous Medium Method.
CP	=	Collapse Prevention performance level.
CRCCB	=	Conventionally Reinforced Concrete Coupling Beam.
CW	=	Coupled Wall.
DOF	=	Degree of Freedom.
DRCCB	=	Diagonally Reinforced Concrete Coupling Beam.
ELF	=	Equivalent Lateral Force procedure (ASCE 7-10).
FEMA	=	Federal Emergency Management Agency.
FPT	=	Fixed Point Theory.
IO	=	Immediate Operation performance level.
LFRS	=	Lateral Force Resisting System.
LRFD	=	Load and Resistance Factor Design.
LS	=	Life Safety performance level.
LWP	=	Linked Wall Piers.
MDOF	=	Multiple Degree of Freedom.
NLTHA	=	Nonlinear Time History Analysis
PBD	=	Performance Based Design.
SBD	=	Strength Based Design.
SDC	=	Seismic Design Category.

SDOF = Single Degree of Freedom.

Notations

A_1 = Wall 1 cross sectional area.

A_2 = Wall 2 cross sectional area.

A_b = Coupling beam cross sectional area.

A_{cw} = Gross area of concrete section of coupling beam resisting shear.

A_{vd} = Area of steel reinforcement in one diagonal bar group.

b_w = Interior width of wall pier.

C = Damping matrix (FPT, Chapter 3)

C = Tension or compression force resulting from coupling action.

C_s = Seismic response coefficient (ASCE 7-10).

C_t = Approximate period parameter (ASCE 7-10).

C_u = Coefficient for upper limit on calculated period (ASCE 7-10).

$\delta_{ground\ motion}$ = Input ground motion displacement.

doc = Degree of coupling.

$\delta_{structure}$ = Lateral deflection at top of the building

E = Young's Modulus.

F(t) = Forcing function.

F_1 = Axial load parameter in the continuous medium method.

F_2 = Shear flow parameter in the continuous medium method.

F_3 = Roof displacement parameter in the continuous medium method.

f_c' = Compressive strength of concrete.

F_x = Lateral force in ELF procedure.

f_y = Yield strength of steel.

g = Coefficient from closed-form solution.

h = Storey height.

h_b = Coupling beam height.

h_x = Height above grade

I_1 = Wall 1 moment of inertia.

I_2 = Wall 2 moment of inertia.

I_b = Coupling beam moment of inertia.

I_c = Effective moment of inertia of the coupling beam.

$I_{frame\ action}$ = Moment of inertia provided by the coupling beams

k	=	Optimal coupling beam stiffness (FPT, Chapter 3).
k	=	Relative flexural to axial stiffness of the wall piers (CMM, Chapter 4).
K	=	Stiffness matrix
K_1	=	Wall 1 stiffness matrix.
k_1	=	Storey level stiffness of Wall 1.
K_1^*	=	Effective equivalent modal stiffness of wall 1.
K_2	=	Wall 2 stiffness matrix.
k_2	=	Storey level stiffness of Wall 2.
K_2^*	=	Effective equivalent modal stiffness of wall 2.
k_o	=	Coupling beam stiffness.
L	=	Coefficient from the closed-form solution.
l_b	=	Length of coupling beam.
L_w	=	Distance between wall centroids.
M	=	Mass matrix
M_1	=	Wall 1 mass matrix.
m_1	=	Wall 1 storey level mass.
M_1	=	Equivalent modal mass of wall 1.
M_1^*	=	Effective equivalent modal mass of wall 1.
M_2	=	Wall 2 mass matrix.
m_2	=	Wall 2 storey level mass.
M_2	=	Equivalent modal mass of wall 2.
M_2^*	=	Effective equivalent modal mass of wall 2.
m_{total}	=	Storey total mass.
NN	=	Number of degrees of freedom.
N	=	Axial load in wall piers.
OTM	=	Overturning moment.
p	=	Lateral load in the continuous medium method.
P	=	Design axial load (tension or compression).
q	=	Shear flow.
R	=	Response modification factor (ASCE 7-10).
r	=	Post yield stiffness factor.
R_T	=	Maximum potential strength of coupled wall system.
R_{wall}	=	Moment resisted by cantilever flexure of each wall pier.

SD_1 = Design, 5-percent-damped, spectral response acceleration parameter at a period of one second (ASCE 7-10).

SD_S = Design, 5-percent-damped, spectral response acceleration parameter at short periods (ASCE 7-10).

T = Natural vibration period of structure.

T_a = Approximate fundamental period of structure (ASCE 7-10).

T_L = Long-period transition period (ASCE 7-10).

U = Lateral displacement.

V_c = Code prescribed base shear

V_u = Shear strength of diagonally reinforced concrete coupling beam.

w_b = width of the coupling beam.

w_x = Storey weight.

y_H = Roof displacement.

α = Angle of inclination in a diagonally reinforced coupling beams.

α = Parameter of the relative flexibility of the coupling beams (CMM, Chapter 4).

α = Unloading stiffness factor.

η = Fixed point stiffness ratio (k / k1).

γ = Frequency ratio of SDOF systems ($\omega 2 / \omega 1$), (FPT, Chapter 3)

λ = Cross-sectional correction coefficient for shear

μ = Mass ratio of Wall 2 to Wall 1 (m_2 / m_1).

ξ = Optimal coupling beam damping ratio.

φ_1 = Normalized first mode shape vector for Wall 1.

φ_2 = Normalized first mode shape vector for Wall 2.

ω_1 = Natural frequency of Wall 1.

ω_2 = Natural frequency of Wall 2.

This document has been prepared using US Standard units of kips, pounds per square foot (psf), inches and feet. The appropriate conversion factors are as follows:

1 inch	=	25.4 mm
1 foot	=	305 mm
1 kip	=	4.448 kN

1 ksi = 6.895 MPa

Reinforcing bar sizes are reported using the standard inch-pound designation used in the United States designated by a ‘#’ followed by a number referring to the bar diameter in eighths of an inch. Thus a #7 bar is a nominal 7/8 inch diameter bar.

ACKNOWLEDGMENTS

I would like to express my sincere appreciation and profound gratitude to my advisor, Dr. Kent A. Harries, for his support, continuous guidance and encouragement throughout my studies.

I would also like to thank Dr. Bahram M. Shahrooz, Dr. Morteza A. Torkamani, Dr. John C. Brigham as well as Dr. Steven P. Levitan for serving on my committee and their suggestions and advice.

Sincere thanks are extended to Dr. Amir Koubaa for his support and unforgettable encouragement throughout my studies.

Finally, I wish to extend my heartfelt thanks to my wife for her great patience, encouragement and support, my parents for their blessing and continuous support of my academic growth.

1.0 INTRODUCTION

Controlling the lateral displacement of a structure subject to seismic loads is a predominant issue in the design of mid to high rise buildings. This lateral displacement is considered to be a primary indicator of the degree of damage imparted to the structure and can additionally lead to unintended structure-structure interaction (i.e., pounding) if not controlled. Performance criteria in the performance-based design (PBD) approach are usually displacement based. Therefore, the goal in a design is to provide an adequate stiffness to ensure that this displacement is within acceptable limits.

Structural walls provide great stiffness as a lateral load resisting system. They reduce the seismic deformation demands and hence the damage to the remainder of the building (i.e., the gravity load-carrying system) due to their high in-plane stiffness. Multiple shear walls are preferred in lateral load resisting systems since they provide redundancy and ductility to building structures through their ability to dissipate energy by forming hinge regions at their bases.

Individual cantilever walls may be subjected to axial, translational, and torsional displacement demands, and the degree to which a cantilever wall contributes to the resistance of overturning moments, storey shear forces, and storey torsion depends primarily on its geometric configuration, orientation, and location within the building plan. While it is comparatively easy to accommodate most wall arrangements in order to resist wind forces, it is more difficult to ensure acceptable overall building response to severe earthquakes especially when wall locations deviate significantly from the center of mass of the building.

This is because a fully elastic response is expected for structures when resisting wind forces, while in the case of large earthquakes, inelastic deformations will likely take place.

One of the key points in the strategy of planning structural walls is to distribute the anticipated inelastic deformations in a reasonably uniform manner over the entire plan of the building rather than concentrating them in only a few walls (Taranath 2009).

Coupled wall structures are outstanding lateral load resisting systems that not only reduce the deformation demands on the building, but also distribute the inelastic deformation both vertically and in plan, between the coupling beams and the wall piers. Different than cantilever walls, where the overturning moment is resisted entirely by flexural stresses, coupled walls resist the overturning moment by a combination of an axial force couple that develops in the wall piers as a result of shear demand in the coupling beams and flexural action in the wall piers.

Some of the components in building structures, such as elevator shafts and stairwells, lend themselves to the use of reinforced concrete cores, particularly in light of post 9/11 force-hardening requirements. These cores are efficiently used to provide the major portion of lateral force resistance in multistorey buildings. Coupled core walls (CCW's) result from the need to provide openings in elevator or stairwell shafts and often take C, L or H shapes. They provide inherent strength and stiffness, and in many cases they result in a compact plan, which results in more available rentable space on a floor plate. In addition, coupled core walls result in a relatively force-hardened and fire resistant structural system.

1.1 OBJECTIVES

The proposed work is intended to contribute to the state of the art of CCW analysis and design by developing a unique design paradigm: expanding the concept of performance-

based design into a domain where the nature of the structural form evolves within the context of the proposed performance objective. In addition, the research is aimed to develop an understanding of the nature and limitations of the behavior of CCW structural systems' evolving in terms of their effective structural form, and to develop guidance to determine and use the optimal coupling properties of CCW systems that may be employed in an environment consistent with structural engineering practice.

It will be shown that damage to the coupling beams in a CCW system likely occurs prior to the plastic capacity of the system being achieved. Furthermore, the damage is progressive, resulting in a structural system that may evolve from behaving as a coupled wall (CW) system to behaving as a collection of linked wall piers (LWP) as shown schematically in Figure 1-1. Based on the proposed evolution of performance, the LWP system will be subject to large demands since the system is presumably behaving as a stiffer CW system at lower performance levels. These behaviors and the implications of this evolution of performance to the dynamic properties of the structure will be investigated.

The present work also aims to provide the designers of CCWs with a straightforward procedure for proportioning the coupling beams that leads to acceptable structural behavior and failure mechanisms of CCW systems. The objective of validation of methodologies for assessing CCW design space will be attempted based on the range of data generated. Guidance with respect to the following questions posed at the initial design stage of a CCW structure will be presented:

1. *Is the proposed 'dual system' or evolving structural behavior viable?* For example, is there adequate reserve capacity in the wall piers to permit LWP behavior to continue to dissipate energy once the coupling beam contributions are exhausted?
2. *When does it become efficient to couple wall piers?* For example, based on architectural considerations, is there any need to couple low- and medium-rise wall piers?

3. *Is there a performance-based basis for the optimization of the degree of coupling* (*doc*)?

4. *Under what conditions is reducing transmissibility a viable performance objective? A*ssuming dual system behavior, what ratios of wall pier dynamic properties may be effectively controlled?

1.2 SCOPE OF THE DISSERTATION

The research in this work considers a prototype 12-storey reinforced concrete CCW building located in Seattle, Washington to achieve the study objectives. Five CCW prototype structures, having varying degrees of coupling and the same wall piers are designed. This approach allows study of the effects of decayed coupling action to be carried out.

Elastic analyses using the equivalent lateral force (ELF) procedure and the continuous medium method (CMM) are utilized to establish initial proportions for the CCW system, and to determine the design forces and moments. Nonlinear static and dynamic analyses are conducted to investigate the CCW structural behavior, adequacy of the design, and the evolution of the structural form from CCW system to a collection of linked wall piers (LWP) (Figure 1-1).

The study is guided by the concepts and terminology of the *Action Plan for Performance Based Seismic Design* (FEMA 2000c). The project activities are founded on extensive parametric analyses using established analytic techniques for the assessment of structural behavior. In this regard most structural analysis is conducted using RUAUMOKO (Carr 2008). XTRACT (Imbsen 2007) is used to conduct nonlinear fiber analyses of wall and beam sections in order to establish robust section parameters for the RUAUMOKO analysis.

1.3 DISSERTATION ORGANIZATION

Chapter 2 presents background and literature review focusing on coupled wall structures, their components, structural behavior, and the methods used to analyze and design them. It also provides a description of the performance objectives and acceptance criteria for the current research.

The remainder of the dissertation is organized in a manner approximately parallel to the design and assessment process briefly described above and shown schematically in Figure 1-2. In Chapter 3, an investigation of the optimization of the coupling beams is carried out. The optimum coupling properties are established based on minimizing the transmissibility between the wall piers. This approach is found to not yield practical structures for the sake of this study. Consequently, Chapter 4 introduces the development of the prototype structure geometry and the structural design of the CCW components that will be utilized through the remainder of the work.

Chapter 5 presents the nonlinear section analysis of the wall piers designed in Chapter 4, and the subsequent nonlinear static (pushover) analyses. Chapter 6 describes the nonlinear time history analysis for the five prototype structures, where the structures are subjected to a suite of four earthquake ground motions. Finally, Chapter 7 synthesizes the results of the previous chapters and presents the conclusion of the study and recommendations for future research.

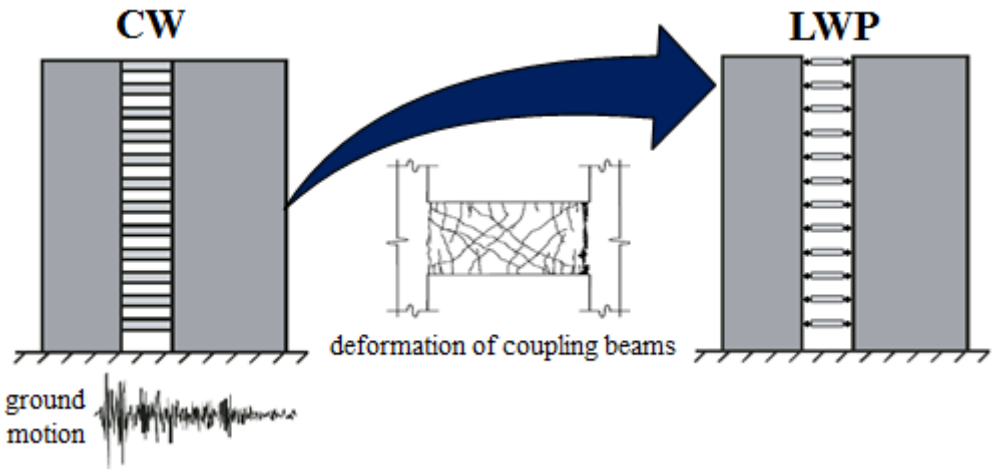

Figure 1-1 Evolution of CCW to LWP

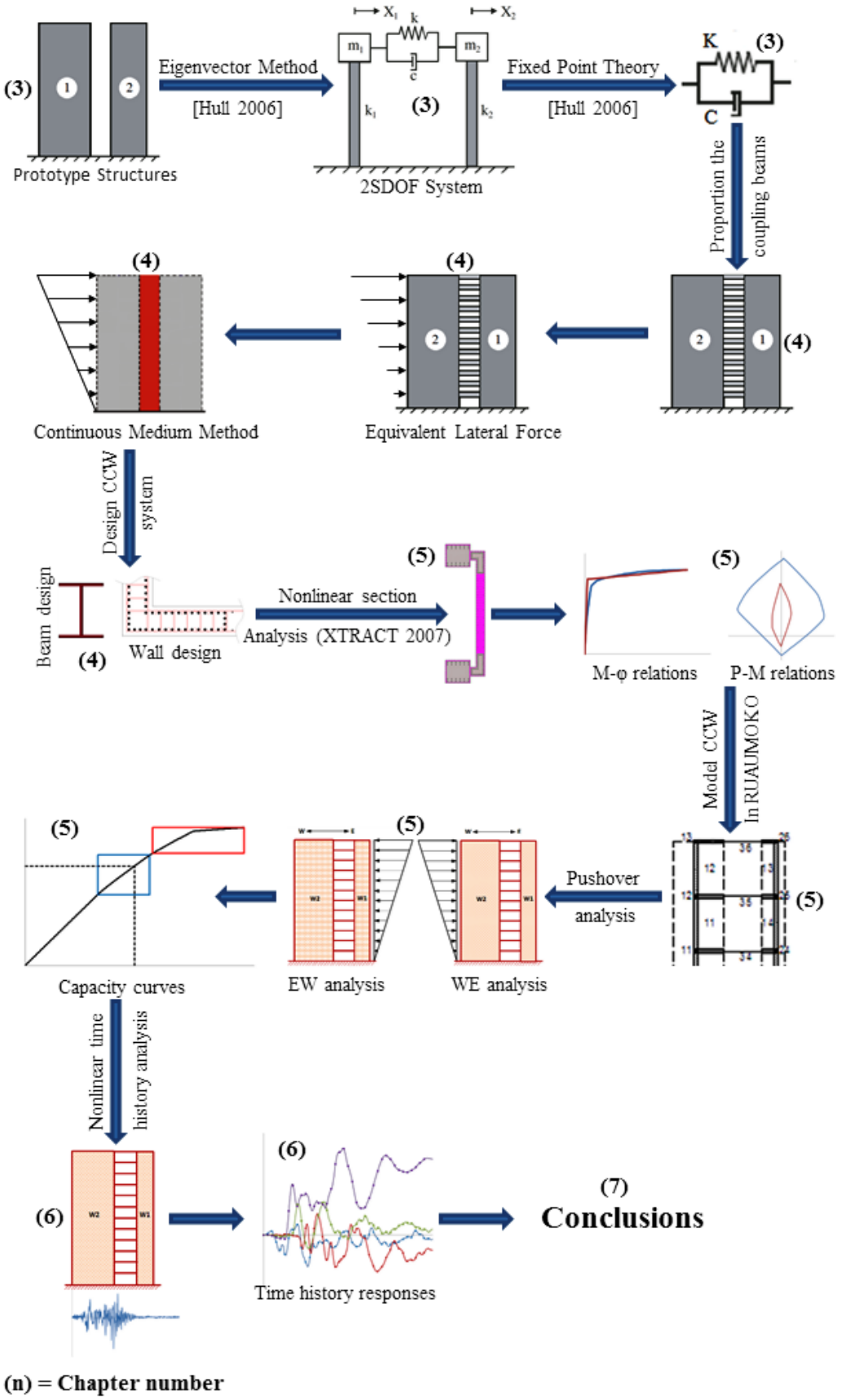

Figure 1-2 Research flowchart

2.0 BACKGROUND AND LITERATURE REVIEW

In many practical situations, structural walls are connected by moment resisting members at each floor level. These connecting members may be stiff coupling beams or relatively flexible floor slabs. In such systems, lateral loads are resisted by the composite action of the individual wall piers and the 'frame' action resulting from the moment connection between them. These systems are referred to as 'coupled walls', 'coupled shear walls', and, depending on the structural plan, 'coupled core walls'. Coupled walls (CW) are a common form of shear wall structure in residential and commercial multi-storey buildings. Practical arrangements of such walls incorporate a single band or multiple bands of openings arranged in elevation, either symmetrically, asymmetrically or in a staggered arrangement.

The degree of rigidity of the coupling beams governs the behavior of CW systems. The impact of the shear resistance of the connecting beams is to make the coupled wall system behave partly as a composite cantilever, bending about the centroidal axis of the wall group. The resulting stiffness of the coupled system is much greater than the summation of stiffnesses of the individual wall piers acting separately as uncoupled walls.

Coupled walls are relatively complex structures and are often used as seismic resisting systems. In structures having typical dimensions and layouts, cantilever wall piers (Figure 2-1) are generally adequate to resist wind-induced lateral loads. The benefit of CWs (Figure 2-2) becomes apparent when resisting much greater seismic lateral loads with the same wall layout required for wind loads. Coupled walls permit more compact wall layouts to resist a given lateral load; for example, CWs were used to great advantage to minimize the lateral

load resisting system footprint in the tallest building in the world, the Burj Khalifa (Lee et al. 2008).

2.1 COUPLED WALLS

Coupled walls (CW) are complex yet attractive lateral load resisting systems that provide extraordinary lateral stiffness without compromising valuable horizontal or vertical space. Coupled walls resist lateral forces through a combination of flexural behavior of the wall piers and 'frame' action imparted by the coupling beams: an axial force couple is developed in the wall piers through the accumulation of shear in the coupling beams (see inset in Figure 2-3). A measure of the structural behavior of CWs is referred to as the 'degree of coupling' (doc) which is defined as the ratio of the overturning moment resisted by the axial couple in the walls to the total structural overturning moment:

$$doc = \frac{CL_W}{CL_W + \sum R_{wall}} = \frac{CL_W}{OTM} \qquad \text{(Eq. 2-1)}$$

Where C is the magnitude of the tension (or compression) force resulting from coupling action; this value is equal to the sum of the shear forces in the coupling beams for a two wall system; L_W is the lever arm between wall pier centroids (i.e.: the location of the resultant of the T-C couple) and R_{wall} is the moment resisted by cantilever flexure of each wall pier. The denominator in Equation 2-1 is equal to the total overturning moment (OTM) applied to the CW system. For CWs to efficiently take advantage of the coupling action, doc (calculated at the base of the structure) ranges from 45-80% (El-Tawil et al. 2009).

In a structural system, where lateral forces are resisted by a combination of systems (such as CWs), the more flexible component will exhibit lower ductility demand than the stiffer component of the structure. In the case of a wall-frame structure, for instance, the

ductility demand on the wall elements will exceed those of the frames (Bertero et al. 1991). Similarly, in a coupled wall structure, the 'frame' action, that is: the axial forces in the walls resulting from the accumulated shear in the beams, is stiffer than the flexural response of the individual wall piers. As a result, the coupling beams exhibit greater ductility demands than do the wall piers. Figure 2-3 shows the idealized response of a coupled wall structure as the sum of the individual pier flexural responses and the 'frame' response resulting from the coupling action of the beams. To allow the structure to achieve its full plastic capacity at its maximum potential strength, $R_T = \Sigma R_w + R_c$, the wall piers must form hinges at their bases. At this stage, the coupling beams must already have undergone significant inelastic deformations. As the structure continues to behave in a ductile manner, the ductility demand on the coupling beams continues to exceed that of the walls. If, for instance, the beams are unable to achieve the ductility ratios demanded of them, a failure occurs. That is to say the potential strength of the 'frame system', R_c, and therefore the potential strength of the entire structure, R_T, is not realized and is limited by the sum of the wall capacities, ΣR_w.

Traditional strength-based design (SBD) of CWs (ACI 2011) often results in coupling beam demands in excess of capacities permitted by the concrete design code (Harries et al. 2004a and 2005). Inherently large redundancy factors associated with CWs, and directional effects (ASCE 2010) also result in increased shear demand on coupling beams. Studies have clearly shown that current strength-based analysis and design procedures typically result in excessive coupling beam shear and inadequate ductility (Harries 2001; Harries et al. 2004a). It is clear from this discussion that the design of the coupling beam elements is critical to the structural performance of a coupled wall system.

2.2 COUPLING BEAMS IN SEISMIC FORCE RESISTING SYSTEMS

2.2.1 Conventionally Reinforced Concrete Coupling Beams (CRCCB)

If the coupling beam length to depth ratio, l_b/h_b, is greater than 4, it is usually designed in accordance with ACI-318 (2011) Chapter 11 provisions using traditional longitudinal and transverse reinforcement as shown schematically in Figure 2-4a. CRCCBs are relatively easy to construct in comparison to diagonally reinforced coupling beams (see Section 2.2.2). However, they have less energy dissipation ability.

In CRCCBs, both top and bottom reinforcement may simultaneously undergo tension as a result of diagonal cracking; this results in the tendency for the beam to elongate (Paulay 2002). For low to moderate levels of damage, vertical cracks develop at the ends of the beam. Together with the observed beam elongation, these cracks become a possible sliding plane (Paulay 2002, FEMA 306 1998). At significant levels of damage, degradation of concrete occurs along these vertical cracks leading to a sliding failure as shown schematically in Figure 2-4b. This failure can occur at relatively low levels of ductility and limits the energy dissipation capacity of the beam (Harries 2001).

2.2.2 Diagonally Reinforced Concrete Coupling Beams (DRCCB)

This reinforcement pattern of coupling beams (shown schematically in Figure 2-5a) is required by ACI-318 (2011) if the beam length to depth ratio (l_b/h_b) is less than 2, and it is recommended for ratios up to 4. For beams with a ratio greater than 4, the diagonal reinforcement will not be effective in resisting the applied forces because of the very low angle of reinforcing bar inclination, α (Harries et al. 2005).

The primary reinforcement of DRCCB consists of two groups of diagonal bars placed symmetrically about the mid span of the beam. Each group is treated like a compression member having a minimum of 4 bars enclosed by transverse reinforcement. In addition, conventional longitudinal and transverse reinforcement are used to confine the entire beam section as shown in Figure 2-5a.

The shear and moment capacities of DRCCB are provided entirely by the diagonal reinforcement. The shear strength of a DRCCB is determined by the following equation (ACI 2011):

$$V_u = 2A_{vd}\ f_y \sin\alpha \le 10\sqrt{f_c'}\ A_{cw} \quad \text{(psi units)} \qquad \text{(Eq. 2-2)}$$

Where A_{vd} is the area of steel in one diagonal bar group, and A_{cw} is the gross area of the concrete coupling beam resisting shear. Neither transverse reinforcement nor concrete contribute to the shear strength of the DRCCB. The limit of $10\sqrt{f_c'}\,A_{cw}$ is based on the observation that DRCCB remain ductile to at least this limit (Nilson 2003) and is otherwise consistent with ACI practice. A particular drawback of DRCCB is that they are difficult to construct and the tradeoff between steel area, A_{vd} and angle of inclination, α, results in an inability to design code-compliant beams in many cases (Harries et al. 2005).

For low-to-moderate levels of damage, shear cracks in DRCCBs develop at low ductility levels. The conventional reinforcing steel helps to control these. Eventual failure (Figure 2-5b) typically results from the opening of a single dominant diagonal shear crack; although this occurs after a great deal of damage and energy dissipation has taken place.

2.2.3 Steel Coupling Beams

Steel coupling beams are used in CW systems as an alternative to reinforced concrete beams (Harries et al. 1992 and 1997; Gong and Shahrooz 1998). Steel beams are advantageous when, due to the architectural restrictions, the available depth for the coupling beams is limited and when large ductility demand is present as a result of seismic loads. When subjected to cyclic loads, it has been shown experimentally that steel beams have superior stiffness and energy dissipation capacity over diagonally reinforced coupling beams (Harries 2001). To insure that the full capacity of the beam is developed, steel coupling beams must be embedded appropriately in the adjacent wall piers (El-Tawil et al. 2009).

2.3 BEHAVIOR OF COUPLED WALLS

As discussed in the previous sections, damage to the coupling beams in a CW system likely occurs prior to the plastic capacity of the system being achieved (Figure 2-3). Furthermore, the damage is progressive, resulting in a structural system that may evolve from behaving as a coupled wall (CW) system to behaving as a collection of linked wall piers (LWP). Allowing the behavior of CW systems to evolve into that of a pair (or collection) of linked cantilever piers raises a number of concerns with regard to the dynamic behavior of such a system. Based on the proposed evolution of performance, the linked wall pier system (LWP) will be subject to large demands since the system is presumably behaving as a stiffer CW system at lower performance levels. In a sense, this evolving behavior may be represented as a progressive reduction in the degree of coupling (doc). If one considers the effective lateral stiffness of a CW system as a function of the doc, the effect of reducing the doc from an initial value (perhaps on the order of 55%) to a very low value (say 10%) results in an

increase in structural flexibility (and therefore demand on the wall piers) on the order of 45%. This is shown schematically in Figure 2-6 where the lateral deflection (stiffness) of a CW is normalized to the deflection of the individual wall piers and plotted against the doc (shown as the “coupling ratio” in the figure).

2.4 FIXED POINT THEORY

Although individual piers must be able to maintain their capacity through larger deformation demands, this is not as critical as it may seem since the extreme axial loads (particularly tension or uplift which generally reduce the flexural capacity of the pier) resulting from the coupling action will be largely diminished as the structure evolves toward LWP behavior. Furthermore, it is likely that the individual wall piers will have different dynamic characteristics due to their geometry and damage accumulated while behaving as a single CW. In this case, a significant aspect of their continued adequate performance is their dynamic interaction. Hull (2006; and Hull and Harries 2008) conducted a preliminary study investigating the performance of LWP systems where performance was defined as the practical minimization of transmissibility of horizontal ground motion in a LWP system having different wall pier geometries. In this work, Fixed Point Theory (FPT, often also referred to as P-Q theory) was used to optimize interaction stiffness and damping properties of two cantilever wall piers that were idealized as a two degree of freedom (2DOF) system as shown schematically in Figure 2-7 (Iwanami et al. 1996).

Traditionally, FPT is used to optimize damping properties for problems of dynamic isolation. In such an application, the two structures considered are the supporting structure (floor or entire building) and the structure to be isolated (often machinery). The two

structures typically have exceptionally different dynamic properties in this case. The objective of applying FPT is to determine the damping required to minimize transmissibility of vibrations between structures (usually to minimize the transmission of machinery vibrations into the supporting structure). Other applications include optimizing passive damping systems for structural control where the damping system is placed between two components of the structure (such as dampers for bridge cable stays). In most applications, the stiffness of the damping system is negligible. Iwanami et al. (1996) demonstrated that FPT may be used to determine an optimal combination of damping and stiffness. The inclusion of stiffness results in a problem analogous to a LWP since the beam (or link) provides both damping and stiffness. Hull (2006) utilized classic FPT and additional closed-form equations for optimized parameters developed by Richardson (2003) to establish optimized link or coupling beam parameters for a range of simplified prototype LWP structures. Hull then conducted linear time history analyses on selected prototypes that were felt to have realistically achievable optimized parameters.

Example displacement-time history results from a single case considered by Hull (2006) are shown in Figures 2-8 and 2-9. The structure considered consisted of two 12- storey LWP systems (similar to those reported in Chapter 3) whose walls are labeled E and A subjected to the 1940 ElCentro NS ground motion record. The walls were idealized as individual SDOFs; thus the analysis corresponds to the 2DOF system shown in Figure 2-7. Four cases are shown: Figure 2-8a shows the dynamic behavior of the two walls acting independently (having no link); the significantly different dynamic properties of the individual wall piers are evident in this figure. Figure 2-8b shows the behavior of the same two walls having a link whose properties were selected to be representative of a coupling beam designed using a conventional strength-based design approach. Hull referred to this case as having ‘arbitrary’ link properties. Figure 2-8c shows the case where the link

properties have been optimized based on FPT. Finally, Figure 2-8d shows the extreme (although quite impractical) case where a rigid link is provided constraining both wall piers to the identical displacement history. The beneficial effect of linking wall piers is evident as one considers the 'spectra' of behavior shown from Figure 2-8a through Figure 2-8d. The improvement in performance (displacement) from an arbitrary link design to an optimized link design is also evident in comparing Figure 2-8b to Figure 2-8c.

Figure 2-9 shows the comparison of the displacement time histories for the individual LWPs, E and A, having optimized and arbitrary link properties. As one would expect, the improvement in dynamic properties associated with optimization is significantly more pronounced for the more flexible of the wall piers comprising the LWP system (wall E; Figure 2-9a).

Hull (2006) draws a number of conclusions with regard to limitations of the proposed procedure and the range of structural properties (and relative properties of individual wall piers) over which it may be applied. Significant conclusions indicate that despite limits to the optimization process, there is a relatively large range of parameters over which 'near-optimal' performance may be achieved. Most relevant in the present context is Hull's conclusion that the FPT approach relies mostly on ratios of dynamic properties of the two individual wall piers. This observation may permit generalization of the approach in a manner analogous to spectral analysis. This approach is explored in Chapter 3.

2.4.1 Transmissibility

Transmissibility in earthquake engineering can simply be defined as the ratio of the lateral deflection of the structure to that of the input horizontal ground motion:

$$Transmissibility = \frac{\delta_{structure}}{\delta_{ground\ motion}} \qquad \text{(Eq. 2-3)}$$

With the exception of extremely stiff structures, transmissibility is typically greater than unity. This indicates that ground motion is amplified by the structure. Thus, a valid performance objective is to minimize this transmissibility. In the work presented in Chapter 3, a CW structure is considered such that the two wall piers are modeled by equivalent SDOF systems connected with damping and spring elements as shown in Figure 2-7 (Iwanami et al. 1996). The connecting elements allow the pier stiffnesses and dynamic properties to interact in order to decrease transmissibility of the overall structure. The transmissibility is reliant upon the stiffness and damping values of the connecting elements. These elements can be optimized for a given pair of equivalent SDOF structures to minimize the transmissibility.

Optimization of transmissibility can be accomplished using a closed-form solution developed by Richardson (2003) for the 2DOF system shown in Figure 2-7. In this approach, the optimized stiffness of the coupling element, k, is obtained through a closed-form equation (presented in Chapter 3). The derivation of the closed-form solution is presented in Hull and Harries (2008).

2.5 METHODS OF ANALYSIS OF COUPLED WALL STRUCTURES

There are a number of analysis procedures suitable for assessing the complex behavior of CWs. As it also results in a closed-form solution, the continuous medium method (CMM) is convenient for integration with fixed point analysis for initial optimization of CW properties. More complex nonlinear methods are required then to verify the expected behavior of these optimizations.

2.5.1 Continuous Medium Method

The continuous medium method, which is also known as Laminar Analysis, was first used to solve the 'dowelled cantilever' problem (analogous to a coupled wall system) by Chitty (1947). The method reduces a coupled wall from a highly statically indeterminate problem to a problem modeled as single fourth-order differential equation. In this method, the connecting members are replaced by a continuum with bending and shear properties equivalent to those of the coupling beams.

The continuous medium method results in closed-form solutions for the internal forces and global deformations of the system. The derivation and resulting closed-form solutions are based on an elastic analysis of a two-dimensional coupled wall structure having two piers and one row of coupling beams as shown in Figure 2-10. The coupled wall system is subject to a lateral load and the inflection point of the coupling beams is assumed to occur at their midspan. In addition, it is assumed in the derivation that the coupling beams do not experience any axial deformation. The resulted governing differential equation in terms of the wall lateral displacement, y, and the vertical distance up the wall in the z direction is (Stafford-Smith and Coull 1991):

$$\frac{d^4y}{dz^4} - (k\alpha)^2 \frac{d^2y}{dz^2} = \frac{1}{EI}\left(\frac{d^2M}{dz^2} - (k\alpha)^2 \frac{k^2-1}{k^2} M\right) \qquad \text{(Eq. 2-4)}$$

Where α and k are parameters describing the properties of the wall piers, beams and their relative stiffnesses (described in depth in Section 4.3.2); and M is the overturning moment applied to the system. Closed-form solutions for different typical lateral load patterns and the definition of all parameters are provided in Stafford-Smith and Coull (1991). Use of this closed-form approach has been developed by Harries (2001) and Harries et al. (2004a), and an approach to developing initial design parameters for CCW systems based on

these closed-form solutions is presented in El-Tawil et al. (2009). The drawback of the use of closed-form solutions is that they are limited to elastic analysis. Details of the CMM, including equations related to the present work, are given in Section 4.3.2.

2.5.2 Equivalent Frame Method

The frame analogy method is more convenient for modeling complex coupled wall systems than the continuous medium method. For example, coupled wall systems comprised of more than two wall piers or an irregular wall configuration make the closed-form solutions difficult to apply (Hassan 2004). The equivalent frame method is versatile, relatively simple and accommodates the nonlinear analysis necessary for performance-based design approaches.

In this method the coupled wall structure is modeled as a series of frame members, where each wall pier is represented by an equivalent column member located at the centroid of the pier. The axial and flexural rigidities (AE and EI) of the column members model those of the actual wall piers. The horizontal frame members consist of two different sections: the coupling beams are represented by beam elements given appropriate structural properties, while the part of the wall pier that spans between the beam-wall connection and the effective column is modeled by rigid arms as shown in Figure 2-10. These rigid arms are used to ensure that the correct rotations and vertical displacements are achieved at the faces of the walls, and also to incorporate the necessary condition that plane wall sections remain plane (Stafford and Coull, 1991). Application of the equivalent frame method is presented in Chapter 5.

2.5.3 Macro Element and Finite Element Models

Macro elements represent a transition between frame element approaches and more complex finite element approaches. A macro element model was proposed by Kabeyasawa et al. (1982) to investigate the behavior of a cantilever shear wall. The model consisted of five nonlinear springs connected at the top and bottom of the wall panel by rigid beam members as shown in Figure 2-11. The vertical springs represent the axial stiffness and strength of the boundary elements and wall web, while the horizontal spring represents the shear stiffness of the wall web. The flexural stiffness and moment strength of the web is represented by the rotational spring. Few studies using macro elements are reported in the literature. The complexity of macro-element and finite element models make them cumbersome for preliminary design. These approaches will not be considered further.

2.6 DESIGN METHODS

2.6.1 Strength Based Seismic Design

In this conventional approach to design, structures are proportioned such that their ultimate capacity is greater than or equal to the required ultimate load demands. The required strength is obtained from the most critical combination of factored loads, while the ultimate capacity of an element is obtained by applying a strength reduction factor to the nominal strength of the element. This load and resistance factor (LRFD) strength-based design (SBD) method is currently the basis of most design codes including ACI (2011) and AISC (2011). Generally, applying an SBD approach is prescriptive in nature; that is; the governing code prescribes how the design will be executed.

In dealing with coupled wall systems, the SBD approach assumes that under the effect of earthquake loads the wall piers and the coupling beams will yield simultaneously at the code-specified base shear. It has already been shown that this is an unrealistic behavior considering the different stiffness of the lateral load carrying mechanisms. To achieve the SBD-assumed mechanism, considering the natural overstrength inherent in all SBD, the wall piers must be designed to handle base shear forces much greater than those nominally required for the coupling beams to yield. Additionally, the traditional SBD of coupled walls often results in coupling beams with shear demands exceeding the permitted shear strength specified by the design code (Harries et al. 2005). For the purpose of reducing these high shear stresses so that they fall within code limits, designers often use unrealistically high values of concrete strength, and/or reduce the effective stiffness of the coupling beams to very small values in their analyses. Neither approach is appropriate nor will either approach capture the expected behavior of coupled wall systems (Harries and McNeice 2004).

2.6.2 Performance-Based Seismic Design

Performance-based design (PBD) (SEAOC 1995) is a burgeoning paradigm in the field of structural engineering, particularly in relation to design for extreme loading conditions such as seismic and blast forces. Largely viewed as assessment tools (FEMA 2000b), performance-based methodologies are being proposed as alternatives to strength-based methodologies and introduced as design tools, typically in relation to specific member types or structural systems (El-Tawil et al. (2009) is one example). PBD generally allows controlled non-linearity in specified structural members as long as certain structural and element performance criteria are satisfied. PBD allows the designer to select how the structure will behave and provides the framework for selecting performance objectives for the

structure. Performance objectives are typically displacement-based objectives; however, they can address any aspect of building performance.

Performance-based approaches are often used to develop novel systems which are then 'standardized' using a prescriptive design approach. In this manner the performance-based aspect is removed by one degree from the final structural design. Recent successful examples of this approach include the development of reduced beam section (RBS) details for steel moment frames (FEMA 2000a) and the development of buckling restrained braces (Watanabe et al. 1988; Black et al. 2002); both concepts were developed with specific performance objectives in mind and subsequently standardized into largely prescriptive design approaches (both: AISC 2005). El-Tawil et al. (2009) present a PBD approach for coupled wall structures. Their approach is presently being incorporated into new AISC seismic design guidelines for hybrid coupled structures (i.e.: those having steel coupling beams linking concrete wall piers).

PBD typically considers 'acceptable design' in the domain of structural behavior – most often defining acceptance criteria in terms of structural deformations. However PBD, by its very nature may define performance in virtually any domain. Examples within the domain of structural engineering include: a) the development of desired yield mechanisms; b) improving constructability; c) acceptable post-event condition of the structure, including damage tolerance and reparability; d) replacement/repair value; e) downtime; f) casualty rate; etc.

Performance objectives represent a spectra rather than a discrete objective. In most building code applications, for instance, the desired performance of a structure is that it will satisfy Immediate Occupancy (IO) requirements for an expected service level earthquake (often defined as having a probability of exceedance of 50% in 50 years), Life Safety (LS) requirements at the design level earthquake (10% in 50 years) and Collapse Prevention (CP)

requirements at the maximum credible event (2% in 50 years). Allowable displacements or damage for CP are greater than those for LS which are, in turn, greater than those for IO. Thus a spectrum of performance results considering both the seismic load and structural performance (resistance). There are spectra of both performance objectives and seismic demand levels which may be combined to develop performance objectives (FEMA 2000b).

2.6.2.1 Proposed Performance Domain for Coupled Wall Structures

In this study, an alternative performance objective based on the behavior of dual or evolving structural systems is investigated. In this case, the performance domain is the *structural form* of the lateral force resisting system (LFRS) itself: the LFRS of a structure is permitted (or encouraged) to evolve from one form to another based on demand. This evolution may then be optimized to affect both rational performance criteria at various demand levels and economy in design. The example considered is the evolution of coupled wall (CW) systems to systems of linked wall piers (LWP) at increasing lateral load demands (Figure 1-1).

At the member level, certain types of fused elements are already designed to behave in this manner; examples include: lead core base isolators (Kelly 1982), friction damping devices (Buckle and Mayes 1990) and fused coupling beams (Fortney et al. 2004). In all of these cases, the element design parameters include a threshold above and below which the element exhibits significantly different behavior. It is conceived in this research that dual structural systems may extend this concept to the structure itself in the performance domain.

The concept is envisioned for a typical dual system as follows: The structure performs as a dual structure (in this case, as a coupled wall) at a particular (design) performance level. At a performance level having a greater demand, the capacity of one of the components of the dual system (coupling beams) is permitted to be exhausted as the structure essentially becomes a single LFRS structure (a collection of linked wall piers). Such an approach will

result in a more rational performance for the structure and a more economical structural design particularly in cases where the components of the dual system have significantly disparate stiffness and thus proportional demands as is the case in CW (see Figure 2-3 and related discussion, above).

2.6.2.2 Acceptance Criteria for CCW Systems

The most important step in the application of PBD is the selection of the definition of 'acceptable behavior' for the structure or individual components for a given seismic event; that is, the selection of the performance objectives. FEMA 356 (2000) refers to this as the building's acceptance criteria and presents tables for acceptance criteria based on plastic hinge rotation capacity for common structural systems and their elements. The values provided in FEMA 356 are for existing structures and may underestimate the capacity of well-detailed new construction (Harries et al. 2004b).

For CW systems, Paulay (2002) provides a method and rationale for determining inelastic deformation capacity of diagonally reinforced coupling beams (DRCCB) and wall piers. Paulay's rationale is based on the fundamental mechanics of DRCCBs and appears to estimate well the experimentally observed behavior of DRCCBs reported in the (admittedly sparse) literature (as reviewed by McNeice 2004). DRCCB and wall pier behavior proposed by Paulay is adopted as the primary acceptance criteria for the current work.

Clearly, nonlinear analysis is required to adequately assess acceptance criteria. Typically, nonlinear static, or pushover, analysis provides the basis for performance-based methodologies, although, validation with nonlinear dynamic (time history) analysis is also often carried out. In the latter case, a suite of three or more representative ground motions are recommended (ASCE 07-10 Section 16.1.3). Pushover analysis is described in greater depth in Chapter 5 and nonlinear time history analysis is described in Chapter 6.

2.6.2.3 Performance Based Design of CW

The difficulties faced by designers attempting to design CWs using current codes should not be underestimated. Departure from accepted SBD practices, however often introduce difficulties associated with the structural peer review and can create expensive delays for the design firm and developer. A rational approach to CW design, founded on a PBD approach has been proposed (El-Tawil et al. 2009). The proposed PBD approach recognizes the preferred yielding mechanism of CWs (Paulay and Santhakumar 1976) and takes advantage of the available ductility of the coupling beams.

Figure 2-12a shows an idealized response of a CW designed using a PBD approach. In the case shown, the coupling beams are permitted to yield (V_B) at a base shear lower than the code-prescribed design base shear (V_C at LS performance objective as described above) and the wall piers will yield (V_W) at essentially V_C. V_D is the base shear corresponding to the CW attaining its code-prescribed drift limit (typically 2%).

Other performance spectra are possible such as allowing inelasticity in the wall piers at design base shear levels ($V_W < V_C$). It is conceived that different behavior may be permitted at different performance levels. For example, a CW may be designed to behave as a coupled wall system at the LS performance level but as a collection of linked wall piers (LWP) at the CP level (essentially, having exhausted the capacity of the beams) as shown in Figure 2-12b. In Figure 2-12, the fundamental structure considered is represented by its structural period: T_{CW} for the CW system (Figure 2-12a) and T_{CW} evolving into T_{LWP} where only the wall piers provide lateral force resistance following designed-for exhaustion of the coupling beam capacity (Figure 2-12b).

2.7 SUMMARY

To the author's knowledge, a unique aspect of the present of the work is the focus on CW systems with notably different wall pier mechanical and dynamic properties. Using this prototype, a performance-based approach to developing an initial viable design for a CCW structure is demonstrated; essentially validating the approach proposed by El-Tawil et al. (2009) while extending it to a more complex structural geometry. Additionally, most previous analytical studies (e.g.: all analytical studies from the 1960's and 1970's; El-Tawil et al. 2002; Xuan et al. 2008) and all previous experimental studies (e.g.: Santhakumar 1974; Aristizabal-Ochoa and Sozen 1976; Lybas and Sozen 1977; Aristizabal-Ochoa et al. 1979; Aktan and Bertero 1981; Teshigawara 1998) have also largely focused on prismatic walls (i.e.: those having the same details over their height). McNeice (2004) is an exception having considered a 30 storey structure with four wall sections and five beam types. The present work will develop a 'realistic' distribution of both wall and beam details vertically over the structure. The application of non-traditional performance objectives based on the recommendations of Hull and Harries (2008) are also explored through the attempted extension of fixed point theory to the coupled wall design problem (Chapter 3).

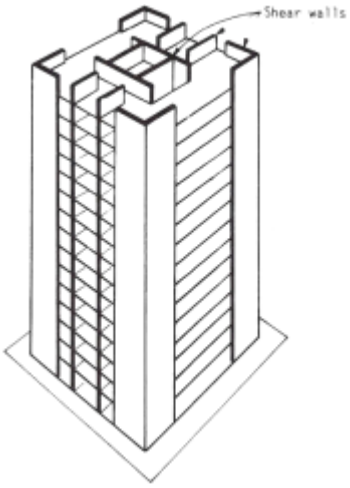

Figure 2-1 Cantilever shear wall structure (Stafford-Smith and Coull 1991)

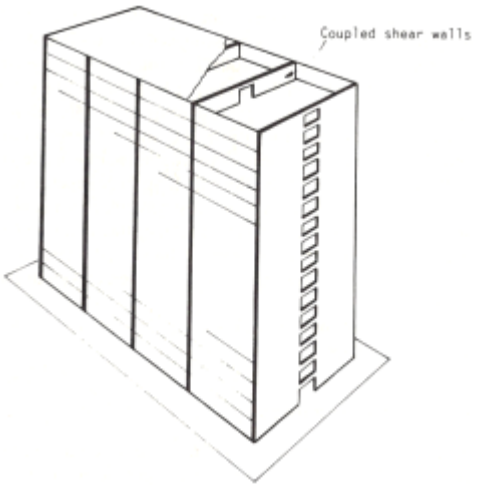

Figure 2-2 Coupled shear wall structure (Stafford-Smith and Coull 1991)

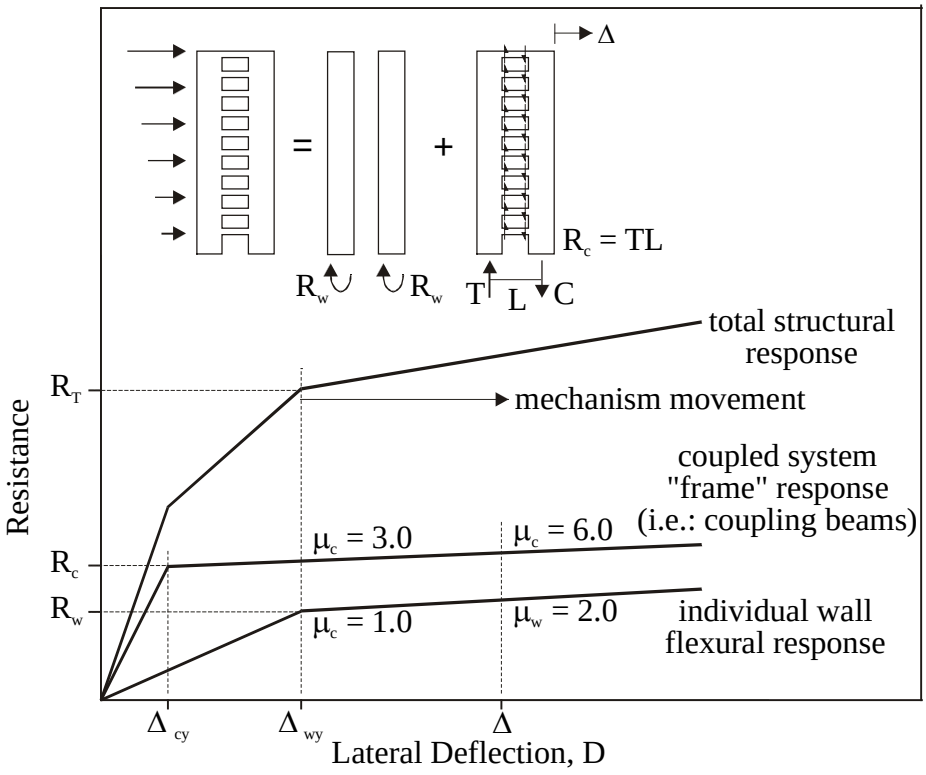

Figure 2-3 Idealized lateral response of CW structure (Harries 2001)

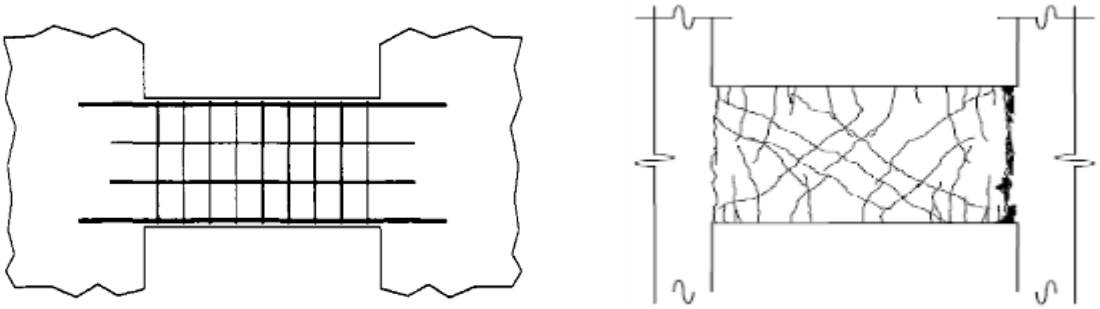

a) reinforcing layout (Boivin 2006) b) typical crack pattern (FEMA 306 1998)

Figure 2-4 Conventionally reinforced coupling beam

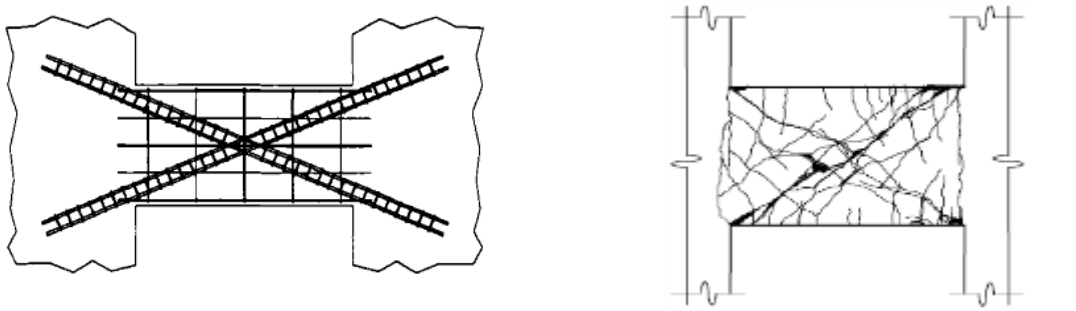

a) reinforcing layout (Boivin 2006) b) typical crack pattern (FEMA 306 1998)

Figure 2-5 Diagonally reinforced coupling beam

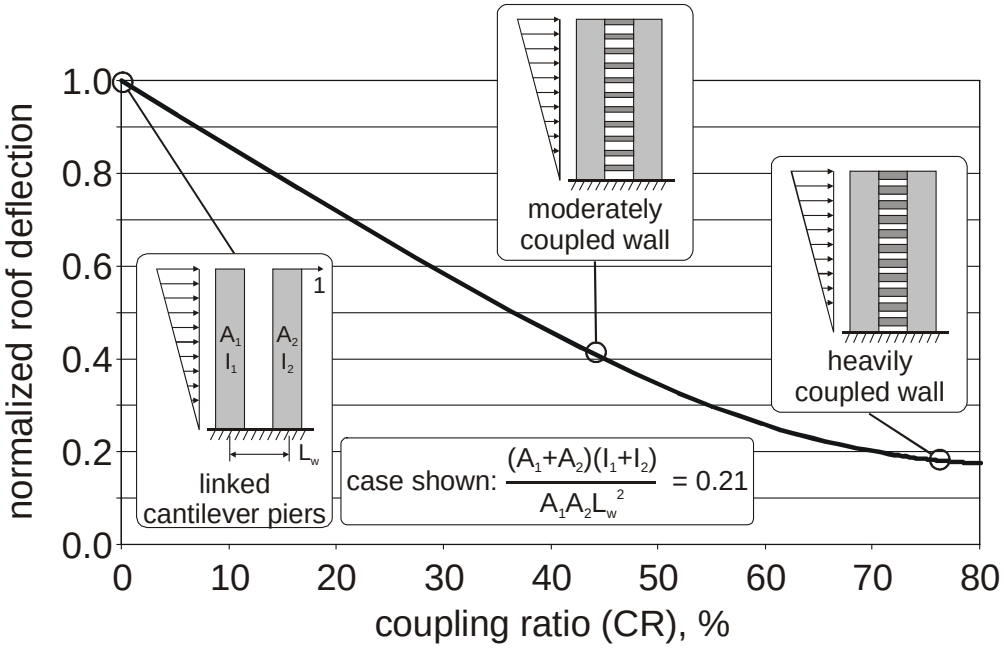

Figure 2-6 Effect of coupling on wall pier roof displacement (El-Tawil et al. 2009)
(coupling ratio = degree of coupling)

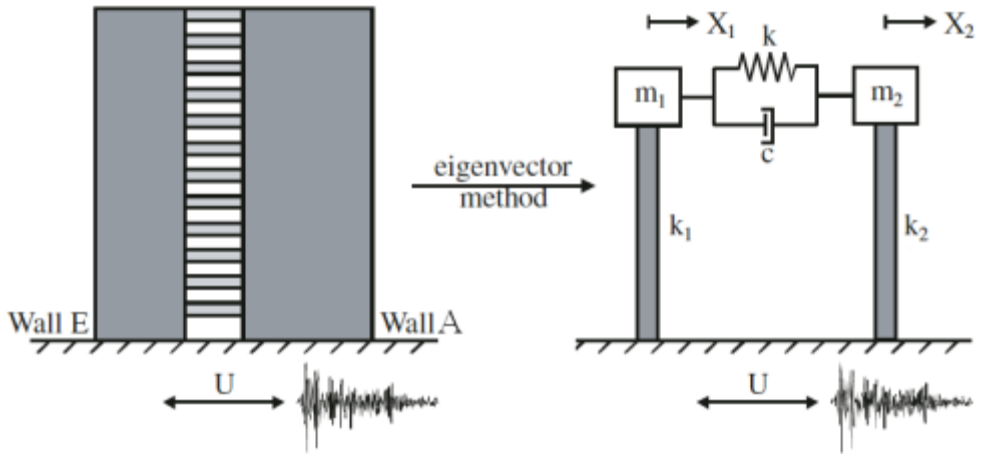

Figure 2-7 Idealized 2DOF system for application of fixed point theory (Hull and Harries 2008)

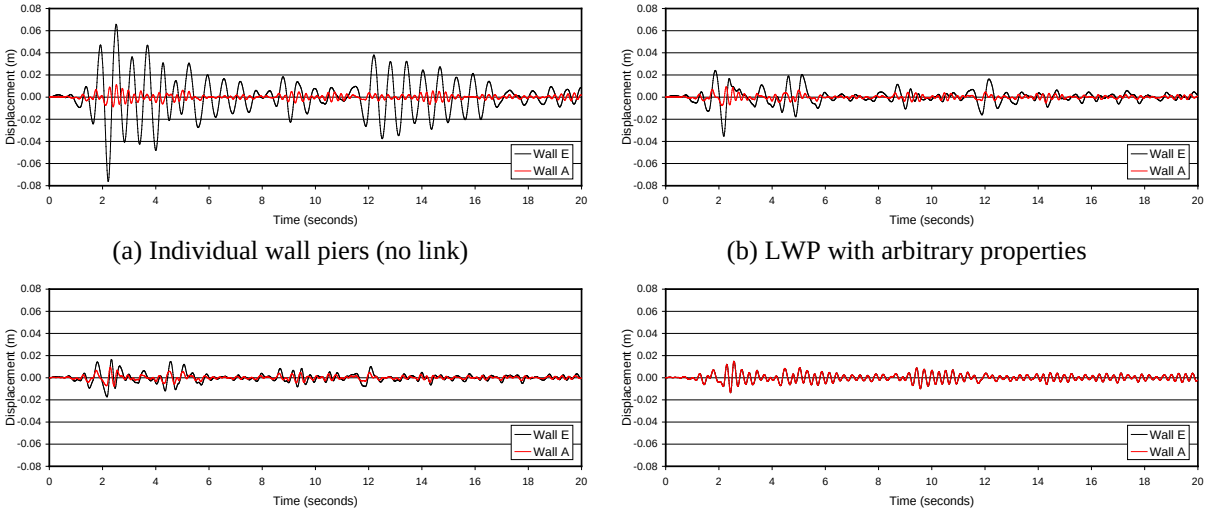

(a) Individual wall piers (no link)

(b) LWP with arbitrary properties

(c) LWP optimized link properties

(d) LWP with rigid link

Figure 2-8 Lateral displacements of walls (labeled E and A) of a LWP system (Hull 2006)

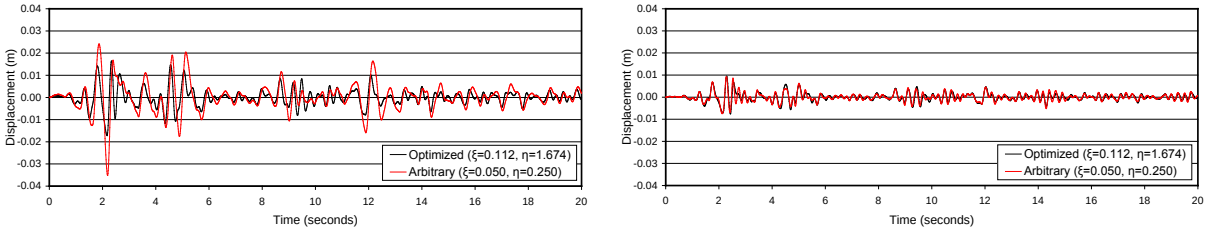

(a) Left hand wall E in LWP system

(b) Right hand wall A in LWP system

Figure 2-9 Wall pier displacements for optimized and arbitrary links (Hull 2006)

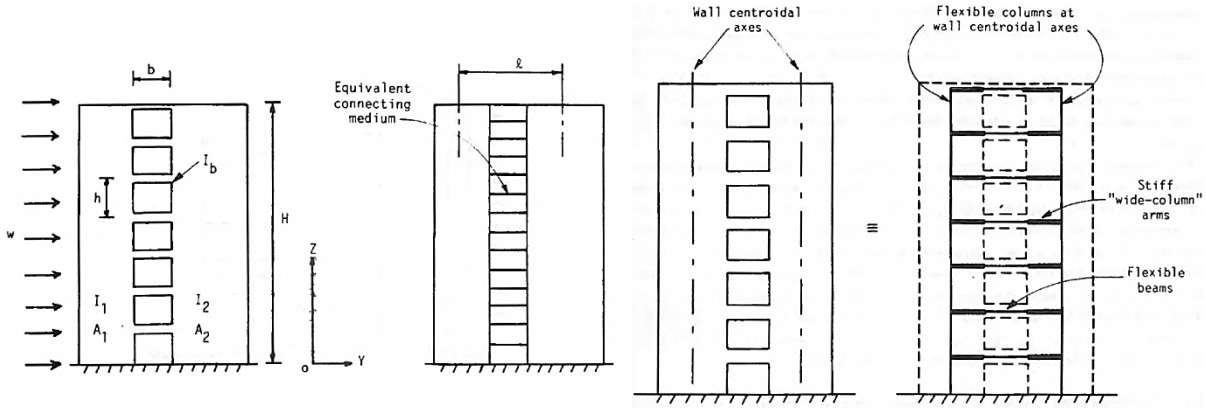

equivalent continuous medium method b) equivalent frame method

Figure 2-10 Modeling of coupled shear wall (Stafford-Smith and Coull 1991)

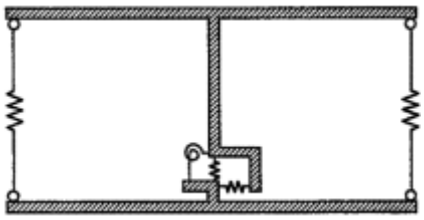

Figure 2-11 Macro element for single floor of wall pier proposed by Kabeyasawa et al. (1982) (Figure from Hassan 2004)

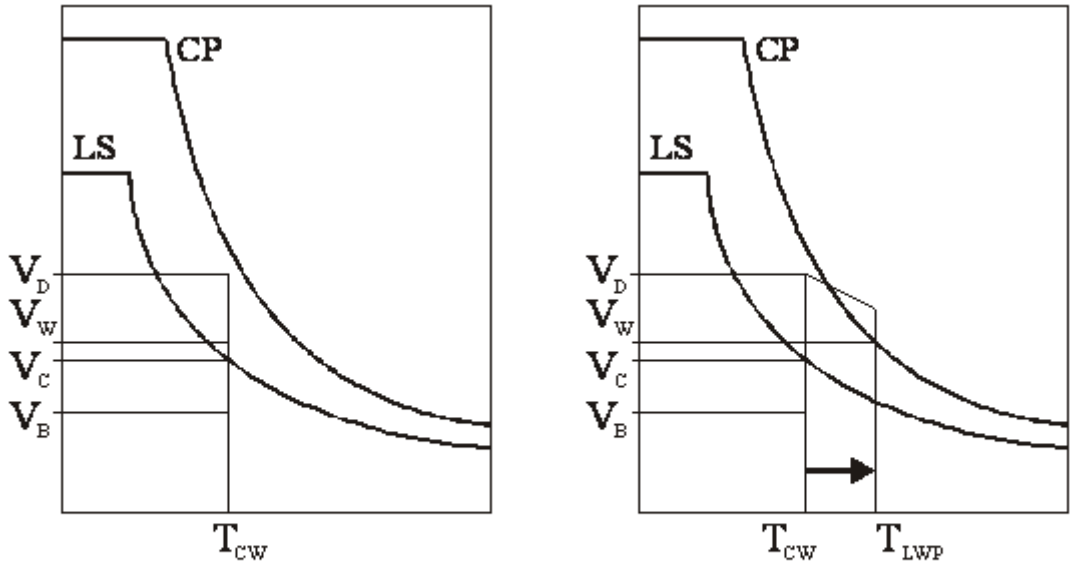

(a) schematic representation of PBD objective as described by Harries and McNeice (2006).

(b) schematic representation of PBD objective of CW treated as dual system.

Figure 2-12 Idealized spectral capacity behavior of a CW

3.0 APPLICATION OF FIXED POINT THEORY TO COUPLED CORE WALLS

Hull and Harries (2008) identified fixed point theory (FPT) as having potential applications to the performance-based design (PBD) of coupled core wall (CCW) systems (see Section 2.4). They identified the potential transition from CCW under service lateral loads to a system of linked wall piers (LWP) under design seismic loads and focused on the performance of the LWP system. Hull and Harries proposed a novel measure of performance: minimization of transmissibility of horizontal ground motion through the optimization of coupling beam stiffness. In this chapter, the practical application of optimizing coupling beams stiffness using FPT will be investigated. The stiffness of the coupling beams for a given set of wall piers may be optimized to improve the CCW, and subsequent LWP, response to earthquake excitation.

The first step in the process is to simplify each of the multi degree of freedom (MDOF) wall piers to single degree of freedom (SDOF) systems, and then apply FPT to determine the optimum coupling beams properties. As described in Section 2.4, the wall piers are idealized as two SDOF systems connected by a spring and dashpot system as shown in Figure 2-7 (Iwanami et al. 1996).

In this study, CCW prototype structures similar to those previously identified by Harries et al. (2004a) are used. These are 12 storey structures that have seven individual pier geometries labeled A through G, shown schematically in Table 3-1. The thickness of the wall piers is 1.15 ft and the uniform storey height is 11.8 ft. The other dimensions and resulting wall pier areas and moments of inertia are presented in Table 3-1. The coupling beam

geometric information is not relevant at this point, as only the wall pier dynamic properties are required. In fact, this analysis is intended to lead to coupling beam stiffness requirements. The individual wall piers are paired into two-pier CCW systems, each pier matched with each other pier resulting in 28 unique analysis cases. Optimal coupling of identical wall piers based on transmissibility is meaningless (i.e.: Wall A coupled to Wall A); thus the number of unique analyses is 21. For example, case 16 (Wall D coupled to Wall E) is shown in Figure 3-1.

3.1 DERIVATION OF THE EQUIVALENT SDOF STRUCTURE

In order to model an MDOF wall pier as a SDOF system, it is represented by a massless beam-column member, where the mass of the structure is lumped at the top of the member. Each beam-column is assigned geometric and material properties of the wall pier. The eigenvector method presented by Seto et al. (1987) is used to establish the equivalent SDOF mass of an MDOF system. For each analysis case, the mass of the MDOF wall pier takes the form of a diagonal matrix, with the diagonal values representing the portion of the storey mass assigned to the wall pier based on its tributary area:

$$\mathbf{M}_X = \begin{bmatrix} m_{X1} & 0 & \dots & 0 \\ 0 & m_{X2} & & \\ \dots & & \dots & \\ 0 & & & m_{X12} \end{bmatrix} \qquad \text{(Eq. 3-1)}$$

Where the subscript X is the wall pier identification (wall 1 or wall 2) and the numeric subscripts are the storey levels 1 through 12, in this case. At each storey, i:

$$m_{1i} = \left(\frac{A_1}{A_1 + A_2} \right) m_{total.i} \quad \text{and} \quad m_{2i} = \left(\frac{A_2}{A_1 + A_2} \right) m_{total,i} \qquad \text{(Eq. 3-2)}$$

Where A_1 and A_2 are the sectional areas of each wall pier and $m_{total,i}$ is the mass of storey i. Thus, piers in a core are assigned structural mass based on their relative areas.

Each MODF wall pier is assumed to have a fixed base and a single DOF at each floor level. Each pier is modeled as a uniform flexural member in which the lateral stiffness associated with each floor is:

$$k_X = \frac{12EI_X}{h^3} \qquad \text{(Eq. 3-3)}$$

Where the subscript X is the wall pier identification (wall 1 or wall 2); h is the storey height; E is the modulus of elasticity of concrete; and I_X is the moment of inertia of the wall pier. For such a uniform MDOF structure, the global stiffness matrix is symmetric and is assembled in the conventional manner:

$$\mathbf{K}_X = \begin{bmatrix} 2k_X & -k_X & 0 & \dots & 0 \\ -k_X & 2k_X & -k_X & & \\ 0 & -k_X & 2k_X & & \\ \dots & & & \dots & -k_X \\ 0 & & 0 & -k_X & k_X \end{bmatrix} \qquad \text{(Eq. 3-4)}$$

In the eigenvector method, the equivalent SDOF mass and stiffness of the structure are determined by applying D'Alembert's principle of dynamic equilibrium to formulate the equation of motion for the system. The equation of motion governing the displacement of the structure is written as

$$\mathbf{M}\,\ddot{x} + \mathbf{C}\,\dot{x} + \mathbf{K}\,x = \mathbf{F}(t) \qquad \text{(Eq. 3-5)}$$

Where **M** and **K** are given in Equations 3-1 and 3-4 respectively; **C** is the damping matrix of the structure; **F**(t) is the forcing function; and x, $\dot{x}$ and $\ddot{x}$, are the DOF displacement, velocity and acceleration vectors, respectively. The equation of motion for the undamped free vibration case reduces to the form shown in Equation 3-6, where both **C** and **F**(t) are set to zero.

$$\mathbf{M}\,\ddot{x} + \mathbf{K}\,x = 0 \qquad \text{(Eq. 3-6)}$$

Equation 3-6 is a set of linear, homogenous, second-order differential equations; its solution has the form:

$$x(t) = \phi_n (A_n \cos \omega_n t + B_n \sin \omega_n t) \qquad \text{(Eq. 3-7)}$$

Where $x(t)$ is the free vibration response; t is the time; ω_n is the modal natural frequency of the structure; ϕ_n is the corresponding mode shape of vibration; n is the number of degrees of freedom defining the motion of the structure; and A_n and B_n are constants that depend on the initial conditions of the displacement and velocity of the system. In Equation 3-7 both ω_n and ϕ_n are unknown. Substituting Equation 3-7 into Equation 3-6 gives:

$$\left(-\omega_n^2 \mathbf{M}\phi_n + \mathbf{K}\phi_n\right)(A_n \cos \omega_n t + B_n \sin \omega_n t) = \mathbf{0} \qquad \text{(Eq. 3-8)}$$

Equation 3-8 can be satisfied in two ways. The trivial solution, *x(t) = 0* implies that there is no motion in the structure. Setting the left term equal to zero and factoring the ϕ_n out, the so-called real eigenvalue problem results:

$$\left(\mathbf{K} - \omega_n^2 \mathbf{M}\right)\phi_n = \mathbf{0} \qquad \text{(Eq. 3-9)}$$

For a nontrivial solution, the determinant of the left term is set to zero resulting in the characteristic equation:

$$\left|\mathbf{K} - \omega_n^2 \mathbf{M}\right| = 0 \qquad \text{(Eq. 3-10)}$$

Expanding the determinant in Equation 3-10 gives N positive roots for ω_n^2, which are the eigenvalues of the system (Chopra 2006). Knowing the natural frequencies ω_n, Equation 3-9 can be solved for the corresponding eigenvectors, ϕ_n, known also as the eigenvectors. In structural applications, it is typical to present the eigenvectors normalized by the roof displacement Equation 3-11, although this is not strictly necessary.

$$\phi_n = \begin{Bmatrix} x_n / x_{roof} \\ \cdots \\ \cdots \\ \cdots \\ x_2 / x_{roof} \\ x_1 / x_{roof} \end{Bmatrix} = \begin{Bmatrix} 1 \\ \cdots \\ \cdots \\ \cdots \\ x_2 / x_{roof} \\ x_1 / x_{roof} \end{Bmatrix} \quad \text{(Eq. 3-11)}$$

The equivalent SDOF modal mass corresponding to each mode is found as the product of the transpose of the eigenvector with the mass matrix and the eigenvector:

$$M_n = \phi_n^T \mathbf{M} \phi_n \quad \text{(Eq. 3-12)}$$

M_n is the equivalent SDOF modal mass of the wall pier for mode n, while **M** is the mass matrix of the MDOF wall pier. The effective equivalent SDOF modal mass of the wall pier is defined as (Chopra 2006):

$$M_n^* = \frac{\left(\sum_i^{NN} m_i \phi_{in}\right)^2}{M_n} \quad \text{(Eq. 3-13)}$$

Where NN is the number of degree of freedom (DOF) of the structures, and m_i is the storey mass associated with each DOF.

Finally, the equivalent stiffness of the SDOF structure is determined as:

$$K_n^* = \omega_n^2 M_n^* \quad \text{(Eq. 3-14)}$$

For the present study, only the fundamental natural frequency is considered, thus only the first mode shape is used and n =1 throughout the preceding equations. In every case, considering only the first mode for these uniform wall piers results in a modal participation factor equal to 0.90 as recommended by ASCE 7-10 section 12.9.1. The optimal properties of the connecting elements are determined using these equivalent SDOF properties of the two wall piers through the closed-form solution provided by the FPT.

3.2 FIXED POINT THOERY

The complete derivations of the closed-form solutions for the FPT approach are presented in Richardson (2003); only necessary equations are presented here. The formulation of the FPT equations begins considering the transmissibility equations of the two wall pier equivalent SDOF structures that are connected with damping and spring elements as shown in Figure 2-7. It is critical to note that in the application of the closed-form solution presented, the wall designations (1 and 2) must be selected such that the frequency ratio, $\gamma = \omega_2/\omega_1 > 1.0$. As discussed in Section 2.4.1, the transmissibility is the ratio of the structure top displacement (x) to the displacement induced by the ground motion (u). The equation of motion for each equivalent SDOF using D'Alembert's principle is presented in Iwanami et al. (1996) as shown in Equations 3-15 and 3-16.

$$m_1 \ddot{x}_1 = k_1 (u - x_1) + k (x_2 - x_1) + c (\dot{x}_2 - \dot{x}_1) \qquad \text{(Eq. 3-15)}$$

$$m_2 \ddot{x}_2 = k_2 (u - x_2) + k (x_1 - x_2) + c (\dot{x}_1 - \dot{x}_2) \qquad \text{(Eq. 3-16)}$$

Where the variables with subscripts 1 and 2 refer to properties of wall 1 and wall 2 respectively; u is the ground displacement; k and c are the stiffness and dashpot damping of the connecting element. Considering that the system is subjected to harmonic motion, Iwanami et al. (1996) derived the displacement transmissibility x_1/u and x_2/u, shown in Equations 3-17 and 3-18 for two SDOF piers connected at the top. The equations are functions of the properties of each SDOF pier as well as the connecting element properties.

$$\left|\frac{x_1}{u}\right| = \sqrt{\frac{\left[1-\left[\frac{\omega}{\omega_2}\right]^2+\left(\frac{\omega_1}{\omega_2}\right)^2\left(\frac{\eta}{\mu}\right)+\eta\right]^2+\left[2\xi\left(\frac{\omega}{\omega_2}\right)\left[1+\mu\left(\frac{\omega_2}{\omega_1}\right)^2\right]\right]^2}{\left[\left[1+\eta-\left(\frac{\omega}{\omega_1}\right)^2\right]\left[1-\left(\frac{\omega}{\omega_2}\right)^2\right]+\left(\frac{\eta}{\mu}\right)\left[\left(\frac{\omega_1}{\omega_2}\right)^2-\left(\frac{\omega}{\omega_2}\right)\right]\right]^2+\left[2\xi\left(\frac{\omega}{\omega_2}\right)\left[1+\mu\left(\frac{\omega_2}{\omega_1}\right)^2-(1-\mu)\left(\frac{\omega}{\omega_1}\right)^2\right]\right]^2}} \qquad \text{(Eq. 3-17)}$$

$$\left|\frac{x_2}{u}\right| = \sqrt{\frac{\left[1-\left[\frac{\omega}{\omega_1}\right]^2+\left(\frac{\omega_1}{\omega_2}\right)^2\left(\frac{\eta}{\mu}\right)+\eta\right]^2+\left[2\xi\left(\frac{\omega}{\omega_2}\right)\left[1+\mu\left(\frac{\omega_2}{\omega_1}\right)^2\right]\right]^2}{\left[\left[1+\eta-\left(\frac{\omega}{\omega_1}\right)^2\right]\left[1-\left(\frac{\omega}{\omega_2}\right)^2\right]+\left(\frac{\eta}{\mu}\right)\left[\left(\frac{\omega_1}{\omega_2}\right)^2-\left(\frac{\omega}{\omega_2}\right)\right]\right]^2+\left[2\xi\left(\frac{\omega}{\omega_2}\right)\left[1+\mu\left(\frac{\omega_2}{\omega_1}\right)^2-(1-\mu)\left(\frac{\omega}{\omega_1}\right)^2\right]\right]^2}}$$

(Eq. 3-18)

Where ω = the forcing function frequency

(Eq. 3-19)

ωi = natural frequency of wall pier i: $\omega_i = \sqrt{\frac{K_i^*}{M_i^*}}$

η = fixed point stiffness ratio: $\eta = \frac{k}{K_1^*}$ (Eq. 3-20)

μ = the mass ratio of the wall piers: $\mu = \frac{M_2^*}{M_1^*}$ (Eq. 3-21)

ζ = damping ratio: $\xi = \frac{c}{2\sqrt{M_2^* K_2^*}}$ (Eq. 3-22)

Figure 3-2 shows schematically the two transmissibility equations plotted by ranging the damping, ζ, between zero and infinity. Three curves result: one for each DOF (wall pier) when the damping is set to zero and third curve for both walls when ζ = ∞. Setting ζ = ∞ in the latter case effectively constrains the two SDOF systems to behave as a single unit, and consequently the two walls have the same displacement and transmissibility (Hull and Harries 2008).

The points P and Q in Figure 3-2 are the fixed points, and the maximum values of the transmissibility equations (Equations 3-17 and 3-18) correspond to these points. Hull and Harries (2008) showed that the maximum transmissibility values always occurs near points P and Q and the optimal transmissibility of the system is achieved when the transmissibility values of P and Q are equal. The value of the fixed point stiffness ratio given by Equation 3-20 corresponding to this optimum case is obtained from the closed-form solution developed by Richardson (2003):

$$\eta = \frac{U}{L}$$ (Eq. 3-23)

Where:

$$U = \frac{1}{4}(-\omega_1 + \omega_2)(\omega_1 + \omega_2)(-3(\mu+5)(\mu+1)^2\,\omega_1^{\,6} - 3\omega_2^{\,2}(7\mu+3)(\mu+1)^2\,\omega_1^{\,4} + \left[(3\mu^5 + 15\mu^2 + 33\mu^3 + 21\mu^4)\omega_2^{\,4} - 3\sqrt{g} + \mu\sqrt{g}\right]\omega_1^{\,2} + (21\mu^5 + 51\mu^4 + 39\mu^3 + 9\mu^2)\omega_2^{\,6} + (3\mu^2\sqrt{g} - \mu\sqrt{g})\omega_2^{\,2})\,\mu \quad \text{(Eq. 3-24)}$$

$$L = (\omega_1^{\,2}(\mu+1)^2(\omega_2^{\,2}\mu + \omega_1^{\,2})[(6\mu + \mu^2 + 5)\omega_1^{\,4} + 13\mu^2 + 3 + \mu^3 + 15\mu)\,\omega_2^{\,2}\omega_1^{\,2} + (7\mu^3 + +3\mu + 10\mu^2)\omega_2^{\,4} + \sqrt{g})] \quad \text{(Eq. 3-25)}$$

Where:

$$g = (\omega_2^{\,2}\mu + \omega_1^{\,2})(\mu^3\omega_2^{\,2} + 26\mu^2\omega_2^{\,2} + 9\mu^2\omega_1^{\,2} + 9\omega_2^{\,2}\mu^2 + 26\omega_1^{\,2}\mu + \omega_1^{\,2})(5\omega_1^{\,2} + 3\omega_2^{\,2} + \omega_1^{\,2}\mu + 7\omega_2^{\,2}\mu)^2 \quad \text{(Eq. 3-26)}$$

The optimum damping ratio (Equation 3-22) of the connecting element is taken as the average of the damping values associated with points P and Q (Hull and Harries 2008). Hull and Harries present the interaction of stiffness and damping properties and demonstrate that near the optimal P and Q points, the optimization itself is relatively insensitive to the selection of damping, particularly in the range typical of engineered structures. In this research only the optimum stiffness of the coupling beams is considered in addressing the objectives of the study.

3.3 PARAMETRIC ANALYSIS OF PROTOTYPE STRUCTURES

Twenty one prototype structures having wall piers provided in Table 3-1 are used to explore the use of the FPT in optimizing CCW behavior. The FPT solution for optimizing the transmissibility requires that the two structures have different dynamic properties to avoid a trivial solution. In these analyses, cracked concrete section properties are considered. The hinge region in these twelve-storey structures is assumed to form in the first two storeys,

where a flexural stiffness of $0.35EI_g$ was used; $0.7\ EI_g$ was used for the upper ten storeys (Equation 3-3). The modulus of elasticity of concrete was assumed to be E = 4134 ksi (Equation 3-3). The storey mass (m_{total} in Equation 3-2) is assumed to 2248 kips.

The results of the FPT analyses are provided in Table 3-2 for the 21 cases. These results include the calculated optimal stiffness and damping ratios for the connecting elements.

When considering the parametric results, it is important to note that when the natural frequency ratio, γ, approaches 1.0, the calculated fixed point stiffness ratio approaches zero. This represents the trivial case where two identical SDOF systems will have continued identical dynamic behavior (and thus equal transmissibility) regardless of the level of coupling and/or damping provided. Additionally, in the closed-form solution, when the product of the mass and frequency ratios, $\mu\gamma$, falls below 1.0, the optimization process yields negative stiffness values (cases 15 and 19 in Table 3-2). Although mathematically correct, such results are not physically meaningful — indicating a negative stiffness is required for optimization. In essence, coupling the wall piers in this case results in increased transmissibility compared to a system of uncoupled walls (Hull and Harries 2008).

3.4 CONSTANT DISTRIBUTION OF THE OPTIMUM STIFFNESS

The next step is to determine the geometric dimensions of the coupling beams for these 12-storey prototype structures. The optimum stiffness obtained from the FPT analysis is distributed to all coupling beams of the CCW system. The distribution of the total stiffness among the coupling beams should be proportional to the shear demand in the coupling beams due to lateral loading, but as preliminary trial, a constant distribution is used.

Once the optimum stiffness of the spring element connecting the two SDOF systems is obtained, it can be used to determine the dimensions of the 24 coupling beams for the prototype structures (two coupling beams at each level). As a starting point, constant distribution of the fixed point stiffness, $k_i = k/12$, to all storeys was used.

The optimum stiffness of the connecting spring represents the axial stiffness of the coupling beams as follows:

$$k_i = \frac{\phi 2AE}{l_b} = \frac{\phi 2h_b w_b E}{l_b} \qquad \text{(Eq. 3-27)}$$

Where $\phi = 0.1$ is the reduction factor for the axial stiffness in tension for coupling beams (Kabeyasawa et al. 1983). The variables h_b, w_b, and l_b are the coupling beams depth, width, and length respectively. The factor 2 accounts for two beams per storey. The width and length of the coupling beams are fixed for all combinations to be equal to 13.78 in. and 6.56 ft respectively (see Figure 3-1). Thus, the required depth, h, of a single coupling beam can be determined. These calculated values are shown in Table 3-2. In most cases, the depth of beam, h, to generate the coupling stiffness required, k_i, is less than the thickness of a typical concrete slab.

3.5 PRACTICAL APPLICATION OF FPT OPTIMIZATION

Based on the fixed point theory (FPT) approach presented in Chapter 3, it is seen that the performance objective of minimization of transmissibility of horizontal ground motion through the optimization of coupling beam stiffness results in very small levels of required coupling stiffness. The ‘required’ coupling beam dimensions are generally smaller than the depth of the concrete slab, let alone a practically dimensioned coupling beam.

Such low levels of coupling stiffness are structurally impractical using either concrete or steel coupling beams and would result in unacceptably low values for the degree of coupling (doc). The premise of the FPT optimization is to permit the structure to degrade from a CCW to a LWP, essentially allowing the doc to fall to zero. Nonetheless, the coupling elements in a typical CCW geometry also participate in the gravity load resistance and must maintain sufficient residual capacity to do so. The calculated beam dimensions in this case were generally inadequate to provide the required capacity. The effect of providing coupling stiffness based on practical coupling beam designs is to move the dynamic system away from the optimum case for minimizing transmissibility. That is to say, other design considerations – primarily the target doc (El-Tawil et al. 2009) will control the design of these coupling beams.

FPT applications in structural engineering are generally most applicable to problems having large frequency ratios ($\gamma = \omega_2/\omega_1$) such as when considering isolating vibrating equipment from a structure. In practice, the frequency ratio of practical CCW systems (considering structural layout and efficient resistance of lateral load) will rarely exceed $\gamma = 2.0$. This relatively low ratio makes optimization impractical or trivial with respect to the global structural performance.

Considerably more research is necessary to identify a design space in which FPT is useful to the structural designer. As guidance for future study, the following applications are suggested:

1. The anticipated seismic performance of shear wall structures (those resisting lateral forces only through the summation of wall moments) may be enhanced by considering the beneficial effect of the small degree of coupling resulting from the floor diaphragm. While the diaphragm is not assumed to develop coupling frame action, it does act as a link between piers, affecting some interaction between

individual piers and therefore the transmissibility of ground motion. Such an approach is not likely necessary in initial design but may serve the objectives of the seismic assessment of existing structures. The beneficial effects of 'slab coupling' may mitigate the need for seismic strengthening in some cases.

2. 'Mega-coupled' wall structures are those having coupling elements at only a few discreet locations rather than at each floor. Such systems are analogous to 'outrigger' structures which are relatively common in modern high-rise design. The performance of such structures, whose performance is dominated by few structural degrees of freedom and have few coupling locations, may benefit from the CCW to LWP design approach and therefore from the FPT optimization approach.

3.5.1 Conclusions

Based on the results presented in this chapter, the primary objectives of this study of investigating the evolution process of a CCW structure to a collection of LWP structures (Figure 1-1) does not appear to be enhanced through the FPT optimization of transmissibility between dynamically different wall piers. Other practical design considerations including the core having a practical floor plan and the need to develop a doc > 50% for an efficient CCW system (El-Tawil et al. 2009) appear to control the design of coupling beams.

Table 3-1 Wall pier dimensions used in FPT analysis (Harries et al. 2004a)

Wall	Wall flange (h_{wall}) ft	Wall web (l_{wall}) ft	Gross wall area (A) ft^2	Gross wall inertia (I) ft^4
A	22.97	29.53	84.0	4658
B	19.69	9.84	53.9	2085
C	13.12	9.84	38.8	675
D	16.40	19.69	57.6	1606
E	9.84	19.69	42.6	385
F	9.84	9.84	31.3	302
G	13.12	29.53	61.4	986

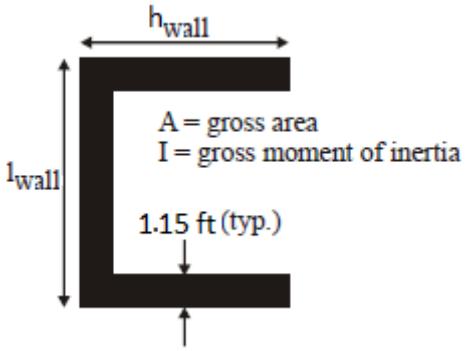

Table 3-2 Optimization results of connecting elements using FPT

Case #	Properties of wall 1				Properties of wall 2				Ratios		Properties connecting elements			
	Wall ID	Equivalent effective mass	Equivalent effective stiffness	Natural frequency	Wall ID	Equivalent effective mass	Equivalent effective stiffness	Natural frequency	Mass Ratio	Frequency Ratio	Coupling Damping Ratio	Coupling Stiffness Ratio	Coupling Stiffness	Depth
		M_1^*	K_1^*	ω_1	-	M_2^*	K_2^*	ω_2	μ	γ	ξ	η	k	h
	Eq.	3-13	3-14	3-10	-	3-13	3-14	3-10	3-21	$\gamma = \omega_2/\omega_1$	3-20	3-22	3-23	3-27
	units	lb sec^2/ft	kip/ft	radians	-	lb sec^2/ft	kip/ft	radians	-	-	-	-	kip/ft	ft
1	B	2.95E+05	8.14E+05	52.54	A	4.60E+05	1.82E+06	62.89	1.56	1.20	0.046	0.059	4.84E+04	0.19
2	C	2.39E+05	2.63E+05	33.22	A	5.16E+05	1.82E+06	59.35	2.16	1.79	0.084	0.632	1.66E+05	0.66
3	D	3.07E+05	6.27E+05	45.18	A	4.48E+05	1.82E+06	63.74	1.46	1.41	0.083	0.149	9.33E+04	0.37
4	E	2.54E+05	1.50E+05	24.32	A	5.01E+05	1.82E+06	60.26	1.97	2.48	0.115	1.518	2.28E+05	0.91
5	F	2.05E+05	1.18E+05	23.96	A	5.50E+05	1.82E+06	57.51	2.68	2.40	0.082	1.760	2.07E+05	0.83
6	G	3.19E+05	3.85E+05	34.75	A	4.36E+05	1.82E+06	64.58	1.37	1.86	0.132	0.430	1.66E+05	0.66
7	C	3.16E+05	2.63E+05	28.86	B	4.39E+05	8.14E+05	43.08	1.39	1.49	0.097	0.181	4.76E+04	0.19
8	D	3.90E+05	6.27E+05	40.09	B	3.65E+05	8.14E+05	47.25	0.93	1.18	0.059	0.007	4.25E+03	0.02
9	E	3.33E+05	1.50E+05	21.23	B	4.22E+05	8.14E+05	43.95	1.27	2.07	0.154	0.556	8.36E+04	0.33
10	F	2.77E+05	1.18E+05	20.59	B	4.77E+05	8.14E+05	41.30	1.72	2.01	0.115	0.731	8.60E+04	0.34
11	G	4.02E+05	3.85E+05	30.94	B	3.53E+05	8.14E+05	48.04	0.88	1.55	0.141	0.072	2.78E+04	0.11
12	C	3.04E+05	2.63E+05	29.44	D	4.51E+05	6.27E+05	37.28	1.48	1.27	0.060	0.082	2.16E+04	0.09
13	E	3.95E+05	1.50E+05	19.50	C	3.60E+05	2.63E+05	27.04	0.91	1.39	0.109	0.037	5.63E+03	0.02
14	F	3.37E+05	1.18E+05	18.68	C	4.18E+05	2.63E+05	25.10	1.24	1.34	0.083	0.082	9.64E+03	0.04
15	G	4.62E+05	3.85E+05	28.85	C	2.92E+05	2.63E+05	30.01	0.63	1.04	0.017	-0.005	-1.89E+03	-
16	E	3.21E+05	1.50E+05	21.64	D	4.34E+05	6.27E+05	38.00	1.35	1.76	0.125	0.345	5.18E+04	0.21
17	F	2.66E+05	1.18E+05	21.04	D	4.89E+05	6.27E+05	35.80	1.84	1.70	0.093	0.454	5.34E+04	0.21
18	G	3.89E+05	3.85E+05	31.44	D	3.65E+05	6.27E+05	41.42	0.94	1.32	0.093	0.028	1.07E+04	0.04
19	E	4.35E+05	1.50E+05	18.58	F	3.20E+05	1.18E+05	19.18	0.73	1.03	0.013	-0.003	-4.30E+02	-
20	E	3.09E+05	1.50E+05	22.04	G	4.46E+05	3.85E+05	29.39	1.44	1.33	0.073	0.107	1.61E+04	0.06
21	F	2.55E+05	1.18E+05	21.48	G	5.00E+05	3.85E+05	27.75	1.96	1.29	0.051	0.143	1.68E+04	0.07

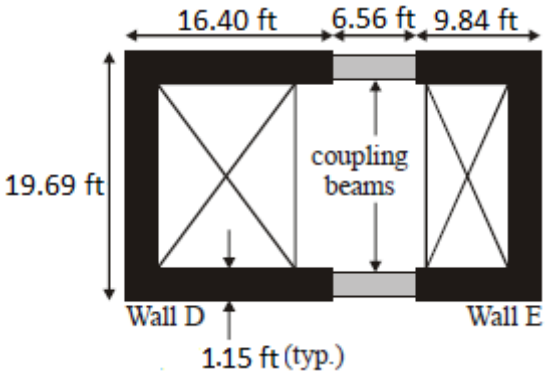

Figure 3-1 Example of prototype CCW Plan: Case 16: coupled Walls D and E

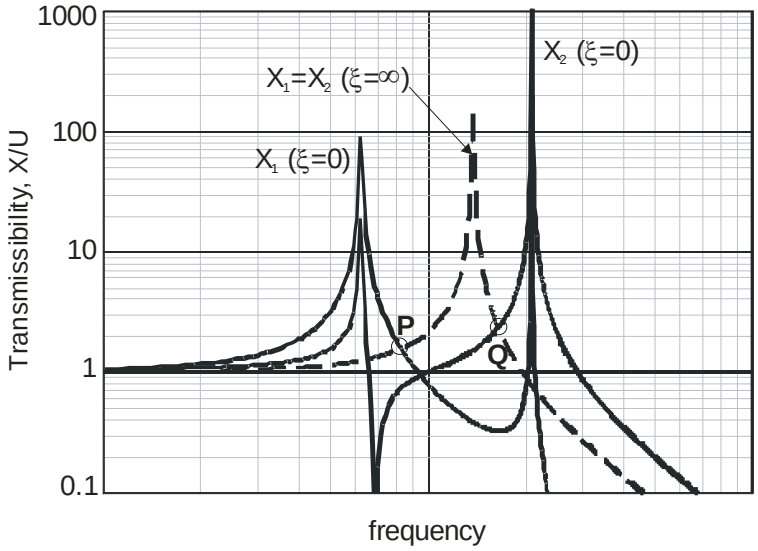

Figure 3-2 Schematic representation of transmissibility (Hull 2006)

4.0 PERFORMANCE BASED DESIGN OF 12-STOREY COUPLED CORE WALL STRUCTURE

The prototype structure considered in this study is a twelve- storey residential structure located in Seattle WA. The structural design includes only the design of the reinforced concrete core wall lateral force resisting system (LFRS) of the building; no other structural components such as slabs, columns, beams, and foundation will be designed. A coupled core wall (CCW) system is provided in the east-west direction to resist 100% of the lateral loads applied to the structure. In the north-south direction, the LFRS consists of two components: the north-south oriented webs of the CCW and two outrigger cantilever shear walls located near the perimeter of the building, as shown in Figure 4-1. The building plan area is 15600 ft^2 with outside dimensions of 129.3 by 120.6 ft. The floor-to-floor height is 11.81 ft for all stories, resulting in an overall building height of 141.7 ft. A 6 in. thick flat plate floor slab is assumed for all floors. A plan of the entire building is shown in Figure 4-1 and an elevation view of the CCW is shown in Figure 4-2. It is acknowledged that the building is an idealization, however its fundamental dimensions, mass and structure are consistent with simple residential and office structures located in the United States. Similar prototypes, designed by practicing engineers, have been used in previous studies (Harries et al. 2004 and 2005).

4.1 DEVELOPMENT OF THE INITIAL CCW GEOMETRY

This study focuses on CCWs having markedly different pier dimensions. The preferred behavior in this case is to have the two wall piers interacting to reduce lateral displacement, transmissibility, damage, and provide sufficient energy dissipation capacity to the system. The geometry of the CCW structure is therefore developed based on this desired behavior of the system.

The process of developing the wall geometry is expected to be iterative, and therefore a parametric study was performed to develop a CCW system that meets the desired performance characteristics. The calculation of the CCW dimensions is based on criteria that ensure a significant interaction between the wall piers while still maintaining a structural geometry that may be considered practical. The following initial criteria were selected to begin the iterative development of the east-west CCW geometry:

1. The natural frequency ratio, γ, between the wall piers is greater than 2.5; this criterion is intended to ensure significant interaction between piers (see Section 3.3).
2. The roof drift at the design load level is less than 1%; this criterion is typical of CCW structures and ensures that the structure has an appropriate overall stiffness.
3. The degree of coupling, doc, is in the range of 0.50; this value is recommended as a reasonable target value for an initial elastic design (El-Tawil et al. 2009).
4. The seismic weight of each floor, w_i = 2248 kips; this is based on the structural geometry described above.

The total moment of inertia of the east-west CCW system is the sum of the contributing moments of inertia from the two wall piers and that resulting from the frame action of the coupling beams:

$$I_{total} = I_1 + I_2 + I_{frameaction} \qquad \text{(Eq. 4-1)}$$

In order to determine an initial estimate of the target moment of inertia of the CCW, the CCW is considered as a cantilever beam subjected to an inverted triangular load. The free end elastic deflection (roof drift) for this condition is given as:

$$\delta = \frac{11 W l^3}{60 E I_{total}} \qquad \text{(Eq. 4-2)}$$

Where δ represents the roof deflection, W is the total lateral load, *l* is the CCW height, and E is the modulus of elasticity of concrete. For the given building height (141.7 ft) and assumed roof drift limit (1%), the target roof deflection is 17 in. From the ASCE 7-10 equivalent lateral force (ELF) method analysis (see Section 4.3.1), the base shear, V, for the prototype structure having a weight of w_i = 2248 kips per floor is found to be 0.063W = $0.063\Sigma w_i$ = 1691 kips. The 28 day compressive strength of concrete is assumed to be 5.4 ksi resulting in a modulus of elasticity of 4134 ksi. Therefore, from Equation 4-2, the target moment of inertia, I_{total} = 1046 ft^4.

The sum of the moments of inertia for the two wall piers is related to the total moment of inertia through the degree of coupling:

$$\sum I_{walls} = (1 - doc) I_{total} \qquad \text{(Eq. 4-3)}$$

Using doc = 0.50, the sum of the walls moment of inertia is found to be 523 ft^4. Frequency is a function of stiffness squared, therefore the ratio of wall pier moments of inertia may be found by equating to γ^2:

$$\frac{I_2}{I_1} = \gamma^2 \qquad \text{(Eq 4-4)}$$

Assuming value of γ = 3.2 the wall piers' moments of inertia are estimated as I_1 = 46.54 ft^4 and I_2 = 476.57 ft^4 (as discussed in Chapter 3, Wall 1 is arbitrarily selected as being the more flexible wall). Through experience gained in this study, it was found that the initial

estimate of γ using this simplified approach must exceed the target value by about 30% in order for the target value to be achieved.

Having established the wall piers' moments of inertia, the initial dimensions can be estimated. The initial arrangement of the CCW system is shown in Figure 4-3. The interior width of the system, b_w = 13.12 ft, and the wall thickness, t = 1.15 ft. The coupling beam length, b = 8.20 ft. With these values, the wall pier lengths, h_{w1} and h_{w2}, are estimated by an iterative process using the Goal Seek Function in Microsoft Excel. The initially selected dimensions of the CCW system are shown in Figure 4-3.

To ensure that the selected wall piers have a frequency ratio greater than 2.5, the eigenvector method (Seto et al. 1987; see Section 3.1), utilizing the effective modal mass concept, is used to calculate natural vibration frequencies of the 2 SDOF systems representing the cantilever wall piers. The parameters describing the wall piers are given in Table 4-1 and the dynamic properties of the initial wall pier design (Figure 4-3) are given in Table 4-2. Note that the initial assumed frequency ratio γ is 3.2, while the calculated ratio based on the equivalent properties of the wall piers is 2.58.

4.2 LOADS APPLIED TO PROTOTYPE STRUCTURE

4.2.1 Dead Loads

The dead loads applied on the structure were determined according to the provisions of Chapter 3 of ASCE 7-10. A 6 in. reinforced concrete flat slab having a specific weight of 150 lb/ft^3 was assumed, resulting in a uniformly distributed areal load of 75 psf for all stories. Additional concrete (walls and columns) self-weight is equivalent to a uniform areal load of 40 psf. In addition to the self-weight of the concrete elements, a superimposed dead load

equal to 31 psf was added to account for cladding (6 psf equivalent areal load) partitions (10 psf), finishes (10 psf) and mechanical (5 psf) loads. An additional dead load of 50 psf was applied over the roof to area above the core to account for elevator machinery loads.

4.2.2 Live Loads

The live loads were determined according to Chapter 4 of ASCE 7-10. The building is assumed to be residential occupancy and therefore a 40 psf live load for a multifamily residential structure was used. A 100 psf live load was assumed for corridors around CCW and a roof live load of 20 psf was used over the entire roof level.

4.2.3 Seismic Loads

The seismic loads for the building structure in this study were determined according to the provisions of Chapters 11 and 12 of ASCE 7-10. The site class for the building location is assumed to be Site Class C. The design, 5% damped spectral response acceleration parameters for the Seattle site for short (0.2 sec.) and 1 second periods are S_{DS} = 1.00g and S_{D1} = 0.433g, respectively, where g is the acceleration of gravity. According to the building occupancy, the structure falls in Seismic Use Group I, and based on the spectral response parameters, the structure belongs to Seismic Design Category D (SDC D).

4.3 ELASTIC ANALYSIS OF THE STRUCTURE

Initial structural analysis was conducting using a two-step process. The Equivalent Lateral Force Method (ELF) prescribed by ASCE 7-10 was implemented to determine the code-

prescribed base shear. The base shear is distributed linearly in an inverted triangular pattern along the height of the structure and the closed-form equations of the Continuous Medium Method (CMM, see Section 2.5.1) were utilized to determine the coupling beam and wall pier demands. The CCW structure was analyzed in only the east-west direction; torsional effects were eliminated by ensuring that the shear center of the LFRS system coincides with the center of mass of the structure. Following design of the CCW in the east-west direction, the north south cantilever wall behavior is verified as will be described subsequently.

4.3.1 Equivalent Lateral Force Procedure

For structures similar to the prototype structure in this study, ASCE 7-10 permits the use of the equivalent lateral force (ELF) procedure. The response modification coefficient is obtained from ASCE 7-10 Table 12.2.1 as R = 6, the importance factor, I_E = 1.00 (ASCE 7-10 Table 1.5-2). The long-period transition period for the building site is obtained from ASCE 7-10 Figure 22-12 as T_L = 6 sec. The approximate fundamental period of the building T_a is calculated using Equation 4-5 and is found to be equal to 0.82 sec.

$$T_a = C_t h_n^x = 0.02\,x\,141.7^{0.75} = 0.82\,\text{sec}. \qquad \text{(Eq. 4-5)}$$

Where h_n is the height of the structure and the coefficients C_t = 0.02 and x = 0.75 are found in ASCE 7-10 Table 12.8-2. The fundamental period of vibration of the structure is determined by multiplying the approximated period, T_a, by the coefficient C_u = 1.4 determined from ASCE 7-10 Table 12.8-1. Thus T = 1.15 sec. From this value, the seismic response coefficient, C_s is calculated using Equation 4-6 and is found to be equal to 0.0627.

$$C_s = \frac{S_{DS}\,I_E}{R} \le \frac{S_{D1}\,I_E}{T\,R} \rightarrow C_s = \frac{1.00\,x\,1.00}{6} \le \frac{0.433\,x\,1.00}{1.15\,x\,6} \rightarrow C_s = 0.0627 \qquad \text{(Eq. 4-6)}$$

Finally, the seismic base shear, V, is calculated as:

$$V = C_s W = C_s \sum w_i \rightarrow V = 0.0627\ x\ 12\ x\ 2248 = 1691\ kips \quad \text{(Eq. 4-7)}$$

Where W = Σw_i = 26976 kips is the seismic weight of the structure (ASCE 7-10 12.7.2). The seismic base shear, V = 1691 kips, is distributed vertically over the height of the structure based on the requirements of ASCE 7-10 12.8.3:

$$F_x = \frac{w_x h_x^k}{\sum_{i=1}^{n} w_i h_i^k} \quad \text{(Eq. 4-8)}$$

Where w_x is the seismic weight at storey x and h_x is the height of storey x above the base of the building. The parameter k is a function of the fundamental period and is taken as k = 1.325 in this case. The resulting ELF distribution of forces is given in Table 4-4 and shown in Figure 4-4.

4.3.2 Continuous Medium Method Analysis

The Continuous Medium Method (CMM) analysis is an elastic analysis of a simplified two-dimensional cantilevered coupled wall structure subject to lateral loads (Stafford-Smith and Coull 1991). The main advantage of the CMM is that it results in closed-form solutions for internal forces and deformation demands allowing for rapid evaluation of design parameters and even parametric study of the selection of design variables (e.g.: Harries et al. 2004).

Closed-form equations are available for uniformly distributed loading, concentrated load at the top of the building, and linearly varying inverted triangular loading. Solutions can be derived for other continuous-function load cases although these are generally not required for initial elastic analysis-based design: the uniform load case is suited to represent wind loading, while the inverted triangle is appropriate for seismic loading. Some seismic codes (e.g.: NBCC 1990) add a concentrated load at the top to the triangle loading case to account

for the higher mode effects. In this study only the triangular load is considered (Figure 4-5); this is deemed to closely match the ELF-prescribed vertical load distribution (Figure 4-4). Detailed derivations of the closed-form equations used are provided in Stafford-Smith and Coull (1991); critical parameters are described below.

Four parameters describe the behavior of a CCW: the total height of the wall, H, the degree of coupling, doc, defined in Equation 2-1, and parameters α and k, defined in Equations 4.9 and 4.10, respectively. In these calculations, the coupling beams are assumed to have a rectangular section with dimensions of 1.64 ft deep and 1.15 ft wide. The geometric and material properties of the CCW used in the CMM are shown in Table 4-5. The CMM calculations are based on service level doc, which means that all mechanical property reduction factors (i.e.: cracked section properties) for both the coupling beams and wall piers are close to unity. However, since the coupling beams are expected to deteriorate faster than the wall piers and the doc falls with increasing loads (Harries 2001), different reduction factors were applied to the moments of inertia of the coupling beams ($I_b = 0.70I_{bg}$) and wall piers ($I_w = 0.95I_{wg}$) to account for concrete cracking at service load levels. The axial rigidity of the beams and walls were not reduced (i.e.: $A_b = A_{bg}$ and $A_w = A_{wg}$).

$$\alpha = \sqrt{\frac{12 I_c L_w^{\,2}}{L_b^{\,3} h I}} \qquad \text{(Eq. 4-9)}$$

$$k = \sqrt{1 + \frac{AI}{A_1 A_2 L_w^{\,2}}} \qquad \text{(Eq. 4-10)}$$

Where

I = sum of the moments of inertia of the individual wall piers ($I = I_1 + I_2$)

= 0.95 (47.5 + 484.3) = 505.16 ft^4

A = sum of the areas of the individual wall piers ($A = A_1 + A_2$)

= 26.37 + 40.31 = 66.68 ft^2

L_w = distance between wall centroids

= 19.08 ft

L_b = length of coupling beam

= 8.20 ft

h = storey height

= 11.81 ft

I_c = the effective moment of inertia of the coupling beam accounting for shear deformations:

$$I_c = \frac{I_b}{1 + \left(\frac{12 E I_b}{L_b^{\,2} G A_b} \lambda \right)} \qquad \text{(Eq. 4-11)}$$

Where

I_b = gross moment of inertia of the coupling beam

= 2 x 0.7 x 1.15 x 1.643^3 / 12 = 0.59 ft^4

A_b = gross area of the coupling beam

= 2 x 1.15 x 1.64 = 3.77 ft^2

The factor 2 in each of the previous calculations accounts for the presence of two coupling beams at each storey level.

E = Young's modulus of the coupling beam

= 4134 ksi

G = Shear modulus of the coupling beam

= 1722 ksi

λ = cross-sectional shape correction coefficient for shear

= 1.2 for thin, vertically oriented rectangular sections.

The term in the parentheses in Equation 4-11 represents the effect of the shear deformation on the calculated flexural deformations over the short span coupling beams.

The parameter α is a measure of the relative flexibility of the coupling beams and wall piers. A higher value of α indicates a stiff coupled system where the coupling beams contribute a greater proportion to the overall stiffness and strength of the CCW through frame action. On the other hand, a low value of α results in a relatively flexible CCW system in which the overall behavior of the system is dominated by the behavior of the individual wall piers (Harries 2004).

The parameter k is a measure of the relative flexural to axial stiffness of the wall piers. For axially rigid wall piers k = 1, which represents the lower bound of k. The upper bound of this parameter is about k = 1.2. From both structural and architectural points of view, practical coupled walls typically have k values less than 1.1.

From Equations 4.9 and 4.10 the parameters are calculated as α = 0.027 ft^{-1} and k = 1.043. The product of these parameters $k\alpha H$ = 3.99 is interpreted as a measure of the stiffness of the coupling beams, and is most sensitive to changes in either the stiffness or length of the coupling beam (which are, of course, related). This parameter is used to calculate the degree of coupling (doc), axial load in the wall piers (N), shear flow in the coupling beams (q) and the lateral deflection (y_H) as shown in Equations 4-12 to 4-15, respectively (doc: Harries et al. 2004; N, q and y_H: Stafford-Smith and Coull 1991).

$$doc = \frac{3}{k^2(k\alpha H)^2}\left[\frac{(k\alpha H)^2}{3} - \cosh(k\alpha H) + \frac{\sinh(k\alpha H) - k\alpha H/2 + 1/k\alpha H}{\cosh(k\alpha H)}\sinh(k\alpha H)\right] \qquad \text{(Eq. 4-12)}$$

$$N = \frac{pH^2}{k^2 L} F_1(z/H, k\alpha H) \qquad \text{(Eq. 4-13)}$$

$$q = \frac{pH}{k^2 L} F_2(z/H, k\alpha H) \qquad \text{(Eq. 4-14)}$$

$$y_H = \frac{11}{120} \frac{pH^4}{EI} F_3(k\alpha H) \qquad \text{(Eq. 4-15)}$$

Where:

$$F_1 = \frac{\sinh k\alpha H - (k\alpha H/2) + (1/k\alpha H)}{(k\alpha H)^2 \cosh k\alpha H} \sinh k\alpha(H-z) - \frac{1}{(k\alpha H)^2} \cosh k\alpha(H-z) + \frac{1}{2}\left(1-\frac{z}{H}\right)^2 - \frac{1}{6}\left(1-\frac{z}{H}\right)^3 + \frac{1}{(k\alpha H)^2}\left(\frac{z}{H}\right) \qquad \text{(Eq. 4-16)}$$

$$F_2 = \frac{\sinh k\alpha H - (k\alpha H/2) + (1/k\alpha H)}{(k\alpha H)\cosh k\alpha H} \cosh k\alpha(H-z) - \frac{1}{(k\alpha H)} \sinh k\alpha(H-z) + \left(1-\frac{z}{H}\right) - \frac{1}{2}\left(1-\frac{z}{H}\right)^2 + \frac{1}{(k\alpha H)^2} \qquad \text{(Eq. 4-17)}$$

$$F_3 = 1 - \frac{1}{k^2} + \frac{120}{11} \frac{1}{k^2 (k\alpha H)^2} \left[\frac{1}{3} - \frac{1 + \{(k\alpha H/2) - (1/k\alpha H)\} \sinh k\alpha H}{(k\alpha H)^2 \cosh k\alpha H} \right] \qquad \text{(Eq. 4-18)}$$

The lateral load, p, is determined by distributing the base shear, V, obtained from the ELF analysis in an inverted triangular pattern as shown in Figure 4-5. The value of p at the top of the wall is calculated as: p = V / (0.5 x H) = 1691 / (0.5 x 141.73) = 23.9 kips/ft. A summary of the wall pier parameters and calculated values for the CMM analysis is given in Table 4-5.

From Equation 4-12, the doc for this structure is found to be 0.61. The calculated values of N, q and y are continuous; these are integrated over the storey heights tributary to

each storey and are reported at the discrete storey levels in Table 4-6 and shown in Figures 4-6a through 4-8a, respectively.

The calculated base overturning moment, M = 159,780 kipft, is shown in Table 4-6 and Figure 4-9a. The frame action component of the overturning resistance is determined by multiplying the axial force in the wall piers resulting from the accumulation of beam shear, N (see Section 2.1), by the lever arm between the tension-compression couple, L_w. The moment resisted by frame action is therefore NL_w = 97,591 kip-ft. The remaining moment is resisted by the individual wall piers, M_w in proportion to their flexural stiffness:

$$M_i = \left(\frac{I_i}{I_1 + I_2} \right) \left(M - NL_w \right) \qquad \text{(Eq. 4-19)}$$

The wall pier base moments are calculated as M_1 = 5555 kipft and M_2 = 56635 kipft. Figure 4-9a shows the moment contribution of each component of the CCW system to the total overturning moment (OTM) along the height of the building.

The calculated elastic roof displacement (Equation 4-15) is 0.646 ft which is equivalent to a roof drift of 0.46%. The CMM analysis of the initial prototype design confirms the design falls within the desired performance parameters and establishes elastic design values for the coupling beams and wall piers from which the design process may progress as described in the following sections.

4.4 CCW DESIGN

As will be shown in the following sections, the design process is iterative and will require additional analyses to update design values.

4.4.1 Initial Design of Coupling Beams

The desired behavior for the coupling beams in a CCW system is to yield essentially simultaneously at the code-prescribed base shear (El-Tawil et al. 2009). To achieve this objective, the coupling beams should optimally be designed to meet the shear demand distribution shown in Figure 4-7a. Typically for a CCW, the most highly stressed coupling beams are located at approximately one third of the height of the structure. The critical coupling beams for the initial prototype twelve-storey building carry 279 kips and are located at the 6^{th} floor.

For the prototype structure, design of the coupling beams using conventional reinforced concrete coupling beams would result in impractical beams with an impractically large amount of reinforcing steel (Harries et al. 2005). As a point of reference, if the coupling beams were designed to carry the maximum ACI 318-11-permitted shear stress of $10\sqrt{f'_c}$ (which is generally not feasible), their dimensions would be on the order of 24 in. deep. Diagonally reinforced coupling beams in this case are also ineffective due to the small angle of inclination resulting from the relatively long beams (Harries et al. 2005). Thus, flexure-critical steel coupling beams are used for the prototype structure (Harries et al. 1992, 1997; El-Tawil et al. 2009). Because the coupling beams are relatively long, they were designed using rolled W-sections in order to simplify the construction process.

One of the primary objectives of this research is to investigate the effects of varying the coupling beam capacity, specifically reducing the beam capacity in order to more efficiently utilize the inherent reserve capacity of the wall piers. Therefore, five different scenarios for the coupling beams are investigated: the beams are designed to resist 100%, 90%, 80%, 70%, and 60% of their shear demand calculated from the CMM analysis (Figure 4-7). Thus five prototype structures will result, each having the same wall details but different

beam details. For reasons of uniformity and constructability, the rolled sections selected for the beams of each individual structure are selected from the same group. W14 sections are used for the 100% and 90% structures, while W12 sections are used for the 80%, 70%, and 60%. Detailed calculations for the design of the steel coupling beams are provided in Appendix A. For the 100% structure, the maximum shear demand in the coupling beams V_u = 279 kips which leads to moment demand, $M_u = V_u b/2$ = 1144 kip-ft. The resulting rolled section selected is a W14x176 and will be used for the beams at the fourth, fifth and sixth storeys.

4.4.2 Revised Wall Dimensions

The W14x176 rolled section has a flange width of 1.31 ft which is greater than the wall thickness, 1.15 ft. There are no suitable rolled sections having sufficiently thin flange widths to be embedded in the wall toes. Nor is it felt practical to design a built up section with a sufficiently narrow flange. Additionally, as the wall reinforcement is detailed (see Section 4.4.3) it becomes apparent that planar walls cannot accommodate both the large amounts of reinforcement and the embedded steel section, regardless of its width. For these reasons, the wall thickness is increased throughout the height of the building for a distance equal to the required development length of the steel coupling beams by the provision of a 'barbell'. The resulting revised wall dimensions are shown in Figure 4-10. The addition of the barbells results in a significant change to the geometric properties of the wall piers necessitating a revised CMM analysis to update design loads. The gross section area increased 40% and 26% for walls 1 and 2, respectively. Similarly, the gross section moments of the inertia increased 78% and 59% for walls 1 and 2, respectively. These non-proportional changes not only result in a stiffer wall pier system but also different relative and overall dynamic properties.

As a result the analyses described previously are repeated. Tables 4-1 and 4-3 summarize the eigenvector analyses for the revised structure. Tables 4-5 and 4-7 summarize the CMM results for the revised structure having barbells added shown in Figure 4-10. Tables 4-3 and 4-7 effectively update Tables 4-2 and 4-6 for the revised structure. Design values from the CMM analyses of the revised structure are shown in Figures 4-6b through 4-9b. The beam and wall design will progress using the revised values after adding the barbells.

The shear demand, final coupling beam selection and beam identification for the final 100% structure are shown in Table 4-8. Table 4-9 shows the final coupling beam selections for all prototype structures.

4.4.3 Design of Wall Piers

The 12-storey prototype structure is designed in accordance with Chapter 21 of ACI 318-11. The coupling beam embedments into the wall piers were designed in accordance with the recommendations of El-Tawil et al. (2009). The wall piers are assumed to resist the entire seismic load in the direction of coupling (east-west direction). In the north-south direction (cantilever piers) the piers are designed to resist lateral forces in proportion to their flexural rigidity. Two additional outrigger cantilever walls (Figure 4-1) are provided near the perimeter of the building in the north-south direction to provide sufficient additional capacity to ensure that the design of the CCW is controlled by the east-west coupling direction (the focus of this work). The design overturning moments in each wall pier are provided in Table 4-10.

The wall piers are designed for the demand generated in the 100% structure. The overstrength factors (El-Tawil et al. 2009) were taken as unity for all structures. Each pier was divided into five sections along the height of the building as shown in Figure 4-12. Detail #1 for both walls denotes the expected plastic hinge region and extends over storeys 1 and 2;

detail #2 includes storeys 3 and 4, detail #3 includes storeys 5, 6 and 7, detail #4 includes storeys 8-10, and detail #5 includes storeys 11-12. Due to the large wall moment demands the 28 day concrete compressive strength used for design is 6.5 ksi and the yield strength of the shear and flexural reinforcing steel is selected to be 75 ksi. The higher grade steel will help to mitigate reinforcing bar congestion in the design.

Two axial load combinations, corresponding to the seismic load cases of ASCE 7-10 Section 2.5.1, were considered for the design of each wall pier:

Compression wall: $$P = 1.2D + 0.5L + 0.2S_{DS}D + \sum V_n \quad \text{(Eq. 4-20)}$$

Tension wall: $$P = 0.9D - 0.2S_{DS}D - \sum V_n \quad \text{(Eq. 4-21)}$$

Where D and L represent the dead load and live load components of the wall gravity loads, respectively. These loads were calculated based on the loaded tributary areas of the wall piers and their self-weight. The term $\sum V_n$ is the axial force resulting from the frame action of the CCW determined as the summation of the coupling beam demand above the point of interest. The term $0.2S_{DS}D$ accounts for the vertical component of ground motion (ASCE 7-10 12.4.2.2). Compression is taken as positive in all cases.

The design of the wall piers was carried out using a customized MathCAD worksheet, examples from the design are provided in Appendix B. The walls were first designed for their east-west moments (Table 4-10). The provision of additional capacity from the outrigger walls meant that the east-west capacity could control the design of the CCW and no additional steel was required to carry north-south moments. In the wall design, #9 primary reinforcing bars and #4 shear, confinement and distributed reinforcing bars were used. Additionally, the wall dimensions result in only a small region of ‘effective flange width’ wall to be engaged in each principle direction (ACI 318-11 21.9.5.2); this limits the placement of the primary ‘boundary element’ reinforcing steel, resulting in relatively

significant steel congestion in the barbells and at the outer corners of the wall piers, particularly lower in the structure. This congestion is partially mitigated by the use of 75 ksi reinforcing bars. For both wall piers, detail #5 in the upper two storeys is controlled by ACI-prescribed minimum reinforcement requirements. In these details, the primary reinforcement is reduced to #6 and #7 bars. Figures 4-13 to 4-17 show the reinforcement details for the five sections of the CCW.

At the beam-wall connection regions, penetration of the confining cross ties through the beam web is avoided – this is felt to be a complex and unnecessary detail (Harries and Shahrooz 2005). Two details – the first immediately above and below the embedded beam section and the second in the web region of the embedded beam section are shown for wall 1 and wall 2 barbells in Figure 4-18. Similar details are used throughout the structure.

4.4.3.1 Outrigger Walls

Two identical outrigger walls are provided to supplement the north-south capacity of the CCW. Without these, additional reinforcing steel is required in the CCW (or the CCW dimensions made larger) which would increase the east-west capacity and affect the objective of the study. These walls were located (see Figure 4-1) so that the resultant lateral force resisted by the CCW and outriggers is coincident with the center of mass of the floor plate; thus avoiding torsional effects. (Accidental torsion prescribed by ASCE 7-10 was intentionally neglected in this study.) Outrigger design moments are given in Table 4-10 and their design is shown in Figure 4-19.

4.5 DISCUSSION OF ELASTIC ANALYSIS OF THE PROTOTYPE STRUCTURES

The equivalent lateral force (ELF) procedure and the continuous medium method (CMM) were used to conduct elastic analyses for the prototype structures. From these analyses, the design forces and bending moments for the structural components were determined.

4.5.1 Equivalent Lateral Force Analysis

The ASCE 7-10 equivalent lateral force (ELF) procedure was used to calculate the base shear demand of the structure based on a given site characteristics (see Section 4.3.1). As described in Section 4.3.1, a base shear value of V = 1691 kips resulted from this procedure. The calculated base shear was then utilized in the continuous medium method to obtain the demands on the CCW components.

The building base shear and the associated lateral loading were determined based on a natural vibration period of T = 1.15 seconds, where the period obtained from Equation 4-5 was modified by a coefficient accounting for the upper limit of the calculated period. However, it has been shown by the subsequent frame analysis of the prototype structure that the fundamental vibration period of the building was twice that obtained from the ELF procedure (T = 2.28 seconds for the 100% structure). The short period of vibration of 1.15 seconds led to a higher base shear which consequently led to an overly designed structure. It is clear that ELF formulas are intended to be conservative, are simple to use and may give good results with respect to the natural vibration period of frame structures, but they underestimate the natural vibration period of CW structures. Refined methods of analysis are permitted by ASCE 7-10; these will inevitably result in longer structural periods and therefore reduced values of base shear. Nonetheless, ASCE 7 clause 12.9.4.1 limits the

resulting reduced base shear to 85% of that calculated using the ELF method (i.e.: $V_{design} \geq 0.85V$). Thus significant reductions through the use of more rigorous analysis are limited.

There are a number of researchers who suggested approximate formulas for the calculation of the natural fundamental period for coupled wall structures; these include Coull and Mukherjee (1973), Rutenberg (1975), Wallace and Moehle (1992), Aksogan et al. (2002), Wang and Wang (2005), Bozdogan and Öztürk (2007), and Chai and Chen (2008 and 2009). Most of the approximate equations proposed by these researchers are intended for preliminary design of CW structures and result in periods longer than would be calculated using the ASCE 7 design procedure. Permitting more realistic period calculations or increasing the C_u coefficient permitted for CW structures in ASCE 7 would result in more economical design for these structures.

4.5.2 Continuous Medium Method Analysis

The continuous medium method (CMM) provides a good approximation of the forces and displacements imparted to CCW structures. The CMM is an acceptable tool in developing preliminary layouts for the relatively uniform CCW structures (El-Tawil et al. 2009). However, the closed-form solutions become increasingly complex for more complex CCW geometries limiting the application of the approach (McNeice 2004).

As described in Section 4.3.2 the base shear obtained from the ELF (V = 1691 kips) was distributed in an inverted triangle pattern along the height of the structure. The frame action (axial couple in the wall piers) generated by the coupling beams, the shear demand in the coupling beams, and displacement of the CCW systems were determined by closed-form equations and are provided in Tables 4-6 and 4-7. Due to the large base shear demand prescribed by the ELF analysis, the wall piers had to be made larger to accommodate the necessary reinforcing steel and to satisfy both practical and ACI 318 limitations on its

placement. Barbells were provided in this case. As expected, in making the wall piers stiffer, the degree of coupling (doc) and the axial load due to coupling action at the base of the wall piers decreased. The doc decreased 21% (see Table 4-5) and the axial load at the base of the structure decreased 9.8%. Although, the axial load in the wall piers decreased in the first 6 storeys, it increased in the upper 6 storeys as shown in Figure 4-6, illustrating the complex interaction of forces occurring in a CW system.

The effect of making the wall piers stiffer is also seen in the distribution of the shear demand in the coupling beams. Figure 4-7 shows that the shear demand is decreased along the height of the structure except for the upper three storeys, and the distribution became more uniform for the final CCW design. As a result, less variation in the coupling beams design was required. The stiffer wall piers also reduced the roof displacement 19.2% as can be seen in Figure 4-8.

Table 4-1 Properties of the 2-SDOF systems

Component	Equation	Symbol	initial CCW design	final CCW design with barbells	unit
Equivalent effective mass of wall 1	Eq. 3-13	m_1 =	2.99E+05	3.17E+05	lb sec^2/ft
Equivalent effective stiffness of wall 1	Eq. 3-15	k_1 =	2.07E+04	3.68E+04	kip/ft
Natural frequency of wall 1	Eq. 3-20	ω_1 =	8.32	10.77	rad/sec
Equivalent effective mass of wall 2	Eq. 3-13	m_2 =	4.56E+05	4.37E+05	lb sec^2/ft
Equivalent effective stiffness of wall 2	Eq. 3-15	k_2 =	2.11E+05	3.36E+05	kip/ft
Natural frequency of wall 2	Eq. 3-20	ω_2 =	21.49	27.70	rad/sec
Mass ratio	Eq. 3-22	μ =	1.53	1.38	-
Frequency ratio	-	γ =	2.58	2.58	-
Damping ratio	Eq. 3-23	ζ =	0.15	0.16	-
Fixed Point stiffness ratio	Eq. 3-21	η =	1.33	1.18	-
Optimum stiffness	Eq. 2-2	k =	2.76E+04	4.34E+04	kip/ft
Total participating mass (%)	Eq. 3-14	%m =	90.05	90.05	-

Table 4-2 Natural frequencies, vibration periods and mode shapes of wall piers for the initial CCW design

Wall 1				Wall 2			
ω, rad/sec	T, sec	ϕ_1	$\phi_{1(Normalized)}$	ω, rad/sec	T, sec	ϕ_1	$\phi_{1(Normalized)}$
8.32	0.755	0.078	0.209	21.49	0.292	0.078	0.209
25.92	0.242	0.155	0.413	66.93	0.094	0.155	0.413
44.36	0.142	0.191	0.509	114.57	0.055	0.191	0.509
61.89	0.102	0.225	0.600	159.84	0.039	0.225	0.600
76.25	0.082	0.257	0.684	196.91	0.032	0.257	0.684
88.88	0.071	0.285	0.760	229.54	0.027	0.285	0.760
103.12	0.061	0.310	0.826	266.32	0.024	0.310	0.826
117.09	0.054	0.331	0.883	302.38	0.021	0.331	0.883
129.33	0.049	0.348	0.929	334.01	0.019	0.348	0.929
139.26	0.045	0.362	0.964	359.65	0.017	0.362	0.964
146.55	0.043	0.371	0.988	378.48	0.017	0.371	0.988
151.00	0.042	0.375	1.000	389.97	0.016	0.375	1.000

Table 4-3 Natural frequencies, vibration periods and mode shapes of wall piers for the final CCW design

Wall 1				Wall 2			
ω, rad/sec	T, sec	ϕ_1	$\phi_{1(Normalized)}$	ω, rad/sec	T, sec	ϕ_1	$\phi_{1(Normalized)}$
10.77	0.583	0.078	0.209	27.70	0.227	0.078	0.209
33.55	0.187	0.155	0.413	86.29	0.073	0.155	0.413
57.42	0.109	0.191	0.509	147.70	0.043	0.191	0.509
80.11	0.078	0.225	0.600	206.07	0.030	0.225	0.600
98.70	0.064	0.257	0.684	253.87	0.025	0.257	0.684
115.05	0.055	0.285	0.760	295.93	0.021	0.285	0.760
133.48	0.047	0.310	0.826	343.34	0.018	0.310	0.826
151.56	0.041	0.331	0.883	389.84	0.016	0.331	0.883
167.41	0.038	0.348	0.929	430.62	0.015	0.348	0.929
180.26	0.035	0.362	0.964	463.68	0.014	0.362	0.964
189.70	0.033	0.371	0.988	487.95	0.013	0.371	0.988
195.46	0.032	0.375	1.000	502.76	0.012	0.375	1.000

Table 4-4 Equivalent lateral force ELF method calculations

Storey	Height above grade, h_x	Storey weight, w_i	Vertical distribution factor, C_{vx}	Lateral force at storey level, F_x	Storey Shear, V	Overturning Moment, M
-	ft	kips	-	kips	kips	kip-ft
12	141.73	2,248	0.176	298	0	0
11	129.92	2,248	0.157	266	298	3524
10	118.11	2,248	0.139	234	564	10188
9	106.30	2,248	0.120	204	799	19619
8	94.49	2,248	0.103	174	1002	31457
7	82.68	2,248	0.086	146	1177	45354
6	70.87	2,248	0.070	119	1323	60976
5	59.06	2,248	0.055	93	1442	78003
4	47.24	2,248	0.041	70	1535	96135
3	35.43	2,248	0.028	47	1605	115088
2	23.62	2,248	0.016	28	1652	134602
1	11.81	2,248	0.007	11	1680	154443
Base	0.00	0	0.000	0	1691	174416
Total	-	26,977	1.0	1691	-	-

Table 4-5 Data used in CMM analysis of CCW

gross section property	initial CCW design	final CCW design with barbells
V_c	1691 kips	
p	23.86 kips	
H	141.73 ft	
h_b	1.64 ft	
w_b	1.15 ft	
L_b	8.20 ft	
L_w	19.08 ft	17.32 ft
h	11.81 ft	
E	4134 ksi	4605 ksi
G	1722 ksi	1919 ksi
ν	0.20	
λ	1.20	
I_1	47.50 ft^4	84.64 ft^4
I_2	484.30 ft^4	771.60 ft^4
A_1	26.37 ft^2	36.89 ft^2
A_2	40.31 ft^2	50.83 ft^2
A_b	3.77 ft^2	3.77 ft^2
I_b	0.59 ft^4	0.59 ft^4
I_c	0.547 ft^4	0.547 ft^4
α	0.027 ft^{-1}	0.019 ft^{-1}
k	1.043	1.062
$k\alpha H$	3.981	2.900
doc	0.611	0.505

Table 4-6 Results of initial CMM analysis

Storey	z	(z/H)	F_2	F_3	p(z/H)	q	N	Q	M	M_1	M_2	N l_w	y
	ft	-	-	-	kips	kip/ft	kips	kips	kip-ft	kip-ft	kip-ft	kip-ft	ft
12	141.73	1.00	0.182	0.331	23.86	92	0	165	0	0	0	0	0.646
11	129.92	0.92	0.187	0.331	21.87	96	336	173	1618	-428	-4362	6408	0.571
10	118.11	0.83	0.197	0.331	19.89	106	699	191	6288	-630	-6420	13337	0.511
9	106.30	0.75	0.211	0.331	17.90	119	1105	215	13731	-657	-6694	21082	0.455
8	94.49	0.67	0.224	0.331	15.91	133	1559	239	23671	-542	-5531	29744	0.397
7	82.68	0.58	0.234	0.331	13.92	144	2059	260	35830	-308	-3135	39273	0.337
6	70.87	0.50	0.238	0.331	11.93	152	2594	274	49931	40	405	49487	0.274
5	59.06	0.42	0.235	0.331	9.94	155	3149	279	65697	502	5113	60082	0.211
4	47.24	0.33	0.221	0.331	7.95	151	3702	271	82849	1092	11132	70626	0.149
3	35.43	0.25	0.193	0.331	5.97	136	4222	245	101111	1838	18734	80539	0.093
2	23.62	0.17	0.150	0.331	3.98	109	4668	197	120205	2782	28363	89060	0.046
1	11.81	0.08	0.087	0.331	1.99	66	4989	118	139854	3990	40679	95186	0.013
Base	0	0	0	0.331	0	0	5115	0	159781	5555	56635	97591	0

Table 4-7 Results of final CMM analysis

Storey	z	(z/H)	F_2	F_3	p(z/H)	q	N	Q	M	M_1	M_2	N l_w	y
	ft	-	-	-	kips	kip/ft	kips	kips	kip-ft	kip-ft	kip-ft	kip-ft	ft
12	141.73	1.00	0.182	0.331	23.86	104	0	186	0	0	0	0	0.542
11	129.92	0.92	0.187	0.331	21.87	106	376	191	1618	-483	-4407	6508	0.457
10	118.11	0.83	0.197	0.331	19.89	112	768	202	6288	-693	-6320	13301	0.396
9	106.30	0.75	0.211	0.331	17.90	120	1186	216	13731	-672	-6131	20534	0.344
8	94.49	0.67	0.224	0.331	15.91	127	1631	229	23671	-452	-4123	28247	0.295
7	82.68	0.58	0.234	0.331	13.92	133	2101	239	35830	-54	-491	36375	0.247
6	70.87	0.50	0.238	0.331	11.93	135	2585	244	49931	511	4657	44763	0.198
5	59.06	0.42	0.235	0.331	9.94	133	3071	240	65697	1238	11288	53171	0.151
4	47.24	0.33	0.221	0.331	7.95	125	3538	226	82849	2133	19444	61272	0.106
3	35.43	0.25	0.193	0.331	5.97	110	3965	198	101111	3209	29253	68650	0.065
2	23.62	0.17	0.150	0.331	3.98	85	4319	154	120205	4489	40928	74788	0.032
1	11.81	0.08	0.087	0.331	1.99	49	4565	89	139854	6010	54792	79052	0.009
Base	0	0	0	0.331	0	0	4659	0	159781	7820	71289	80672	0

Table 4-8 Coupling beams design shear demand and beam selection for 100% structure

Storey #	**z**	**Initial CCW design V_u**	**Final CCW design with barbells V_u**	**Beam Identification**	**Beam Selected**
	ft	kips	kips	-	
12	141.73	173	191	4	W14 x 120
11	129.92	173	191	4	W14 x 120
10	118.11	197	202	3	W14 x 132
9	106.30	215	229	2	W14 x 145
8	94.49	245	229	2	W14 x 145
7	82.68	260	244	1	W14 x 159
6	70.87	279	244	1	W14 x 159
5	59.06	279	244	1	W14 x 159
4	47.24	279	229	2	W14 x 145
3	35.43	245	202	3	W14 x 132
2	23.62	197	191	4	W14 x 120
1	11.81	118	89	5	W14 x 61

Table 4-9 Final design of steel coupling beams for all prototype structures

Storey	Structure				
	100%	90%	80%	70%	60%
12	W14 x 120	W14 x 109	W12 x 120	W12x 96	W12 x 87
11	W14 x 120	W14 x 109	W12 x 120	W12x 96	W12 x 87
10	W14 x 132	W14 x 120	W12 x 120	W12 x 106	W12x 96
9	W14 x 145	W14 x 132	W12 x 136	W12 x 120	W12 x 106
8	W14 x 145	W14 x 132	W12 x 136	W12 x 120	W12 x 106
7	W14 x 159	W14 x 145	W12 x 136	W12 x 120	W12 x 106
6	W14 x 159	W14 x 145	W12 x 136	W12 x 120	W12 x 106
5	W14 x 159	W14 x 145	W12 x 136	W12 x 120	W12 x 106
4	W14 x 145	W14 x 132	W12 x 136	W12 x 120	W12 x 106
3	W14 x 132	W14 x 120	W12 x 120	W12 x 106	W12x 96
2	W14 x 120	W14 x 109	W12x 96	W12 x 79	W12 x 72
1	W14 x 61	W14 x 61	W12 x 58	W12 x 50	W12 x 45

Table 4-10 Design moments for wall piers along the height of the structure

Storey	east-west coupled direction			north-south cantilever direction			
	OTM	M_1	M_2	OTM	M_1	M_2	2 x $M_{outrigger}$
	kip-ft	kip-ft	kip-ft	kip-ft	kip-ft	kip-ft	kip-ft
12	6,288	693	6,320	6,288	2,127	3,291	870
11	6,288	693	6,320	6,288	2,127	3,291	870
10	35,830	672	6,131	35,830	12,367	18,593	4,870
9	35,830	762	6,131	35,830	12,367	18,593	4,870
8	35,830	672	6,131	35,830	12,367	18,593	4,870
7	82,849	2,133	19,444	82,849	28,840	42,878	11,131
6	82,849	2,133	19,444	82,849	28,840	42,878	11,131
5	82,849	2,133	19,444	82,849	28,840	42,878	11,131
4	120,205	4,489	40,928	120,205	41,918	62,677	15,610
3	120,205	4,489	40,928	120,205	41,918	62,677	15,610
2	159,781	7,820	71,289	159,781	54,426	85,405	19,949
1	159,781	7,820	71,289	159,781	54,426	85,405	19,949

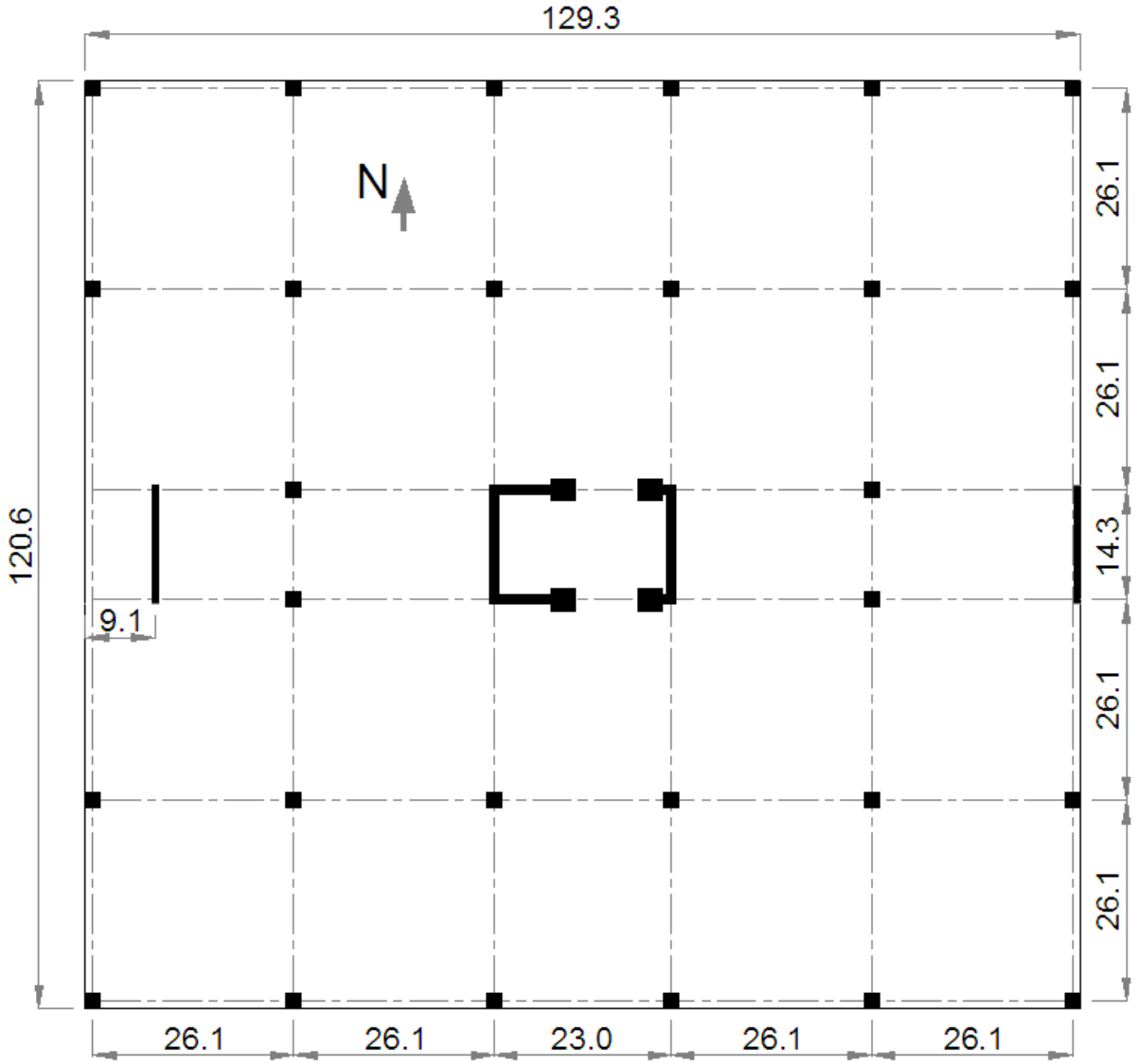

Figure 4-1 Layout plan of the 12-storey building, dimensions are in feet.

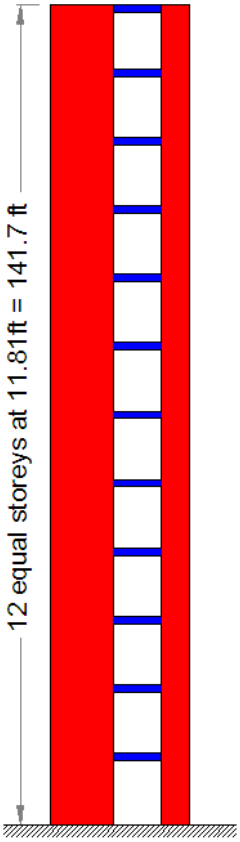

Figure 4-2 An elevation view of the 12-storey CCW in EW coupling direction

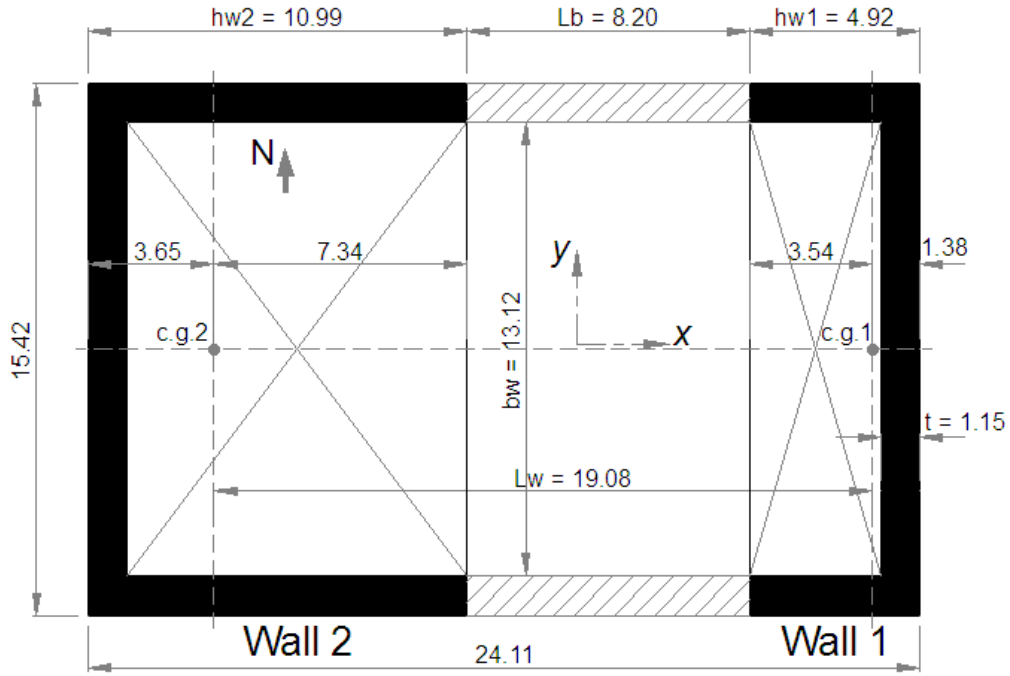

Figure 4-3 Arrangement of the CCW system, dimensions are in feet

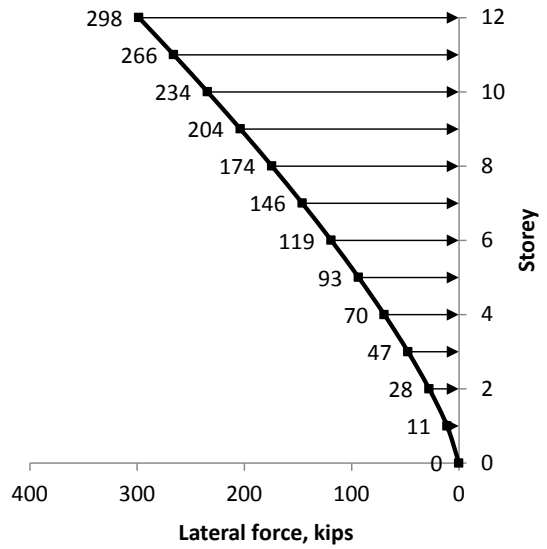

Figure 4-4 Force distribution from ASCE 7-10 ELF analysis

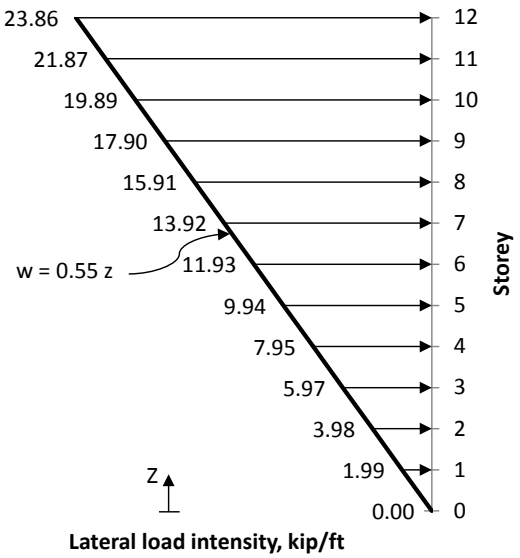

Figure 4-5 Inverted triangular load distribution used in CMM analysis

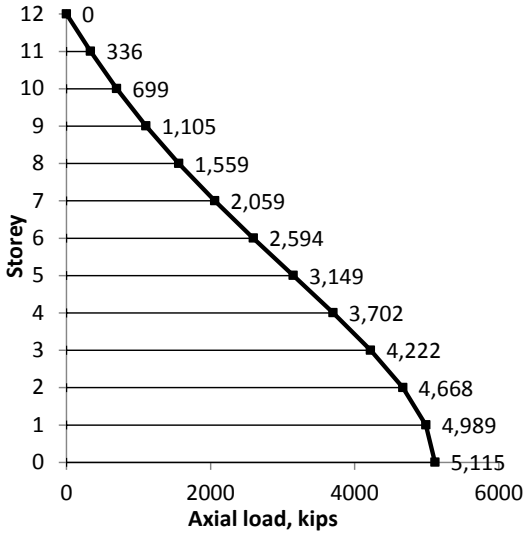

a) Initial CCW design

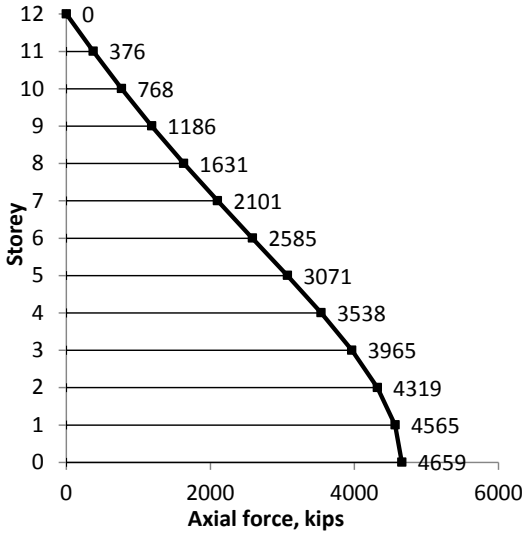

b) Final CCW design

Figure 4-6 Axial load in the wall piers along the height of the structure due to coupling action only

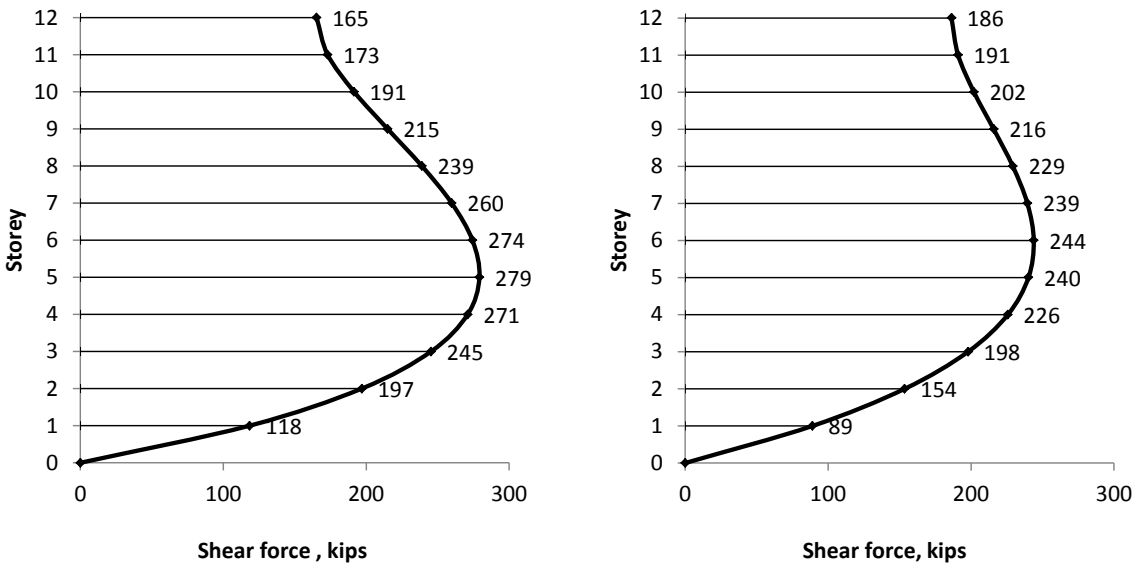

a) Initial CCW design b) Final CCW design

Figure 4-7 Shear demand in a single coupling beam

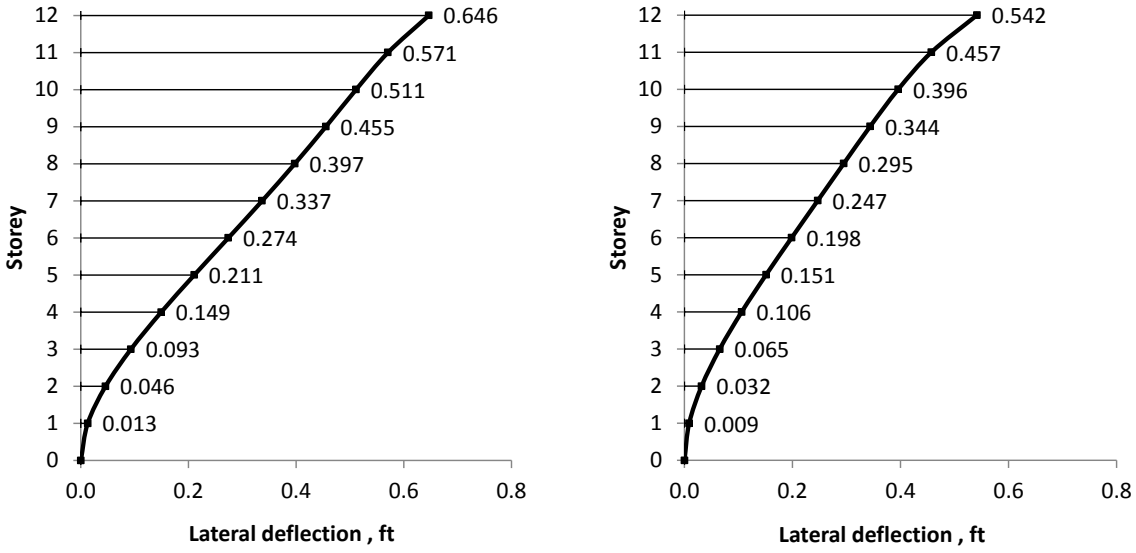

a) Initial CCW design b) Final CCW design

Figure 4-8 Lateral deflection along the height of the structure

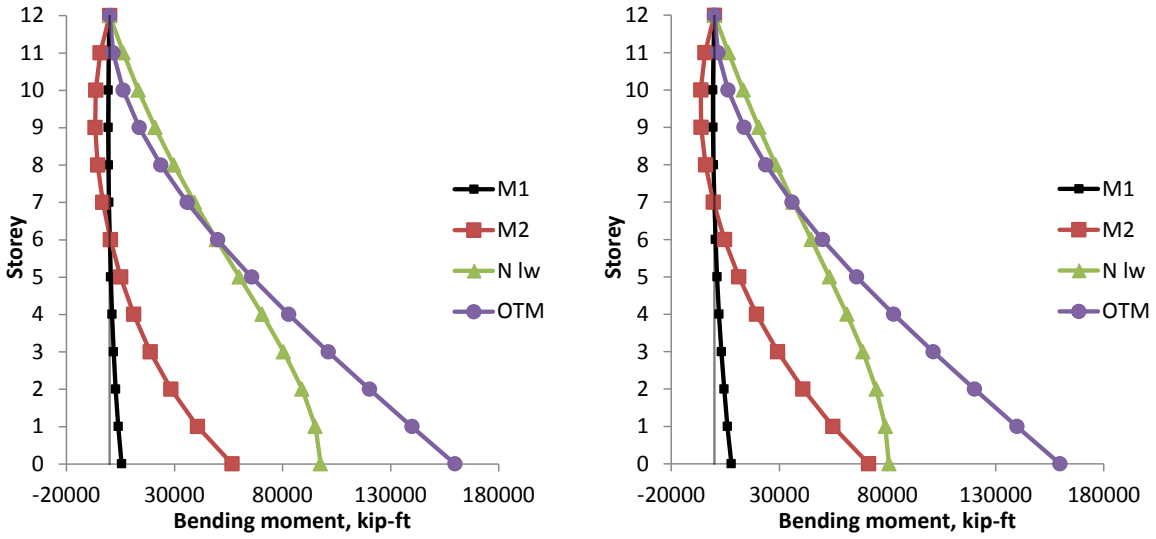

a) Initial CCW design

b) Final CCW design

Figure 4-9 CCW overturning moments

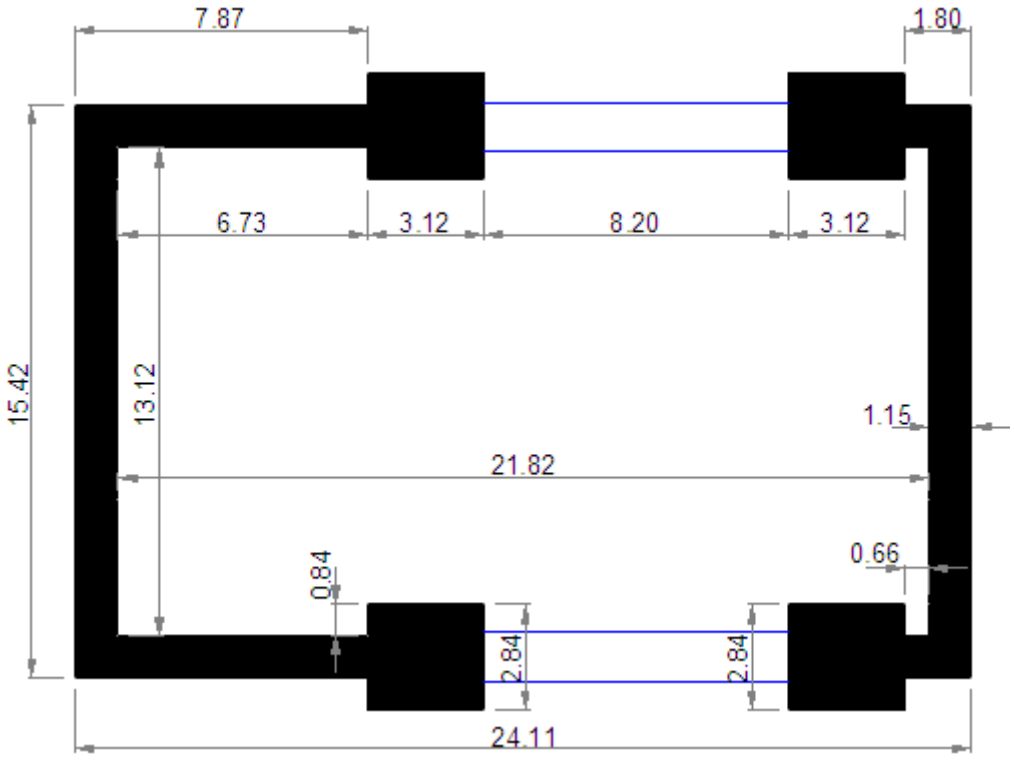

Figure 4-10 Plan of the CCW system after adding the barbells, dimensions are in feet

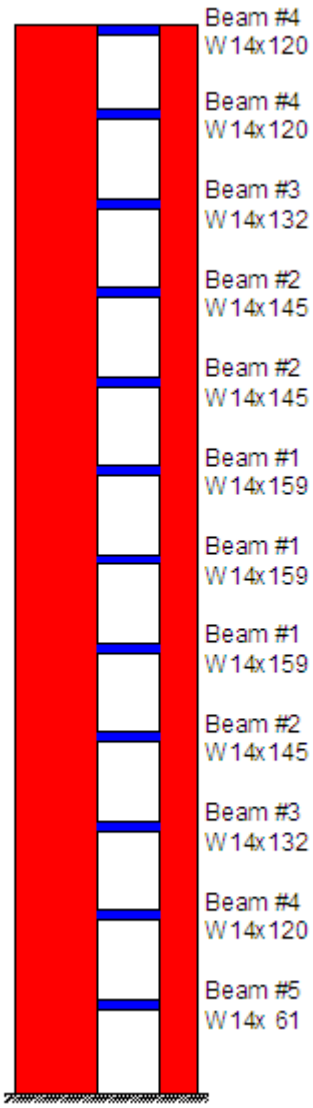

Figure 4-11 Distribution of coupling beams along the height for 100% structure

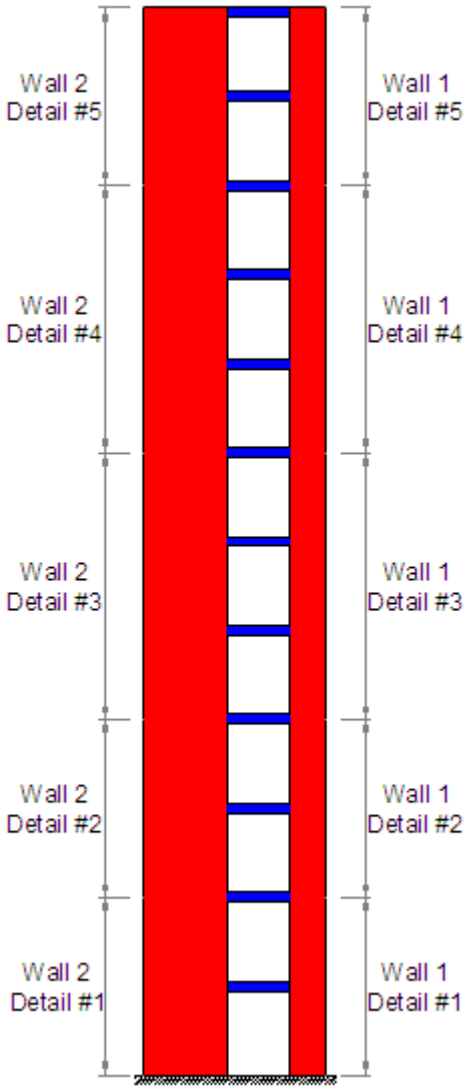

Figure 4-12 Distribution of the wall pier sections along the height for all structures

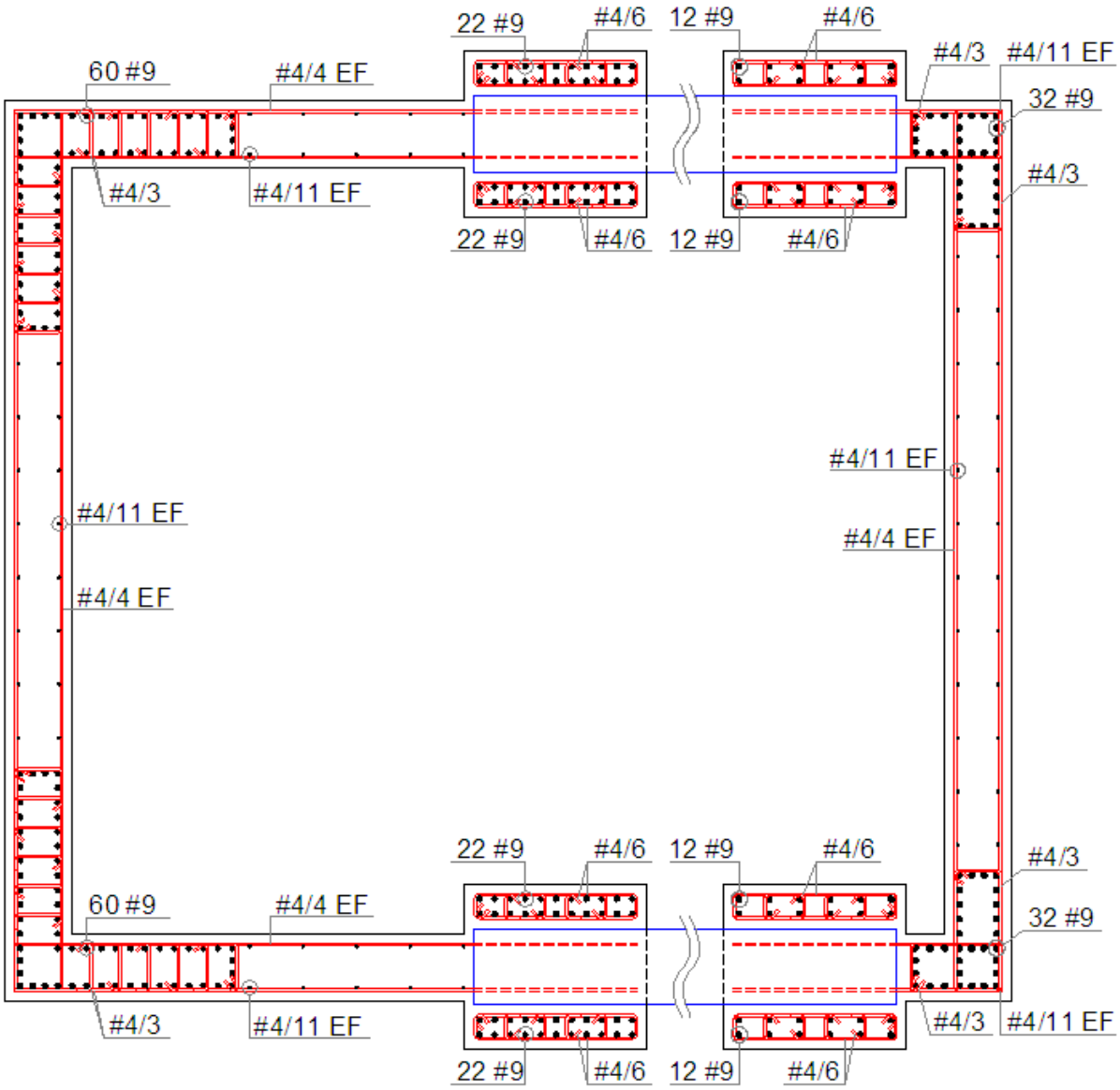

Figure 4-13 Section 1 reinforcement detail of CCW (stories 1-2)

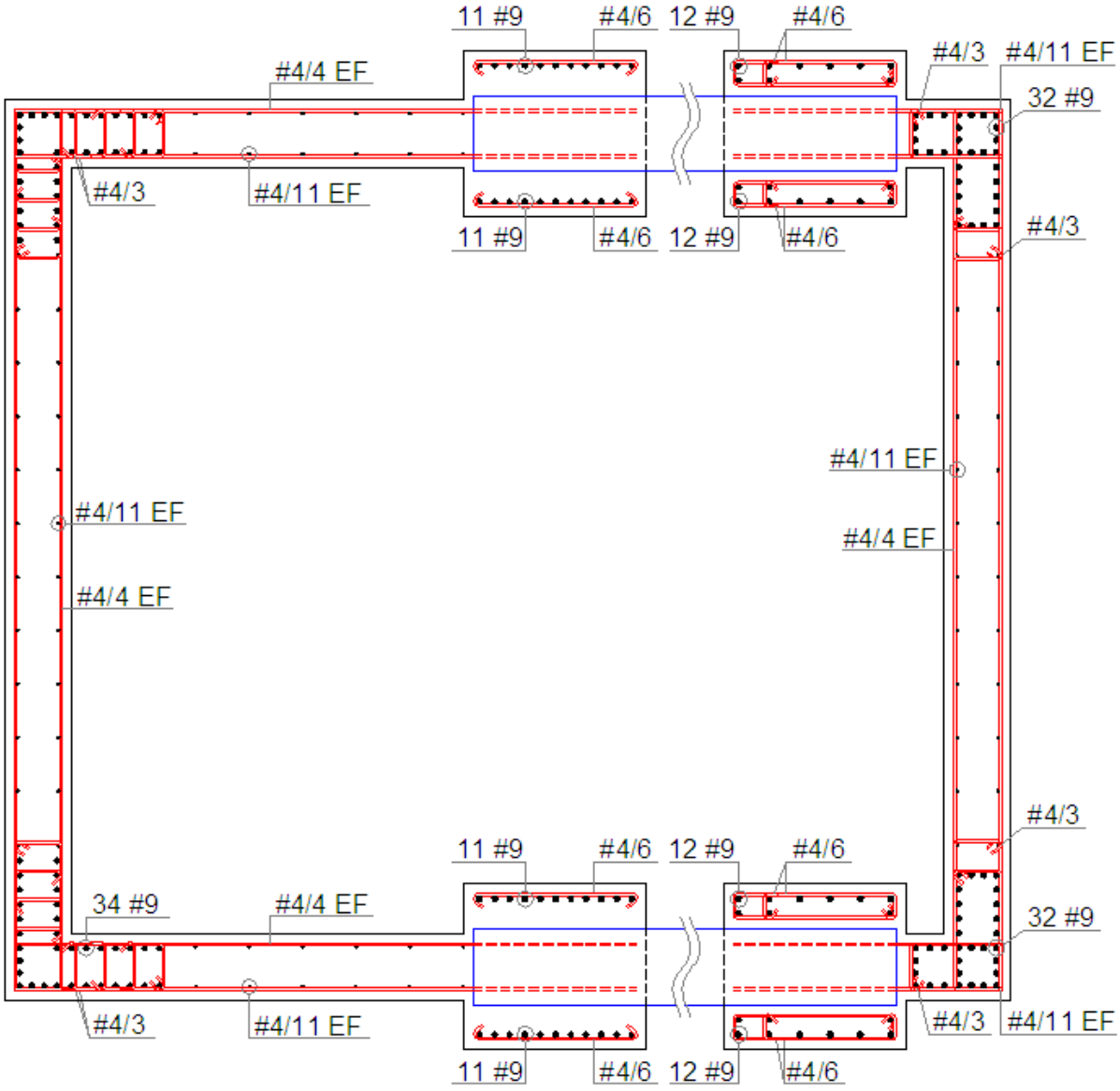

Figure 4-14 Section 2 reinforcement detail of CCW (stories 3-4)

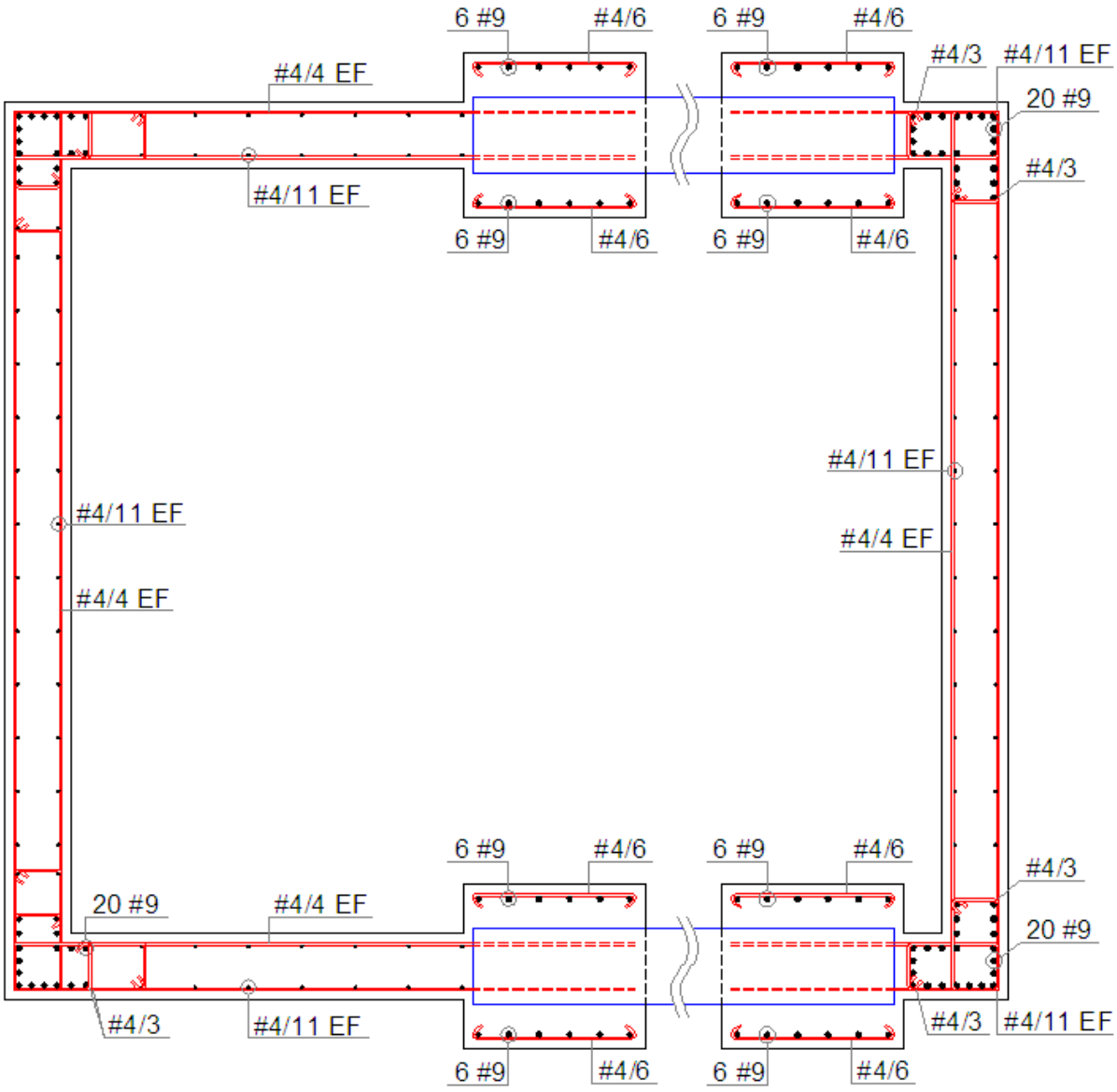

Figure 4-15 Section 3 reinforcement detail of CCW (stories 5-7)

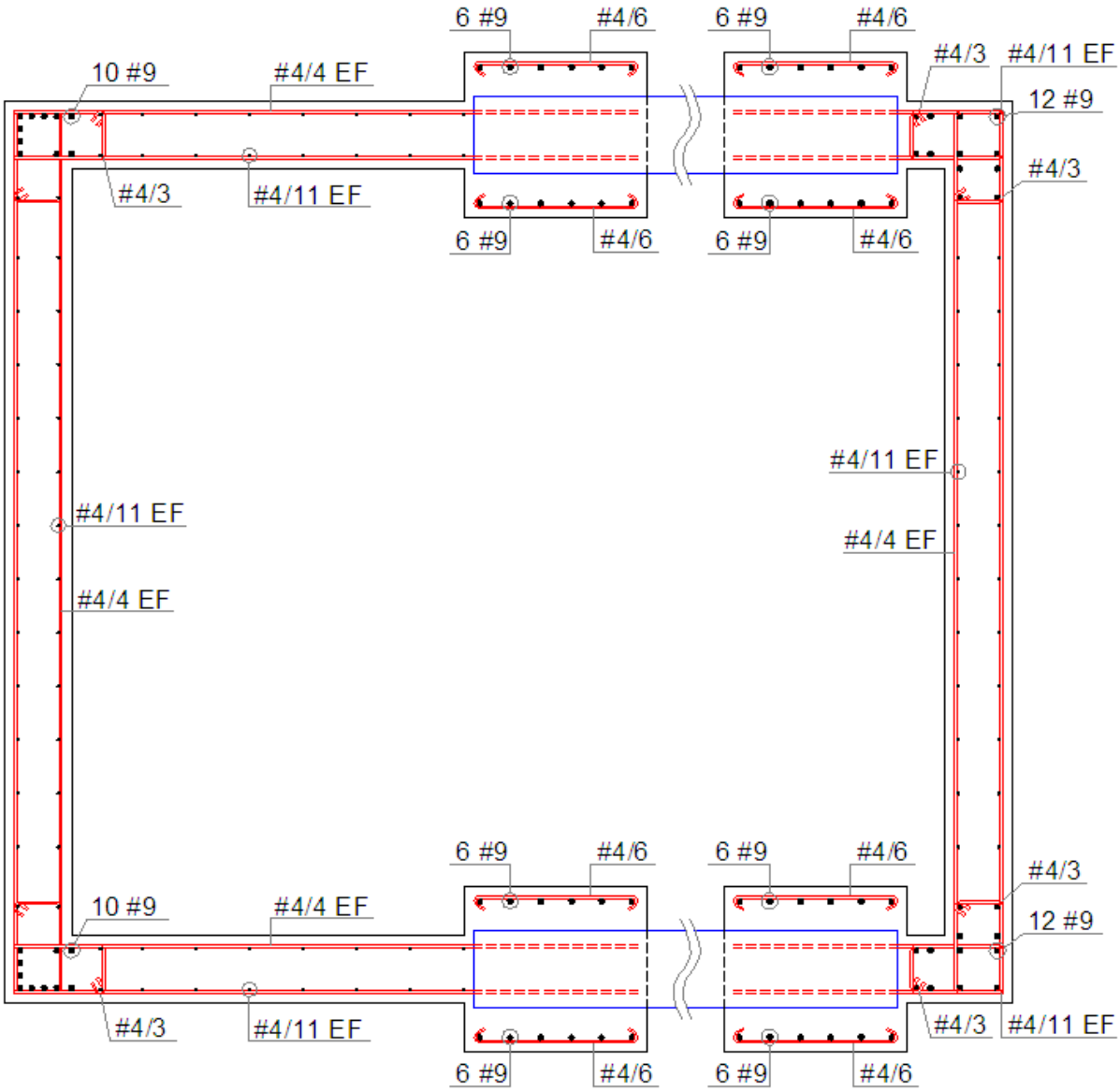

Figure 4-16 Section 4 reinforcement detail of CCW (stories 8-10)

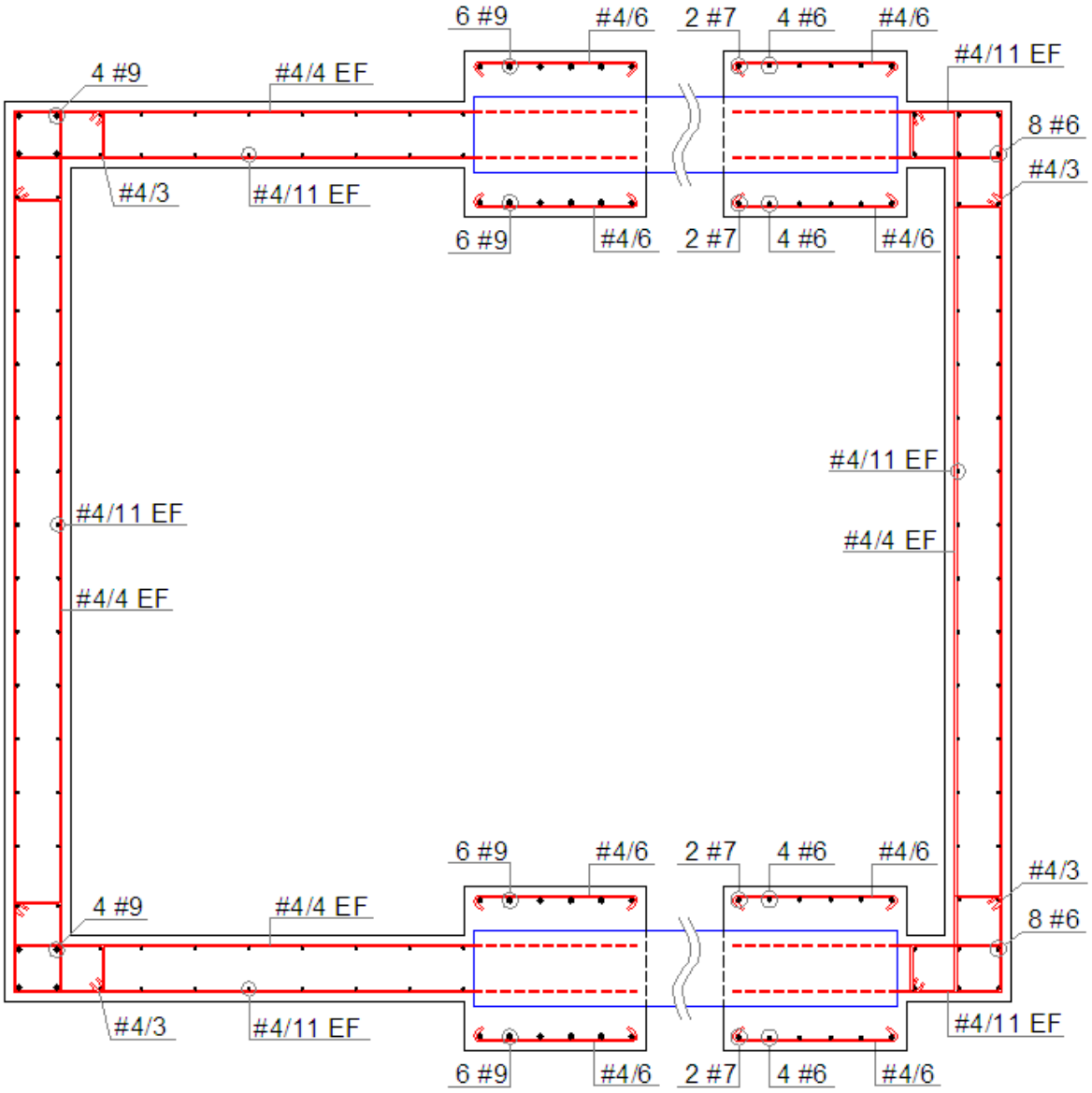

Figure 4-17 Section 5 reinforcement detail of CCW (stories 11-12)

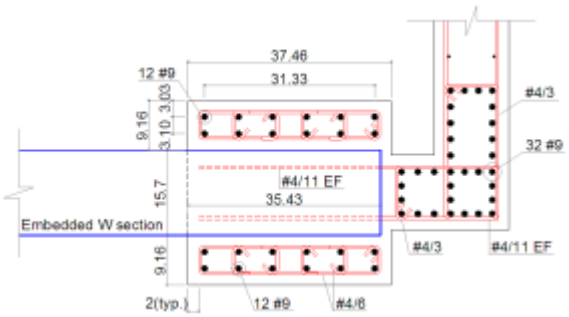

a) Detail of wall 1 barbell in the web region of the coupling beam

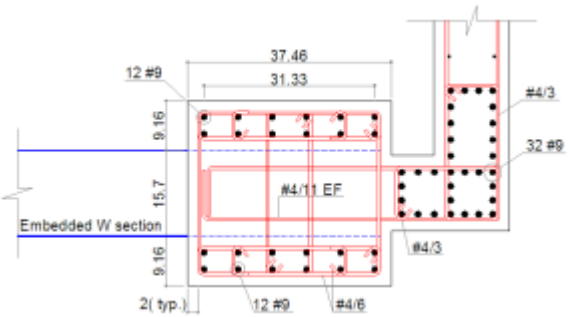

b) Detail of wall 1 barbell at level above/below the coupling beam

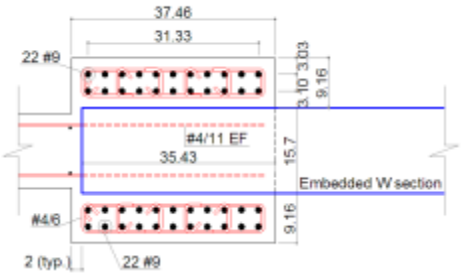

c) Detail of wall 2 barbell in the web region of the coupling beam

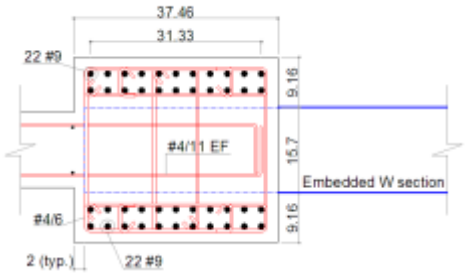

d) Detail of wall 2 barbell at level above/below the coupling beam

Figure 4-18 Details of barbells at the base level for the two walls, dimensions in inches

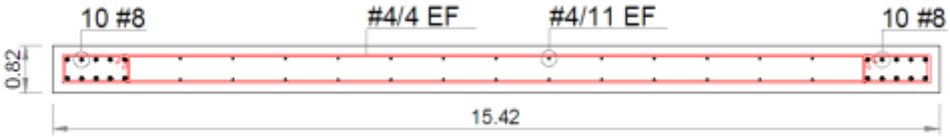

Figure 4-19 Typical reinforcement detail for outrigger cantilever walls (stories 1-2)
Note that walls are oriented in the north-south direction in the structure.

5.0 NONLINEAR STATIC ANALYSIS

When a structure deforms while its elements are yielding sequentially, the force-deformation relationship cannot be determined by simple limit analysis. In such a case, the need for other methods of analysis becomes apparent. One, relatively simple, method of nonlinear analysis is the nonlinear static analysis, also known as a 'pushover' analysis. This method is intended to provide a simple way for determining a 'backbone' nonlinear response for a structure subject to incrementally increasing lateral forces and/or displacements. In such an analysis, the structural response is 'pushed' through the initial elastic response, through sequential yielding of the elements to the eventual formation of a failure mechanism and therefore collapse.

The nonlinear static procedure was documented as an acceptable method of analysis in FEMA 356 (2000). The so-called pushover analysis has become popular because it avoids the complexity of a response history analysis, but still includes significant aspects of degradation that are critical to seismic behavior (El-Tawil et al. 2009). However, the conventional pushover procedure presented in FEMA-356 does not directly account for the presence of higher modes, which may be particularly critical in taller buildings, and therefore the procedure should be limited to low to mid-rise buildings whose behavior is dominated by first mode response. Chopra and Goel (2002) have presented a modal pushover procedure suitable for capturing higher mode effects. The modal pushover procedure has not been integrated into codes or standards yet and is sufficiently computationally expensive that it partially negates the simplicity of the pushover procedure, particularly in the conceptual design stage. Because of the

dominance of the first mode of behavior for the prototype structures (see Section 5.2), only a conventional pushover analysis will be carried out in this study. A more detailed description of the conventional pushover analysis procedure can be found in the Applied Technology Council Report ATC-40 (1996).

5.1 NONLINEAR MODELING OF THE PROTOTYPE STRUCTURES

Once the structural design of the CCW elements was complete (Chapter 4), the structure is modeled for conducting the nonlinear static analysis. The computer software RUAUMOKO (Carr 2008) is used to perform all nonlinear static and dynamic analyses. In this study, the CCW system is modeled in two dimensions since the effect of torsion is eliminated by positioning the center of rigidity of the LFRS coincident with the center of mass of the building (Figure 4-1). Also, the ASCE 7-prescribed accidental torsion is neglected for simplicity.

A model similar to that developed for the pushover analysis will be subsequently used for dynamic analyses described in Chapter 6. Thus the complete model properties – static and dynamic – are described in the following sections.

5.1.1 Pushover Analysis

A conventional pushover analysis is conducted by applying an incrementally increasing pattern of lateral loads distributed along the height of the structure (similar to those shown in Figures 4-4 and 4-5). RUAUMOKO permits an adaptive pushover procedure to be used. In an adaptive pushover analysis, the loading pattern is revised at each analysis step to reflect the deformation pattern of the structure (Satyarno et al. 1998). This is an approximate method

of addressing higher-mode effects that result from variation of inertial forces over the structure's height. Using RUAUMOKO, an initial load pattern is selected (in this study, the inverted triangular load of the ELF method) and the adaptive pushover refines this based on displacement. Carr (2008) reported that the results using this approach are largely independent of the initial load pattern selected. The analysis continually traces the internal distribution of loads and deformations as the load progressively increases and automatically terminates when the structure reaches its ultimate capacity (Carr 2008).

Because the wall piers are C-shaped, their capacities in the EW direction vary. Therefore two pushover analyses are required: one with the load acting in the west-to-east (WE) direction and the second with load acting east-to-west (EW). In the WE pushover, Wall 1 will be the 'compression' wall (leeward wall in a wind analysis) and Wall 2 will be the 'tension' wall (windward). In the EW direction, the wall forces are reversed.

5.1.2 Dynamic Properties

Several options are available in RUAUMOKO for modeling the stiffness, mass and damping properties of structural components. In this study, the diagonal mass representation where mass is lumped at each translational degree of freedom (DOF) and the contribution of the rotational DOF is obtained as the diagonal term of the appropriate consistent mass matrix for the member considered (Carr 2008), is used. Because the CCW resists 100% of the lateral loads in the direction of analysis, 100% of the storey mass is applied at each storey level. The mass is divided between the wall piers based on their relative area although since lateral degrees of freedom are constrained, this is not strictly necessary. In RUAUMOKO, the mass applied in this fashion only affects the calculation of dynamic properties and is not treated as an applied load. As will be described, it is additionally necessary to apply gravity loads to the wall piers. 5% Rayleigh damping proportional to the initial stiffness matrix (Carr 2008) is

applied in modeling the prototype structure. Finally, P-Δ effects considering only small displacements are accounted for.

5.1.3 Equivalent Frame Model

The model uses the Equivalent Frame Method described in Section 2.5.2, and Giberson one-component beam model (Carr 2008) to represent the steel coupling beams (See Figure 5-1). The Giberson model defines a plastic hinge at both ends of an otherwise elastic. Using RUAUMOKO any of a number of hysteresis rules may be used to describe the hinge behavior. Also, a bilinear axial load- axial displacement hysteresis rules may be applied to the member. However, no interaction between the axial and moment responses is modeled. In the two-dimensional frame analysis, each beam element in the model represents the two coupling beams at a respective storey level; therefore the properties assigned to the element are twice those of a single coupling beam. The wall piers are modeled using a general quadratic beam-column model. This element is conceptually the same as the one-component beam but includes axial springs at both ends and an elastic axial member between these. The general quadratic element may be programmed to capture appropriate axial load-moment interaction (P-M) behavior as shown in Figure 5-2. Additionally, this element has the advantage of capturing the behavior of non-symmetric geometry such as the C-shaped wall piers in this study.

Figure 5-3 shows the equivalent frame idealization of the CCW model and the node and element numbering along the height of the structure. The wall elements are located at the centroids of each C-shaped wall pier. Since the beam elements span the entire lever arm between the piers' centroids, they must be connected to wall elements by rigid links of lengths equal to the distances between the centroids and beam-wall interfaces. These links affect the 'plane sections' response of the wall pier and result in the beams spanning their

appropriate lengths. The lengths of the rigid links are 2.97 ft and 6.14 ft from walls 1 and 2, respectively. As described previously, the nonlinear properties and effective properties of the structural elements should be used in the pushover analysis. In this study the expected hinge region at the base of the walls is assumed to extend through the second floor; greater stiffness reduction factors are therefore used for the first two storeys. Based on previous studies (Harries and McNeice 2006) and a synthesis of international code-prescribed values (Harries 2001), the effective flexural and axial stiffness of the 'tension' wall pier are taken as $0.35I_g$ and $0.75A_g$, respectively. The effective values for the 'compression' pier and for both piers above the expected hinge region are taken as $0.70I_g$ and $1.00A_g$, respectively. These effective properties are shown schematically in Figure 5-4 for loading in the West-to-East (WE) direction. Modeled stiffness values for both wall piers are given in Table 5-1. No reductions are applied to the stiffness of the steel coupling beams. The moments of inertia of the steel coupling beams (see Table 5-2) are obtained from the AISC *Steel Construction Manual* (AISC 2011).

The two-dimensional model shown in Figure 5-3 is fully fixed at the base of each wall. All other nodes have all three degrees of freedom (horizontal and vertical translation and rotation) released. Consistent with the restraint provided by the floor diaphragms, the lateral degrees of freedom at each level of Wall 1 are constrained to those of Wall 2. Thus no axial forces will be developed in the coupling beams and there is no need to model the in-plane axial stiffness of the floor plates.

5.1.4 Element Hysteresis Models

In the pushover analysis, the structural components are modeled using elements with stiffness properties dependent on the amount of imposed deformation on the element. The degradation in stiffness of the components is incorporated using appropriate hysteresis rules. In this work,

a simple bilinear hysteresis rule, shown schematically in Figure 5-5, is used to model the steel coupling beams. This rule requires the following parameters (shown in Figure 5-5):

k_o = beam stiffness which is a function of EI_b, where I_b is the moment of inertia of the W-section found in AISC (2011) and reported in Table 5-2.

F_y = yield capacity of beam taken as the yield moment, $M_y = Sf_y$, where S is the elastic section modulus of the W-section, also found in AISC (2011) and f_y is the yield strength of the steel, taken as 50 ksi in this study. The values of M_y are reported in Table 5-2.

r = post-yield stiffness factor, assumed to be 0.02 (Gudimetla et al. 2010)

The wall piers are modeled using the Q-HYST degrading stiffness hysteresis rule (Saiidi 1979), shown schematically in Figure 5-6. This rule requires the following parameters (shown in Figure 5-6):

k_o = wall stiffness which is a function of EI_{eff}, where I_{eff} is the effective moment of inertia of the wall piers as described above and given in Table 5-1.

F_y = yield capacity of the wall as described in the following section.

r = post-yield stiffness factor given in Table 5-1 and described in the following section.

α = unloading stiffness factor, taken as 0.5 for all analyses.

The value of F_y, in this case is the moment capacity of the wall pier in the presence of axial load. Due to both coupling action and gravity loads, the axial load varies along the height of the wall piers. This value and the post yield stiffness factor were obtained from nonlinear section analyses of the piers conducted using a commercially available non-linear fiber sectional analysis software package XTRACT (Imbsen 2007) as described in the following section.

5.1.4.1 XTRACT Wall Pier Sections Analysis

In XTRACT, the section geometry is 'drawn' and an automated discretization procedure divides this into triangulated fiber elements. The concrete fiber element size for all models was 1 in., which is felt to be adequate given the complexity and size of the section. Mild steel reinforcing bars are modeled as individual fiber elements and are located exactly as they occur in the section. Customized non-linear stress-strain relationships are defined for all materials. XTRACT can be used to perform moment curvature (M-φ) and axial load-moment interaction (P-M) analyses about both principle axes of the modeled section.

Nonlinear models for both unconfined and confined concrete were used. The unconfined model was used for the concrete cover and wall webs that were reinforced with only minimum reinforcement requirements. The unconfined concrete strength was taken as 6.5 ksi. The confined concrete model, based on that of Mander et al. (1988) was used for the boundary elements and barbells (minus their cover concrete) where significant transverse (confining) reinforcement is provided. The concrete stress-strain behavior is modified from the unconfined behavior based on the confining reinforcement ratio provided. A bilinear stress-strain relationship with 2% strain hardening was used to capture the nonlinear behavior of the 75 ksi reinforcing steel.

The predicted moment curvature behavior for each wall at each storey and for each analysis direction (48 M-φ curves in all) were constructed using XTRACT. Individual curves are required since moment capacity is a function of axial load and this varies both over the height of the structure and with the direction of the applied pushover load. The axial loads used were calculated at each storey using Equations 4-20 and 4-21. An example of the resulting M-φ curves is shown in Figure 5-7. These curves are bilinearized (as shown in Figure 5-7) to obtain the post yield stiffness factor, r. These values were averaged for each wall pier and the values of r used in subsequent RUAUMOKO analyses are reported in Table

5-1. The values of yield moment, M_y, determined from the bilinearization of the M-φ curves are also reported in Table 5-1. While these are not used directly in analysis, they were used to validate the development of the axial load-moment (P-M) interaction surfaces also calculated using XTRACT.

Because this study will progress to include time history analyses, it is necessary to model the wall piers in such a way that alternating tension and compression capacity may be captured. Using XTRACT, complete axial load-moment (P-M) interaction yield surfaces were calculated. These are shown in Figure 5-8. From these, the six control points necessary to define the P-M interaction surface (shown schematically in Figure 5-2) for the RUAUMOKO general quadratic beam elements are found; these are reported in Table 5-3.

It is noted that XTRACT and RUAUMOKO use different sign conventions, and consequently the signs of both axial loads and moments obtained from XTRACT are reversed from those used in RUAUMOKO. The sign convention used in XTRACT is such that positive moments impart axial tension in the webs of the C-shaped wall piers, and consequently negative moments generate axial compression in the webs of the C-shapes (see Figure 5-8f).

Finally, XTRACT was also used to verify that the NS capacity of the wall piers was adequate and would not control structural behavior. This was found to be the case and is no presented here.

5.2 MODAL ANALYSIS

Although not necessary for a pushover analysis, conducting a modal analysis of a constructed model is good practice. Such an analysis may be compared with approximations and serve to troubleshoot the model. Additionally, such analyses may verify some of the assumptions or

limitations used in the design process. RUAUMOKO is used to conduct such a modal analysis of the prototype structures. The results, in terms of modal periods (T) and the proportional of modal mass (mass participation factor, mpf) are provided in Table 5-4.

The first mode periods are longer than the ASCE 7-10 (see Section 4.3.1) approximations although this should be expected. The ASCE approximations are intended for use with typical cantilever wall structures and have been observed in the past to be poor indicators of CCW behavior as discussed in Section 4.5.1. The calculated periods are longer: 2.28 seconds as compared to 1.15 seconds used in the ELF design procedure. The effect of this shift is that the ELF procedure will overestimate the design base shear (see Equation 4-6). Although refined methods of analysis (including modal procedures) are permitted by ASCE 7-10, clause 12.9.4.1 limits the resulting reduced base shear to 85% of that calculated using the ELF method. Thus significant reductions are limited.

The fundamental periods elongate as the coupling beams become more flexible (Table 5-4). This is expected since the flexible coupling beams (with the same wall piers) result in a more flexible structure. The period elongation is relatively small (2.28 sec. to 2.57 sec.), indicating the dominance of the wall pier properties in the dynamic response of the structures.

As indicated by the mass participation factors (Table 5-4), the prototype structures are dominated by first mode behavior (expected for relatively uniform structures) and the first 3 modes are adequate to capture 90% of the structural response in all cases.

5.3 PUSHOVER ANALYSIS

The pushover analyses conducted in this study were intended to verify the performance of the prototype structures, and estimate their ultimate capacities for eventual comparison with earthquake demands and results presented in Chapter 6. As described, two pushover analyses

were conducted on each prototype: one in the WE direction and one in the EW direction. The purpose of conducting the analysis in two directions is to investigate the variations in overall CCW system capacity, ultimate displacement, and sequence of hinge formation associated with the compression and tension stresses in both walls resulting from the coupling (frame) action. As described, the adaptive pushover procedure in RUAUMOKO was used; the initial lateral load pattern used was the modified inverted triangular load obtained from the equivalent lateral force (ELF) procedure described by Equation 4-8 and shown in Figure 4-4. Through the course of the analysis, the load pattern is updated automatically based on the structural deformations (Carr 2008).

Prior to application of lateral loads, appropriate gravity loads tributary to the wall piers were applied. These loads are treated as forces and do not affect the seismic mass (i.e.: dynamic properties) of the structure. While the walls resist 100% of lateral loads, they carry only tributary gravity loads; therefore, the gravity loads tributary to the walls are significantly less than the seismic mass assigned to the walls. The presence of gravity loads is important as these resist uplift in the tension wall; their magnitude can be an important design parameter since typically designers prefer to avoid the situation of uplift. Once gravity loads are applied, the lateral pushover loads are applied incrementally.

5.4 PUSHOVER RESULTS

Base shear versus roof displacement pushover curves for the WE and EW analyses are presented in Figures 5-9 and 5-10, respectively. A summary of base shear and roof displacement at a) the ELF prescribed base shear, V = 1691 kips; b) first yield of a wall pier; and, c) the predicted ultimate capacity (formation of sufficient hinges to form a mechanism) are summarized in Table 5-5. The ASCE 7-prescribed base shear (V = 1691 kips) and the 1%

drift limit used in initial design (Chapter 4) are also shown in Figures 5-9 and 5-10 for reference. These elastic design values appear to capture the limit of elastic behavior reasonably well indicating a relatively 'tight' CCW design with only marginal overstrength, as intended, for this study.

Figures 5-9 and 5-10 are similar to the schematic pushover behavior shown in Figure 2-3. The curves shown are the pushover responses of the 'total' structure. Additionally, in Figures 5-9 and 5-10, two 'windows' are identified:

1. The left-most rectangle represents the yield window of the coupling beams where the bottom left corner denotes the first yield of a coupling beam and the upper right corner is the twelfth or last beam to yield. The sequence of coupling beam yielding, with the corresponding base shear (normalized to the ELF value V = 1691 kips) and roof displacement, is reported in Tables 5-6 through 5-10 for the five prototype structures, respectively. The beam yield window shows the range of response representing the 'frame' curve in Figure 2-3.
2. The right rectangle is the yield window of the wall piers at the base of the structure where the bottom left point is the first yield of a wall pier and upper right point is the yield of the second pier, resulting in the formation of a mechanism and representing the point of failure for the CCW system. The wall yield window shows the range of response representing the 'wall' curve in Figure 2-3.

In Figures 5-9 and 5-10, the initial slope of each curve represents the elastic behavior of the CCW system. In this range, the lateral force is resisted by the combined action of the coupling beams and wall piers in the manner assumed in design and in the elastic-based continuous medium method (see Section 4.3.2)

Once beams begin to yield (left window), the coupling action begins to degrade and the lateral forces once resisted by coupling frame action are redistributed to the wall piers. As

can be seen in Tables 5-6 through 5-10 and Figure 5-11, the progression of coupling beam yield initiated near the one third height of the structure and progressed both upwards and downwards. Typically the roof beam will remain elastic the longest since its demand is significantly reduced since no forces are applied above this point. In this analysis, the first floor beam yield is also delayed. This is a result of the very stiff restraining effect resulting from this beam being located so close to the fixed bases of the walls. A taller first storey (typical in many structures) will often lead the first floor beam to yield earlier in the analysis (Harries and McNeice 2006).

As the coupling beams yield, the properties of the CCW system change resulting in a) a decrease in the degree of coupling, doc; b) a decrease in structural stiffness resulting in c) an increase in the natural period of vibration; and d) an increase in the damping properties of the structure resulting from increased concrete damage. In subsequent nonlinear time-history analyses (Chapter 6), all of these effects, with the exception of the change in damping, are captured.

In the range beyond the left window, once all coupling beams have yielded, the structure is no longer a CCW but a collection of two linked wall piers (LWP). From left to right in the left window, the structure is transitioning from being a CCW to being a LWP.

As the prototype coupling beams become more flexible (100% to 60% structures), the beam yield windows shift to the left – the beams yield at a lower base shear. Nonetheless, the beam yield progression does not vary substantially as shown in Figure 5-11. As a result of the more flexible beams, the overall CCW capacity falls and the wall piers yield at a lower base shear. Nonetheless, all capacities exceed the ASCE 7 design basis.

The EW pushover analyses results in higher ultimate strengths than the WE analysis. This is attributed to the higher resistance of the system resulting from the stiffer pier (Wall 2) being in compression. Added compression will generally increase the wall moment capacity

while tension reduces the capacity (Figure 5-8). The dominance of Wall 2 in this analysis is apparent in the pushover results. For the purposes of design or evaluation, clearly the lower WE capacity would be adopted. The pushover analyses validated the CCW designs and will serve as a basis of comparison with the nonlinear time history analyses presented in Chapter 6.

5.5 DISCUSSION OF PUSHOVER ANALYSIS

As described in Section 5.1.1, since the CCW system in this study consists of two very different C-shape wall piers, the structural behavior of the system is expected to be different when the stiffer or flexible wall is in tension or compression. Thus pushover analyses must be conducted in both directions (EW and WE, in this case). In these analyses and under load control, the structure is subjected to gradually increasing lateral loads. The analysis is terminated when the structure achieves its performance criteria (see Section 2.6.2.1) or fails (defined as a negative value in the diagonal stiffness matrix).

In the WE analysis (wall 1 is in compression and wall 2 is in tension), the CCW systems of the five structures have good behavior in the elastic range; the elastic range on the capacity curves (Figure 5-9) is represented by the region enclosed by the dashed lines representing fundamental ELF analysis design criteria (base shear and 1% drift). It can be seen from Figure 5-9 that even the softest structure (60%) exhibited relatively small roof displacement - on order of 12.1 in. - at the code-prescribed base shear, and consequently satisfied the 1% roof drift limit (17.0 in.).

In all five prototype structures analyzed in the WE direction, the initiation of the yield in the coupling beams started before the code base shear was achieved. This is shown in Figure 5-9, where the left bottom corner of the left window (coupling beams yield process) is

located inside the elastic range. In the 100% structure the process of the coupling beams yielding was complete beyond the elastic base shear, while for the 90% structure all beams had yielded at the code base shear. The coupling beam yielding for the 80%, 70% and 60% structures was completed before the code base shear was achieved (see Figure 5-9 c, d and e). As the strength of the coupling beams is reduced from 100% to 60%, the beams yield earlier in the pushover analysis (the coupling beams yield process (left window) moves to the left as shown in the Figures 5-9a through e) and force the CCW system to evolve more rapidly to a collection of two linked wall piers (LWP) (Figure 1-1). From the capacity curves of the five structures, it is also seen that even once the coupling beams had yielded and the structures functionally became sets of LWP's, the yield of wall piers at their base (right window) had not yet taken place; thus significant reserve stiffness and capacity remained.

The right window in Figure 5-9 represents the wall yield process defined at the base of the structure. In the region between the beam yield and wall yield windows on the capacity curves, one can see the difference between a system of two cantilever walls designed to work separately and a system resulting from the evolution of a CCW system. The former system would have less capacity and stiffness, and hinge initiation would form immediately at the base of the walls when the system achieves the code base shear. Furthermore, it can be seen that this region increases as the strength of the coupling beams decreases (100% to 60%). This observation suggests that the wall piers in this study are over designed for the demands on the structure which reflects the inherent over strength prescribed by ASCE 7 (see Section 4.5).

As described earlier, following yield initiation at the base of wall piers (represented by the left bottom corner of the right window on the capacity curves (Figure 5-9)), the structures continue to show an increase in strength and roof displacement. Finally, the

stiffness falls to essentially zero representing the formation of a complete mechanism (yield of all beams and both piers at their base).

The parts of Figure 5-9 show that as the coupling beams become more flexible (100% - 60%) the ultimate capacity of the system (base shear) decreases, although it always exceeds the code design base shear. Additionally, the ultimate roof displacement of the 100%, 90% and 80% satisfied the roof drift limit of 1% (17 in.), although the roof displacement exceeded this limit in the 70% and 60% structures by 10 and 17% respectively. Nonetheless, all structures satisfy the typical performance-based limit of 2% (34 in.).

When conducting the pushover analysis in the EW direction (wall 1 is in tension and wall 2 is in compression), a different behavior is expected due to the large difference in wall pier geometry. In addition, there should be concern about the ability of the smaller wall 1 to handle the uplift axial force resulting from coupling action. For the prototype structure, uplift was not a great concern due partially to the large tributary gravity loads applied to the core walls. Additionally, as the coupling beams yield, the axial forces in the wall piers stabilize and may eventually diminish as the coupling beams lose their shear strengths (not modeled here since steel coupling beams having large ductility were used). Once the coupling beams yield, the frame action of the coupling beams is redistributed to the wall pier flexural action. Thus, in the case of wall piers having significantly different geometries, permitting dual action or allowing 'weaker' coupling beams (60% in lieu of 100%) may mitigate uplift in piers. (Uplift is very undesirable from a design perspective since it requires significant foundation engineering.)

The results of the EW pushover analysis showed that the ultimate capacities of the five structures exceeded their counterparts in WE analysis (see Table 5-5 and Figures 5-9 and 5-10). The higher capacities in the EW analyses result from the stiffer wall 2 being in compression and thus being even more dominant in the behavior of the system. In the WE

analysis, when this wall was in tension, the overall system was more flexible since the dominant element was more flexible. Since the pushover analysis for the CCW system in the two directions results in two different capacities, the lower result would control the ultimate capacity of the system.

From the results of the pushover analysis, the following points are concluded:

1- Considering the performance criteria of limiting roof drift, it is seen that reducing coupling beams strength could be a key in developing constructible design (the need for this is developed by Harries et al. 2005), as the analysis indicated little significant change to global structural performance from coupling beams designed for 100% of their demand. Prototype structures with coupling beams strengths to 80% satisfied the 1% drift limit, and all prototype structures satisfied the 2% drift limit.

2- If the 60% structure is considered as a 'step' in the deterioration process of the 100% structure, the system at this stage is still showing acceptable behavior by satisfying the 2% drift limit and having an ultimate capacity exceeding the code design basis.

3- Using two geometrically different wall piers does not produce a lower ultimate capacity for the CCW system as it intuitively seem. Nonetheless pushover analyses must be conducted in both principle directions. In this study, the results of the EW pushover analysis provided higher ultimate capacities for the five prototype structures.

The observations from the nonlinear static analyses would appear to vindicate the dual system approach proposed in this work: The structure behaves as a stiff coupled system for wind and moderate seismic loads and degrades to a collection of linked piers for high seismic loads. The inherent stiffness of a CW permits this evolution without exceeding performance drift limits (1-2%). Additionally, this behavior can be achieved using 'weaker' coupling beams. Such beams are easier to design (Harries et al. 2005) and may result in a wider practical use of CW systems.

Table 5-1 Modeling parameters for wall piers (see Figure 5-6)

analysis:	**WE**						**EW**						**all**
pier:	**Wall 1 (compression)**			**Wall 2 (tension)**			**Wall 1 (tension)**			**Wall 2 (compression)**			**both**
	I_{eff}	M_y	r	I_{eff}	M_y	r	I_{eff}	M_y	r	I_{eff}	M_y	r	α
storey	in^4	kip-in		in^4	kip-in		in^4	kip-in		in^4	kip-in		
11	1267700	52583	0.01	11620000	176752	0.03	1267700	37265	0.04	11620000	226942	0.004	0.50
10		65642			166216			34183			271865		
9	1296400	110634		11760000	279695		1296400	76536		11760000	427325		
8		121024			253710			67484			471958		
7		132689			213942			57724			518483		
6	1313200	147231		11830000	316495		1313200	52014		11830000	649465		
5		156338			282428			42246			692911		
4		166816			249655			32975			735562		
3	1359400	204162		12320000	560293		1359400	73894		12320000	1024643		
2		207849			536935			66628			1023253		
1	1369900	231087		6540000	933257		684950	96449		13090000	1470131		
base		233715			927027			94342			1482105		

Table 5-2 Modeling parameters for steel coupling beams (see Figure 5-5)

model:	**100%**			**90%**			**80%**			**70%**			**60%**			**all**
	Section	I_b	M_y	Section	I_b	M_y	Section	I_b	M_y	Section	I_b	M_y	Section	I_b	M_y	r
storey		in^4	kip-in		in^4	kip-in		in^4	kip-in		in^4	kip-in		in^4	kip-in	
12	W14 x 120	1380	9540	W14 x 109	1240	8640	W12 x 120	1070	8376	W12x 96	833	6612	W12 x 87	740	5940	0.02
11	W14 x 120	1380	9540	W14 x 109	1240	8640	W12 x 120	1070	8376	W12x 96	833	6612	W12 x 87	740	5940	0.02
10	W14 x 132	1530	10536	W14 x 120	1380	9540	W12 x 120	1070	8376	W12 x 106	933	7380	W12x 96	833	6612	0.02
9	W14 x 145	1710	11700	W14 x 132	1530	10536	W12 x 136	1240	9636	W12 x 120	1070	8376	W12 x 106	933	7380	0.02
8	W14 x 145	1710	11700	W14 x 132	1530	10536	W12 x 136	1240	9636	W12 x 120	1070	8376	W12 x 106	933	7380	0.02
7	W14 x 159	1900	12960	W14 x 145	1710	11700	W12 x 136	1240	9636	W12 x 120	1070	8376	W12 x 106	933	7380	0.02
6	W14 x 159	1900	12960	W14 x 145	1710	11700	W12 x 136	1240	9636	W12 x 120	1070	8376	W12 x 106	933	7380	0.02
5	W14 x 159	1900	12960	W14 x 145	1710	11700	W12 x 136	1240	9636	W12 x 120	1070	8376	W12 x 106	933	7380	0.02
4	W14 x 145	1710	11700	W14 x 132	1530	10536	W12 x 136	1240	9636	W12 x 120	1070	8376	W12 x 106	933	7380	0.02
3	W14 x 132	1530	10536	W14 x 120	1380	9540	W12 x 120	1070	8376	W12 x 106	933	7380	W12x 96	833	6612	0.02
2	W14 x 120	1380	9540	W14 x 109	1240	8640	W12x 96	833	6612	W12 x 79	662	5352	W12 x 72	597	4860	0.02
1	W14 x 61	640	4596	W14 x 61	640	4596	W12 x 58	475	3888	W12 x 50	391	3240	W12 x 45	348	2892	0.02

Table 5-3 Control points used for the general quadratic beam-column elements in pushover analyses (see Figure 5-2)

Detail #	Storeys	PYC	PB	MB	PC	MC	PYT
		kips	kips	kip-in	kips	kip-in	kips
Wall 1							
1	1 - 2	-44290	-12760	342400	-18000	-371000	8689
2	3 - 4	-43130	-9890	336700	-18470	-359500	7789
3	5 - 7	-40290	-14710	310300	-17780	-321200	5150
4	8 - 10	-39130	-14860	301600	-16930	-310200	3801
5	11 - 12	-37340	-14490	287800	-17880	-286800	1774
Wall 2							
1	1 - 2	-63740	-21200	1647000	-17950	-1611000	16120
2	3 - 4	-55820	-21790	1337000	-17730	-1356000	9101
3	5 - 7	-52160	-21390	1174000	-20590	-1209000	5016
4	8 - 10	-51330	-20470	1132000	-23300	-1175000	4181
5	11 - 12	-50750	-18850	1109000	-23610	-1145000	3282

Table 5-4 Natural vibration periods of the five prototype structures

Mode	**100%**		**90%**		**80%**		**70%**		**60%**	
	sec.	mpf	sec.	mpf	sec.	mpf	sec.	mpf	sec.	mpf
1	2.28	70.79	2.33	70.67	2.40	70.71	2.49	70.41	2.57	70.17
2	0.57	15.51	0.58	15.50	0.59	15.40	0.61	15.50	0.62	15.61
3	0.25	5.65	0.25	5.72	0.25	5.73	0.25	5.85	0.26	5.93
4	0.14	3.19	0.14	3.22	0.14	3.23	0.14	3.27	0.14	3.30
5	0.09	1.91	0.09	1.93	0.09	1.95	0.09	1.97	0.09	1.98
6	0.07	1.18	0.07	1.19	0.07	1.20	0.07	1.21	0.07	1.22
7	0.05	0.76	0.05	0.76	0.05	0.77	0.05	0.77	0.05	0.78
8	0.04	0.49	0.04	0.50	0.04	0.50	0.04	0.50	0.04	0.50
9	0.04	0.30	0.04	0.30	0.04	0.30	0.04	0.30	0.04	0.30
10	0.03	0.15	0.03	0.15	0.03	0.15	0.03	0.15	0.03	0.15
11	0.03	0.05	0.03	0.05	0.03	0.06	0.03	0.06	0.03	0.06
12	0.03	0.01	0.03	0.01	0.03	0.01	0.03	0.01	0.03	0.01
mpf = modal mass participation factor (%)										

Table 5-5 Base shear and roof displacement at different loading stages for the five structures

Structure	Elastic		at first yield of wall piers		ultimate capacity	
	normalized base shear	roof disp., in.	normalized base shear	roof disp., in.	normalized base shear	roof disp., in.
WE direction						
100%	1.00 (1691 kips)	7.64	1.13	8.90	1.39	15.30
90%		8.20	1.13	9.90	1.36	15.95
80%		9.08	1.11	10.67	1.34	17.10
70%		10.85	1.06	11.73	1.28	18.74
60%		12.09	1.02	12.46	1.25	19.91
EW direction						
100%	1.00 (1691 kips)	5.89	1.59	11.15	2.01	17.05
90%		6.30	1.54	11.72	1.96	15.86
80%		6.71	1.52	12.55	1.98	19.40
70%		8.03	1.30	11.90	1.58	15.88
60%		9.05	1.21	11.97	1.51	17.71

Table 5-6 Initiation of nonlinear behavior in beam elements for 100% structure

WE direction			EW direction		
beam at storey	normalized base shear	roof disp. in.	beam at storey	normalized base shear	roof disp. in.
3-4	0.71	5.07	5	0.90	5.18
5	0.73	5.21	6	0.90	5.23
6	0.76	5.42	4	0.91	5.25
2	0.76	5.45	7	0.94	5.48
7	0.80	5.77	3	0.97	5.65
8	0.85	6.22	8	0.99	5.80
9	0.91	6.83	9	1.05	6.28
10	0.98	7.45	2	1.11	6.73
1	1.01	7.78	10	1.13	6.83
11	1.05	8.13	11	1.20	7.37
12	1.11	8.71	12	1.28	8.06
			1	1.53	10.56

Table 5-7 Initiation of nonlinear behavior in beam elements for 90% structure

WE direction			EW direction		
beam at storey	normalized base shear	roof disp. in.	beam at storey	normalized base shear	roof disp. in.
4	0.66	4.92	5	0.83	5.02
3	0.67	4.97	4, 6	0.84	5.11
5	0.67	5.03	7	0.87	5.27
6	0.70	5.23	3, 8	0.90	5.50
2	0.72	5.45	9	0.96	5.98
7	0.73	5.54	10	1.02	6.44
8	0.77	5.90	2	1.07	6.83
9	0.83	6.43	11	1.09	6.99
10	0.88	7.00	12	1.15	7.55
11	0.95	7.68	1	1.45	10.75
1	0.97	7.89			
12	1.00	8.17			

Table 5-8 Initiation of nonlinear behavior in beam elements for 80% structure

WE direction			EW direction		
beam at storey	normalized base shear	roof disp. in.	beam at storey	normalized base shear	roof disp. in.
4	0.61	4.70	5	0.75	4.67
5	0.61	4.74	6	0.76	4.75
3	0.62	4.80	4, 7	0.78	4.89
6	0.63	4.92	8	0.82	5.24
7	0.66	5.19	3	0.84	5.37
2	0.67	5.31	9	0.87	5.65
8	0.70	5.60	10	0.93	6.13
9	0.75	6.11	2	0.99	6.61
10	0.81	6.68	11	1.00	6.68
11	0.87	7.29	12	1.05	7.17
12	0.91	7.75	1	1.44	11.70
1	0.96	8.57			

Table 5-9 Initiation of nonlinear behavior in beam elements for 70% structure

WE direction			EW direction		
beam at storey	normalized base shear	roof disp. in.	beam at storey	normalized base shear	roof disp. in.
4-5	0.54	4.60	5-6	0.66	4.52
6	0.55	4.70	7	0.68	4.63
3	0.56	4.77	4	0.69	4.72
7	0.58	4.93	8	0.71	4.87
8	0.61	5.26	9	0.75	5.19
2	0.61	5.29	3	0.76	5.31
9	0.65	5.68	10	0.79	5.61
10	0.69	6.17	11	0.83	5.99
11	0.73	6.63	12	0.87	6.39
12	0.76	6.97	2	0.89	6.63
1	0.84	8.26	1	1.24	11.20

Table 5-10 Initiation of nonlinear behavior in beam elements for 60% structure

WE direction			EW direction		
beam at storey	normalized base shear	roof disp. in.	beam at storey	normalized base shear	roof disp. in.
5	0.50	4.50	6	0.61	4.38
4	0.50	4.54	5	0.62	4.44
6	0.51	4.58	7	0.62	4.47
3	0.53	4.75	4, 8	0.65	4.69
7	0.53	4.79	9	0.68	4.98
8	0.55	5.07	3, 10	0.72	5.33
2	0.57	5.28	11	0.74	5.61
9	0.59	5.42	12	0.77	5.94
10	0.62	5.88	2	0.83	6.68
11	0.65	6.20	1	1.17	11.39
12	0.67	6.48			
1	0.78	8.42			

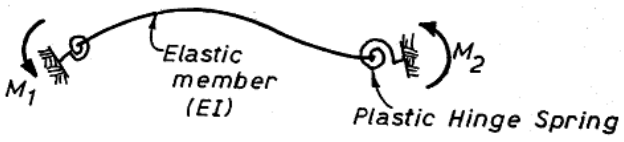

Figure 5-1 Giberson one component beam model used for steel coupling beams (Carr 2008)

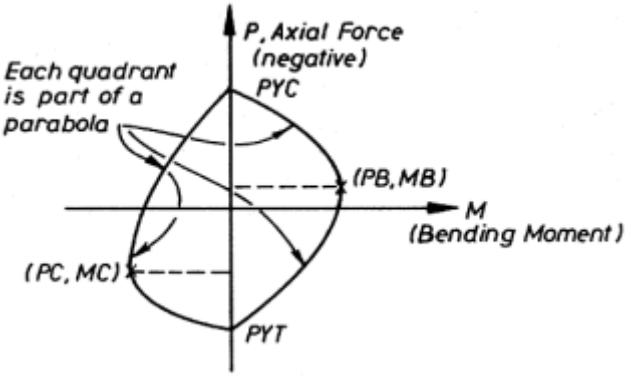

Figure 5-2 Quadratic beam-column yield surface used to model used for wall piers (Carr 2008)

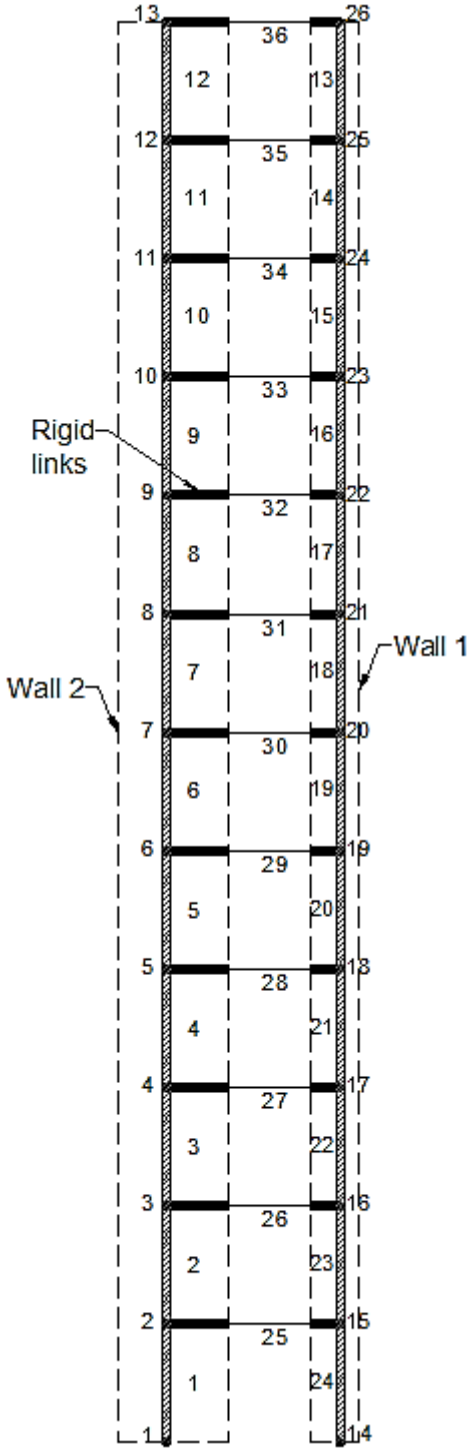

Figure 5-3 Equivalent frame model with node and element numbering scheme used to model the prototype structures

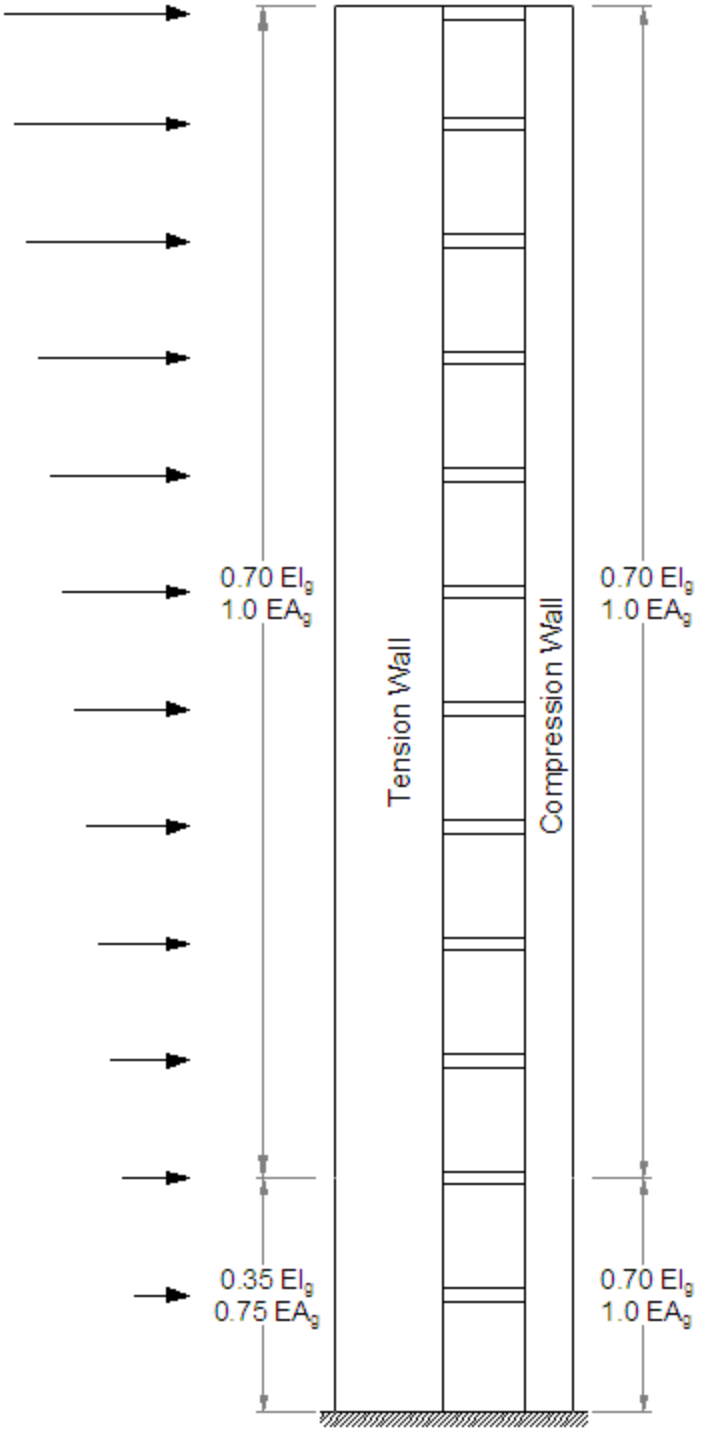

Figure 5-4 Effective wall pier properties used in modeling the prototype structure in pushover analysis (WE direction shown)

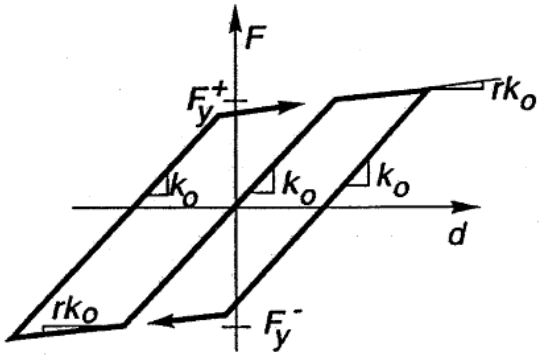

Figure 5-5 Bilinear hysteresis rule to model the steel coupling beams in Ruaumoko

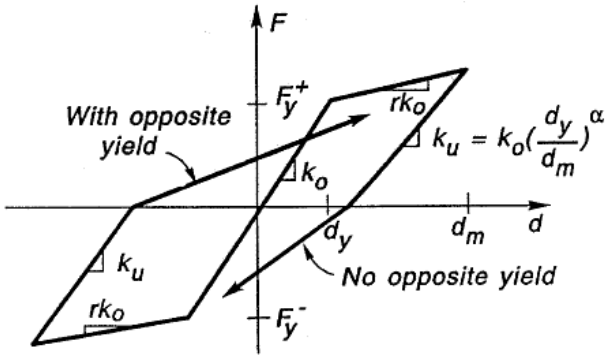

Figure 5-6 Q-HYST hysteresis rule to model the wall piers in Ruaumoko

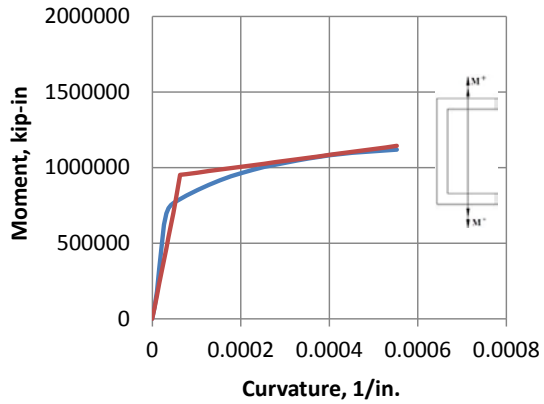

a) WE loading (tension wall)

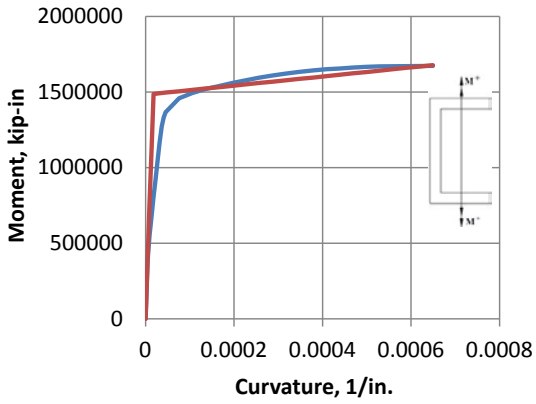

b) EW loading (compression wall)

Figure 5-7 Example of calculated and bilinearized moment curvature for the base of Wall 2.

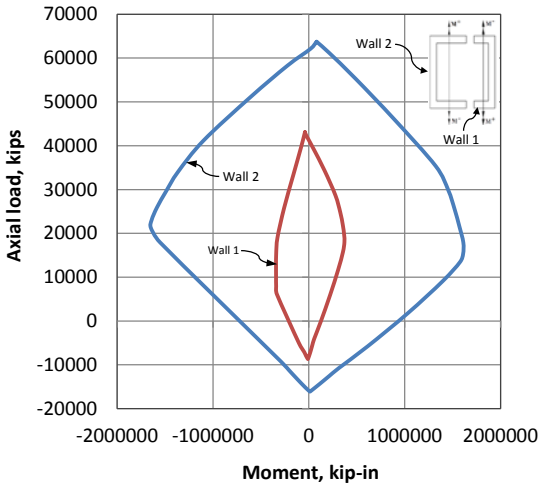

a) Section 1

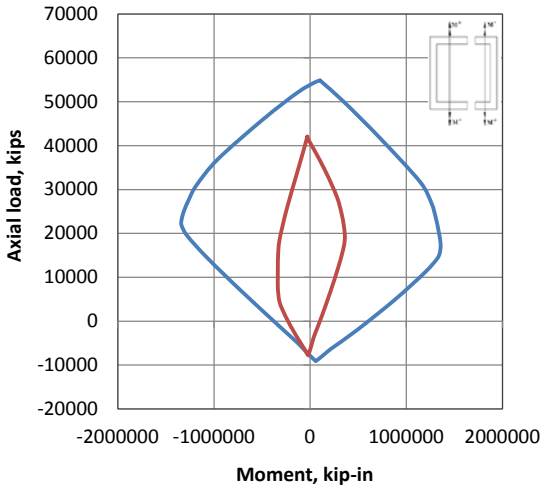

b) Section 2

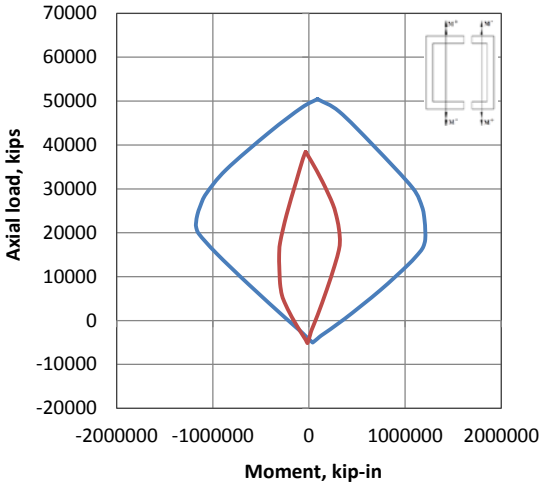

c) Section 3

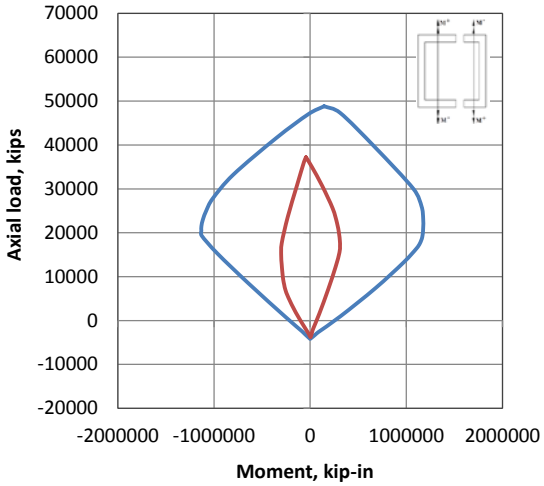

d) Section 4

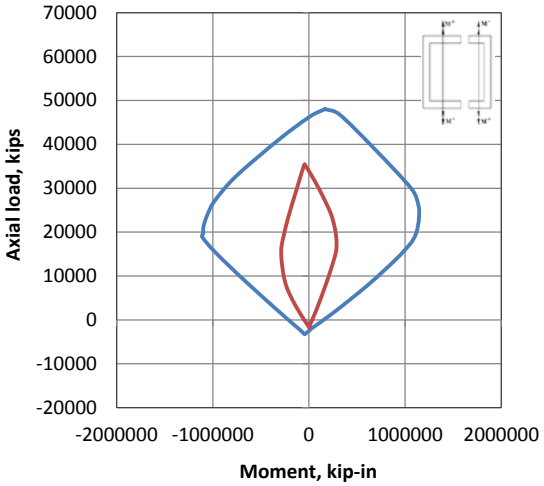

e) Section 5

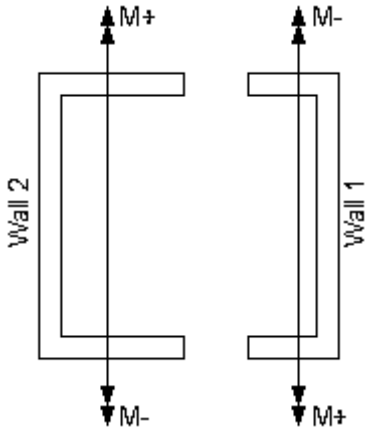

f) sign convention

Figure 5-8 Axial load-moment interaction surfaces of the two walls

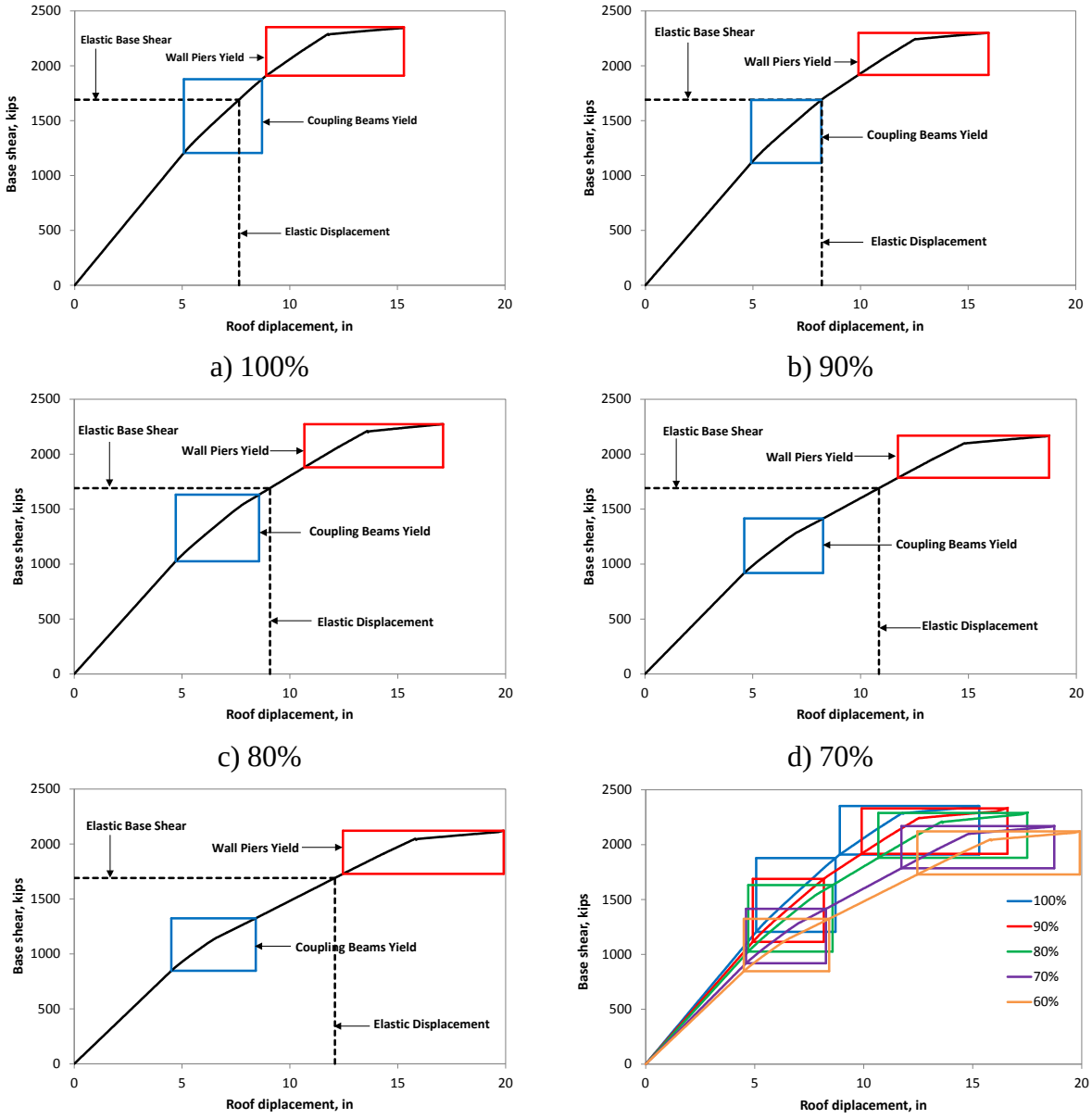

Figure 5-9 Pushover curves for WE direction

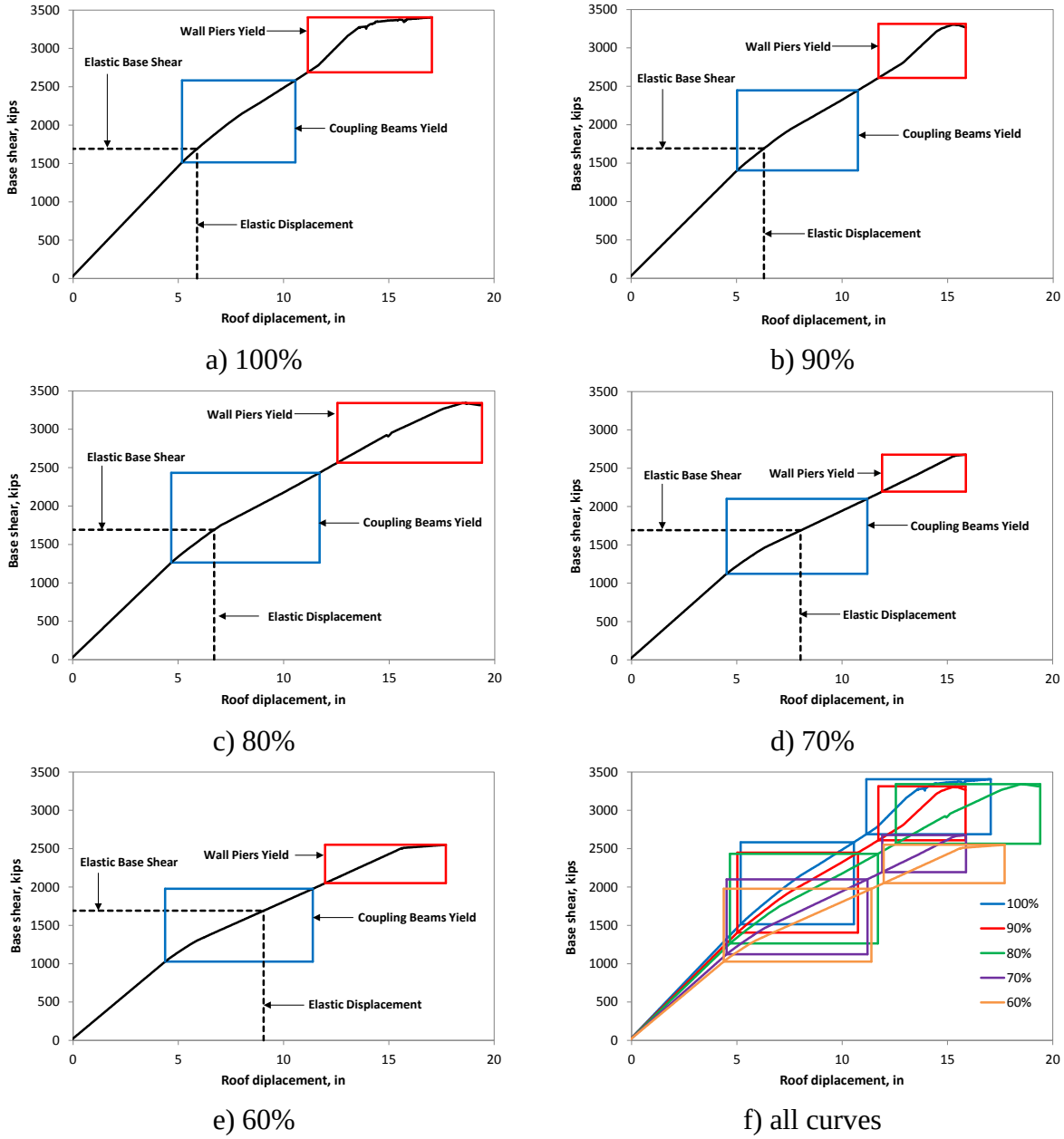

Figure 5-10 Pushover curves for EW direction

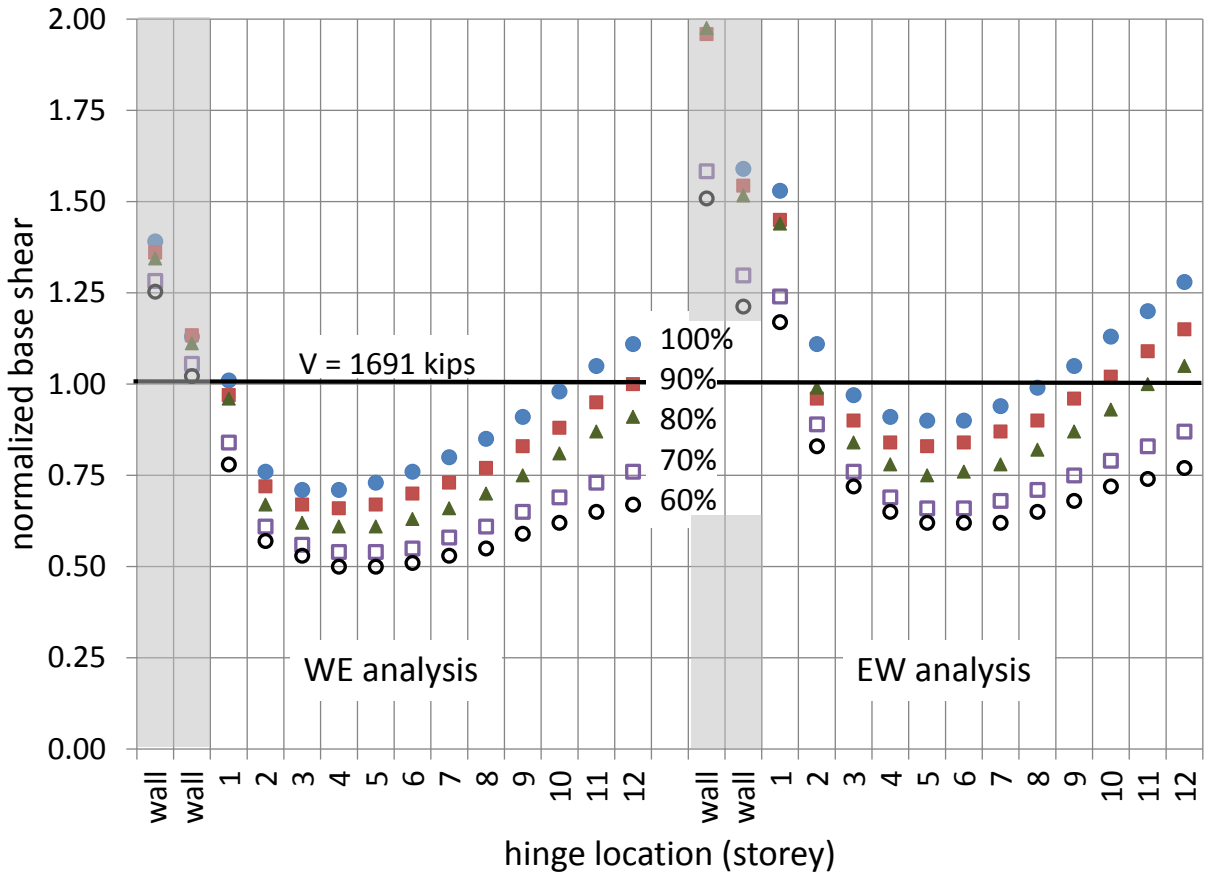

Figure 5-11 Progression of hinge formation in beams and walls (see Tables 5-6 through 5-10)

6.0 NONLINEAR DYNAMIC ANALYSIS

When buildings are subjected to significant dynamic loads such as seismic excitation, their nonlinear response must be assessed. This is required in particular for structures that are designed to dissipate inelastic energy. Coupled core walls (CCW), due to their stiffness, are usually the principal lateral force resisting system in a structure. As discussed previously, the efficacy of CCW is based on their excellent energy dissipation characteristics. Therefore, to be efficient, the response of CCW to earthquake excitation is expected to extend into the nonlinear range.

Nonlinear time history analysis (NLTHA) is considered by design codes (ASCE 7-10) to be the most comprehensive level of analysis, where the effect of the transient and cyclic nature of the ground motion can be simulated. The influence of the ground motion characteristics, including the frequency content, magnitude, and its ability to trigger higher modes may be significant, requiring a suite of ground motions to be considered.

Structural characteristics beyond simply mass and stiffness and their distribution must also be considered. Stiffness and/or strength degradation, are particularly important as these impact the change in dynamic properties with accumulated energy dissipation (damage).

The pushover analyses described in Chapter 5 demonstrated that the prototype CCW structure behaved in an acceptable manner, in which reasonable hinge formation, base shear and roof displacement levels were achieved. This Chapter describes the extension of these analyses

to NLTHA, subjecting the same five prototype structures described in Chapters 4 and 5 to a suite of ground motions. The NLTHA were carried out using frame models similar to those described in Section 5.1.

6.1 NONLINEAR MODELING AND PARAMETERS

The computer program RUAUMOKO (Carr 2008) was utilized to conduct the nonlinear time history analyses. The 2D model used for the pushover analysis (Chapter 5) is modified for the nonlinear dynamic analysis. Additional input parameters are required to conduct the dynamic analysis. Unlike the pushover analysis, during response history analysis, the two walls will sway back and forth resulting in each wall alternating between being the tension and compression wall piers (gravity loads are also applied, in which case the 'tension' wall may still have a net compressive force). Because the wall axial stress varies, the instantaneous flexural stiffness, moment capacity and post peak behavior also vary.

Using the P-M interaction surfaces described in Section 5.1.4.1 and shown in Figure 5-8, the wall pier strength envelope is determined and variation in axial load accounted for. It is impractical, however, to vary wall pier stiffness and post peak behavior. In these cases, both the effective of moment of inertia of the pier, I, and the post-yield stiffness factor, r, are taken as the average of the values used in the pushover analysis (see Table 5-1) as shown in Table 6-1. Similar to the pushover analysis, the bilinear and Q-HYST (see Section 5.1.4) hysteresis rules are also used to represent the inelastic behavior of the beam and wall pier members respectively.

In RUAUMOKO, both the bilinear and the Q-HYST hysteresis rules allow for degradation of strength that is independent of the stiffness degradation associated with the

hysteresis rule. The yield moments are allowed to degrade as a function of member ductility or the number of cycles of inelastic actions (Carr 2008). In this study, strength degradation of the members due to cyclic loading is considered as a function of the member ductility demand as shown schematically in Figure 6-1. The strength degradation parameters are provided in Table 6-2, where the parameter DUCT1 represents the ductility of the member at which degradation begins, DUCT2 is the ductility at which degradation stops, RDUCT denotes to the residual strength as a fraction of the initial yield strength. In Figure 6-1, DUCT3 is the ductility at 0.01 initial strength, and RCYC is the percentage of the reduction of strength per cycle of inelastic behavior; these two parameters are not used in the present study as they do not apply if the strength degradation is taken as function of the ductility demand. DUCT parameters are determined based on engineering judgment; values used in this study are consistent with those used in related and comparable studies (Harries and McNeice 2006).

6.2 EARTHQUAKE GROUND MOTION RECORDS

Nonlinear response of structural systems to earthquake ground motion is significantly affected by earthquake magnitude, duration and frequency content. Therefore, a number of ground motions representing a range of frequencies and amplitudes should be used to establish the upper and lower bounds of nonlinear behavior of a system. ASCE 7-10 requires using a suite of not fewer than three appropriate ground motion histories, and these histories should be scaled to be consistent with the magnitude, distance, and source mechanism of the maximum considered earthquake expected at the site. In this study, no site specific characteristics are assumed; thus

ground motions are scaled to the ASCE 7 (2010) design spectra determined for a 10% probability of exceedance in 50 years (Figure 6-2) as described below.

In this study, each of the five prototype buildings is subjected to a suite of four ground motions. The motions range from moderate to severe records from past earthquakes. They are:

1. north-south ground motion record of the El Centro earthquake recorded at Imperial Valley on May 18, 1940 (El Centro);
2. north-south ground motion record of the Kobe earthquake of January 17, 1995 (Kobe);
3. north-south ground motion record of the Northridge recorded at Sylmar Hospital on January 17, 1994 (Northridge); and,
4. north-south ground motion record of the San Fernando earthquake recorded at Pacoima Dam on February 9, 1971 (San Fernando).

Each record was available in a suite included in the RUAUMOKO software package. Each record is digitized at a time step of 0.02 seconds and has a duration exceeding 20 seconds. Analyses were cut off at 20 seconds in all cases.

Each ground motion record was scaled such that its acceleration response spectral ordinate at T = 2.28 seconds – the first mode of the 100% prototype (see Table 5-4) – was equal to that of the ASCE 7 design spectra as shown in Figure 6-2. The resulting scale factors and other key parameters for each ground motion record are given in Table 6-3. The scaled spectra are shown in Figure 6-2 and can be seen to generally exceed the ASCE 7 spectra for all higher modes (T < 2.28 sec.). The scaled ground motion acceleration-time histories are shown in Figures 6-3 to 6-6.

6.3 NONLINEAR TIME HISTORY ANALYSIS

The nonlinear analysis time history analysis performed in this study was based on the Newmark integration method with constant average acceleration, which assumes that the acceleration during the time step from time t to $t+\Delta t$ is constant (Carr 2008). The constant average acceleration method has the advantages of being unconditionally stable and that not all of the degrees of freedom need to have associate mass (Carr 2008).

The time step used in the time history analysis should be less than 0.1 of the natural vibration period of the highest mode of free vibration that contributes significantly to the response of the structure. In this study, a time step of 0.01 seconds was used for all analyses. For the five prototype structures in this study, the first three modes are sufficient the capture 90% of the modal mass (as required by ASCE 7) as shown in Table 5-4. The third mode period is 0.25 seconds, thus the 0.01 second time step is sufficient to capture the behavior of the model. Finally, a diagonal mass matrix (masses lumped at nodes) and 5% Rayleigh damping were used in the analysis.

6.4 RESULTS OF NLTHA

6.4.1 Roof Displacements

The roof displacement time histories for the five prototype structures are shown in Figures 6-7 through 6-11, while the maximum values and the time at which they were obtained are shown in Table 6-4. A comparison of all twenty roof displacement histories obtained is shown in Figure 6-

12. The overall building high is 1700 in. (141 ft- 8 in.); thus the 1% and 2% drift limits are 17 in. and 34 in., respectively.

The El Centro earthquake resulted in peak roof displacements ranging from 10.52 in. for the 70% prototype structure to 17.04 in. for the 80% structure. The 100% structure had a maximum roof displacement of 12.99 in. Similar behavior was observed for the Kobe records, with a maximum roof displacement of 18.99 in. observed in the 70% structure. The Northridge earthquake results exceeded the 1% drift limit for the 100% and 80% structures but fell below the 2% limit in all cases. The San Fernando ground motion represents the most severe event in the suite. All five structures exceeded the 2% drift limit as shown in Table 6-4 and Figures 6-7 to 6-11. This behavior will be discussed further in Section 6.5.

From the roof displacement time history plots (Figures 6-7 to 6-11), it can be clearly seen that all structures exhibited some degree of permanent deformation following the 20 second-duration ground motions. Permanent deformations generally are established relatively earlier in the ground motion records, often following the peak observed displacement (Table 6-4). Permanent set is observed as a bias in the mean displacement and indicates the existence of nonlinear behavior. Generally, the extent of nonlinear behavior is proportional to the severity of the ground motion record (scaled PGA in Table 6-3 and Figure 6-2). The progression of nonlinear behavior in the structure itself; that is: the number and order of beam yielding, followed by the wall pier yielding, also effects the permanent distortions of the structure. These progressions are described in Section 6.4.5.

6.4.2 Base Shear Forces

The base shear time histories for the five structures for each ground motion record are shown in Figures 6-13 to 6-16. The maximum base shear values for each structure and their time of occurrence in the records for each earthquake are provided in Table 6-5.

Base shear demand is highly sensitive to the dynamic properties of the structure. While, in general, base shear may be expected to decrease as the first mode period increases (Table 6-3), the importance of higher mode behavior in CCWs makes this generalization difficult. The influence of higher mode behavior is apparent in the base shear time histories. In the El Centro and Kobe responses, the first mode behavior (T≈ 2.25 s) is clearly dominant. Particularly in the Northridge response, the second mode behavior (T ≈ 0.6 s) is especially evident notably between 5 and 10 seconds.

6.4.3 Interstorey Drift

ASCE 7 (2010) provisions limit the interstorey drift to 2% of the storey height. For the five structures in this study the storey height is 142 in. which corresponds to an interstorey drift limit of 2.84 in. The interstorey drift results help in the understanding of the performance of the building and its structural behavior over its height. The positive and negative envelopes of the maximum observed interstorey drifts for the five buildings for the suite of the earthquakes are shown in Figure 6-17 to 6-21. The envelopes are also plotted on a single chart for comparison in Figure 6-22.

For the relative moderate El Centro ground motions, all five prototype structures satisfied the 2% drift limit with exception of the 80% structure as can be seen in Figure 6-19. For the

Kobe excitation, the 100%, 70%, and 60% structure interstorey drifts only marginally exceeded the 2% limit, while the 90% and 80% structures almost satisfied this requirement. Similarly, for the Northridge ground motion, the interstorey drift limit was not exceeded for the 90%, 70%, and 60% buildings, while the 100% and 80% buildings exceeded the limit only marginally, as shown in Figures 6-17 and 6-19. The San Fernando ground motion resulted in significant inelastic deformation and the 2% drift limit was exceeded in all cases. As expected, however, drift envelopes reflect the severity of the ground motions considered (Table 6-3).

6.4.4 Axial Load-Moment Interaction

Figures 6-23 to 6-26 show the axial load-moment hysteretic responses at the base of each wall pier plotted on the P-M interaction capacity surfaces for the wall section at the base of the structure (previously presented in Figure 5-8). Considering, for example the El Centro behavior shown in Figure 6-23: It is apparent that the response of wall 2 exceeded the P-M interaction envelope, indicating significant excursions into nonlinear behavior. Conversely, the wall 1 response remained within the P-M interaction envelope indicating that this wall remained essentially elastic.

Significant inelastic excursions of both walls were exhibited in the Kobe ground motions (Figure 6-24). On the other hand, no inelastic excursions at the base of the wall piers were exhibited for either the Northridge or San Fernando records. This latter observation is explained by significant inelasticity occurring in the beams and elsewhere in the wall piers as described in the following section.

6.4.5 Progression of Inelastic Behavior

Tables 6-6 to 6-9 summarize the times at which each structural element exhibited its first yield. During the El Centro ground motion, the coupling beams in the five structures started to yield at approximately one third of the structure height (fourth floor), and in all of the structures the yield in this beam occurred at 1.57 seconds into the record. At this time in the record, the ground acceleration has only just exceeded about 0.06g (Figure 6-3), corresponding, approximately to the design base shear (i.e.: V = 0.063W; see Equation 4-6). The yield of the coupling beams then spread vertically both up and down the structure as observed in the pushover analysis (Figure 5-11). Wall 1 did not yield at the base at all in this event as can be seen in Figure 6-23. The wall did however yield higher up the structure primarily in the positive direction (indicating yield while resisting the tension couple). Significantly fewer excursions beyond yielding were evident in the negative (compression couple) direction. Wall 2 yielded at its base only in the positive direction (compression couple) from 2.14 to 2.18 seconds in each of the five structures. This single excursion (which can be seen in Figure 6-23) would be relatively insignificant in the global response of this structure. The wall started to yield at a time close to the time of yield for the less stressed coupling beams (beam 1 in 80%, 70%, and60% structure, see Table 6-6). Wall 2 did not yield in either tension or compression.

In the Kobe ground motion (Table 6-7), the coupling beams started to yield at time ranges between 4.42 and 4.45 seconds, and then the yield spread vertically in both directions (up and down). It is noted for the five structures that the first yield occurred at the third floor at both ends of the beams. The coupling beams yielded faster as the stiffness of the coupling beams decreased (100% to 60%). Wall 1 yielded only in tension at the base in all structures with the exception of the 70% structure, although, excursions were observed in both tension and compression in other

storeys along the height of the structure. Wall 2 exhibited an inelastic behavior in both tension and compression for most of the prototype structures. However, this wall did not yield in compression at the base of the 70% structure.

Table 6-8 shows the progression of the inelastic behavior for the five prototype structures in the Northridge earthquake. In this event, the most highly stressed coupling beams yielded at time ranges between 3.58 and 3.61 seconds at both ends of these beams. The first yield occurred at the third floor of the structures. The yield then propagated vertically up and down. It is noted during this earthquake that the first floor beams in 100%, 80%, 70% and 60% structures showed an inelastic behavior much later than beams in other floors. However, the first floor beam did not yield at all in 90% structure. Wall 1 did not show any inelastic behavior at the base for all prototype structures, but it did yield in tension in some upper storeys. Also, wall 2 did not yield at the base in all structures. The wall started to yield in both tension and compression at the fourth floor of the 90%, 80%, 70% and 60% structures. However, it yielded in tension (positive) at the second floor of the 100% structure.

During the San Fernando ground motion (Table 6-9) the time of first yield ranges between 2.77 and 2.88 seconds, and it was observed at different storeys for five the prototype structures. The coupling beams at fourth, fifth, sixth and seventh floors yielded simultaneously at time of 2.88 seconds in the 100% structures as shown in Table 6-9. Also, it is noted in this event that the first floor beams yielded at time relatively close to the time of yield of the upper storeys. With respect to wall1, it did not yield at the base except in 90% structure, where it yielded in tension (Table 6-9). Also, wall 1 did not yield at all in compression along the height in the 100%, 70% and 60% structures. It exhibited an inelastic behavior at the roof in 90% structure and eleventh floor in the 80% structure. On the other hand wall 2 showed an inelastic behavior in

both tension and compression along the height in the five structures. The wall yielded only in tension at the base of the 100%, 90%, 80% and 70% structures, and it did not yield neither in tension nor in compression at the base of the 60% structure (Table 6-9), although the excursions were very close to the capacity curve as can be seen in Figure 6-26.

6.5 DISCUSSION OF TIME HISTORY ANALYSIS

The nonlinear time history analysis was conducted for a two-dimensional model similar to that used for the pushover analysis described in Chapter 5. A necessary simplification was that the wall pier properties were obtained by averaging the tension and compression properties used in pushover model. As discussed in Section 6.2, each prototype structure was subjected to four different ground motions. Figures 6-7 to 6-11 show the time history responses of the prototype structures during the suite of ground motions. From Figure 6-7, it can be seen that the 100% structure exhibited a good behavior during the El Centro, Kobe, and Northridge events. The structure satisfied the roof drift limit specified by design codes of 2% (34 in.). However, permanent deformations were observed in the Kobe and Northridge ground motions indicating moderate to severe yielding of the wall piers. The structure suffered the largest roof displacement during the Fan Fernando earthquake. In this event the roof displacement exceed the 2% drift limit, so the event could be considered as representative of the collapse prevention (CP) performance level.

The time history response of the roof displacement for the 90% structure is shown in Figure 6-8, the structure response satisfied the drift limit, and showed little permanent drift in the El Centro, Kobe, and Northridge ground motions. It can be also seen that the structure satisfied

the acceptance criteria for life safety (LS) performance level for these events. On the other hand, the structure exhibited very large roof drift during the San Fernando earthquake. This may be due to an occurrence of resonance in which one of the modal frequencies is excited to resonance by the ground motion. As the 90% structure exhibited such significant damage during the San Fernando earthquake, it can be said that this structure is not viable for this event as it does not satisfy the acceptance criteria of the CP performance level.

The roof displacement time history response of the 80% structure (Figure 6-9) shows that permanent deformation occurred in all of the ground motions, although the response satisfied the 2% drift limit with the exception of the San Fernando earthquake where the roof drift exceeded the 34 in. limit at a few points. The structure can be considered as an acceptable CCW for the suite of the ground motions examined.

Figure 6-10 displays the time history roof displacement response for the 70% structure. The response barely exceeded the 2% drift limit at one point during the San Fernando earthquake. The structure exhibited good behavior in the other events, even though a permanent drift was observed after approximately 6 seconds (Figure 6-10).

The 60% structure roof displacement time history response satisfied the code drift limit during all ground motions as shown in Figure 6-11, and consequently the acceptance criteria for LS and CP performance levels.

Figures 6-13 to 6-16 show the time history of the base shear for the five prototype structures. During the suite of earthquakes, the maximum base shear demand for the five structures exceeded the code specified base shear (V = 1691 kips) estimated by the equivalent lateral force (ELF) procedure as shown in Table 6-5. From this table, the largest base shear for all structures occurred during the course of the Kobe excitation, while the smallest were

observed for the Northridge event. The large level of base shear demand can be attributed to the effects of higher structural modes. The natural periods of the second and third modes for the five structures range from 0.57 to 0.62 seconds and 0.25 to 0.26 seconds respectively (Table 5-4). Referring to Figure 6-2, it can be seen that the Kobe and El-Centro earthquakes have high spectral acceleration values at the period of the second mode, while Northridge has the lowest. The levels of base shear imparted to the structures by this suite of ground motions seem to be representative of the design level spectra for which they were scaled.

The interstorey drift envelopes are shown in Figures 6-17 to 6-21. From these figures, it is clearly that no structure satisfied the 2% interstorey drift limit in the San Fernando earthquake, where significant drift occurred above the 6^{th} floor. During the El Centro ground motion, it is observed that all structures, with the exception of the 80% structure, behaved very well and fulfilled the 2% interstorey drift requirement. In the 80% structure, large drift took place in the upper storeys which implies large coupling beams rotation at theses floors. Similar behavior was observed during the Kobe earthquake, where the 70% and 60% structures showed large interstorey drifts in the upper three storeys.

This observed behavior of large drifts in upper storeys sheds some light on the seemingly anomalous behavior of the prototype structures to the San Fernando ground motion. The wall piers are not uniform along their height. The significant effects of higher modes or the combined effects of first plus higher modes may be exciting the levels at which the wall piers transition from one section (capacity) to another. In such a case, hinges form in the wall piers at these transitions (discontinuities) earlier in the time history (see Tables 6-6 to 6-9) and the once the coupling beams yield above this point, a mechanism forms resulting in very high interstorey and roof drifts. This highlights the complexity associated with the dynamic characteristics of non-

uniform structures and structures having multiple lateral force resisting mechanisms such as coupled walls.

Addressing the drift requirement could be difficult when the design is based on elastic analysis. Drift is a function of the overall lateral stiffness of the structure. The lateral stiffness of the CCW system could be enhanced by providing stiffer coupling beams or stiffening the wall piers. For instance, for the prototype structure, the issue of interstorey drift in the upper three storeys could be addressed by extending the wall's section detail #4 up to the roof level. This would provide more lateral stiffness and it won't affect the properties of the CCW system such as the doc at the base. In this case, extending detail #4 may prove an economical solution having little impact on the rest of the structure.

The axial load-moment hysteresis responses at the base of the wall piers are shown in Figure 6-23 to 6-26. During the El Centro ground motion (Figure 6-23) wall 2 response exceeded the P-M interaction surface indicating significant nonlinear behavior at the pier base. From this figure, it can be seen also that the wall response crosses the capacity surface in the negative moment and positive axial load quadrant, indicating that the nonlinear excursion occurred when wall 2 was resisting the compression couple. The sign convention for the positive wall pier moment for both walls is shown at the lower right of the figures.

The higher demand in wall 2 for all analyses corresponds to peaks in base shear demands and indicates that the pier participated in dissipating the energy along with the coupling beams for these design earthquake event. On the other hand, the smaller and flexible wall 1 remained elastic throughout most analyses.

In Kobe ground motion (Figure 6-24), both wall piers experience significant inelastic excursions at their bases. In this event wall 2 yielded in tension and compression, while wall 1

yielded only in tension. The two piers showed no inelastic excursions at their base in the Northridge earthquake, indicating that both walls maintained their axial and flexural capacities. Similarly, the wall bases experienced only nominal inelastic deformation during the San Fernando earthquake were both walls yielded in tension; wall 2 multiple times while wall 1 yielded only once (Figure 6-26). As noted above, however, the behavior of the wall piers, especially for the San Fernando event, was dominated by behavior at higher stories rather than the pier bases. Finally, it should also be noted that the hysteretic properties used to define the wall piers in the analytical models are based on averaged parameters. This would underestimate the hysteretic characteristics of the compression wall and overestimate the hysteretic characteristics of the tension wall.

Table 6-1 Moments of inertia and post yield parameters of wall piers used for NLTHA

Wall section	Storey	proportion of I_g	Wall 1		Wall 2	
			I, in^4	r	I, in^4	r
1	1-2	$0.53I_g$	1,027,425	0.025	9,817,500	0.017
2	3-4	$0.70I_g$	1,359,400	0.025	12,320,000	0.017
3	5- 7	$0.70I_g$	1,313,200	0.025	11,830,000	0.017
4	8-10	$0.70I_g$	1,296,400	0.025	11,760,000	0.017
5	11-12	$0.70I_g$	1,267,700	0.025	11,620,000	0.017

Table 6-2 Strength degradation parameters used for NLTHA (see Figure 6-1)

ELEMENT	DUCT1	DUCT2	RDUCT	DUCT3
WALL 1	6	10.5	0.8	-
WALL 2	10	16	0.8	-
BEAMS	4	10	0.85	30

Table 6-3 Ground motion parameters

ground motion	recorded value		scaled values		
	PGA	acceleration ordinate at T = 2.28 sec.	scale factor	PGA	acceleration ordinate at T = 2.28 sec.
El Centro	0.35g	0.19g	1.00	0.35g	0.19g
Kobe	0.84g	0.26g	0.73	0.61g	
Northridge	0.79g	0.44g	0.43	0.34g	
San Fernando	1.17g	0.35g	0.55	0.64g	

Table 6-4 Maximum roof displacements and time of occurrence for the five structures

Structure	Earthquake							
	El Centro		Kobe		Northridge		San Fernando	
	disp.	time	disp.	time	disp.	time	disp.	time
-	in	sec	in	sec	in	sec	in	sec
100%	12.99	17.92	15.23	6.38	31.67	13.65	42.32	9.46
90%	12.23	17.95	15.19	15.41	15.19	7.01	60.47	19.99
80%	17.04	17.94	14.03	6.38	28.75	7.27	36.95	9.48
70%	10.52	16.62	18.99	17.74	12.3	7.04	36.15	9.47
60%	12.39	5.22	14.33	13.41	13.06	7.07	34.03	9.32

Table 6-5 Maximum base shear forces and time of occurrence for the five structures

Structure	Earthquake							
	El Centro		Kobe		Northridge		San Fernando	
	base shear	time	base shear	time	base shear	time	base shear	time
-	kips	sec	kips	sec	kips	sec	kips	sec
100%	4687	2.17	5467	5.6	2704	4.21	4049	3.52
90%	4317	2.17	5772	5.57	2753	4.43	3419	8.39
80%	4162	2.17	5947	5.6	2623	3.63	3277	2.79
70%	3783	2.18	5898	5.55	2720	3.62	3402	2.79
60%	3930	5.75	6125	7.93	2777	3.63	3416	2.79

Table 6-6 Time (seconds) of first yield of structural elements for El Centro ground motion

Storey	100% structure						90% structure					
	Beam		Wall Pier 1		Wall Pier 2		Beam		Wall Pier 1		Wall Pier 2	
	pos.	neg.	pos.	neg.	pos.	neg.	pos.	neg.	pos.	neg.	pos.	neg.
12	1.81	1.81	-	-	-	-	1.81	1.81	-	-	-	-
11	1.80	1.80	-	12.89	12.83	-	1.80	1.80	-	-	5.00	-
10	1.80	1.79	12.68	-	2.24	1.96	1.79	1.79	5.00	-	2.24	1.93
9	1.77	1.77	-	19.95	2.23	1.90	1.77	1.77	2.32	18.25	2.24	1.90
8	1.75	1.75	2.29	-	2.18	1.88	1.74	1.74	3.99	-	2.20	1.88
7	1.72	1.72	2.98	1.91	2.16	1.87	1.72	1.72	2.95	-	2.17	1.87
6	1.68	1.68	3.53	-	2.16	2.59	1.68	1.67	3.41	-	2.18	1.88
5	1.61	1.61	5.73	-	2.23	2.49	1.60	1.60	-	-	2.17	2.51
4	1.57	1.57	-	-	2.21	2.59	1.57	1.57	-	-	2.19	2.54
3	1.56	1.56	-	-	-	5.02	1.56	1.56	-	-	-	5.00
2	1.57	1.57	-	-	-	4.99	1.58	1.58	-	-	-	4.89
1	1.62	1.63	-	-	-	-	1.63	1.64	-	-	-	-
base	-	-	-	-	-	2.14	-	-	-	-	-	2.16
	80% structure						70% structure					
12	1.81	1.81	-	-	-	-	1.81	1.81	-	-	-	-
11	1.81	1.80	-	-	2.33	-	1.80	1.80	-	-	2.33	-
10	1.79	1.79	2.35	-	2.25	1.94	1.79	1.79	-	-	2.25	1.93
9	1.77	1.77	2.30	5.98	2.24	1.90	1.76	1.76	2.30	12.40	2.25	1.90
8	1.74	1.74	2.29	-	2.20	1.88	1.74	1.74	2.39	12.41	2.22	1.89
7	1.71	1.71	3.39	-	2.18	1.88	1.71	1.70	3.22	-	2.20	1.88
6	1.66	1.65	3.31	-	2.19	1.88	1.64	1.64	-	-	2.20	1.88
5	1.59	1.59	12.65	-	2.18	2.50	1.59	1.58	-	-	2.20	1.91
4	1.57	1.57	-	-	2.20	2.53	1.57	1.57	-	-	-	2.53
3	1.57	1.57	-	-	-	5.02	1.57	1.57	-	-	-	5.01
2	1.58	1.58	-	-	-	4.98	1.59	1.59	-	-	-	4.89
1	2.17	2.17	-	-	-	-	2.17	2.17	-	-	-	-
base	-	-	-	-	-	2.16	-	-	-	-	-	2.17
	60% structure											
12	1.81	1.81	-	-	-	-						
11	1.80	1.80	-	-	2.31	-						
10	1.79	1.79	-	-	2.26	1.94						
9	1.76	1.76	-	-	2.25	1.91						
8	1.73	1.73	2.32	-	2.21	1.89						
7	1.70	1.70	3.95	-	2.21	1.88						
6	1.64	1.64	-	-	2.22	1.87						
5	1.59	1.59	-	-	5.72	1.88						
4	1.58	1.57	-	-	-	2.51						
3	1.58	1.58	-	-	-	5.01						
2	1.59	1.59	-	-	-	4.88						
1	2.18	2.18	-	-	-	-						
base	-	-	-	-	-	2.18						

- = did not yield

Table 6-7 Time (seconds) of first yield of structural elements for Kobe ground motion

Storey	100% structure						90% structure					
	Beam		Wall Pier 1		Wall Pier 2		Beam		Wall Pier 1		Wall Pier 2	
	pos.	neg.	pos.	neg.	pos.	neg.	pos.	neg.	pos.	neg.	pos.	neg.
12	4.64	4.63	-	-	-	-	4.63	4.62	-	-	-	-
11	4.63	4.63	-	-	4.98	-	4.62	4.62	-	-	6.04	-
10	4.62	4.62	4.99	9.90	4.97	4.75	4.61	4.61	5.86	9.90	4.97	4.74
9	4.61	4.61	8.02	5.67	4.95	4.71	4.60	4.60	8.03	5.65	4.97	4.71
8	4.60	4.60	5.09	4.76	4.93	4.69	4.58	4.58	5.15	4.75	4.95	4.68
7	4.57	4.57	5.04	4.65	4.93	4.68	4.56	4.55	6.03	4.70	4.94	4.67
6	4.53	4.52	5.09	-	4.94	4.68	4.51	4.51	5.07	-	5.00	4.67
5	4.49	4.48	5.18	-	5.01	4.68	4.47	4.47	5.15	-	5.01	4.67
4	4.46	4.46	7.87	-	5.02	5.53	4.45	4.45	7.92	-	5.03	4.69
3	4.45	4.45	-	-	-	8.76	4.45	4.45	-	-	-	-
2	4.49	4.48	-	-	-	8.73	4.75	5.26	-	-	-	8.09
1	5.56	5.57	-	-	5.69	-	5.29	5.56	-	-	5.69	-
base	-	-	5.71	-	5.59	7.93	-	-	5.61	-	5.58	7.90
	80% structure						70% structure					
12	4.62	4.62	-	-	-	-	4.61	4.61	-	-	-	-
11	4.61	4.61	-	-	6.01	-	4.60	4.60	-	-	5.98	-
10	4.60	4.60	5.88	8.38	4.98	4.74	4.59	4.59	5.99	-	4.96	4.72
9	4.59	4.59	8.12	5.56	4.98	4.70	4.58	4.58	9.43	5.79	4.97	4.69
8	4.57	4.57	5.09	4.76	4.96	4.68	4.55	4.55	5.16	4.76	4.95	4.67
7	4.53	4.53	5.92	4.73	4.95	4.67	4.51	4.51	6.03	4.73	4.96	4.66
6	4.49	4.49	5.09	-	5.01	4.66	4.48	4.48	5.21	-	5.01	4.66
5	4.46	4.46	6.00	-	5.02	4.67	4.45	4.45	6.07	-	5.04	4.66
4	4.45	4.45	-	-	5.04	4.68	4.44	4.44	7.89	-	5.05	4.66
3	4.44	4.44	-	-	-	8.77	4.43	4.43	-	-	-	-
2	4.47	4.47	-	-	5.76	8.72	4.45	4.45	-	-	5.78	-
1	5.28	5.57	-	-	-	-	5.31	5.32	-	-	5.76	-
base			5.60	-	5.58	5.28	-	-	-	-	5.60	-
	60% structure											
12	4.60	4.60	-	-	-	-						
11	4.60	4.60	-	-	5.46	-						
10	4.59	4.59	5.26	8.52	4.96	4.71						
9	4.57	4.57	8.03	5.80	4.98	4.68						
8	4.55	4.55	5.19	4.81	4.99	4.67						
7	4.51	4.51	5.95	4.73	4.98	4.66						
6	4.47	4.47	5.19	5.65	5.03	4.65						
5	4.45	4.45	6.07	-	5.05	4.65						
4	4.43	4.43	7.93	-	5.06	4.66						
3	4.42	4.42	-	-	-	-						
2	4.43	4.43	-	-	5.76	8.06						
1	5.28	5.29	-	-	5.72	-						
base	-	-	5.69	-	5.60	5.30						

- = did not yield

Table 6-8 Time (seconds) of first yield of structural elements for Northridge ground motion

Storey	100% structure						90% structure					
	Beam		Wall Pier 1		Wall Pier 2		Beam		Wall Pier 1		Wall Pier 2	
	pos.	neg.	pos.	neg.	pos.	neg.	pos.	neg.	pos.	neg.	pos.	neg.
12	3.80	3.79	-	-	-	-	3.79	3.78	-	-	-	-
11	3.78	3.78	-	-	4.46	-	3.77	3.77	-	-	4.29	-
10	3.77	3.77	-	-	3.94	-	3.76	3.76	4.28	-	3.94	-
9	3.76	3.76	-	-	3.95	4.80	3.75	3.75	-	-	3.94	-
8	3.75	3.75	3.98	-	3.95	4.74	3.74	3.74	3.99	-	3.93	5.15
7	3.73	3.73	4.02	-	3.95	4.57	3.72	3.72	3.99	-	3.91	7.66
6	3.70	3.70	-	-	3.94	4.68	3.69	3.68	-	-	3.89	8.29
5	3.66	3.66	3.92	-	3.81	4.62	3.65	3.65	4.15	-	3.82	5.01
4	3.63	3.63	4.13	-	3.77	4.67	3.62	3.62	4.11	-	3.78	4.97
3	3.61	3.61	-	-	-	-	3.60	3.60	-	-	-	-
2	3.63	3.63	-	-	3.77	-	3.62	3.62	-	-	-	-
1	5.09	5.09	-	-	-	-	-	-	-	-	-	-
base	-	-	-	-	-	-	-	-	-	-	-	-
	80% structure						70% structure					
12	3.78	3.78	-	-	-	-	3.77	3.77	-	-	-	-
11	3.77	3.77	-	-	3.96	-	3.76	3.76	-	-	-	-
10	3.76	3.76	-	-	3.94	-	3.76	3.75	-	-	3.93	-
9	3.75	3.75	-	-	3.93	-	3.74	3.74	-	-	3.93	7.69
8	3.73	3.73	3.97	-	3.92	5.42	3.72	3.72	3.97	-	3.91	7.68
7	3.71	3.70	3.99	-	3.91	4.77	3.70	3.69	3.99	-	3.90	7.68
6	3.67	3.67	-	-	3.93	-	3.66	3.66	-	-	3.89	8.31
5	3.64	3.64	-	-	3.82	-	3.63	3.63	-	-	3.84	5.29
4	3.61	3.61	4.07	-	3.79	4.71	3.61	3.61	-	-	3.80	5.27
3	3.59	3.59	-	-	-	-	3.59	3.59	-	-	-	-
2	3.60	3.61	0.00	-	-	-	3.59	3.59	-	-	-	-
1	6.73	6.73	0.00	-	-	-	6.74	-	-	-	-	-
base	-	-	0.00	-	-	-	-	-	-	-	-	-
	60% structure											
12	3.77	3.77	-	-	-	-						
11	3.76	3.76	-	-	-	-						
10	3.75	3.75	-	-	3.92	-						
9	3.74	3.74	-	-	3.92	5.44						
8	3.72	3.72	3.96	-	3.91	5.42						
7	3.69	3.69	3.95	-	3.90	5.35						
6	3.66	3.66	-	-	3.89	5.31						
5	3.63	3.63	-	-	3.84	5.28						
4	3.60	3.60	-	-	3.80	5.28						
3	3.58	3.58	-	-	-	-						
2	3.58	3.58	-	-	-	-						
1	6.74	6.74	-	-	-	-						
base	-	-	-	-	-	-						

- = did not yield

Table 6-9 Time (seconds) of first yield of structural elements for San Fernando ground motion

Storey	100% structure						90% structure					
	Beam		Wall Pier 1		Wall Pier 2		Beam		Wall Pier 1		Wall Pier 2	
	pos.	neg.	pos.	neg.	pos.	neg.	pos.	neg.	pos.	neg.	pos.	neg.
12	2.97	2.96	-	-	-	-	2.96	2.95	-	-	-	-
11	2.95	2.95	7.72	-	-	-	2.94	2.94	-	9.66	3.33	-
10	2.94	2.93	7.72	-	3.32	4.02	2.93	2.92	8.82	-	3.31	4.82
9	2.91	2.91	-	-	3.31	3.18	2.90	2.90	3.55	-	3.30	2.94
8	2.89	2.89	3.36	-	3.30	3.96	2.89	2.89	3.33	-	3.29	4.84
7	2.88	2.88	3.37	-	3.29	3.93	2.88	2.88	3.35	-	3.27	4.00
6	2.88	2.88	3.36	-	3.30	3.84	2.88	2.88	3.44	-	3.26	-
5	2.88	2.88	3.42	-	2.92	3.88	2.87	2.87	3.42	-	2.92	-
4	2.88	2.88	3.16	-	2.90	3.90	2.87	2.87	3.20	-	2.90	-
3	2.93	2.93	-	-	3.20	-	2.86	2.86	-	-	3.17	-
2	2.96	2.96	-	-	3.11	-	2.96	2.96	8.32	-	3.14	-
1	3.00	3.00	-	-	-	-	3.00	3.01	-	-	8.44	-
base	-	-	-	-	2.99	-	-	-	8.39	-	3.02	-
	80% structure						70% structure					
12	2.95	2.95	-	-	-	-	2.95	2.94	-	-	-	-
11	2.94	2.94	-	-	3.33	-	2.94	2.94	-	-	3.33	-
10	2.92	2.92	-	3.95	3.31	2.96	2.92	2.92	8.49	-	3.31	7.28
9	2.90	2.90	6.25	-	3.30	2.93	2.90	2.90	9.60	-	3.30	2.94
8	2.89	2.89	3.34	-	3.29	4.02	2.89	2.89	3.36	-	3.28	4.83
7	2.88	2.88	3.36	-	3.27	3.98	2.89	2.88	3.36	-	3.26	4.01
6	2.88	2.88	3.45	-	3.26	7.41	2.88	2.88	3.49	-	3.23	5.78
5	2.87	2.87	3.43	-	2.93	7.42	2.87	2.87	3.25	-	3.17	7.18
4	2.86	2.86	3.17	-	2.91	7.39	2.84	2.84	3.19	-	2.92	6.59
3	2.82	2.82	-	-	3.18	-	2.80	2.80	-	-	3.17	-
2	2.81	2.81	-	-	3.17	-	2.78	2.78	-	-	3.15	-
1	3.02	3.02	-	-	-	-	3.02	3.02	-	-	-	-
base	-	-	-	-	3.04	-	-	-	-	-	3.10	-
	60% structure											
12	2.67	2.66	-	-	-	-						
11	2.66	2.66	-	-	8.69	-						
10	2.67	2.67	-	-	3.30	4.82						
9	2.91	2.91	9.57	-	3.31	2.94						
8	2.90	2.90	3.36	-	3.28	4.82						
7	2.89	2.89	3.33	-	3.26	4.01						
6	2.88	2.88	3.44	-	3.22	5.80						
5	2.86	2.86	3.24	-	3.16	7.39						
4	2.83	2.83	3.19	-	2.95	7.17						
3	2.79	2.79	-	-	3.16	-						
2	2.77	2.78	-	-	3.15	-						
1	3.02	3.02	-	-	-	-						
base	-	-	-	-	-	-						

- = did not yield

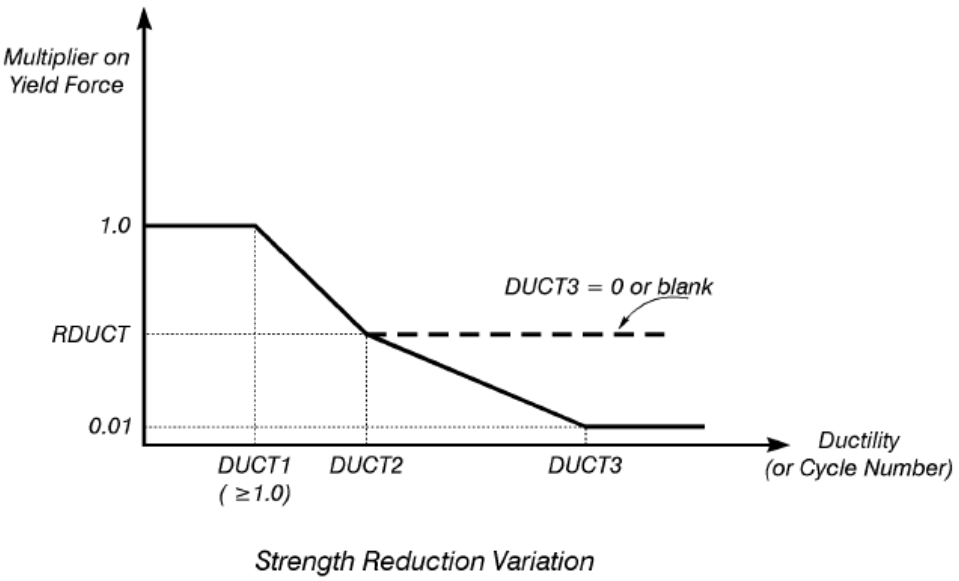

Figure 6-1 Strength degradation rule used for NLTH analysis in RUAUMOKO

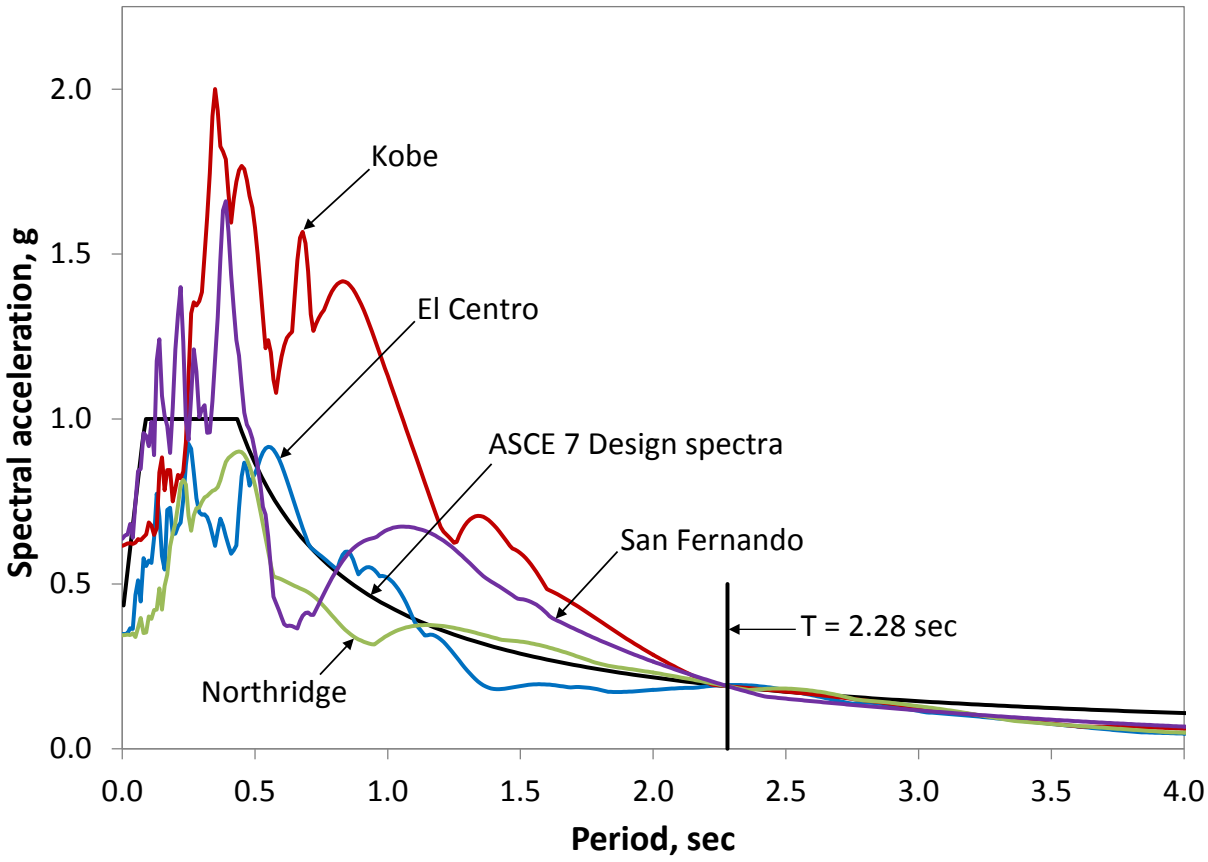

Figure 6-2 Response spectra for all ground motions

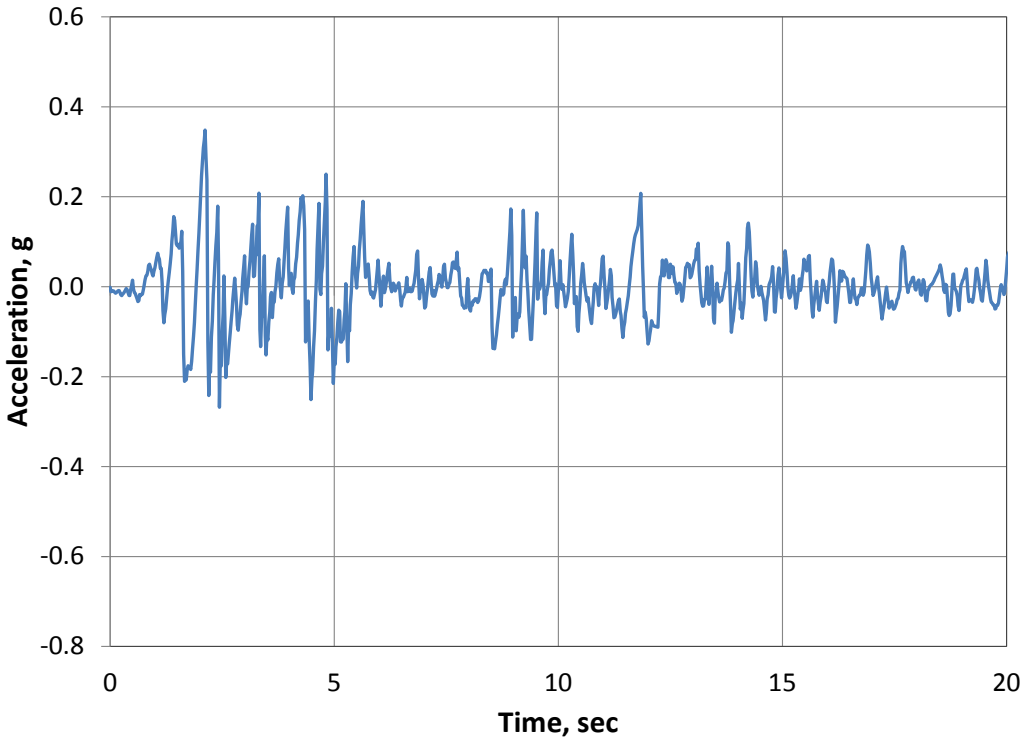

Figure 6-3 Scaled El Centro ground motion record

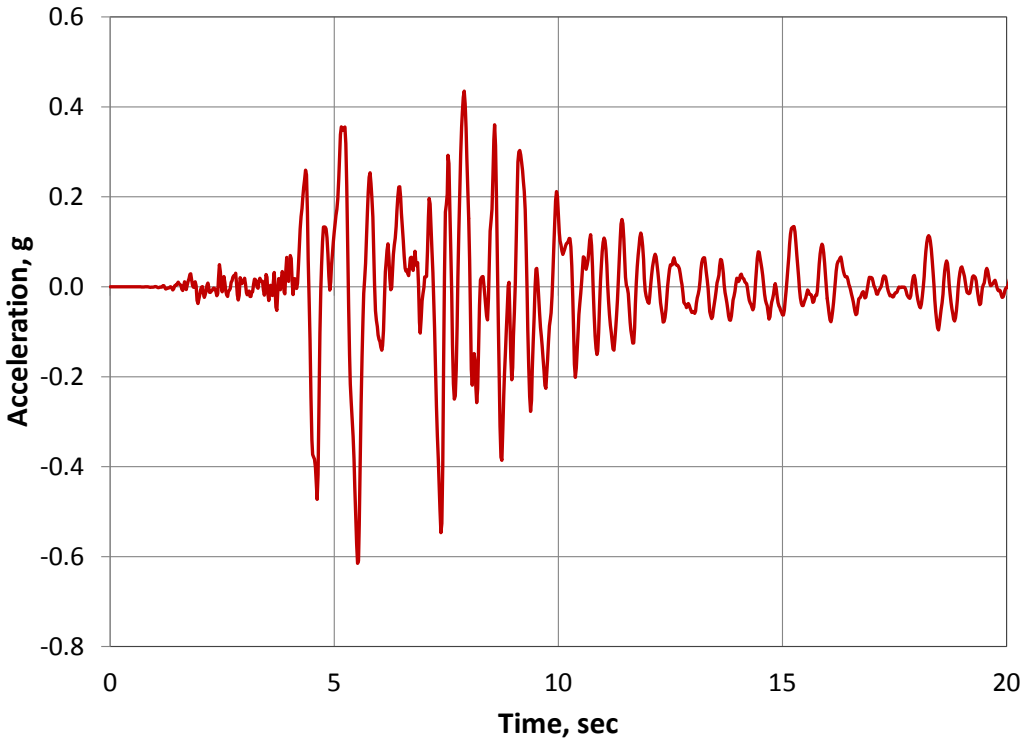

Figure 6-4 Scaled Kobe ground motion record

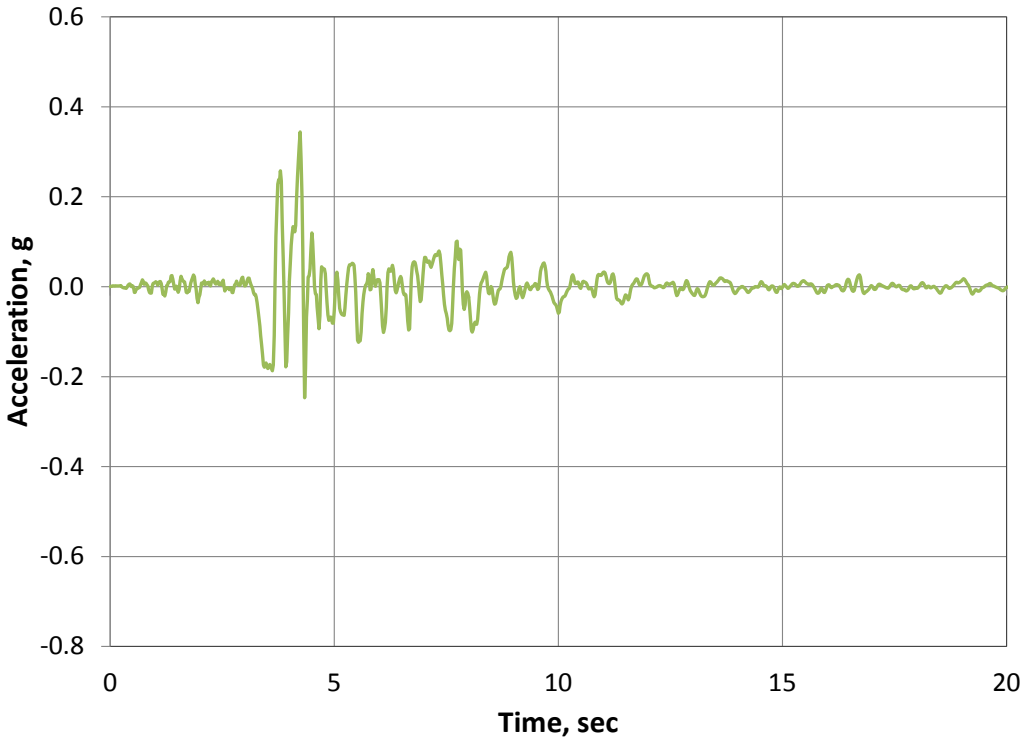

Figure 6-5 Scaled Northridge ground motion record

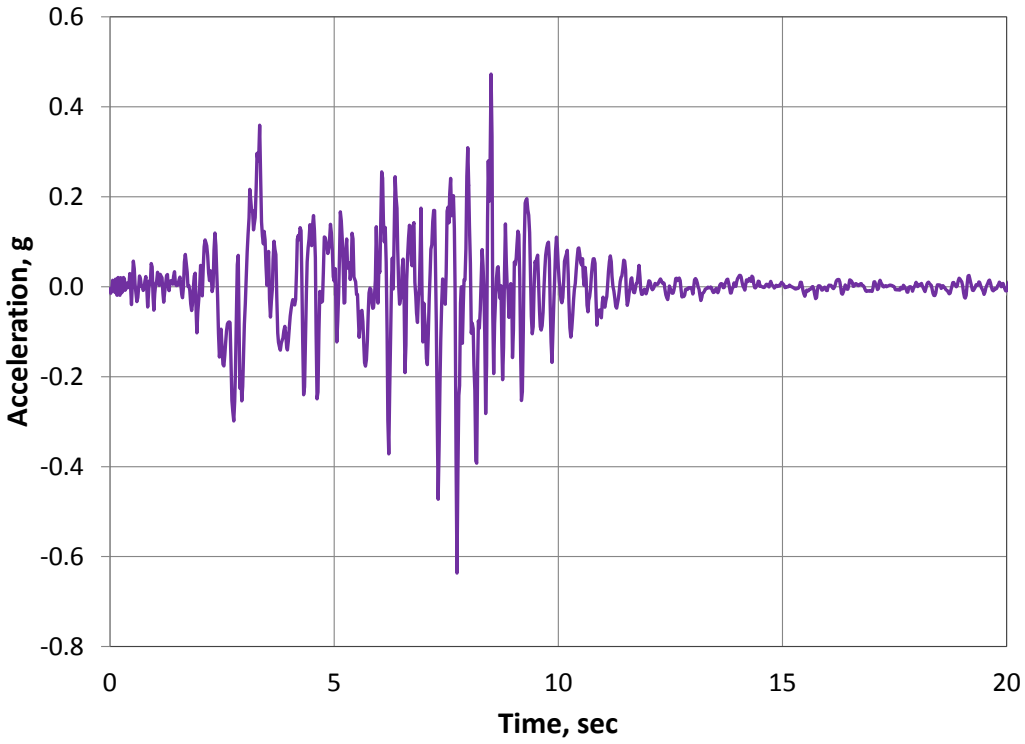

Figure 6-6 Scaled San Fernando ground motion record

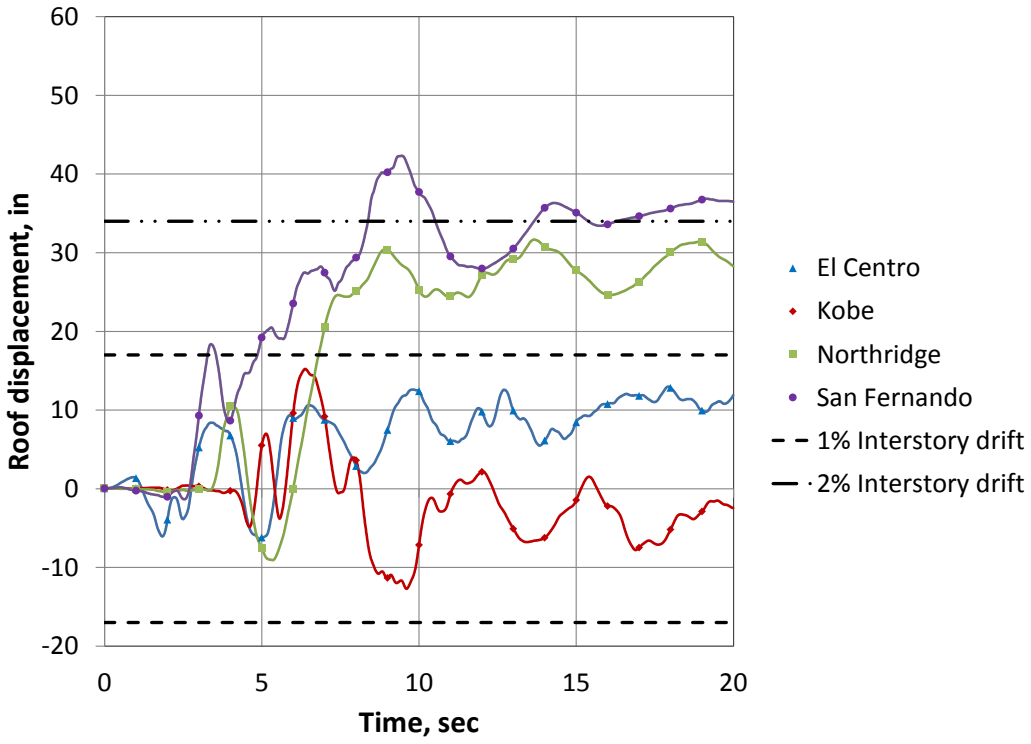

Figure 6-7 Roof displacement histories for the 100% prototype structure

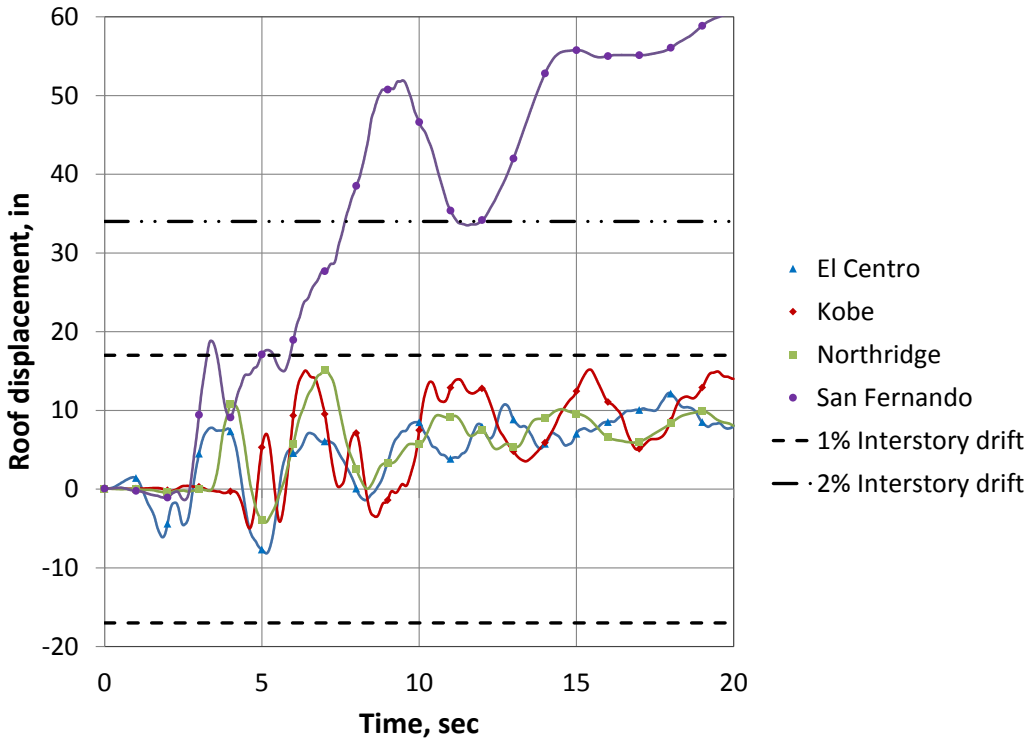

Figure 6-8 Roof displacement histories for the 90% prototype structure

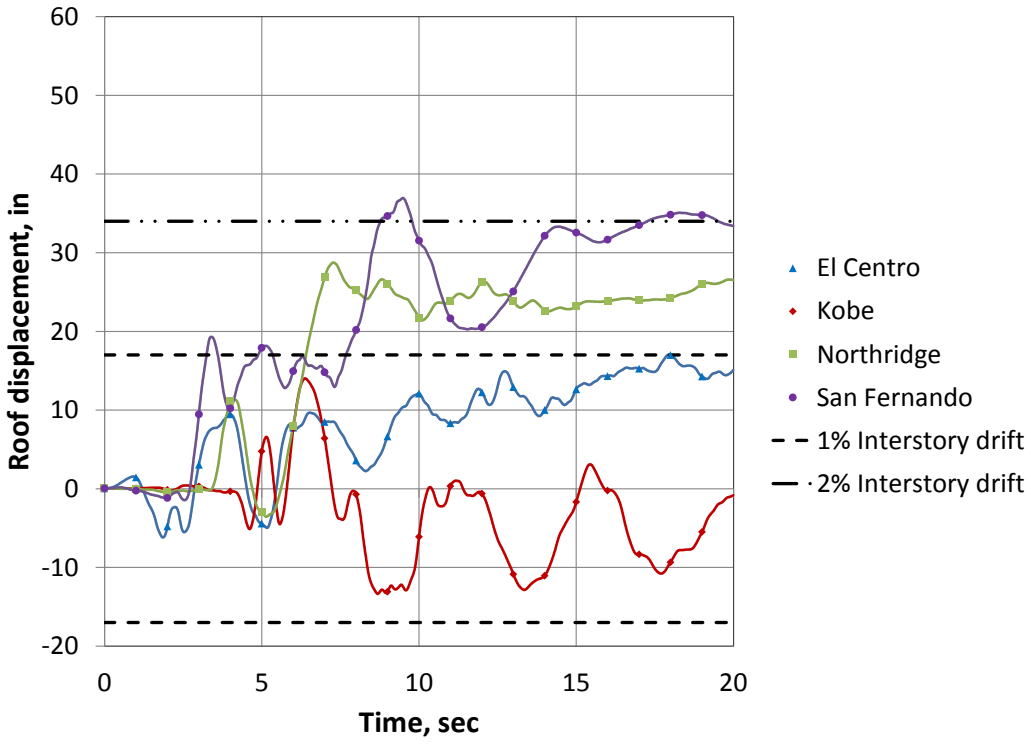

Figure 6-9 Roof displacement histories for the 80% prototype structure

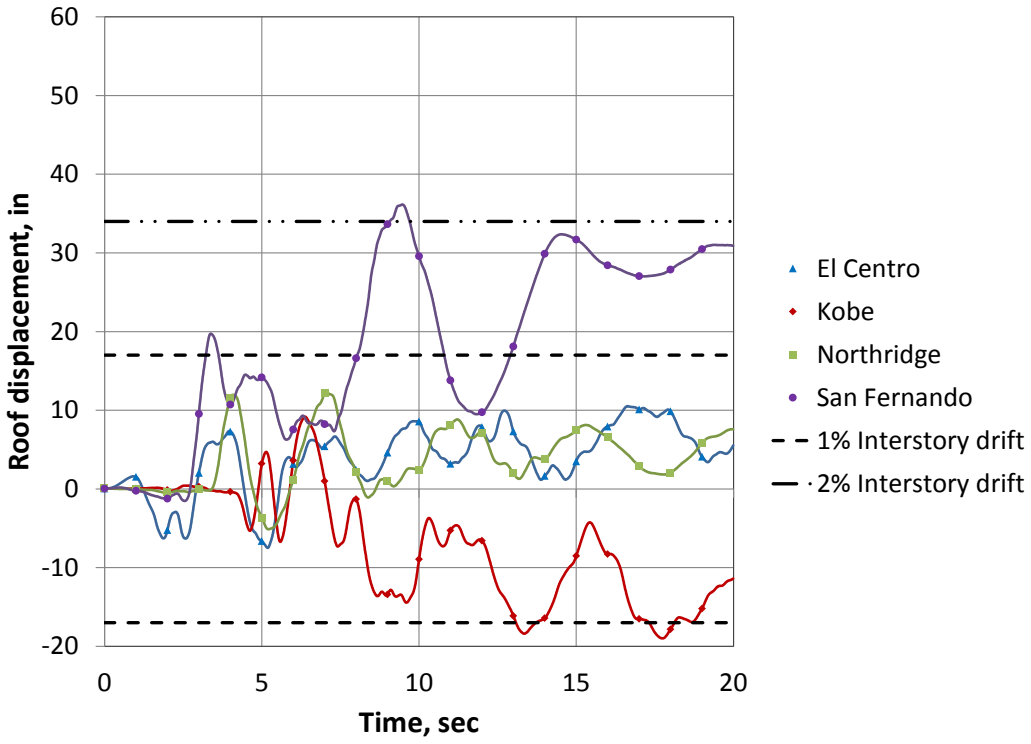

Figure 6-10 Roof displacement histories for the 70% prototype structure

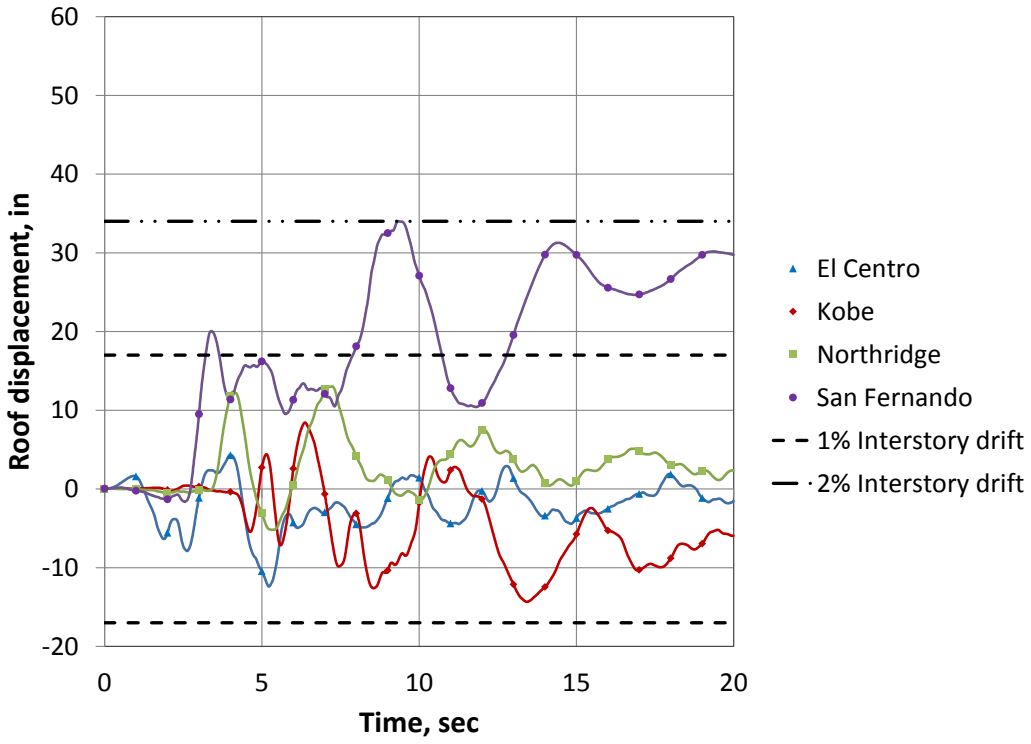

Figure 6-11 Roof displacement histories for the 60% prototype structure

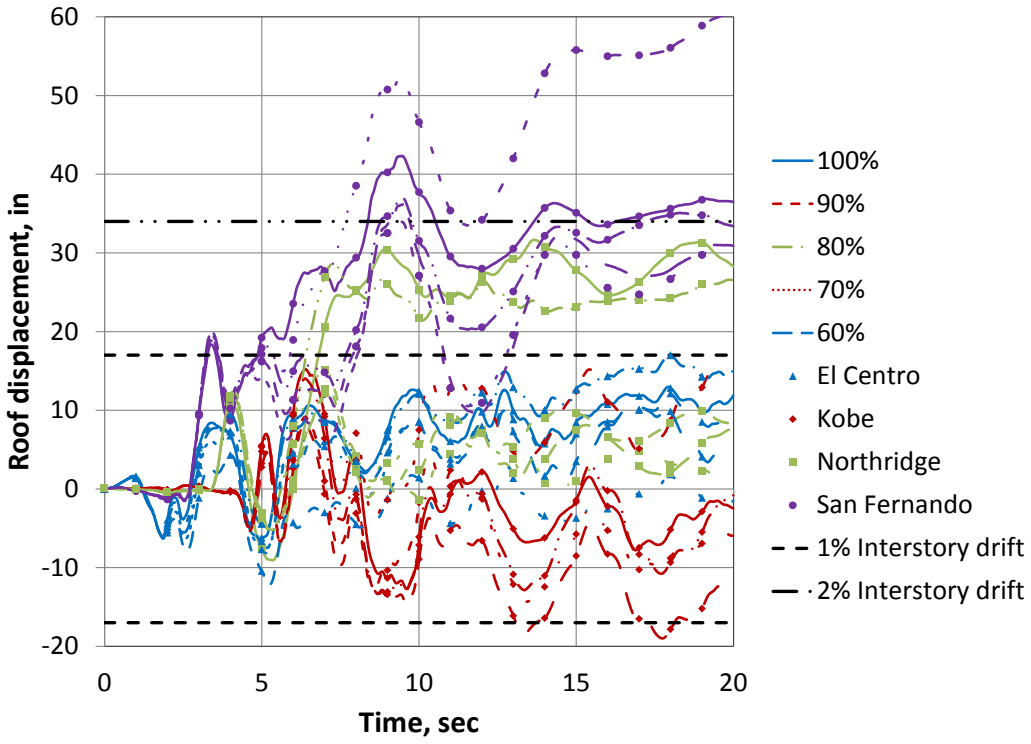

Figure 6-12 Roof displacement histories for all buildings for the suite of earthquakes considered

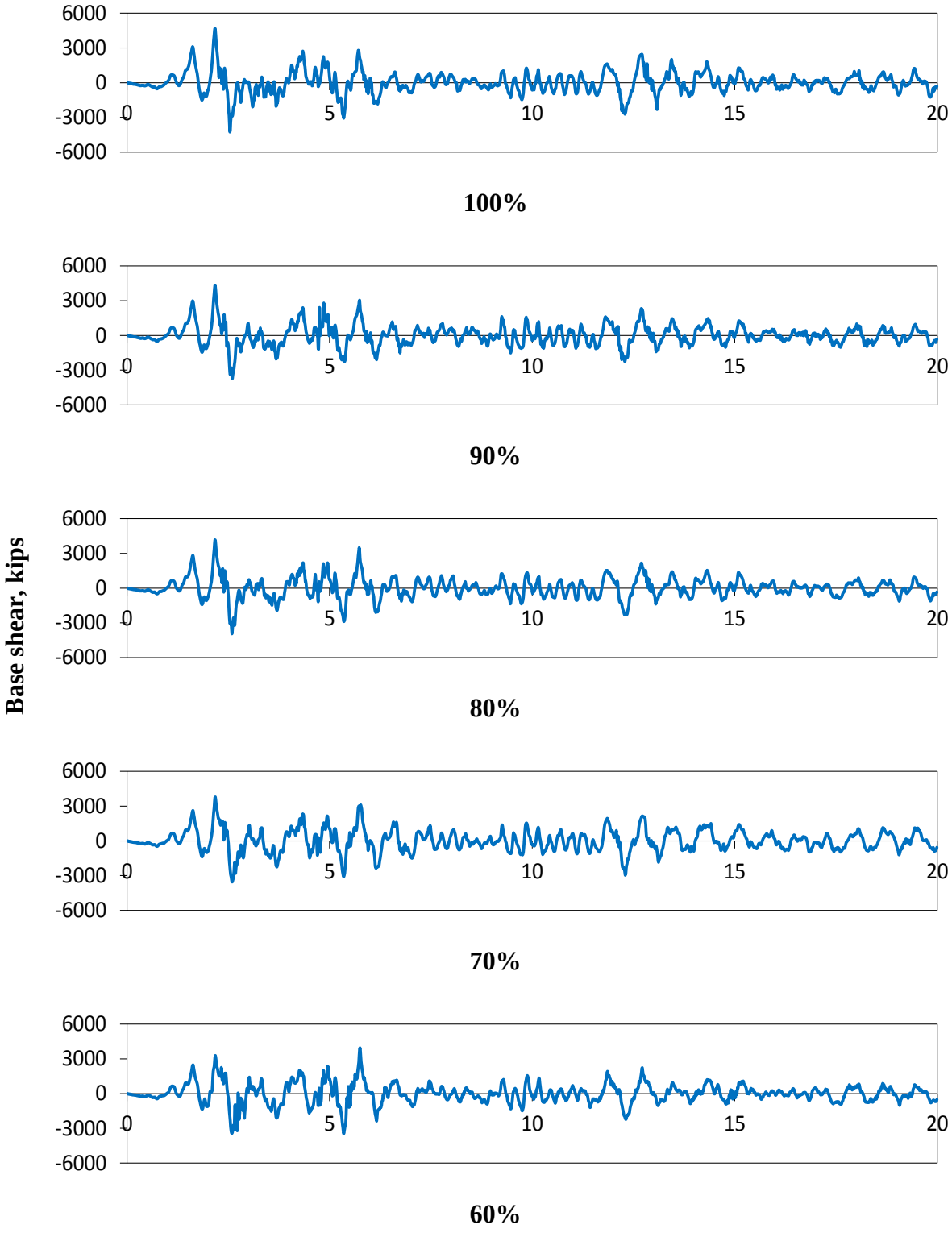

Figure 6-13 Base shear histories for all buildings during El Centro earthquake

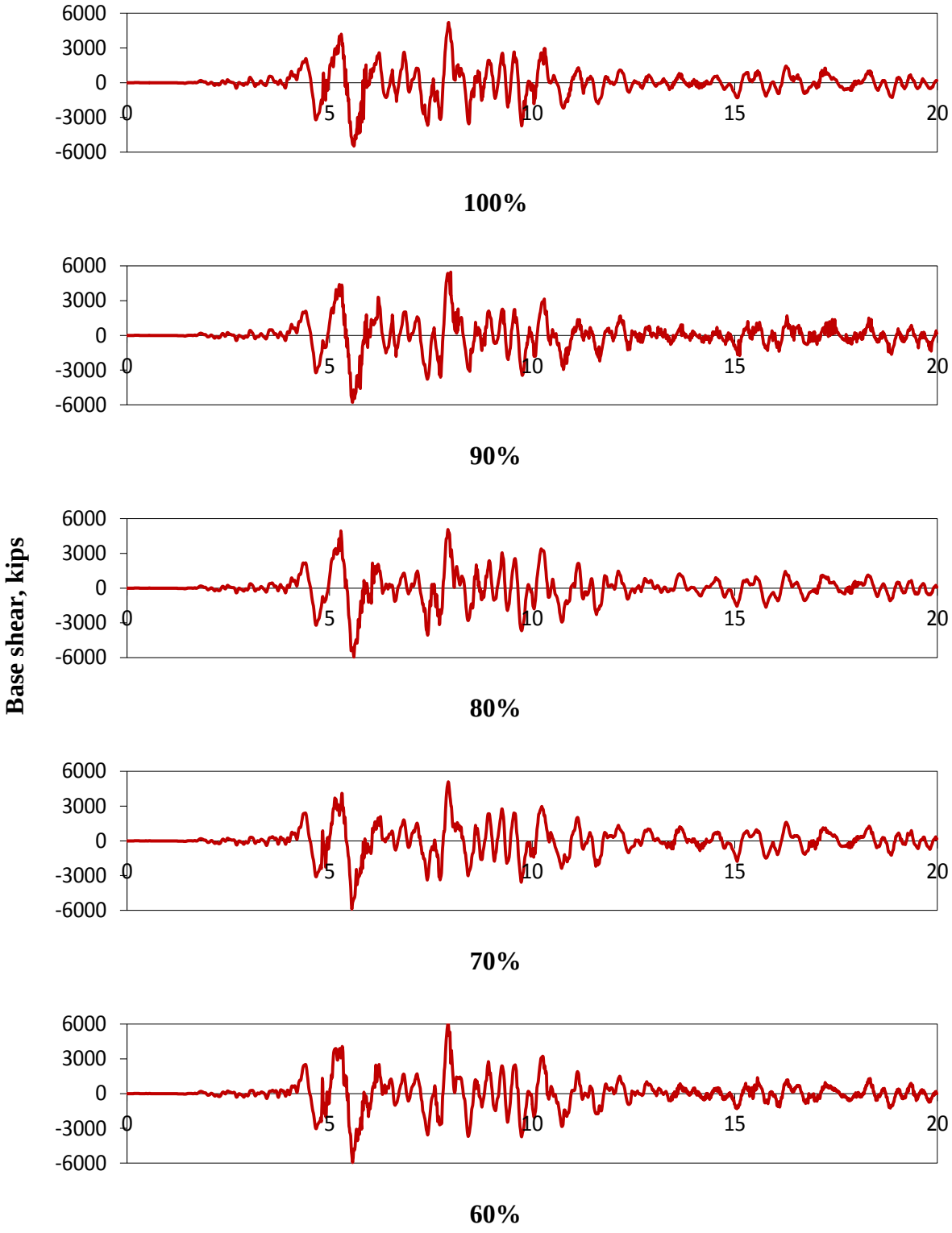

Figure 6-14 Base shear histories for all buildings during Kobe earthquake

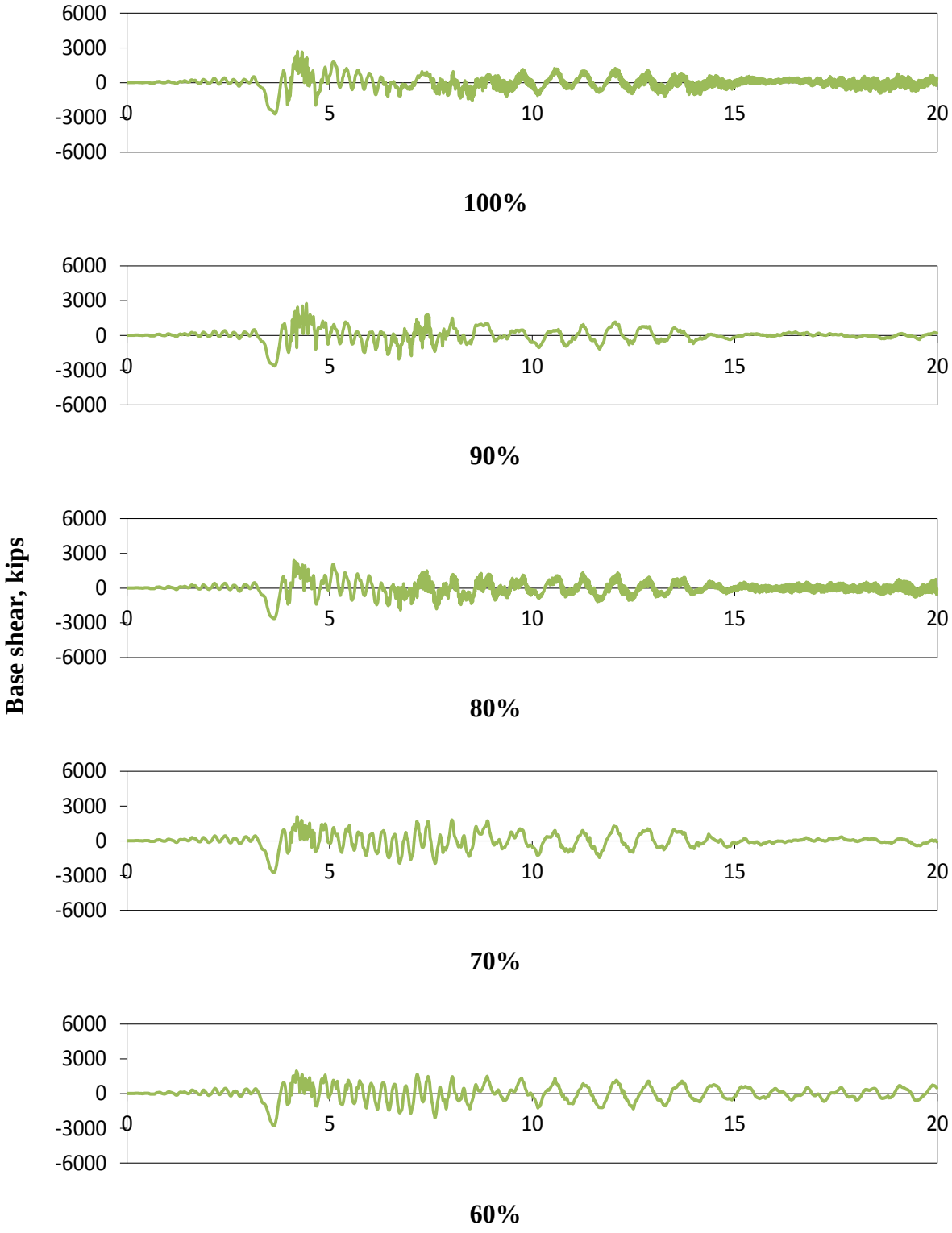

Figure 6-15 Base shear histories for all buildings during Northridge earthquake

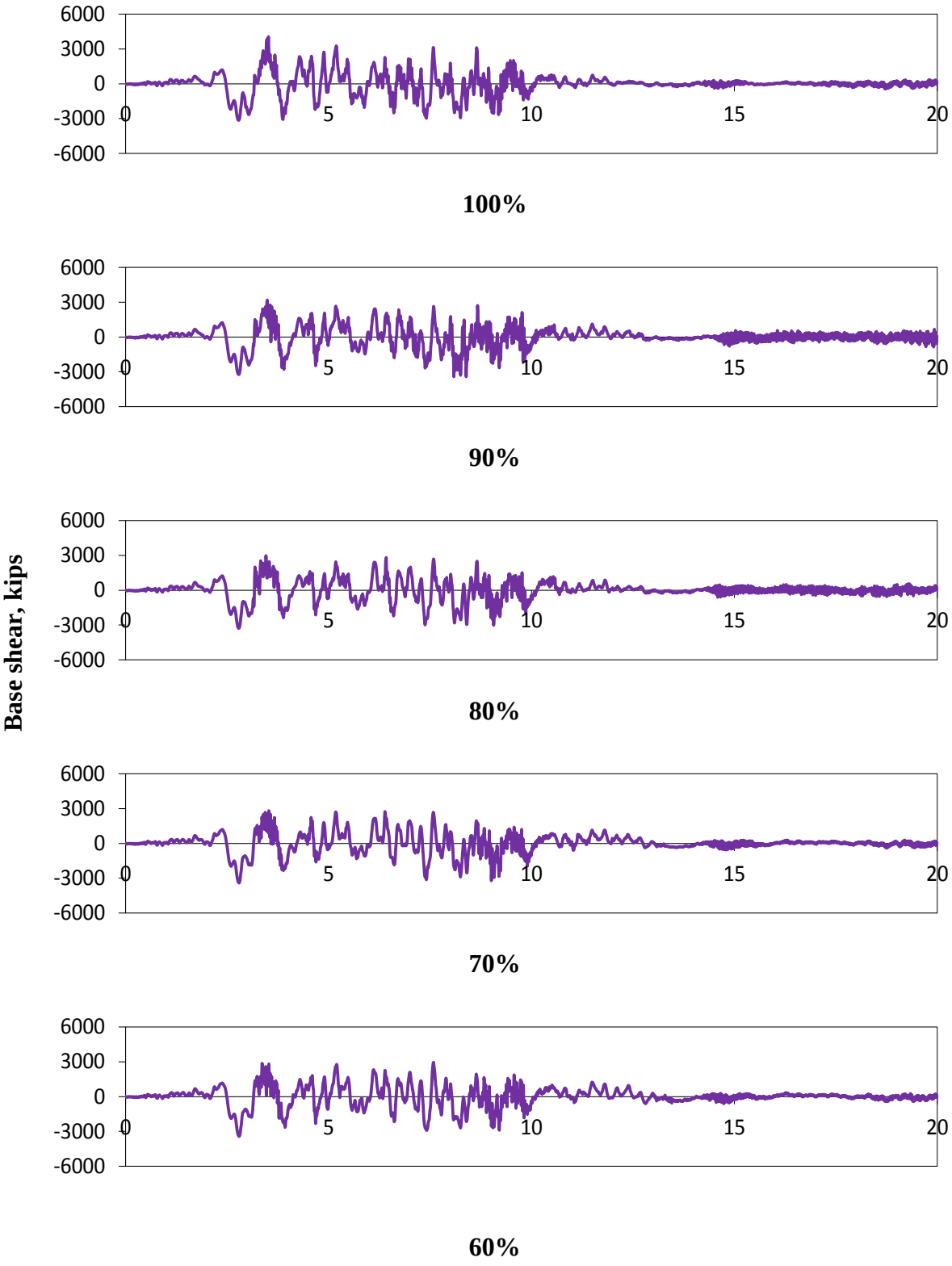

Figure 6-16 Base shear histories for all buildings during San Fernando earthquake

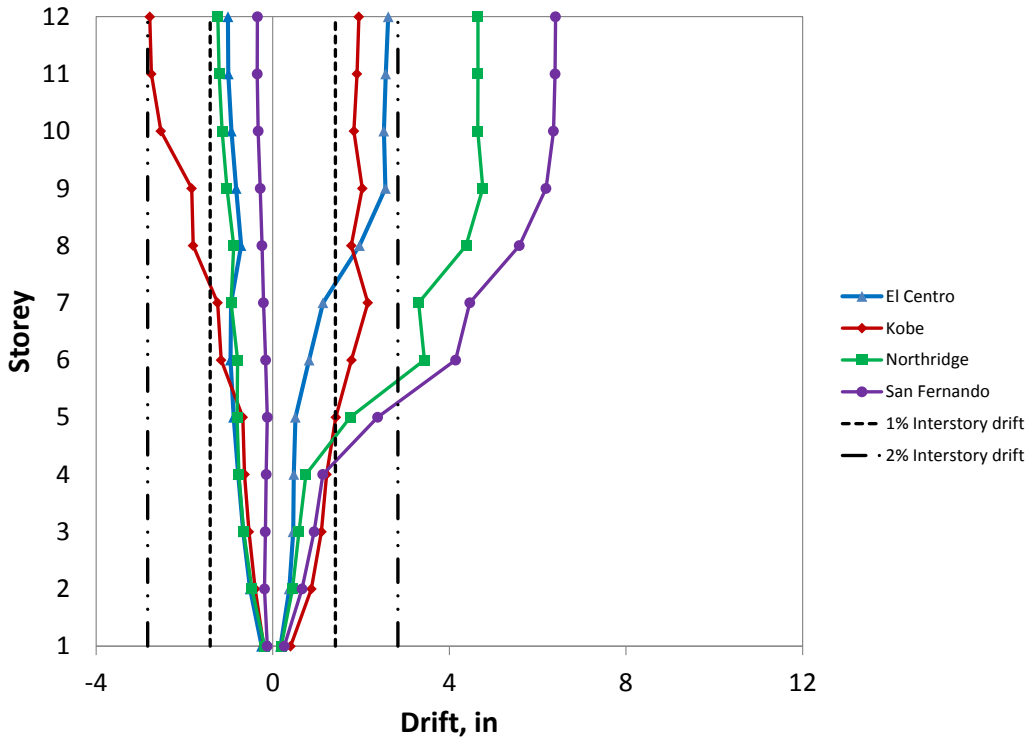

Figure 6-17 Interstorey drift envelopes for the 100% prototype structure

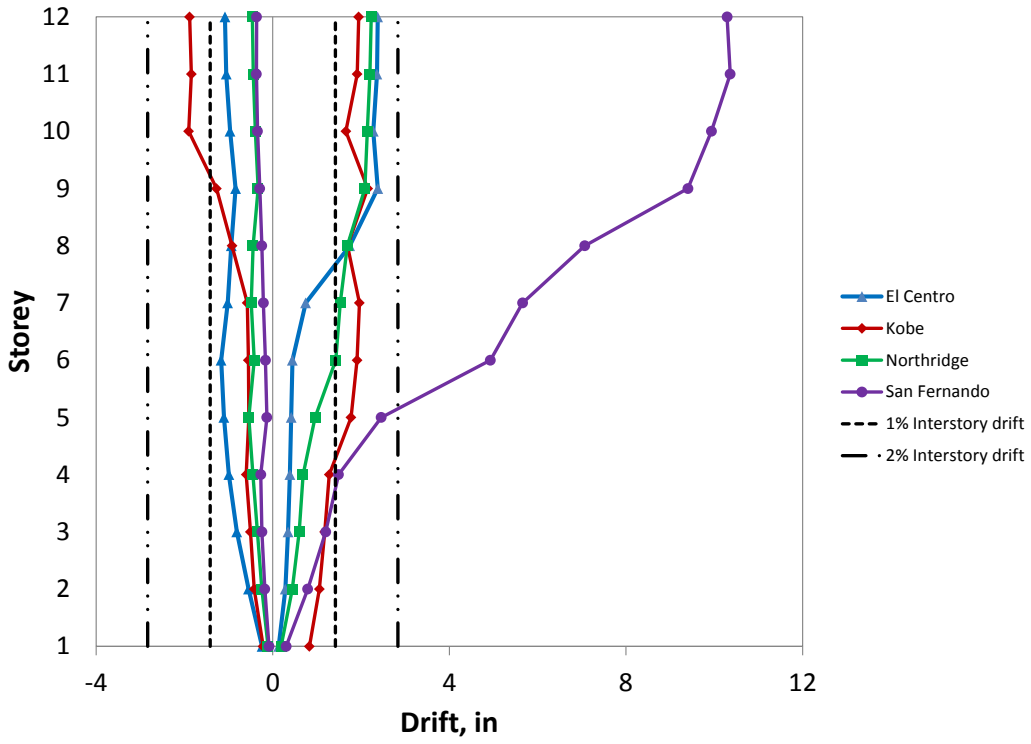

Figure 6-18 Interstorey drift envelopes for the 90% prototype structure

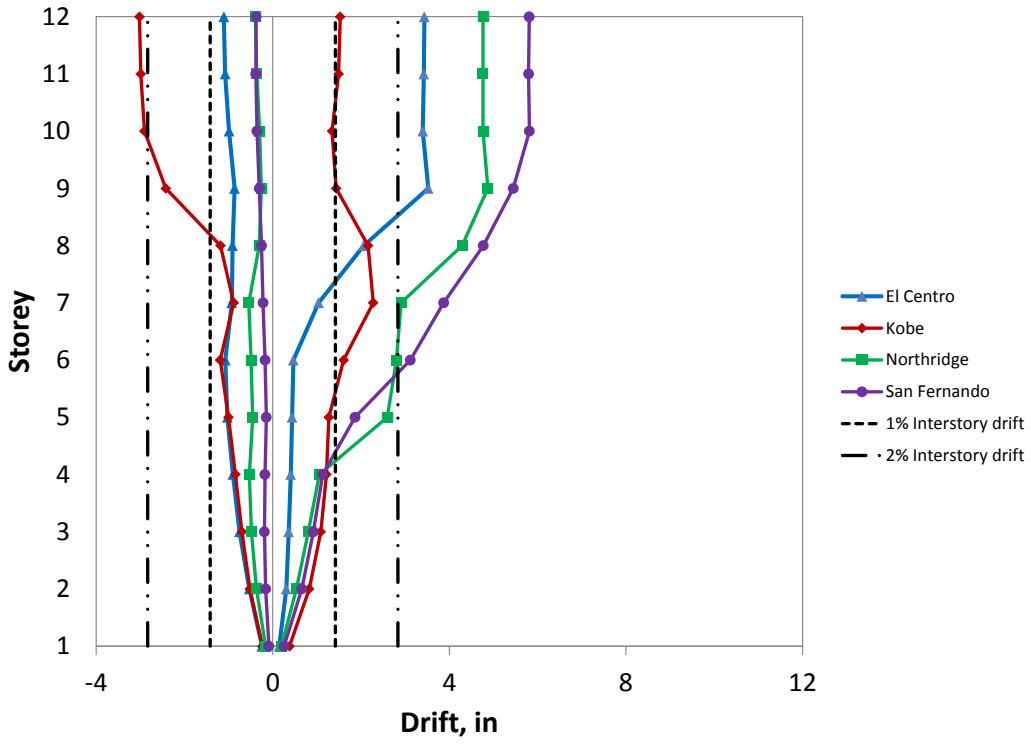

Figure 6-19 Interstorey drift envelopes for the 80% prototype structure

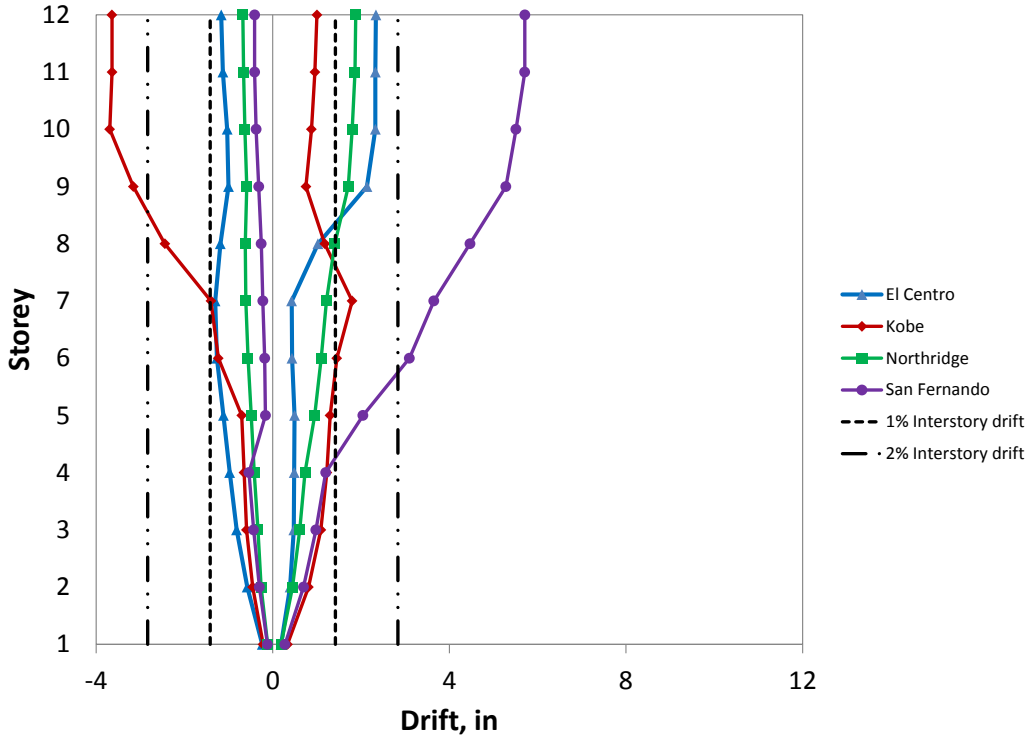

Figure 6-20 Interstorey drift envelopes for the 70% prototype structure

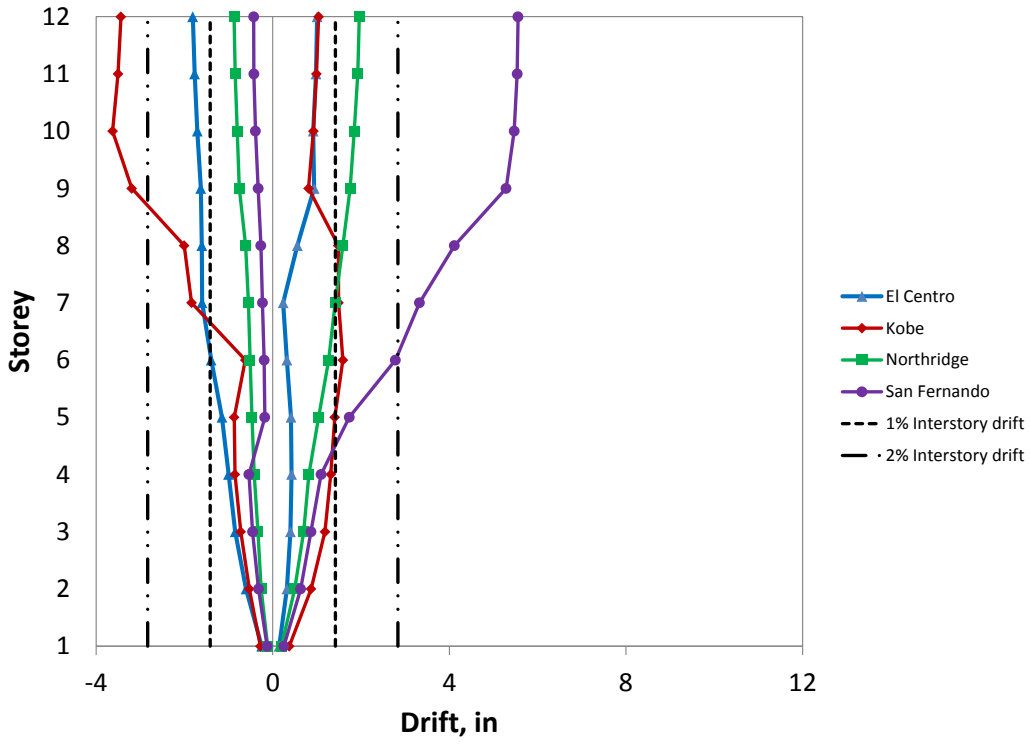

Figure 6-21 Interstorey drift envelopes for the 60% prototype structure

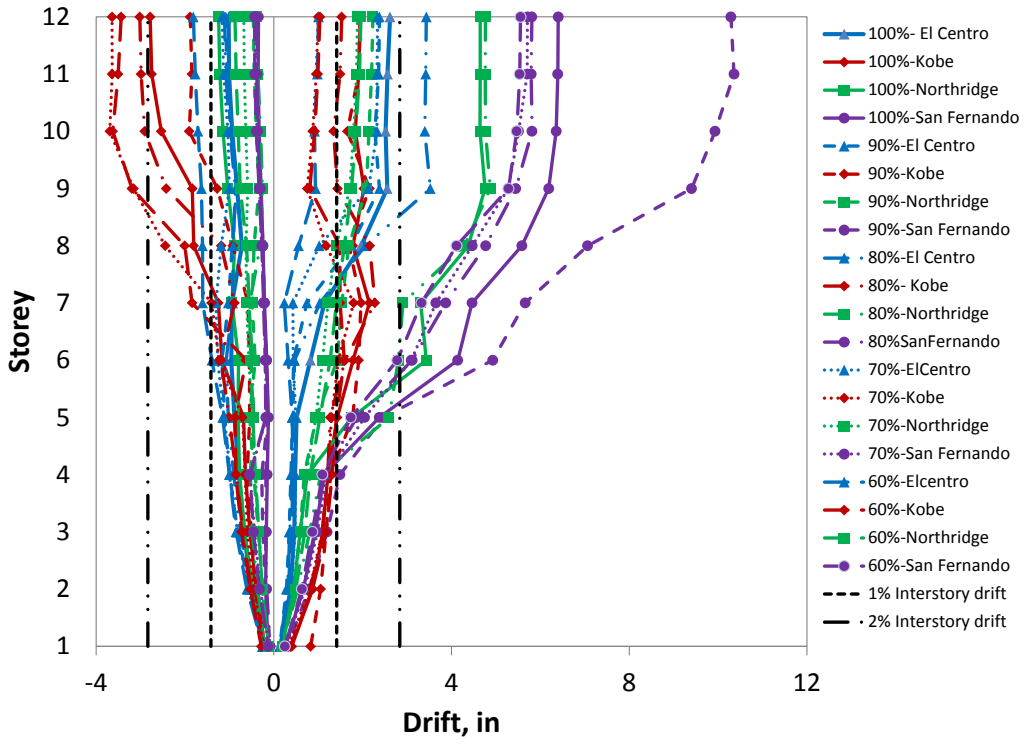

Figure 6-22 Interstorey drift envelopes for all buildings for the suite of earthquakes considered

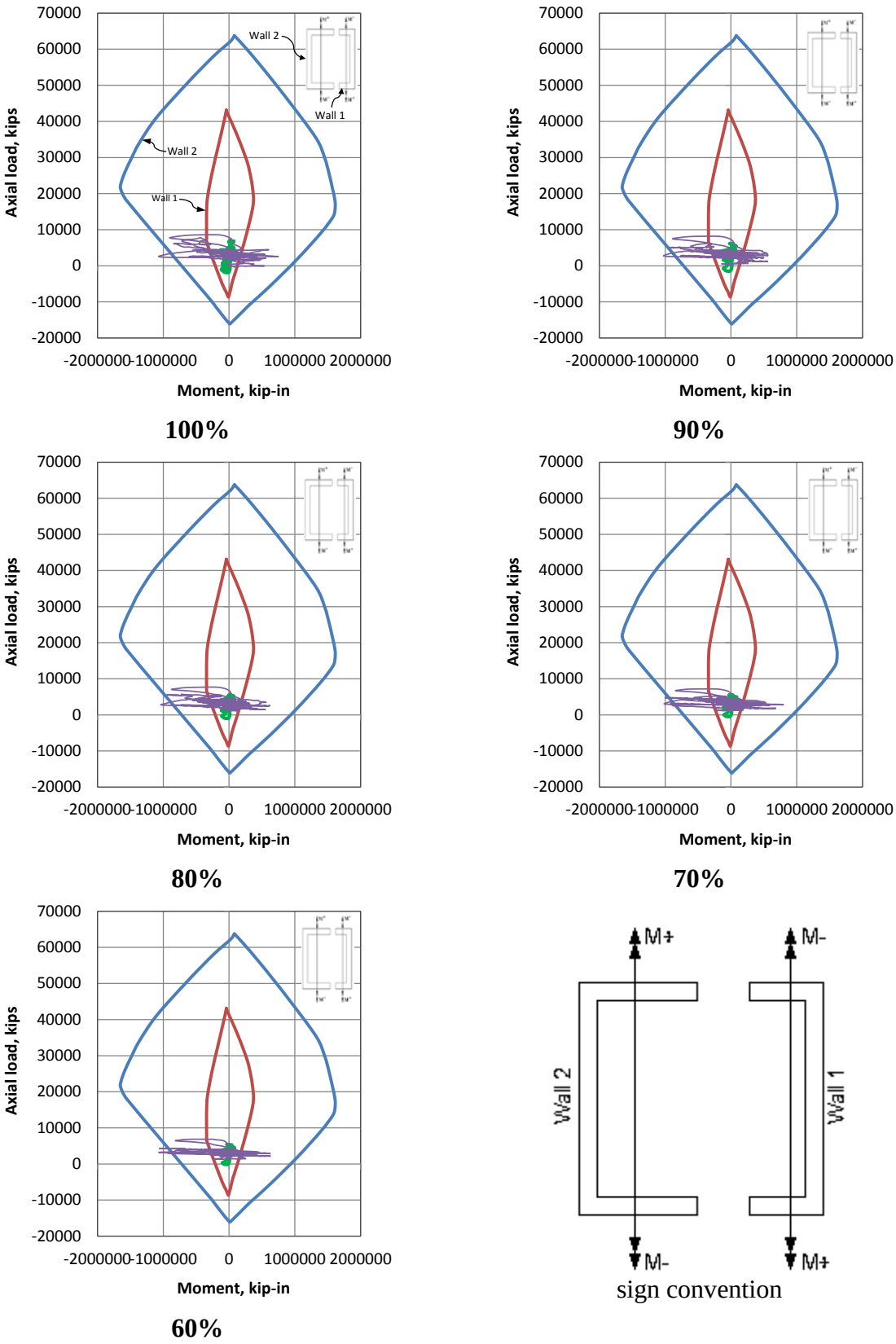

Figure 6-23 Axial load-moment interaction at the base of the two walls for the El Centro ground motion

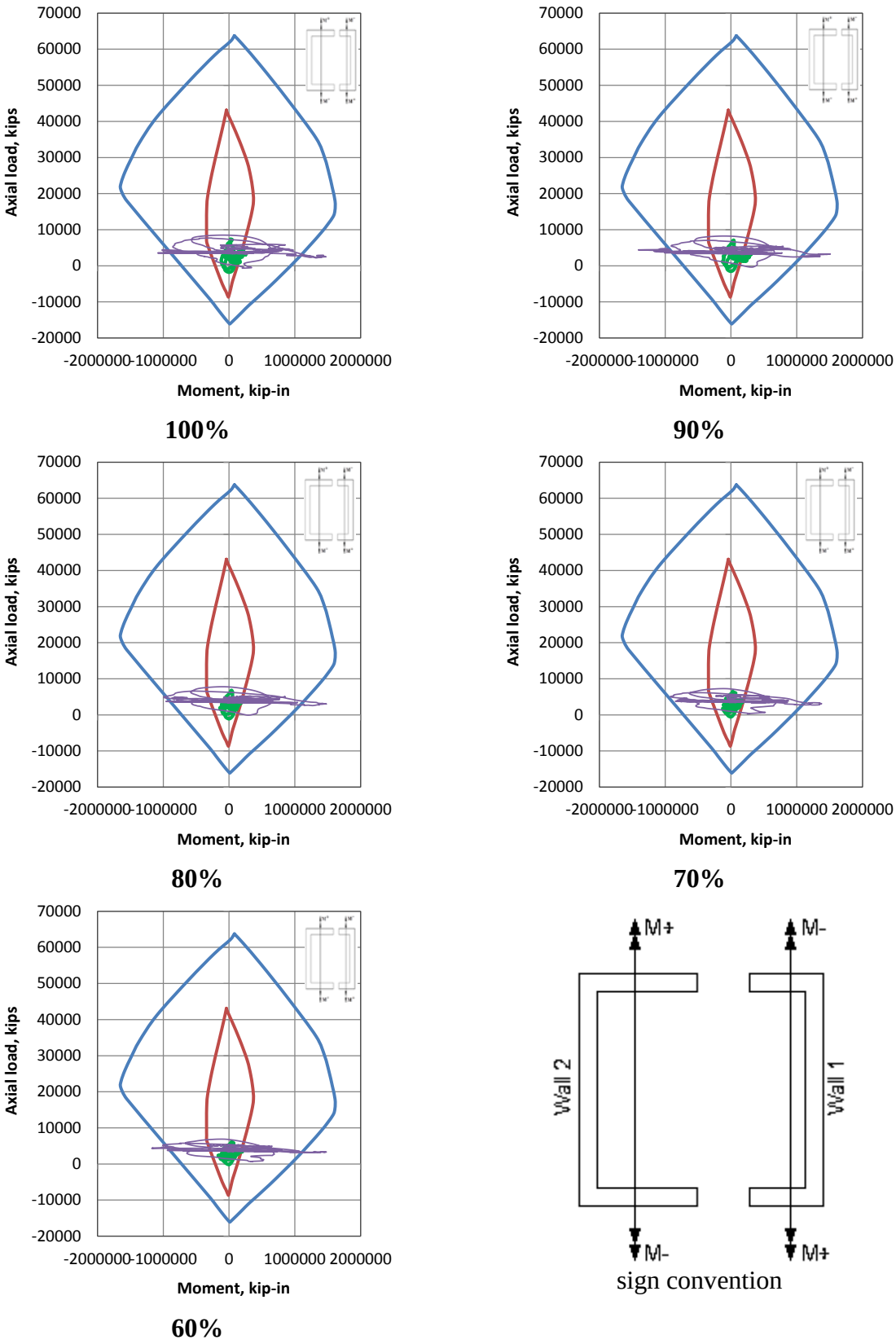

Figure 6-24 Axial load-moment interaction at the base of the two walls for the Kobe ground motion

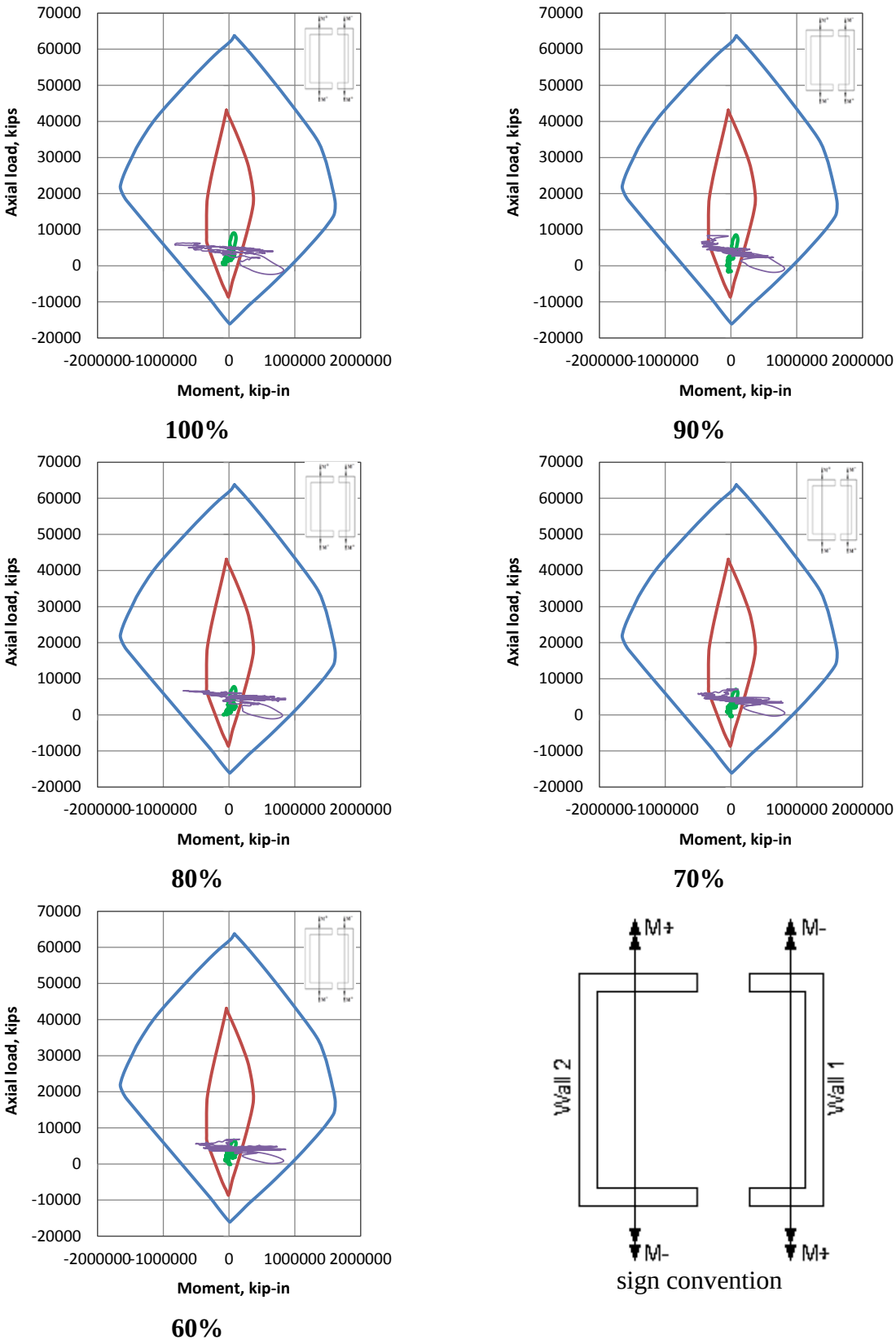

Figure 6-25 Axial load-moment interaction at the base of the two walls for the Northridge ground motion

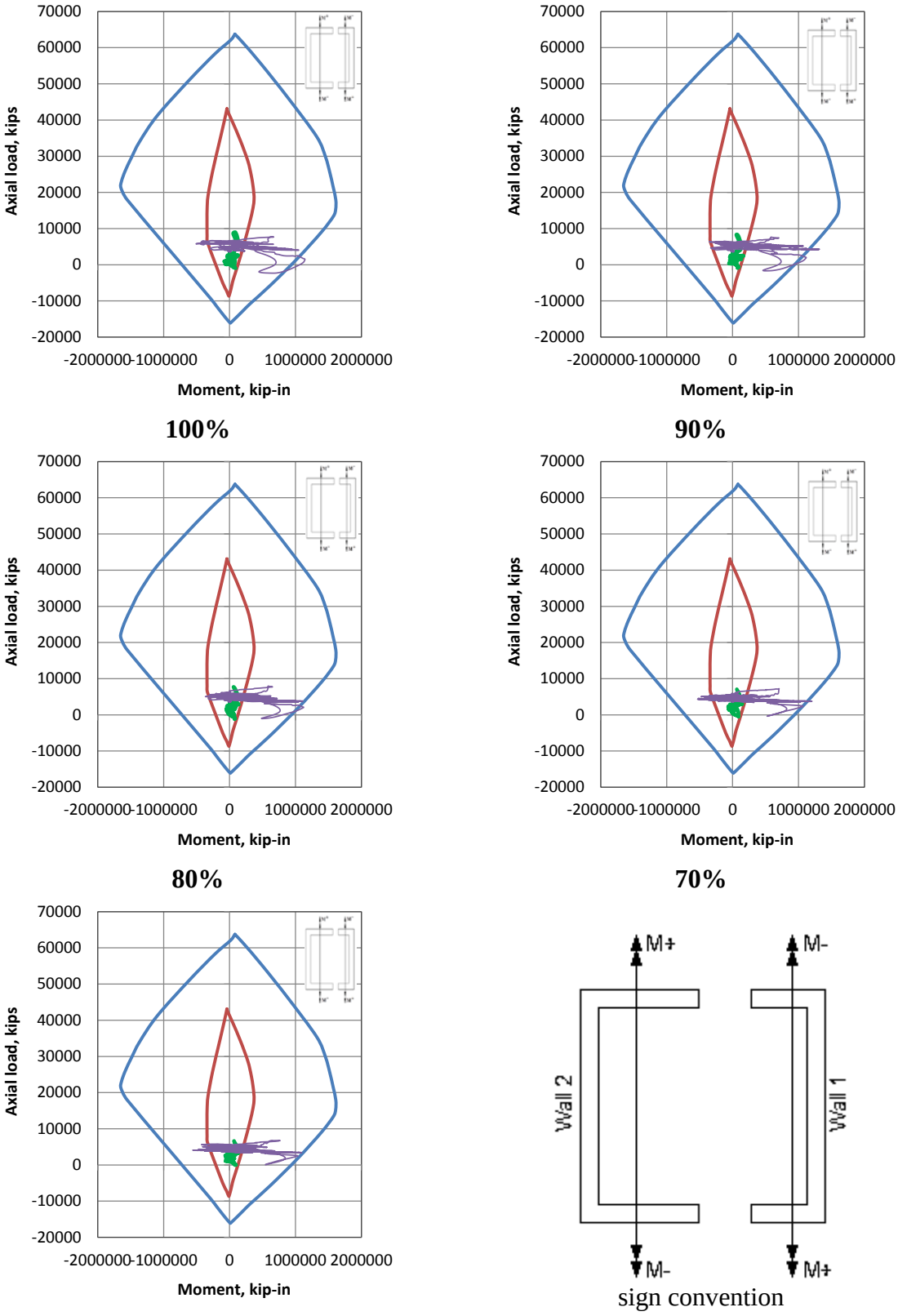

Figure 6-26 Axial load-moment interaction at the base of the two walls for the San Fernando ground motion

7.0 CONCLUSIONS AND RECOMMENDATIONS

The work presented in this dissertation contributes to the state of the art of coupled wall (CW) analysis and design by developing a unique design paradigm: expanding the concept of performance-based design into a domain where the nature of the structural form evolves within the context of the proposed performance objective. It was shown that damage to the coupling beams in a CW system occurs prior to the plastic capacity of the system being achieved. Furthermore, the damage is progressive; resulting in a structural system that does, in fact, evolve from behaving as a coupled wall (CW) system to behaving as a collection of linked wall piers (LWP) as shown schematically in Figure 1-1. Based on this evolution of performance, the LWP system was found to be subject to large demands since the system is behaving as a stiffer CW system at lower performance levels. The work also investigated a procedure for proportioning the coupling beams that leads to acceptable structural behavior and failure mechanisms of the CW systems.

The research in this work considered a prototype 12-storey reinforced concrete coupled core wall (CCW) building located in Seattle, Washington. Five CCW prototype structures, having varying degrees of coupling and the same wall piers are designed allowing the study of the effects of decayed coupling action to be carried out. Elastic analyses using the equivalent lateral force (ELF) procedure and the continuous medium method (CMM) were successfully utilized to establish initial proportions for the CCW system, and to determine the design forces

and moments. Nonlinear static and dynamic analyses are conducted to investigate the CCW structural behavior, adequacy of the design, and the evolution of the structural form from CCW system to a collection of linked wall piers (LWP). An additional unique aspect of this work was that the wall piers in the CCW were significantly different in terms of their dynamic and geometric properties: the moments of inertia of the two wall piers differed by almost an order of magnitude.

The analyses presented represent a methodology for examining CCW behavior and may be extended to a variety of other structural parameters or to other types of dual structural systems.

7.1 EVOLUTION OF CCW TO LWP

The performance objective based on the behavior of dual or evolving structural systems was investigated in this study. The nonlinear static analysis results presented in Chapter 5 showed that the CCW structures exhibited reasonable behavior as all prototype structures achieved ultimate capacities greater than the design capacity, and satisfied the roof drift requirement of 2%, indicating that the structures fulfilled the acceptance performance criteria for the life safety performance level (LS).

From the behavior of the five prototype structures in this analysis, it can be confidently said that the dual systems, consisted of reinforced concrete wall piers and steel coupling beams, performed very well and as what would be expected. The dual system provided superior lateral stiffness as a CCW in the elastic range, and maintained a good stiffness during the evolution toward a collection of linked wall piers (LWP). When the CCW structure (dual system) was

subjected to lateral demand, the system first resisted the lateral loads by a combination of actions: frame action generated by shear in the coupling beams and flexural behavior of the individual wall piers. During the evolution process, the frame action degraded as the steel coupling beams yielded and formed hinges at their ends and the moment resistance was redistributed to the walls piers.

The prototype structures satisfied even the 1% drift limit until the first yield of wall piers for both directions of analysis (WE & EW). This means that the prototype structures, working as LWP, fulfilled the life safety (LS) performance criteria.

At both the first yield of wall piers and the ultimate capacity stages, the coupling beams had essentially exhausted their capacities and experienced significant inelastic deformation demands, thus the CCW systems at these stages resist additional load as a collection of linked wall piers (LWP).

The different wall pier capacities also affected performance although did not result in a significant reduction in capacity as may be initially intuited. The results of the EW pushover analysis showed that the ultimate capacities of the five structures exceeded their counterparts in WE analysis. The higher capacities in the EW analyses result from the stiffer wall 2 being in compression and thus being even more dominant in the behavior of the system. In the WE analysis, when this wall was in tension, the overall system was more flexible since the dominant element was more flexible. Because the coupling beams in the WE pushover analysis yielded at a lower base shear than the EW analysis, the CCW evolved at lower applied lateral loads.

As expected, the structures having weaker coupling beams exhibited yield at lower lateral loads. The accompanying reduction in coupling stiffness, and therefore degree of coupling (doc), mitigated this effect although the wall pier demand clearly rose with reduced coupling. In every

case, however, the walls embodied sufficient overstrength to permit the overall structure to perform well.

The CCW system showed good energy dissipation capacity, as even with the coupling beam capacity exhausted, the system still had a reserve capacity greater than the design basis. Importantly, energy dissipation is distributed throughout the structure in both the coupling beams and wall piers making the CCW structure a very attractive option as lateral force resisting system (LFRS).

In the nonlinear analyses conducted (Chapter 6) the structures exhibited similar behavior to that predicted in the pushover analyses, although dynamic aspects of the structural behavior such as the effects of higher modes were identified. The dynamic analyses showed that, in general, all of the CCW systems behaved very well during the El Centro, Kobe and Northridge ground motions from the performance perspective of controlling roof drift.

Higher modes effects significantly affected all analyses. For the structures considered, both the second and third modes had relatively large participation factors and very high (15% and 6%, respectively) spectral ordinates for some of the ground motions used. This led to high base shear values, exceeding the code prescribed values, and some concentrated high interstorey drift values particularly at locations where the wall details transitioned vertically. The dynamic analyses supported the observations of the structural performance for the CCW systems in the pushover analyses, and consequently enhance the dual system evolution philosophy.

Considering the performance criteria of limiting the roof drift, it is seen that reducing coupling beams strength could be a key in developing constructible design (the need for this is developed by Harries et al. 2005), as the analyses indicated little significant change to global structural performance from coupling beams designed for 100% of their demand. Prototype

structures with coupling beams strengths to 80% satisfied the 1% drift limit, and all prototype structures satisfied the 2% drift limit.

Furthermore, the consideration of analyzing five CCW structures that differ by 10% in their coupling beams stiffness could be seen as standing surrogate for the deterioration process of the 100% structure. So, if the 60% structure is considered as a 'step' in this deterioration process, the system at this stage is still showing acceptable behavior by satisfying the 2% drift limit and having ultimate capacity exceeding the code design basis. The five analyses of different-strength/stiffness coupling beams allowed the visualization of how would the 100% structure respond to different levels of lateral demand at different levels of deteriorated strengths and stiffnesses.

The observations from the nonlinear static analyses would appear to vindicate the dual system approach proposed in this work: The structure behaves as a stiff coupled system for wind and moderate seismic loads and degrades to a collection of linked piers for high seismic loads. The inherent stiffness of a CW permits this evolution without exceeding performance drift limits (1-2%). Additionally, this behavior can be achieved using 'weaker' coupling beams. Such beams are easier to design (Harries et al. 2005) and may result in a wider practical use of CW systems.

7.1.1 A Note of the ELF Method of Design

Throughout this work, an inherent overstrength of the CCW design has been noted and described. Much of the inherent overstrength in the system is shown to have resulted from the ASCE 7-prescribed design procedure. The building base shear and the associated lateral loading were determined based on an ASCE 7-prescribed natural vibration period of T = 1.15 seconds, where the period obtained from Equation 4-5 was modified by a coefficient accounting for the

upper limit of the calculated period. However, it was shown by the subsequent frame analyses that the fundamental vibration period of the building was twice that obtained from the ELF procedure (T = 2.28 seconds for the 100% structure). The short period of vibration of 1.15 seconds led to a higher base shear which consequently led to an overly designed structure. It is clear that ELF formulas are intended to be conservative, are simple to use and may give good results with respect to the natural vibration period of frame structures, but they underestimate the natural vibration period of CW structures. Refined methods of analysis are permitted by ASCE 7-10; these will inevitably result in longer structural periods and therefore reduced values of base shear. Nonetheless, ASCE 7 clause 12.9.4.1 limits the resulting reduced base shear to 85% of that calculated using the ELF method (i.e.: $V_{design} \geq 0.85V$). Thus significant reductions through the use of more rigorous analysis are limited.

There are a number of researchers who suggested approximate formulas for the calculation of the natural fundamental period for coupled wall structures intended for preliminary design of CW structures that result in periods longer than would be calculated using the ASCE 7 design procedure. Permitting more realistic period calculations or increasing the C_u coefficient permitted for CW structures in ASCE 7 would result in more economical design for these structures.

7.2 OPTIMZATION USING FIXED POINT THEORY

Based on the fixed point theory (FPT) approach presented in Chapter 3, it is seen that the performance objective of minimization of transmissibility of horizontal ground motion through the optimization of coupling beam stiffness results in very small levels of required coupling

stiffness. The ‘required’ coupling beam dimensions are generally smaller than the depth of the concrete slab, let alone a practically dimensioned coupling beam.

Such low levels of coupling stiffness are structurally impractical using either concrete or steel coupling beams and would result in unacceptably low values for the degree of coupling (doc). The premise of the FPT optimization is to permit the structure to degrade from a CCW to a LWP, essentially allowing the doc to fall to zero. Nonetheless, the coupling elements in a typical CCW geometry also participate in the gravity load resistance and must maintain sufficient residual capacity to do so. The calculated beam dimensions in this case were generally inadequate to provide the required capacity. The effect of providing coupling stiffness based on practical coupling beam designs is to move the dynamic system away from the optimum case for minimizing transmissibility. That is to say, other design considerations – primarily the target doc (El-Tawil et al. 2009) will control the design of these coupling beams.

FPT applications in structural engineering are generally most applicable to problems having large frequency ratios ($\gamma = \omega_2/\omega_1$) such as when considering isolating vibrating equipment from a structure. In practice, the frequency ratio of practical CCW systems (considering structural layout and efficient resistance of lateral load) will rarely exceed $\gamma = 2.0$. This relatively low ratio makes optimization impractical or trivial with respect to the global structural performance.

7.3 RECOMMENDATIONS FOR FUTURE RESEARCH

7.3.1 Design of CCW Dual Systems

The current work presents a preliminary exploration of the use of the evolution of structural form for dual systems (CCW to LWP) in the context of performance-based design. For better understanding of this process, and before the generalization of results of this study, further research is required especially in terms of the following:

1. Other performance objectives such as the post-earthquake condition and reparability of the CCW components must also be considered to optimize the design of these structures.
2. Consideration of using different coupling details such as diagonally reinforced concrete coupling beams, and their effect on the evolution process must be investigated. This can be done using the approach demonstrated in this work.
3. The behavior of slab coupling should be investigated as described briefly in the following section.
4. Consideration of using more appropriate formulation for determining the natural vibration period of CW structures, as this is especially critical in the preliminary design stage.

7.3.2 Application of FPT

Considerably more research is necessary to identify a design space in which FPT is useful to the structural designer. As guidance for future study, the following applications are suggested:

1. The anticipated seismic performance of shear wall structures (those resisting lateral forces only through the summation of wall moments) may be enhanced by considering the beneficial effect of the small degree of coupling resulting from the floor diaphragm. While the diaphragm is not assumed to develop coupling frame action, it does act as a link between piers, affecting some interaction between individual piers and therefore the transmissibility of ground motion. Such an approach is not likely necessary in initial design but may serve the objectives of the seismic assessment of existing structures. The beneficial effects of 'slab coupling' may mitigate the need for seismic strengthening in some cases.
2. 'Mega-coupled' wall structures are those having coupling elements at only a few discreet locations rather than at each floor. Such systems are analogous to 'outrigger' structures which are relatively common in modern high-rise design. The performance of such structures, whose performance is dominated by few structural degrees of freedom and have few coupling locations, may benefit from the CCW to LWP design approach and therefore from the FPT optimization approach.

APPENDIX A

WALL PIERS DESIGN

Appendix A presents wall piers design worksheet. This worksheet was created using the computer program Mathcad 14 developed by Parametric Technology Corporation (PTC).

Design of Wall Piers

Note: The wall piers are designed to 100% of their demand

Walls Material Properties

$f_c := 45MPa = 6527 \cdot psi$

$f_y := 520MPa = 75420 \cdot psi$

$f_{yt} := 520MPa = 75420 \cdot psi$

$E_s := 200GPa = 29007548 \cdot psi$

Coupled Core Wall System Layout Plan

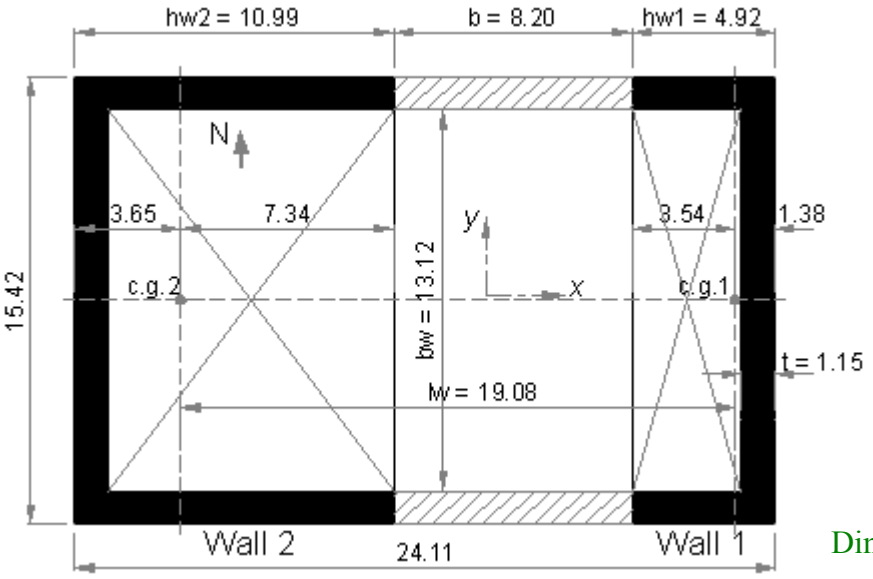

Dimensions are in feet

Geometric Properties of Wall Piers

$H_w := 141.73\ ft$ Total height of the Wall

$H_s := 11.81\ ft$ Story height

$h_{w1} := 4.92\ ft$ Wall 1 web length

$h_{w2} := 10.99\ ft$ Wall 2 web length

$l_w := 15.42\ ft$ Wall flange length

$t_w := 13.78\ in$ Wall thickness

$b_w := \left(l_w - 2 \cdot t_w\right) = 13.12 \cdot ft$ Wall interior width

$A_{w1} := 36.89\ ft^2$ Total area of the wall pier 1

$A_{w2} := 50.8272\ ft^2$ Total area of the wall pier 2

$X_{1\_Centroid} := 1.947\ ft$ X centroid of wall pier 1

$X_{2\_Centroid} := 4.851\ ft$ X centroid of wall pier 2

$I_{w1\_y} := 94.38\ ft^4$

$I_{w2\_y} := 901.81\ ft^4$

$I_{w1\_x} := 1533.56\ ft^4$

$I_{w2\_x} := 2406.44\ ft^4$

$I_{outrigger\_x} := 281.06\ ft^4$

$A_{c\_w1\_EW} := 21.82\ ft^2$ Total area of wall pier 1 web in EW directio

$A_{c\_w2\_EW} := 35.76\ ft^2$ Total area of wall pier 2 web in EW directio

$A_{cv\_w1\_EW} := A_{c\_w1\_EW}$

$A_{cv\_w2\_EW} := A_{c\_w2\_EW}$

$A_{c\_NS} := l_w \cdot t_w = 2549.85 \cdot in^2$ Area of one wall pier web in NS direction

Demand

Base Shear := 1691.01 kip

Total Overturning Moment := 159780.74 kip·ft

Axial Load Due to Frame Action := 4658.84 kip

Moment of Wall 1 in Coupling Direction := 7819.64 kip·ft

Moment of Wall 2 in Coupling Direction := 71288.8 kip·ft

Dead Load of Wall 1 := 2065.97 kip

Dead Load of Wall 2 := 2475.27 kip

Live Load of Wall 1 := 1077.19 kip

Live Load of Wall 2 := 1377.23 kip

$S_{DS} := 1$

Designations, Diameters, and Areas of Standard Bars:

Bar Number	3	4	5	6	7	8	9	10	11	14	18
Bar Diameter, in	0.375	0.5	0.625	0.75	0.875	1	1.128	1.27	1.41	1.693	2.257
Bar Area, in^2	0.11	0.20	0.31	0.44	0.60	0.79	1.00	1.27	1.56	2.25	4.00

Minimum Reinforcement:

Minimum vertical (ρ_v) and horizontal (ρ_h) web reinforcement ratios , by section 21.9.2.1 is 0.0025

Concrete cover: $cover := 2in$

First Design of Wall 1 (the Flexible Wall Pier)

a) Design in the Coupling Direction (EW Direction)

Design Forces

$V_{u\_w1\_EW} := \text{Base Shear}\cdot\left[I_{w1\_y} \div \left(I_{w1\_y} + I_{w2\_y}\right)\right] = 160\cdot kip$

$M_{u\_w1\_EW} := \text{Moment of Wall 1 in Coupling Direction} = 7820\cdot kip\cdot ft$

$P_{u\_w1\_Tension} := 0.9\cdot\text{Dead Load of Wall 1} - 0.2\cdot S_{DS}\cdot\text{Dead Load of Wall 1} - \text{Axial Load Due to Frame Action} = -3213\cdot kip$

$P_{u\_w1\_Compression} := 1.2\cdot\text{Dead Load of Wall 1} + 0.5\cdot\text{Live Load of Wall 1} + 0.2\cdot S_{DS}\cdot\text{Dead Load of Wall 1 ...} = 8090\cdot kip$
$+ \text{Axial Load Due to Frame Action}$

Check the Reinforcemnt Ratios Reduction Condition

Section 14.3 permits a reduction in the minimum vertical and horizontal reinforcement ratios if:

$V_u \le A_c\sqrt{f'_c}$

$V_{u\_w1\_EW} = 160\cdot kip$

$\text{Redution Limit}_{w1\_EW} := A_{c\_w1\_EW}\cdot\sqrt{\frac{f_c}{psi}}\cdot psi = 253.84\cdot kip$

$case_1 := \text{"Permitted"} \qquad case_2 := \text{"Not permitted"}$

$\text{Reduction in minimum reiforcement ratios}_{w1\_EW} := \text{if}\left(V_{u\_w1\_EW} \le \text{Redution Limit}_{w1\_EW}, case_1, case_2\right)$

$\text{Reduction in minimum reiforcement ratios}_{w1\_EW} = \text{"Permitted"}$

The minimum vertical & horizontal reinforcement ratio will be kept for consistency as

$\rho_{min\_w1\_EW} := 0.0025$

Check Two Curtains Requirment

Section 21.9.2.2 requires at least two curtains of reinforcemnt, for both ρ_v and ρ_h if:

$$V_u > 2A_c\sqrt{f_c'}$$

$V_{u\_w1\_EW} = 160.21 \cdot kip$

$\text{Two curtains limit}_{w1\_EW} := 2 \cdot A_{c\_w1\_EW} \cdot \sqrt{\frac{f_c}{psi}} \cdot psi = 507.68 \cdot kip$

$\text{Case}_1 :=$ "One curtain is enough in each direction" $\quad \text{Case}_2 :=$ "Two curtains are required for each direction"

$\text{Numer of reinforcemnt curtains}_{w1\_EW} := \text{if}\left(V_{u\_w1\_EW} \le \text{Two curtains limit}_{w1\_EW}, \text{Case}_1, \text{Case}_2\right)$

$\text{Numer of reinforcemnt curtains}_{w1\_EW} =$ "One curtain is enough in each direction"

Design for Shear

The shear strength is given by

$$\varphi V_n = \varphi A_{cv}\left(\alpha_c\sqrt{f_c'} + \rho_n f_y\right)$$

$\phi := 0.6$

Set $\alpha_c := 2.0$

Set $\phi V_n = V_u$

$$\rho_h = \frac{1}{f_y}\cdot\left(\frac{V_u}{\phi \cdot A_{cv}} - \alpha_c \cdot \sqrt{f_c}\right)$$

$$\rho_{h\_w1\_EW\_required} := \max\left[\frac{1}{f_y}\cdot\left[\frac{V_{u\_w1\_EW}}{\phi\cdot\left(A_{cv\_w1\_EW}\right)} - \alpha_c\cdot\sqrt{\frac{f_c}{psi}}\cdot psi\right], \rho_{min\_w1\_EW}\right] = 0.0025$$

Select Reinforcement

Try # 4 each face in horizontal direction

$\text{Horizontal Bar \#}_{w1\_EW} := 4$

$d_{b\_h\_w1\_EW} := \#4 \text{ daimeter} \cdot in = 0.5 \cdot in$

$A_{b\_h\_w1\_EW} := \#4 \text{ area} \cdot in^2 = 0.2 \cdot in^2$

$$S_{h\_w1\_EW} := \text{floor}\left[\frac{\left(2 \cdot A_{b\_h\_w1\_EW}\right)}{\left(\rho_{h\_w1\_EW\_required}\right)\cdot t_w \cdot in}\right]\cdot in = 11 \cdot in$$

Consider Maximum Reinforcement Spacing

$\text{Maximum Spacing} := 18\text{in}$

$S_{h\_w1\_EW} := \text{if}\left(S_{h\_w1\_EW} < \text{Maximum Spacing}, S_{h\_w1\_EW}, \text{Maximum Spacing}\right) = 11\cdot\text{in}$

$\rho_{h\_w1\_EW\_provided} := \dfrac{2\cdot\left(A_{b\_h\_w1\_EW}\right)}{\left(S_{h\_w1\_EW}\right)\cdot t_w} = 0.00264$

Calculate Nominal Shear Strength

$\phi V_{n\_w1\_EW} := \phi\cdot A_{cv\_w1\_EW}\cdot\left(2\cdot\sqrt{\dfrac{f_c}{\text{psi}}}\cdot\text{psi} + \rho_{h\_w1\_EW\_provided}\cdot f_y\right) = 679.82\cdot\text{kip}$

$\text{Result}_1 := \text{"Check is OK"}$ $\text{Result}_2 := \text{"Check is NOT OK"}$

Check Shear Strength

$\text{Shear Strengh}_{w1\_EW} := \text{if}\left(\phi V_{n\_w1\_EW} > V_{u\_w1\_EW}, \text{Result}_1, \text{Result}_2\right)$

$\text{Shear Strengh}_{w1\_EW} = \text{"Check is OK"}$

Use #4 at 11in each face in horizontal direction

Check for Maximum Allowable Nominal Shear Strength

$V_n \le 10A_{cv}\sqrt{f_c'}$

$\text{Nominal Shear Strength Limit}_{w1\_EW} := 10\cdot A_{cv\_w1\_EW}\cdot\left(\sqrt{\dfrac{f_c}{\text{psi}}}\cdot\text{psi}\right) = 2538.42\cdot\text{kip}$

$\text{Max Allowable Nominal Shear Strength}_{w1\_EW} := \text{if}\left(\phi V_{n\_w1\_EW} \le \text{Nominal Shear Strength Limit}_{w1\_EW}, \text{Result}_1, \text{Result}_2\right)$

$\text{Max Allowable Nominal Shear Strength}_{w1\_EW} = \text{"Check is OK"}$

Need for Boundary Elements

Stress index procedure

Sections 21.9.6.3 requires special boundary elements at boundaries and edges around openings of structu walls where the maximum extreme fiber compressive stress, corresponding to load combinations includin earthquake effects exceeds $0.2f_c'$

$0.2\cdot f_c = 1.31\cdot\text{ksi}$

The states of stresses will be checked at two extreme points 'points A and B in the figure below'

$$S_{A\_w1} = \frac{I_{w1\_y}}{c_{A\_w1}} \qquad c_{A\_w1} := 1.381\ ft \quad c_{B\_w1} := 3.54\ ft$$

$$S_{A\_w1} := \frac{I_{w1\_y}}{c_{A\_w1}} = 118094.6 \cdot in^3$$

$$S_{B\_w1} := \frac{I_{w1\_y}}{c_{B\_w1}} = 46070.24 \cdot in^3$$

$$\sigma_{A\_w1} := \frac{M_{u\_w1\_EW}}{S_{A\_w1}} + \frac{P_{u\_w1\_Compression}}{A_{w1}} = 2.317 \cdot ksi$$

$$\sigma_{B\_w1} := \frac{M_{u\_w1\_EW}}{S_{B\_w1}} + \frac{P_{u\_w1\_Compression}}{A_{w1}} = 3.56 \cdot ksi$$

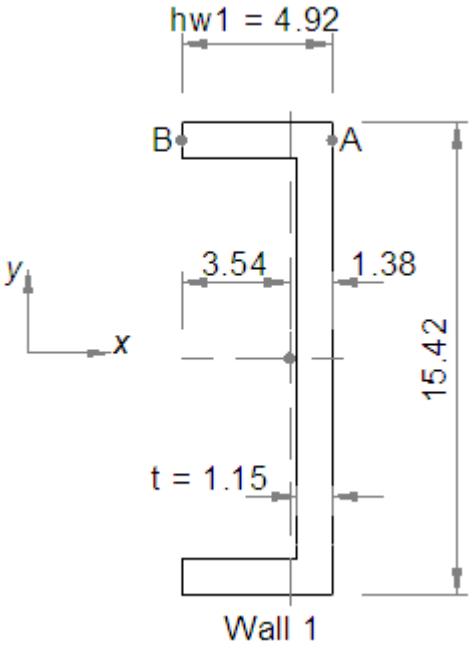

Case1 := "Boundary element is required"

Case2 := "Boundary element is not required"

Need For Boundary Element at inner end (point A)$_{w1}$:= if$\left(\sigma_{A_w1} > 0.2 \cdot f_c, Case1, Case2\right)$

Need For Boundary Element at inner end (point A)$_{w1}$ = "Boundary element is required"

Need For Boundary Element at outer end (point B)$_{w1}$:= if$\left(\sigma_{B_w1} > 0.2 \cdot f_c, Case1, Case2\right)$

Need For Boundary Element at outer end (point B)$_{w1}$ = "Boundary element is required"

Design for Flexure [Longitudinal (Vertical) Reinforcement]

Initial estimate of required area of steel for the boundary element is calculated as

$$A_{s\_w1\_EW} := \frac{M_{u\_w1\_EW}}{0.8 \cdot (h_{w1})(f_y)} = 26.34 \cdot in^2$$

Consider Minimum Reinforcement for the Barbell as a Short Column

$$\rho\_w1\_Barbell := \max\left[\frac{A_{s\_w1\_EW}}{2(2.84ft)(3.12ft)}, 0.01\right] = 0.01032$$

Select Reinforcement

Try # 9

Boundary Element Vertical Bar #$_{w1\_EW}$:= 9

$d_{b\_v\_BE\_w1\_EW}$:= #9 daimeter$\cdot$in = 1.128$\cdot$in

$A_{b\_v\_BE\_w1\_EW}$:= #9 area$\cdot in^2$ = 1.000$\cdot in^2$

$$\text{Total Number of Bars per Pier}_{w1\_EW} := 2\,\text{ceil}\left(\frac{A_{s\_w1\_EW}}{2A_{b\_v\_BE\_w1\_EW}}\right) = 28$$

$$\text{One Boundary Element \# of Bars}_{w1\_EW} := \frac{\text{Total Number of Bars per Pier}_{w1\_EW}}{2} = 14$$

Select Web Vertical Reinforcement

Initially a minimum vertical reinforcement will be provided in the web [regions between the B.E's]

$\rho_{min\_w1\_EW} = 0.0025$

$\text{Web Vertical Bar \#}_{w1\_EW} := 4$

$d_{b\_v\_web\_w1\_EW} := \#4\ \text{daimeter}\cdot\text{in} = 0.5\cdot\text{in}$

$A_{b\_v\_web\_w1\_EW} := \#4\ \text{area}\cdot\text{in}^2 = 0.200\cdot\text{in}^2$

$$S_{v\_web\_w1\_EW} := \text{floor}\left[\frac{2\cdot\left(A_{b\_v\_web\_w1\_EW}\right)}{\left(\rho_{min\_w1\_EW}\right)\cdot t_w\cdot\text{in}}\right]\cdot\text{in} = 11\cdot\text{in}$$

$$\rho_{v\_web\_w1\_EW} := \frac{2\cdot\left(A_{b\_v\_web\_w1\_EW}\right)}{\left(S_{v\_web\_w1\_EW}\right)\cdot t_w} = 0.00264$$

Use 14 #9 rebars at each boundary zone, with #4 at 11in at each face in between the boundary elements

Shear Friction (Sliding Shear)

The sliding shear resistance is given by

$V_{n\_sliding} = A_{vf}\, f_y\, \mu$

$\mu = 1.0\ \lambda$

$\lambda := 1$ for normal weight concrete

$\mu := 1.0\cdot\lambda$

A_{vf} = total area of vetical reinforcement 'including boundary elements'

$\text{Total Number of Vertical Bars in the Pier Web}_{w1\_EW} := 0$

$$A_{vf\_w1\_EW} := (112)\cdot\left(A_{b\_v\_BE\_w1\_EW}\right) \cdots + \left(\text{Total Number of Vertical Bars in the Pier Web}_{w1\_EW}\right)\cdot\left(A_{b\_v\_web\_w1\_EW}\right) = 112\cdot\text{in}^2$$

$V_{n\_sliding\_w1\_EW} := A_{vf\_w1\_EW}\cdot f_y\cdot\mu = 8447\cdot\text{kip}$

The shear friction strength should be less than the smallest of $0.2\ f_c'\ A_c$ or $800\ A_c$

$Limit_{1\_w1\_EW} := 0.2 \cdot f_c \cdot (A_{c\_w1\_EW}) = 4101.48 \cdot kip$

$Limit_{2\_w1\_EW} := 800psi \cdot (A_{c\_w1\_EW}) = 2513.66 \cdot kip$

$V_{n\_sliding\_w1\_EW} := \min(A_{vf\_w1\_EW} \cdot f_y \cdot \mu, Limit_{1\_w1\_EW}, Limit_{2\_w1\_EW}) = 2513.66 \cdot kip$

Sliding Shear Capacity Check

$V_{u\_w1\_EW} = 160.21 \cdot kip$

$\text{Sliding Shear Capacity}_{w1} := \text{if}(V_{n\_sliding\_w1\_EW} > V_{u\_w1\_EW}, Result_1, Result_2)$

$\text{Sliding Shear Capacity}_{w1} = \text{"Check is OK"}$

b) Design in the Uncoupling Direction (NS Direction)

Design Forces

$V_{u\_w1\_NS} := \text{Base Shear} \cdot [I_{w1\_x} \div (I_{w1\_x} + I_{w2\_x} + 2 \cdot I_{outrigger\_x})] = 576 \cdot kip$

$M_{u\_w1\_NS} := \text{Total Overturning Moment} \cdot [I_{w1\_x} \div (I_{w1\_x} + I_{w2\_x} + 2 \cdot I_{outrigger\_x})] = 54426 \cdot kip \cdot ft$

$P_{u\_w1\_Tension} = -3213 \cdot kip$

$P_{u\_w1\_Compression} = 8090 \cdot kip$

Check the Reinforcemnt Ratios Reduction Condition

Section 14.3 permits a reduction in the minimum vertical and horizontal reinforcement ratios if:

$V_u \le A_c \sqrt{f'_c}$

$V_{u\_w1\_NS} = 576 \cdot kip$

$\text{Redution Limit}_{w1\_NS} := A_{c\_NS} \cdot \sqrt{\frac{f_c}{psi}} \cdot psi = 206 \cdot kip$

$\text{Reduction in minimum reiforcement ratios}_{w1\_NS} := \text{if}(V_{u\_w1\_NS} \le \text{Redution Limit}_{w1\_NS}, case_1, case_2)$

$\text{Reduction in minimum reiforcement ratios}_{w1\_NS} = \text{"Not permitted"}$

Therefore, minimum vertical & horizontal reinforcement ratio is

$\rho_{min\_w1\_NS} := 0.0025$

Check Two Curtains Requirment

Section 21.9.2.2 requires at least two curtains of reinforcemnt, for both ρ_v and ρ_h if:

$V_u > 2A_c\sqrt{f_c'}$

$V_{u\_w1\_NS} = 576 \cdot kip$

$\text{Two curtains limit}_{w1\_NS} := 2 \cdot A_{c\_NS} \cdot \sqrt{\frac{f_c}{psi}} \cdot psi = 411.99 \cdot kip$

$\text{Numer of reinforcemnt curtains}_{w1\_NS} := \text{if}\left(V_{u\_w1\_NS} \le \text{Two curtains limit}_{w1\_NS}, \text{Case}_1, \text{Case}_2\right)$

$\text{Numer of reinforcemnt curtains}_{w1\_NS} = \text{"Two curtains are required for each direction"}$

Design for Shear

The shear strength is given by

$\varphi V_n = \varphi A_{cv}\left(\alpha_c\sqrt{f_c'} + \rho_n f_y\right)$

$\phi := 0.6$

Set $\alpha_c := 2.0$

Set $\phi V_n = V_u$

$\rho_h = \frac{1}{f_y} \cdot \left(\frac{V_u}{\phi \cdot A_{cv}} - \alpha_c \cdot \sqrt{f_c}\right)$

$\rho_{h\_w1\_NS\_required} := \max\left[\frac{1}{f_y} \cdot \left[\frac{V_{u\_w1\_NS}}{\phi \cdot \left(A_{c\_NS}\right)} - \alpha_c \cdot \sqrt{\frac{f_c}{psi}} \cdot psi\right], \rho_{min\_w1\_NS}\right] = 0.00285$

Select Reinforcement

Try # 4 each face in horizontal direction

$\text{Horizontal Bar \#}_{w1\_NS} := 4$

$d_{b\_h\_w1\_NS} := \#4\ \text{daimeter} \cdot in = 0.5 \cdot in$

$A_{b\_h\_w1\_NS} := \#4\ \text{area} \cdot in^2 = 0.2 \cdot in^2$

$S_{h\_w1\_NS} := \text{floor}\left[\frac{\left(2 \cdot A_{b\_h\_w1\_NS}\right)}{\left(\rho_{h\_w1\_NS\_required}\right) \cdot t_w \cdot in}\right] \cdot in = 10 \cdot in$

Consider Maximum Reinforcement Spacing

$S_{h\_w1\_NS} := \text{if}\left(S_{h\_w1\_NS} < \text{Maximum Spacing}, S_{h\_w1\_NS}, \text{Maximum Spacing}\right) = 10 \cdot in$

$$\rho_{h\_w1\_NS\_provided} := \frac{2\cdot\left(A_{b\_h\_w1\_NS}\right)}{\left(S_{h\_w1\_NS}\right)\cdot t_w} = 0.0029$$

Calculate Nominal Shear Strength

$$\phi V_{n\_w1\_NS} := \phi\cdot A_{c\_NS}\cdot\left(2\cdot\sqrt{\frac{f_c}{psi}}\cdot psi + \rho_{h\_w1\_NS\_provided}\cdot f_y\right) = 582.13\cdot kip$$

Check Shear Strength

$$\text{Shear Strengh}_{w1\_NS} := \text{if}\left(\phi V_{n\_w1\_NS} > V_{u\_w1\_NS}, \text{Result}_1, \text{Result}_2\right)$$

$$\text{Shear Strengh}_{w1\_NS} = \text{"Check is OK"}$$

Use #4 at 10 in. each face in horizontal direction

Check for Maximum Allowable Nominal Shear Strength

$$V_n \le 10A_{cv}\sqrt{f_c'}$$

$$\text{Nominal Shear Strength Limit}_{w1\_NS} := 10\cdot A_{c\_NS}\cdot\left(\sqrt{\frac{f_c}{psi}}\cdot psi\right) = 2059.97\cdot kip$$

$$\text{Max Allowable Nominal Shear Strength}_{w1\_NS} := \text{if}\left(\phi V_{n\_w1\_NS} \le \text{Nominal Shear Strength Limit}_{w1\_NS}, \text{Result}_1, \text{Result}_2\right)$$

$$\text{Max Allowable Nominal Shear Strength}_{w1\_NS} = \text{"Check is OK"}$$

Need for Boundary Elements

Stress index procedure

$$0.2\cdot f_c = 1.31\cdot ksi$$

The states of stresses will be checked at one of the two extreme points 'points C and D in the figure below

$$S_{C\_w1} = \frac{I_{w1\_x}}{c_C}$$

$$c_C := \frac{l_w}{2} = 7.71\ \text{ft}$$

$$S_{C\_w1} := \frac{I_{w1\_x}}{c_C} = 343708.39 \cdot \text{in}^3$$

$$\sigma_{C\_w1} := \frac{M_{u\_w1\_NS}}{S_{C\_w1}} + \frac{P_{u\_w1\_Compression}}{A_{w1}} = 3.423 \cdot \text{ksi}$$

$\text{Case}_1 :=$ "Boundary elements are required"

$\text{Case}_2 :=$ "Boundary elements are not required"

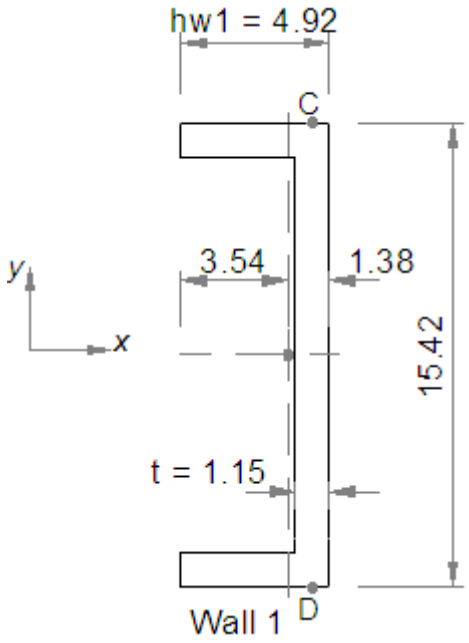

Need For Boundary Element at both ends (points C&D)$_{w1} := \text{if}\left(\sigma_{C\_w1} > 0.2 \cdot f_c, \text{Case}_1, \text{Case}_2\right)$

Need For Boundary Element at both ends (points C&D)$_{w1}$ = "Boundary elements are required"

Design for Flexure [Longitudinal (vertical) reinforcement]

Initial estimate of required area of steel for the boundary element is calculated as

$$A_{s\_w1\_NS} := \frac{M_{u\_w1\_NS}}{0.8 \cdot \left(l_w\right)\left(f_y\right)} = 58.5 \cdot \text{in}^2$$

Select Reinforcement

Try # 9

Boundary Element Vertical Bar #$_{w1\_NS} := 9$

$d_{b\_v\_BE\_w1\_NS} :=$ #9 daimeter$\cdot$in $= 1.128 \cdot \text{in}$

$A_{b\_v\_BE\_w1\_NS} :=$ #9 area$\cdot\text{in}^2 = 1 \cdot \text{in}^2$

Total Number of Bars per Pier$_{w1_NS} := 2\ \text{ceil}\left(\frac{A_{s_w1_NS}}{2A_{b_v_BE_w1_NS}}\right) = 60$

Select Web Vertical Reinforcement

Initially a minimum vertical reinforcement will be provided in the web [regions between the B.E's]

$\rho_{min\_w1\_NS} = 0.0025$

Web Vertical Bar $\#_{w1\_NS} := 4$

$d_{b\_v\_web\_w1\_NS} := \#4\ \text{daimeter} \cdot \text{in} = 0.5 \cdot \text{in}$

$A_{b\_v\_web\_w1\_NS} := \#4\ \text{area} \cdot \text{in}^2 = 0.2 \cdot \text{in}^2$

$$S_{v\_web\_w1\_NS} := \text{floor}\left[\frac{2 \cdot \left(A_{b\_v\_web\_w1\_NS}\right)}{\left(\rho_{min\_w1\_NS}\right) \cdot t_w \cdot \text{in}}\right] \cdot \text{in} = 11 \cdot \text{in}$$

$$\rho_{v\_web\_w1\_NS} := \frac{2 \cdot \left(A_{b\_v\_web\_w1\_NS}\right)}{\left(S_{v\_web\_w1\_NS}\right) \cdot t_w} = 0.00264$$

Use 60 #9 rebars at each boundary zone, with #4 at 11in at each face in between the boundary elements

Shear Friction (Sliding Shear)

$V_{n\_sliding} = A_{vf}\, f_y\, \mu$

A_{vf} = total area of vetical reinforcement 'including boundary elements'

Total Number of Vertical Bars in the Pier $\text{Web}_{w1\_NS} := 20$

$$A_{vf\_w1\_NS} := (72) \cdot \left(A_{b\_v\_BE\_w1\_NS}\right) \ldots + \left(\text{Total Number of Vertical Bars in the Pier Web}_{w1\_NS}\right) \cdot \left(A_{b\_v\_web\_w1\_NS}\right) = 76 \cdot \text{in}^2$$

$V_{n\_sliding\_w1\_NS} := A_{vf\_w1\_NS} \cdot f_y \cdot \mu = 5731.89 \cdot \text{kip}$

The shear friction strength should be less than the smallest of $0.2\, f_c'\, A_c$ or $800\, A_c$

$\text{Limit}_{1\_w1\_NS} := 0.2 \cdot f_c \cdot \left(A_{c\_NS}\right) = 3328.42 \cdot \text{kip}$

$\text{Limit}_{2\_w1\_NS} := 800\text{psi} \cdot \left(A_{c\_NS}\right) = 2039.88 \cdot \text{kip}$

$V_{n\_sliding\_w1\_NS} := \min\left(A_{vf\_w1\_NS} \cdot f_y \cdot \mu, \text{Limit}_{1\_w1\_NS}, \text{Limit}_{2\_w1\_NS}\right) = 2039.88 \cdot \text{kip}$

Sliding Shear Capacity Check

$\text{Sliding Shear Capacity}_{w1\_NS} := \text{if}\left(V_{n\_sliding\_w1\_NS} > V_{u\_w1\_NS}, \text{Result}_1, \text{Result}_2\right)$

$\text{Sliding Shear Capacity}_{w1\_NS} = \text{"Check is OK"}$

Boundary Element Details

Length of the Boundary Element

According to ACI 318-08 21.9.5.2, the effective flange widths of flanged sections shall extend from the fa
of the web a distance equal to the smaller of one-half the distance to an adjacent wall web and 25 percent

the total wall height.

The distances between the webs are:

In EW direction:

$L_{EW} := 21.82\ ft$

In NS direction:

$L_{NS} := 13.12\ ft$

The wall height (story height) i $H_s = 11.81 \cdot ft$

The effective flange width (EFW) in EW direction is

$EFW_{EW} := \min\left(0.5 \cdot L_{EW}, 0.25 \cdot H_s\right) = 2.95 \cdot ft$

The effective flange width (EFW) in NS direction is

$EFW_{NS} := \min\left(0.5 \cdot L_{NS}, 0.25 \cdot H_s\right) = 2.95 \cdot ft$

Thus, the effective flange width (EFW) in both directions is

$EFW := EFW_{NS} = 2.95\ ft$

According to the *Recommendations for Seismic Design of Hybrid Coupled Wall Systems*, the effective flange width should be resuced by a factor of 0.75 for drift level of 1% if the compression force in the wa greater than $0.05\ f'_c\ A_g$

$IFTrue := \text{"Required"}$

$IFFalse := \text{"NOT Required"}$

$\text{Reduction in Effective Flange Width}_{w1} := \text{if}\left(P_{u\_w1\_Compression} > 0.05 \cdot f_c \cdot A_{w1}, IFTrue, IFFalse\right)$

$\text{Reduction in Effective Flange Width}_{w1} = \text{"Required"}$

Therefore, the final effective flange width (EFW) in both directions is

$EFW := 0.75 \cdot EFW = 2.214 \cdot ft$

Easr-West Direstion (EW)

Extension of the Boundary Element

The required vertical extension of boundary element Ex_b must not be less than h_w, l_w or $\frac{M_n}{4V_n}$

$$\text{Boundary Elment Vertical Extension}_{w1\_EW} := \max\left[h_{w1}, l_w, \frac{\left(\frac{M_{u\_w1\_EW}}{0.9}\right)}{4 \cdot \left(\frac{V_{u\_w1\_EW}}{0.85}\right)}\right] = 185.04 \cdot in$$

$$\text{Boundary Elment Vertical Extension}_{w1\_EW} := \text{Ceil}\left(\frac{\text{Boundary Elment Vertical Extension}_{w1\_EW}}{in}, 2\right)\cdot in = 186\cdot in$$

Confinement for the Boundary Element

Transverse Steel

$$\text{Boundary Element Transverse Steel Bar \#}_{w1\_EW} := 4$$

$$d_{b\_T\_BE\_w1\_EW} := \#4\ \text{daimeter}\cdot in = 0.5\cdot in$$

$$A_{b\_T\_BE\_w1\_EW} := \#4\ \text{area}\cdot in^2 = 0.2\cdot in^2$$

Inner Boundary Element

Number of shear legs parallel/perpendicular to the wall contributing to shear resistance is

$$\text{No of shear legs}_{Parallel\_w1\_EW\_inner} := 8$$

$$\text{No of shear legs}_{Perpendicular\_w1\_EW\_inner} := 8$$

$h_{x\_w1\_EW\_inner} := 0.67\ ft$ maximum horizontal spacing of hoops or crosstie legs on all faces of colu

$h_{c\_parallel\_w1\_EW\_inner} := 2.75\ ft$ boundary element dimension measured c-c of confining rei

$h_{c\_perpendicular\_w1\_EW\_inner} := 2.46\ ft$

Calculate Transverse Reinforcement Spacing

The minimum cross-sectional area of confining reinforcement is given by

$$A_{sh} = 0.09 s\cdot h_c\left(\frac{f_c}{f_y}\right) \qquad s = \left(\frac{A_{sh}}{0.09\cdot h_c\left(\frac{f_c}{f_y}\right)}\right)$$

In parallel direction

$$S_{t\_w1\_EW\_inner\_parallel} := \frac{\text{No of shear legs}_{Parallel\_w1\_EW\_inner}\cdot A_{b\_T\_BE\_w1\_EW}}{0.09\cdot h_{c\_parallel\_w1\_EW\_inner}\cdot\left(\frac{f_c}{f_y}\right)} = 6.23\cdot in$$

In perpendicular direction

$$S_{t\_w1\_EW\_inner\_perpendicular} := \frac{\text{No of shear legs}_{Perpendicular\_w1\_EW\_inner}\cdot A_{b\_T\_BE\_w1\_EW}}{\left[0.09\cdot h_{c\_perpendicular\_w1\_EW\_inner}\cdot\left(\frac{f_c}{f_y}\right)\right]} = 6.96\cdot in$$

$$S_{t\_w1\_EW\_inner} := \text{floor}\left(\frac{\min\left(S_{t\_w1\_EW\_inner\_parallel}, S_{t\_w1\_EW\_inner\_perpendicular}\right)}{in}\right)\cdot in = 6\cdot in$$

Check Maximum Spacing

Maximum allowable spacing (S_{max}) of hoops and crossties is the smallest of the following:

$S_1 = 0.25 \times$ the minimum member dimension

$S_2 = 6 \times$ the diameter of longitudinal bar

$$S_3 = 4 + \left(\frac{14 - h_x}{3}\right)$$

$$S_{max\_w1\_EW\_inner} := \text{floor}\left[\frac{\min\left[0.25\cdot(0.864\,\text{m}), 6\cdot d_{b\_v\_BE\_w1\_EW}, 4\,\text{in} + \left(\frac{14\,\text{in} - h_{x\_w1\_EW\_inner}}{3}\right)\right]}{\text{in}}\right]\cdot\text{in} = 5\cdot\text{in}$$

$$S_{t\_w1\_EW\_inner} := \text{if}\left(S_{t\_w1\_EW\_inner} < S_{max\_w1\_EW\_inner}, S_{t\_w1\_EW\_inner}, S_{max\_w1\_EW\_inner}\right) = 5\cdot\text{in}$$

Outer Boundary Element

Number of shear legs parallel/perpendicular to the wall contributing to shear resistance is

$$\text{No of shear legs}_{Parallel\_w1\_EW\_outer} := 4$$

$$\text{No of shear legs}_{Perpendicular\_w1\_EW\_outer} := 8$$

$$h_{x\_w1\_EW\_outer} := 0.35\ \text{ft}$$

$$h_{c\_parallel\_w1\_EW\_outer} := 1.67\ \text{ft}$$

$$h_{c\_perpendicular\_w1\_EW\_outer} := 0.78\ \text{ft}$$

Calculate Transverse Reinforcement Spacing

The minimum cross-sectional area of confining reinforcement is given by

$$A_{sh} = 0.09 s\cdot h_c\left(\frac{f_c}{f_y}\right) \qquad s = \left(\frac{A_{sh}}{0.09\cdot h_c\left(\frac{f_c}{f_y}\right)}\right)$$

In parallel direction

$$S_{t\_w1\_EW\_outer\_parallel} := \frac{\text{No of shear legs}_{Parallel\_w1\_EW\_outer}\cdot A_{b\_T\_BE\_w1\_EW}}{0.09\cdot h_{c\_parallel\_w1\_EW\_outer}\cdot\left(\frac{f_c}{f_y}\right)} = 5.13\cdot\text{in}$$

In perpendicular direction

$$S_{t\_w1\_EW\_outer\_perpendicular} := \frac{\text{No of shear legs}_{Perpendicular\_w1\_EW\_outer}\cdot A_{b\_T\_BE\_w1\_EW}}{\left[0.09\cdot h_{c\_perpendicular\_w1\_EW\_outer}\cdot\left(\frac{f_c}{f_y}\right)\right]} = 21.95\cdot\text{in}$$

$$S_{t\_w1\_EW\_outer} := \text{floor}\left(\frac{\min\left(S_{t\_w1\_EW\_outer\_parallel}, S_{t\_w1\_EW\_outer\_perpendicular}\right)}{\text{in}}\right)\cdot\text{in} = 5\cdot\text{in}$$

Check Maximum Spacing

Maximum allowable spacing (S_{max}) of hoops and crossties is the smallest of the following:

$S_1 = 0.25 \times$ the minimum member dimension

$S_2 = 6 \times$ the diameter of longitudinal bar

$$S_3 = 4 + \left(\frac{14 - h_x}{3}\right)$$

$$S_{max\_w1\_EW\_outer} := \text{floor}\left[\frac{\min\left[0.25\cdot(0.35\text{m}), 6\cdot d_{b\_v\_BE\_w1\_EW}, 4\text{in} + \left(\frac{14\text{in} - h_{x\_w1\_EW\_outer}}{3}\right)\right]}{\text{in}}\right]\cdot\text{in} = 3\cdot\text{in}$$

$$S_{t\_w1\_EW\_outer} := \text{if}\left(S_{t\_w1\_EW\_outer} < S_{max\_w1\_EW\_outer}, S_{t\_w1\_EW\_outer}, S_{max\_w1\_EW\_outer}\right) = 3\cdot\text{in}$$

North-South Direction (NS)

Extension of the Boundary Element

$$\text{Boundary Elment Vertical Extension}_{w1\_NS} := \max\left[h_{w1}, l_w, \frac{\left(\frac{M_{u\_w1\_NS}}{0.9}\right)}{4\cdot\left(\frac{V_{u\_w1\_NS}}{0.85}\right)}\right] = 267.72\cdot\text{in}$$

$$\text{Boundary Elment Vertical Extension}_{w1\_NS} := \text{Ceil}\left(\frac{\text{Boundary Elment Vertical Extension}_{w1\_NS}}{\text{in}}, 2\right)\cdot\text{in} = 268\cdot\text{in}$$

Confinement for the Boundary Element

Transverse Steel

$$\text{Boundary Element Transverse Steel Bar \#}_{w1\_NS} := 4$$

$$d_{b\_T\_BE\_w1\_NS} := \#4\ \text{daimeter}\cdot\text{in} = 0.5\cdot\text{in}$$

$$A_{b\_T\_BE\_w1\_NS} := \#4\ \text{area}\cdot\text{in}^2 = 0.2\cdot\text{in}^2$$

Number of shear legs parallel/perpendicular to the wall contributing to shear resistance is

$$\text{No of shear legs}_{Parallel\_w1\_NS} := 8$$

$$\text{No of shear legs}_{Perpendicular\_w1\_NS} := 10$$

$h_{x\_w1\_NS} := 0.65\ ft$

$h_{c\_parallel\_w1\_NS} := 2.54\ ft$

$h_{c\_perpendicular\_w1\_NS} := 0.78\ ft$

Calculate Transverse Reinforcement Spacing

In parallel direction

$$S_{t\_w1\_NS\_parallel} := \frac{No\ of\ shear\ legs_{Parallel\_w1\_NS} \cdot A_{b\_T\_BE\_w1\_NS}}{0.09 \cdot h_{c\_parallel\_w1\_NS} \cdot \left(\frac{f_c}{f_y}\right)} = 6.74 \cdot in$$

In perpendicular direction

$$S_{t\_w1\_NS\_perpendicular} := \frac{No\ of\ shear\ legs_{Perpendicular\_w1\_NS} \cdot A_{b\_T\_BE\_w1\_NS}}{\left[0.09 \cdot h_{c\_perpendicular\_w1\_NS} \cdot \left(\frac{f_c}{f_y}\right)\right]} = 27.43 \cdot in$$

$$S_{t\_w1\_NS} := floor\left(\frac{\min\left(S_{t\_w1\_NS\_parallel}, S_{t\_w1\_NS\_perpendicular}\right)}{in}\right) \cdot in = 6 \cdot in$$

Check Maximum Spacing

$$S_{max\_w1\_NS} := floor\left[\frac{\min\left[0.25 \cdot (0.35m), 6 \cdot d_{b\_v\_BE\_w1\_NS}, 4in + \left(\frac{14in - h_{x\_w1\_NS}}{3}\right)\right]}{in}\right] \cdot in = 3 \cdot in$$

$$S_{t\_w1\_NS} := if\left(S_{t\_w1\_NS} < S_{max\_w1\_NS}, S_{t\_w1\_NS}, S_{max\_w1\_NS}\right) = 3 \cdot in$$

Outer Boundary Element Confinement Reinforcement Spacing Considering Both Directions

Final transverse reinforcement spacing for the outer boundary element is the minimum of spacings in EW NS directions

$$S_{t\_w1\_outer} := \min\left(S_{t\_w1\_EW\_outer}, S_{t\_w1\_NS}\right) = 3 \cdot in$$

Second Design of Wall 2 (the Stiffer Wall Pier)

a) Design in the Direction of Coupling (EW Direction)

Design Forces

$V_{u\_w2\_EW} := \text{Base Shear} \cdot \left[I_{w2\_y} \div \left(I_{w1\_y} + I_{w2\_y} \right) \right] = 1531 \cdot \text{kip}$

$M_{u\_w2\_EW} := \text{Moment of Wall 2 in Coupling Direction} = 71289 \cdot \text{kip} \cdot \text{ft}$

$P_{u\_w2\_Tension} := 0.9 \cdot \text{Dead Load of Wall 2} - 0.2 \cdot S_{DS} \cdot \text{Dead Load of Wall 2} - \text{Axial Load Due to Frame Action} = -2926 \cdot \text{kip}$

$P_{u\_w2\_Compression} := 1.2 \cdot \text{Dead Load of Wall 2} + 0.5 \cdot \text{Live Load of Wall 2} + 0.2 \cdot S_{DS} \cdot \text{Dead Load of Wall 2} \ldots + \text{Axial Load Due to Frame Action} = 8813 \cdot \text{kip}$

Check the Reinforcemnt Ratios Reduction Condition

$V_{u\_w2\_EW} = 1531 \cdot \text{kip}$

$\text{Redution Limit}_{w2\_EW} := A_{c\_w2\_EW} \cdot \sqrt{\frac{f_c}{\text{psi}}} \cdot \text{psi} = 416.01 \cdot \text{kip}$

$\text{case}_1 := \text{"Permitted"} \qquad \text{case}_2 := \text{"Not permitted"}$

$\text{Reduction in minimum reiforcement ratios}_{w2\_EW} := \text{if}\left(V_{u\_w2\_EW} \le \text{Redution Limit}_{w2\_EW}, \text{case}_1, \text{case}_2 \right)$

$\text{Reduction in minimum reiforcement ratios}_{w2\_EW} = \text{"Not permitted"}$

Therefore, minimum vertical & horizontal reinforcement ratio is

$\rho_{min\_w2\_EW} := 0.0025$

Check Two Curtains Requirment

$V_{u\_w2\_EW} = 1530.8 \cdot \text{kip}$

$\text{Two curtains limit}_{w2\_EW} := 2 \cdot A_{c\_w2\_EW} \cdot \sqrt{\frac{f_c}{\text{psi}}} \cdot \text{psi} = 832.03 \cdot \text{kip}$

$\text{Case}_1 := \text{"One curtain is enough in each direction"} \qquad \text{Case}_2 := \text{"Two curtains are required for each direction"}$

$\text{Numer of reinforcemnt curtains}_{w2\_EW} := \text{if}\left(V_{u\_w2\_EW} \le \text{Two curtains limit}_{w2\_EW}, \text{Case}_1, \text{Case}_2 \right)$

$\text{Numer of reinforcemnt curtains}_{w2\_EW} = \text{"Two curtains are required for each direction"}$

Design for Shear

$$\rho_h = \frac{1}{f_y} \cdot \left(\frac{V_u}{\phi \cdot A_{cv}} - \alpha_c \cdot \sqrt{f_c} \right)$$

$$\rho_{h\_w2\_EW\_required} := \frac{1}{f_y} \cdot \left[\frac{V_{u\_w2\_EW}}{\phi \cdot \left(A_{cv\_w2\_EW} \right)} - \alpha_c \cdot \sqrt{\frac{f_c}{\text{psi}}} \cdot \text{psi} \right] = 0.00443$$

Consider Minimum Reinforcement

$\rho_{h\_w2\_EW\_required} := \max\left(\rho_{h\_w2\_EW\_required}, \rho_{min\_w2\_EW}\right) = 0.00443$

Select Reinforcement

Try # 4 each face in horizontal direction

$\text{Horizontal Bar \#}_{w2\_EW} := 4$

$d_{b\_h\_w2\_EW} := \#4\ \text{daimeter} \cdot \text{in} = 0.5 \cdot \text{in}$

$A_{b\_h\_w2\_EW} := \#4\ \text{area} \cdot \text{in}^2 = 0.2 \cdot \text{in}^2$

$S_{h\_w2\_EW} := \text{floor}\left[\frac{\left(2 \cdot A_{b\_h\_w2\_EW}\right)}{\left(\rho_{h\_w2\_EW\_required}\right) \cdot t_w \cdot \text{in}}\right] \cdot \text{in} = 6 \cdot \text{in}$

Consider Maximum Reinforcement Spacing

$S_{h\_w2\_EW} := \text{if}\left(S_{h\_w2\_EW} < \text{Maximum Spacing}, S_{h\_w2\_EW}, \text{Maximum Spacing}\right) = 6 \cdot \text{in}$

$\rho_{h\_w2\_EW\_provided} := \frac{2 \cdot \left(A_{b\_h\_w2\_EW}\right)}{\left(S_{h\_w2\_EW}\right) \cdot t_w} = 0.00484$

Calculate Nominal Shear Strength

$\phi V_{n\_w2\_EW} := \phi \cdot A_{cv\_w2\_EW} \cdot \left(2 \cdot \sqrt{\frac{f_c}{\text{psi}}} \cdot \text{psi} + \rho_{h\_w2\_EW\_provided} \cdot f_y\right) = 1626.56 \cdot \text{kip}$

Check Shear Strength

$\text{Shear Strengh}_{w2\_EW} := \text{if}\left(\phi V_{n\_w2\_EW} > V_{u\_w2\_EW}, \text{Result}_1, \text{Result}_2\right)$

$\text{Shear Strengh}_{w2\_EW} = \text{"Check is OK"}$

Use #4 at 4 in. each face in horizontal direction

Check for Maximum Allowable Nominal Shear Strength

$V_n \le 10 A_{cv} \sqrt{f_c'}$

$\text{Nominal Shear Strength Limit}_{w2\_EW} := 10 \cdot A_{cv\_w2\_EW} \cdot \left(\sqrt{\frac{f_c}{\text{psi}}} \cdot \text{psi}\right) = 4160.13 \cdot \text{kip}$

$\text{Max Allowable Nominal Shear Strength}_{w2\_EW} := \text{if}\left(\phi V_{n\_w2\_EW} \le \text{Nominal Shear Strength Limit}_{w2\_EW}, \text{Result}_1, \text{Result}_2\right)$

$\text{Max Allowable Nominal Shear Strength}_{w2\_EW} = \text{"Check is OK"}$

Need for Boundary Elements

Stress index procedure

$0.2 \cdot f_c = 1.31 \cdot ksi$

The states of stresses will be checked at two extreme points 'points A and B in the figure below'

$$S_{A\_w2} = \frac{I_{w2\_y}}{c_{A\_w2}}$$

$c_{A\_w2} := 7.34\ ft \qquad c_{B\_w2} := 3.65\ ft$

$$S_{A\_w2} := \frac{I_{w2\_y}}{c_{A\_w2}} = 212306.22 \cdot in^3$$

$$S_{B\_w2} := \frac{I_{w2\_y}}{c_{B\_w2}} = 426939.09 \cdot in^3$$

$$\sigma_{A\_w2} := \frac{M_{u\_w2\_EW}}{S_{A\_w2}} + \frac{P_{u\_w2\_Compression}}{A_{w2}} = 5.233 \cdot ksi$$

$$\sigma_{B\_w2} := \frac{M_{u\_w2\_EW}}{S_{B\_w2}} + \frac{P_{u\_w2\_Compression}}{A_{w2}} = 3.208 \cdot ksi$$

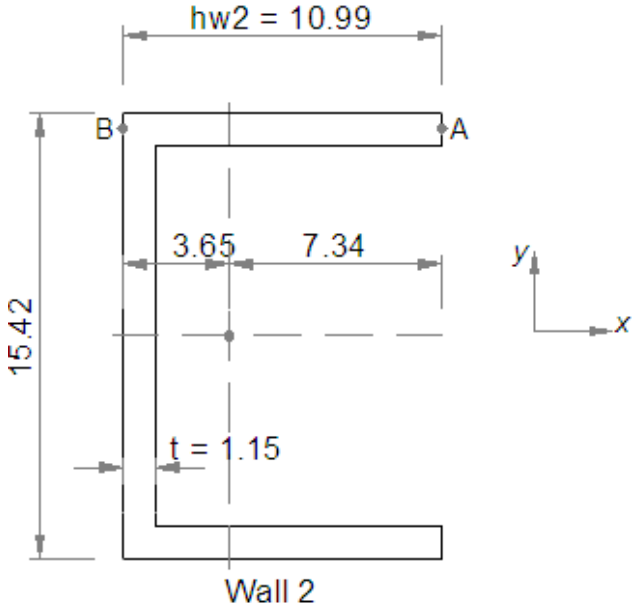

Case1 := "Boundary element is required" Case2 := "Boundary element is not required"

Need For Boundary Element at inner end (point A)$_{w2}$:= if$\left(\sigma_{A_w2} > 0.2 \cdot f_c, Case1, Case2\right)$

Need For Boundary Element at inner end (point A)$_{w2}$ = "Boundary element is required"

Need For Boundary Element at outer end (point B)$_{w2}$:= if$\left(\sigma_{B_w2} > 0.2 \cdot f_c, Case1, Case2\right)$

Need For Boundary Element at outer end (point B)$_{w2}$ = "Boundary element is required"

Design for Flexure [Longitudinal (vertical) reinforcement]

Initial estimate of required area of steel for the boundary element is calculated as

$$A_{s\_w2\_EW} := \frac{M_{u\_w2\_EW}}{0.8 \cdot (h_{w2})(f_y)} = 107.51 \cdot in^2$$

Consider Minimum Reinforcement for the Barbell as a Short Column

$$\rho\_w2\_Barbell := if\left[\frac{A_{s\_w2\_EW}}{2(2.84\ ft)(3.12\ ft)} > 0.01, \frac{A_{s\_w2\_EW}}{2(2.84\ ft)(3.12\ ft)}, 0.01\right] = 0.04213$$

Select Reinforcement

Try # 9

Boundary Element Vertical Bar #$_{w2\_EW}$:= 9

$d_{b\_v\_BE\_w2\_EW} := \#9\ \text{daimeter} \cdot in = 1.128 \cdot in$

$A_{b\_v\_BE\_w2\_EW} := \#9\ \text{area} \cdot in^2 = 1.000 \cdot in^2$

$$\text{Total Number of Bars per Pier}_{w2\_EW} := 2\ \text{ceil}\left(\frac{A_{s\_w2\_EW}}{2A_{b\_v\_BE\_w2\_EW}}\right) = 108$$

$$\text{One Boundary Element \# of Bars}_{w2\_EW} := \frac{\text{Total Number of Bars per Pier}_{w2\_EW}}{2} = 54$$

Select Web Vertical Reinforcement

Initially a minimum vertical reinforcement will be provided in the web [regions between the B.E's]

$\rho_{min\_w2\_EW} = 0.0025$

$\text{Web Vertical Bar \#}_{w2\_EW} := 4$

$d_{b\_v\_web\_w2\_EW} := \#4\ \text{daimeter} \cdot in = 0.5 \cdot in$

$A_{b\_v\_web\_w2\_EW} := \#4\ \text{area} \cdot in^2 = 0.200 \cdot in^2$

$$S_{v\_web\_w2\_EW} := \text{floor}\left[\frac{2 \cdot \left(A_{b\_v\_web\_w2\_EW}\right)}{\left(\rho_{min\_w2\_EW}\right) \cdot t_w \cdot in}\right] \cdot in = 11 \cdot in$$

$$\rho_{v\_web\_w2\_EW} := \frac{2 \cdot \left(A_{b\_v\_web\_w2\_EW}\right)}{\left(S_{v\_web\_w2\_EW}\right) \cdot t_w} = 0.00264$$

Use 54 #9 rebars at each boundary zone, with #4 at 11 in. at each face in between the boundary elements

Shear Friction (Sliding Shear)

A_{vf} = total area of vetical reinforcement 'including boundary elements'

$\text{Total Number of Vertical Bars in the Pier Web}_{w2\_EW} := 20$

$$A_{vf\_w2\_EW} := (216) \cdot \left(A_{b\_v\_BE\_w2\_EW}\right) \cdots + \left(\text{Total Number of Vertical Bars in the Pier Web}_{w2\_EW}\right) \cdot \left(A_{b\_v\_web\_w2\_EW}\right) = 220 \cdot in^2$$

$V_{n\_sliding\_w2\_EW} := A_{vf\_w2\_EW} \cdot f_y \cdot \mu = 16592.32 \cdot kip$

The shear friction strength should be less than the smallest of $0.2\ f_c'\ A_c$ or $800\ A_c$

$\text{Limit}_{1\_w2\_EW} := 0.2 \cdot f_c \cdot \left(A_{c\_w2\_EW}\right) = 6721.77 \cdot kip$

$\text{Limit}_{2\_w2\_EW} := 800psi \cdot \left(A_{c\_w2\_EW}\right) = 4119.55 \cdot kip$

$V_{n\_sliding\_w2\_EW} := \min\left(A_{vf\_w2\_EW} \cdot f_y \cdot \mu, Limit_{1\_w2\_EW}, Limit_{2\_w2\_EW}\right) = 4119.55 \cdot kip$

Sliding Shear Capacity Check

$V_{u\_w2\_EW} = 1530.8 \cdot kip$

$\text{Sliding Shear Capacity}_{w2} := \text{if}\left(V_{n\_sliding\_w2\_EW} > V_{u\_w2\_EW}, Result_1, Result_2\right)$

$\text{Sliding Shear Capacity}_{w2} = \text{"Check is OK"}$

b) Design in the Opposite Direction (NS Direction)

Design Forces

$V_{u\_w2\_NS} := \text{Base Shear} \cdot \left[I_{w2\_x} \div \left(I_{w1\_x} + I_{w2\_x} + 2 \cdot I_{outrigger\_x}\right)\right] = 904 \cdot kip$

$M_{u\_w2\_NS} := \text{Total Overturning Moment} \cdot \left[I_{w2\_x} \div \left(I_{w1\_x} + I_{w2\_x} + 2 \cdot I_{outrigger\_x}\right)\right] = 85405 \cdot kip \cdot ft$

$P_{u\_w2\_Tension} = -2926 \cdot kip$

$P_{u\_w2\_Compression} = 8813 \cdot kip$

Check the Reinforcemnt Ratios Reduction Condition

$V_{u\_w2\_NS} = 904 \cdot kip$

$\text{Redution Limit}_{w2\_NS} := A_{c\_NS} \cdot \sqrt{\frac{f_c}{psi}} \cdot psi = 206 \cdot kip$

$\text{Reduction in minimum reiforcement ratios}_{w2\_NS} := \text{if}\left(V_{u\_w2\_NS} \le \text{Redution Limit}_{w2\_NS}, case_1, case_2\right)$

$\text{Reduction in minimum reiforcement ratios}_{w2\_NS} = \text{"Not permitted"}$

Therefore, minimum vertical & horizontal reinforcement ratio is

$\rho_{min\_w2\_NS} := 0.0025$

Check Two Curtains Requirment

$V_{u\_w2\_NS} = 904 \cdot kip$

$\text{Two curtains limit}_{w2\_NS} := 2 \cdot A_{c\_NS} \cdot \sqrt{\frac{f_c}{psi}} \cdot psi = 411.99 \cdot kip$

$\text{Number of reinforcemnt curtains}_{w2\_NS} := \text{if}\left(V_{u\_w2\_NS} \le \text{Two curtains limit}_{w2\_NS}, Case_1, Case_2\right)$

$\text{Number of reinforcemnt curtains}_{w2\_NS} = \text{"Two curtains are required for each direction"}$

Design for Shear

$$\rho_h = \frac{1}{f_y} \cdot \left(\frac{V_u}{\phi \cdot A_{cv}} - \alpha_c \cdot \sqrt{f_c}\right)$$

$$\rho_{h\_w2\_NS\_required} := \frac{1}{f_y}\cdot\left[\frac{V_{u\_w2\_NS}}{\phi\cdot\left(A_{c\_NS}\right)} - \alpha_c\cdot\sqrt{\frac{f_c}{psi}}\cdot psi\right] = 0.00569$$

Consider Minimum Reinforcement

$$\rho_{h\_w2\_NS\_required} := \max\left(\rho_{h\_w2\_NS\_required}, \rho_{min\_w2\_NS}\right) = 0.00569$$

Select Reinforcement

Try # 4 each face in horizontal direction

$$\text{Horizontal Bar \#}_{w2\_NS} := 4$$

$$d_{b\_h\_w2\_NS} := \#4\ \text{daimeter}\cdot in = 0.5\cdot in$$

$$A_{b\_h\_w2\_NS} := \#4\ \text{area}\cdot in^2 = 0.2\cdot in^2$$

$$S_{h\_w2\_NS} := \text{floor}\left[\frac{\left(2\cdot A_{b\_h\_w2\_NS}\right)}{\left(\rho_{h\_w2\_NS\_required}\right)\cdot t_w\cdot in}\right]\cdot in = 5\cdot in$$

Consider Maximum Reinforcement Spacing

$$S_{h\_w2\_NS} := \text{if}\left(S_{h\_w2\_NS} < \text{Maximum Spacing}, S_{h\_w2\_NS}, \text{Maximum Spacing}\right) = 5\cdot in$$

$$\rho_{h\_w2\_NS\_provided} := \frac{2\cdot\left(A_{b\_h\_w2\_NS}\right)}{\left(S_{h\_w2\_NS}\right)\cdot t_w} = 0.00581$$

Calculate Nominal Shear Strength

$$\phi V_{n\_w2\_NS} := \phi\cdot A_{c\_NS}\cdot\left(2\cdot\sqrt{\frac{f_c}{psi}}\cdot psi + \rho_{h\_w2\_NS\_provided}\cdot f_y\right) = 917.07\cdot kip$$

Check Shear Strength

$$\text{Shear Strengh}_{w2\_NS} := \text{if}\left(\phi V_{n\_w2\_NS} > V_{u\_w2\_NS}, \text{Result}_1, \text{Result}_2\right)$$

$$\text{Shear Strengh}_{w2\_NS} = \text{"Check is OK"}$$

Use #4 at 4 in. each face in horizontal direction

Check for Maximum Allowable Nominal Shear Strength

$$V_n \le 10A_{cv}\sqrt{f_c'}$$

$$\text{Nominal Shear Strength Limit}_{w2\_NS} := 10\cdot A_{c\_NS}\cdot\left(\sqrt{\frac{f_c}{psi}}\cdot psi\right) = 2059.97\cdot kip$$

$$\text{Max Allowable Nominal Shear Strength}_{w2\_NS} := \text{if}\left(\phi V_{n\_w2\_NS} \le \text{Nominal Shear Strength Limit}_{w2\_NS}, \text{Result}_1, \text{Result}_2\right)$$

Max Allowable Nominal Shear Strength$_{w2_NS}$ = "Check is OK"

Need for Boundary Elements

Stress index procedure

$0.2 \cdot f_c = 1.31 \cdot ksi$

The states of stresses will be checked at one of the two extreme points 'points C and D in the figure below

$$S_{C\_w2} = \frac{I_{w2\_x}}{c_C}$$

$$c_C := \frac{l_w}{2} = 7.71\ ft$$

$$S_{C\_w2} := \frac{I_{w2\_x}}{c_C} = 539342.19 \cdot in^3$$

$$\sigma_{C\_w2} := \frac{M_{u\_w2\_NS}}{S_{C\_w2}} + \frac{P_{u\_w2\_Compression}}{A_{w2}} = 3.104 \cdot ksi$$

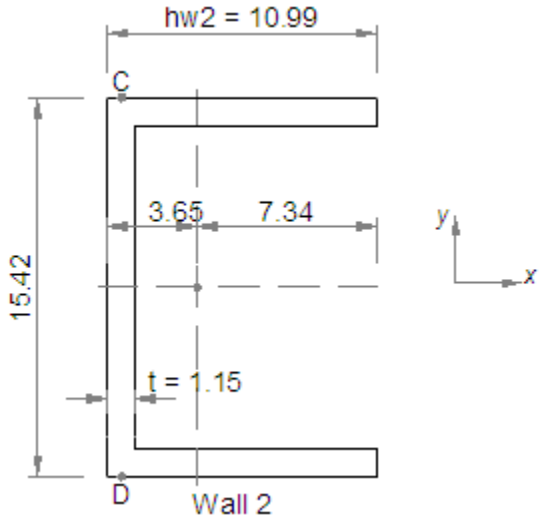

$Case_1$:= "Boundary elements are required" $Case_2$:= "Boundary elements are not required"

Need For Boundary Element at both ends (points C&D)$_{w2}$:= $if(\sigma_{C\_w2} > 0.2 \cdot f_c, Case_1, Case_2)$

Need For Boundary Element at both ends (points C&D)$_{w2}$ = "Boundary elements are required"

Design for Flexure [Longitudinal (vertical) reinforcement]

Initial estimate of required area of steel for the boundary element is calculated as

$$A_{s\_w2\_NS} := \frac{M_{u\_w2\_NS}}{0.8 \cdot (l_w)(f_y)} = 91.8 \cdot in^2$$

Select Reinforcement

Try # 9

Boundary Element Vertical Bar #$_{w2\_NS}$:= 9

$d_{b\_v\_BE\_w2\_NS}$:= #9 daimeter·in = 1.128·in

$A_{b\_v\_BE\_w2\_NS}$:= #9 area·in^2 = 1·in^2

$$\text{Total Number of Bars per Pier}_{w2\_NS} := 2\,\text{ceil}\left(\frac{A_{s\_w2\_NS}}{2A_{b\_v\_BE\_w2\_NS}}\right) = 92$$

Select Web Vertical Reinforcement

Initially a minimum vertical reinforcement will be provided in the web [regions between the B.E's]

$\rho_{min\_w2\_NS} = 0.0025$

$\text{Web Vertical Bar \#}_{w2\_NS} := 4$

$d_{b\_v\_web\_w2\_NS} := \#4\ \text{daimeter}\cdot\text{in} = 0.5\cdot\text{in}$

$A_{b\_v\_web\_w2\_NS} := \#4\ \text{area}\cdot\text{in}^2 = 0.2\cdot\text{in}^2$

$$S_{v\_web\_w2\_NS} := \text{floor}\left[\frac{2\cdot\left(A_{b\_v\_web\_w2\_NS}\right)}{\left(\rho_{min\_w2\_NS}\right)\cdot t_w\cdot\text{in}}\right]\cdot\text{in} = 11\cdot\text{in}$$

$$\rho_{v\_web\_w2\_NS} := \frac{2\cdot\left(A_{b\_v\_web\_w2\_NS}\right)}{\left(S_{v\_web\_w2\_NS}\right)\cdot t_w} = 0.00264$$

Use 92 #9 rebars at each boundary zone, with #4 at 11in at each face in between the boundary elements

Shear Friction (Sliding Shear)

$V_{n\_sliding} = A_{vf}\, f_y\, \mu$

A_{vf} = total area of vetical reinforcement 'including boundary elements'

$\text{Total Number of Vertical Bars in the Pier Web}_{w2\_NS} := 16$

$$A_{vf\_w2\_NS} := (128)\cdot\left(A_{b\_v\_BE\_w2\_NS}\right) \ldots + \left(\text{Total Number of Vertical Bars in the Pier Web}_{w2\_NS}\right)\cdot\left(A_{b\_v\_web\_w2\_NS}\right) = 131.2\cdot\text{in}^2$$

$V_{n\_sliding\_w2\_NS} := A_{vf\_w2\_NS}\cdot f_y\cdot\mu = 9895.05\cdot\text{kip}$

The shear friction strength should be less than the smallest of $0.2\, f_c'\, A_c$ or $800\, A_c$

$\text{Limit}_{1\_w2\_NS} := 0.2\cdot f_c\cdot\left(A_{c\_NS}\right) = 3328.42\cdot\text{kip}$

$\text{Limit}_{2\_w2\_NS} := 800\text{psi}\cdot\left(A_{c\_NS}\right) = 2039.88\cdot\text{kip}$

$V_{n\_sliding\_w2\_NS} := \min\left(A_{vf\_w2\_NS}\cdot f_y\cdot\mu, \text{Limit}_{1\_w2\_NS}, \text{Limit}_{2\_w2\_NS}\right) = 2039.88\cdot\text{kip}$

Sliding Shear Capacity Check

$\text{Sliding Shear Capacity}_{w2\_NS} := \text{if}\left(V_{n\_sliding\_w2\_NS} > V_{u\_w2\_NS}, \text{Result}_1, \text{Result}_2\right)$

$\text{Sliding Shear Capacity}_{w2\_NS} = \text{"Check is OK"}$

Boundary Element Details

Length of the Boundary Element

Thus, the effective flange width (EFW) in both directions was calculated in wall 1 and equal to

$EFW := EFW_{NS} = 2.95\ ft$

According to the *Recommendations for Seismic Design of Hybrid Coupled Wall Systems*, the effective flange width should be resuced by a factor of 0.75 for drift level of 1% if the compression force in the wa greater than $0.05\ f'_c\ A_g$

$IFTrue := "Required"$

$IFFalse := "NOT\ Required"$

$Reduction\ in\ Effective\ Flange\ Width_{w2} := if\left(P_{u\_w2\_Compression} > 0.05 \cdot f_c \cdot A_{w2}, IFTrue, IFFalse\right)$

$Reduction\ in\ Effective\ Flange\ Width_{w2} = "Required"$

Therefore, the final effective flange width (EFW) in both directions is

$EFW := 0.75 \cdot EFW = 2.214 \cdot ft$

East-West Direction (EW)

Extension of the Boundary Element

$$Boundary\ Elment\ Vertical\ Extension_{w2\_EW} := \max\left[h_{w2}, l_w, \frac{\left(\frac{M_{u\_w2\_EW}}{0.9}\right)}{4 \cdot \left(\frac{V_{u\_w2\_EW}}{0.85}\right)}\right] = 185.04 \cdot in$$

$$Boundary\ Elment\ Vertical\ Extension_{w2\_EW} := Ceil\left(\frac{Boundary\ Elment\ Vertical\ Extension_{w2\_EW}}{in}, 2\right) \cdot in = 186 \cdot in$$

Confinement for the Boundary Element

Transverse Steel

$Boundary\ Element\ Transverse\ Steel\ Bar\ \#_{w2\_EW} := 4$

$d_{b\_T\_BE\_w2\_EW} := \#4\ daimeter \cdot in = 0.5 \cdot in$

$A_{b\_T\_BE\_w2\_EW} := \#4\ area \cdot in^2 = 0.2 \cdot in^2$

Inner Boundary Element

Number of shear legs parallel/perpendicular to the wall contributing to shear resistance is

$No\ of\ shear\ legs_{Parallel\_w2\_EW\_inner} := 8$

$No\ of\ shear\ legs_{Perpendicular\_w2\_EW\_inner} := 8$

$h_{x\_w2\_EW\_inner} := 0.67\ ft$ maximum horizontal spacing of hoops or crosstie legs on all faces of colu

$h_{c\_parallel\_w2\_EW\_inner} := 2.75\ ft$ boundary element dimension measured c-c of confining rei

$h_{c\_perpendicular\_w2\_EW\_inner} := 2.46\ ft$

Calculate Transverse Reinforcement Spacing

In parallel direction

$$S_{t\_w2\_EW\_inner\_parallel} := \frac{No\ of\ shear\ legs_{Parallel\_w2\_EW\_inner} \cdot A_{b\_T\_BE\_w2\_EW}}{0.09 \cdot h_{c\_parallel\_w2\_EW\_inner} \cdot \left(\frac{f_c}{f_y}\right)} = 6.23 \cdot in$$

In perpendicular direction

$$S_{t\_w2\_EW\_inner\_perpendicular} := \frac{No\ of\ shear\ legs_{Perpendicular\_w2\_EW\_inner} \cdot A_{b\_T\_BE\_w2\_EW}}{\left[0.09 \cdot h_{c\_perpendicular\_w2\_EW\_inner} \cdot \left(\frac{f_c}{f_y}\right)\right]} = 6.96 \cdot in$$

$$S_{t\_w2\_EW\_inner} := floor\left(\frac{\min\left(S_{t\_w2\_EW\_inner\_parallel}, S_{t\_w2\_EW\_inner\_perpendicular}\right)}{in}\right) \cdot in = 6 \cdot in$$

Check Maximum Spacing

$$S_{max\_w2\_EW} := floor\left[\frac{\min\left[0.25 \cdot (0.864m), 6 \cdot d_{b\_v\_BE\_w2\_EW}, 4in + \left(\frac{14in - h_{x\_w2\_EW\_inner}}{3}\right)\right]}{in}\right] \cdot in = 5 \cdot in$$

$$S_{t\_w2\_EW\_inner} := if\left(S_{t\_w2\_EW\_inner} < S_{max\_w2\_EW}, S_{t\_w2\_EW\_inner}, S_{max\_w2\_EW}\right) = 5 \cdot in$$

Outer Boundary Element

Number of shear legs parallel/perpendicular to the wall contributing to shear resistance is

$No\ of\ shear\ legs_{Parallel\_w2\_EW\_outer} := 15$

$No\ of\ shear\ legs_{Perpendicular\_w2\_EW\_outer} := 15$

$h_{x\_w2\_EW\_outer} := 0.35\ ft$ maximum horizontal spacing of hoops or crosstie legs on all faces of colu

$h_{c\_parallel\_w2\_EW\_outer} := 3.16\ ft$ boundary element dimension measured c-c of confining rei

$h_{c\_perpendicular\_w2\_EW\_outer} := 0.78\ ft$

Calculate Transverse Reinforcement Spacing

In parallel direction

$$S_{t\_w2\_EW\_outer\_parallel} := \frac{\text{No of shear legs}_{Parallel\_w2\_EW\_outer} \cdot A_{b\_T\_BE\_w2\_EW}}{0.09 \cdot h_{c\_parallel\_w2\_EW\_outer} \cdot \left(\frac{f_c}{f_y}\right)} = 10.16 \cdot in$$

In perpendicular direction

$$S_{t\_w2\_EW\_outer\_perpendicular} := \frac{\text{No of shear legs}_{Perpendicular\_w2\_EW\_outer} \cdot A_{b\_T\_BE\_w2\_EW}}{\left[0.09 \cdot h_{c\_perpendicular\_w2\_EW\_outer} \cdot \left(\frac{f_c}{f_y}\right)\right]} = 41.15 \cdot in$$

$$S_{t\_w2\_EW\_outer} := \text{floor}\left(\frac{\min\left(S_{t\_w2\_EW\_outer\_parallel}, S_{t\_w2\_EW\_outer\_perpendicular}\right)}{in}\right) \cdot in = 10 \cdot in$$

Check Maximum Spacing

$$S_{max\_w2\_EW\_outer} := \text{floor}\left[\frac{\min\left[0.25 \cdot (1.15\ ft), 6 \cdot d_{b\_v\_BE\_w2\_EW}, 4in + \left(\frac{14in - h_{x\_w2\_EW\_outer}}{3}\right)\right]}{in}\right] \cdot in = 3 \cdot in$$

$$S_{t\_w2\_EW\_outer} := \text{if}\left(S_{t\_w2\_EW\_outer} < S_{max\_w2\_EW\_outer}, S_{t\_w2\_EW\_outer}, S_{max\_w2\_EW\_outer}\right) = 3 \cdot in$$

Norht-South Direction (NS)

Extension of the Boundary Element

$$\text{Boundary Elment Vertical Extension}_{w2\_NS} := \max\left[h_{w2}, l_w, \frac{\left(\frac{M_{u\_w2\_NS}}{0.9}\right)}{4 \cdot \left(\frac{V_{u\_w2\_NS}}{0.85}\right)}\right] = 267.72 \cdot in$$

$$\text{Boundary Elment Vertical Extension}_{w2\_NS} := \text{Ceil}\left(\frac{\text{Boundary Elment Vertical Extension}_{w2\_NS}}{in}, 2\right) \cdot in = 268 \cdot in$$

Confinement for the Boundary Element

Transverse Steel

$$\text{Boundary Element Transverse Steel Bar \#}_{w2\_NS} := 4$$

$$d_{b\_T\_BE\_w2\_NS} := \#4\ \text{daimeter} \cdot in = 0.5 \cdot in$$

$$A_{b\_T\_BE\_w2\_NS} := \#4\ \text{area} \cdot in^2 = 0.2 \cdot in^2$$

Number of shear legs parallel/perpendicular to the wall contributing to shear resistance is

$\text{No of shear legs}_{\text{Parallel\_w2\_NS}} := 15$

$\text{No of shear legs}_{\text{Perpendicular\_w2\_NS}} := 15$

$h_{x\_w2\_NS} := 0.35\ \text{ft}$

$h_{c\_parallel\_w2\_NS} := 3.16\ \text{ft}$

$h_{c\_perpendicular\_w2\_NS} := 0.78\ \text{ft}$

Calculate Transverse Reinforcement Spacing

In parallel direction

$$S_{t\_w2\_NS\_parallel} := \frac{\text{No of shear legs}_{\text{Parallel\_w2\_NS}} \cdot A_{b\_T\_BE\_w2\_NS}}{0.09 \cdot h_{c\_parallel\_w2\_NS} \cdot \left(\frac{f_c}{f_y}\right)} = 10.16 \cdot \text{in}$$

In perpendicular direction

$$S_{t\_w2\_NS\_perpendicular} := \frac{\text{No of shear legs}_{\text{Perpendicular\_w2\_NS}} \cdot A_{b\_T\_BE\_w2\_NS}}{\left[0.09 \cdot h_{c\_perpendicular\_w2\_NS} \cdot \left(\frac{f_c}{f_y}\right)\right]} = 41.15 \cdot \text{in}$$

$$S_{t\_w2\_NS} := \text{floor}\left(\frac{\min\left(S_{t\_w2\_NS\_parallel}, S_{t\_w2\_NS\_perpendicular}\right)}{\text{in}}\right) \cdot \text{in} = 10 \cdot \text{in}$$

Check Maximum Spacing

$$S_{max\_w2\_NS} := \text{floor}\left[\frac{\left[\min\left[0.25 \cdot (0.35\text{m}), 6 \cdot d_{b\_v\_BE\_w2\_NS}, 4\text{in} + \left(\frac{14\text{in} - h_{x\_w2\_NS}}{3}\right)\right]\right]}{\text{in}}\right] \cdot \text{in} = 3 \cdot \text{in}$$

$$S_{t\_w2\_NS} := \text{if}\left(S_{t\_w2\_NS} < S_{max\_w2\_NS}, S_{t\_w2\_NS}, S_{max\_w2\_NS}\right) = 3 \cdot \text{in}$$

Outer Boundary Element Confinement Reinforcement Spacing Considering Both Directions

Final transverse reinforcement spacing for the outer boundary element is the minimum of spacings in EW NS directions

$$S_{t\_w2\_outer} := \min\left(S_{t\_w2\_EW\_outer}, S_{t\_w2\_NS}\right) = 3 \cdot \text{in}$$

APPENDIX B

STEEL COUPING BEAM DESIGN EXAMPLE

Appendix B presents a sample steel coupling beam design worksheet. This worksheet was created using the computer program Mathcad 14 developed by Parametric Technology Corporation (PTC).

Design of Steel Coupling Beam

100% Structure

Coupling Beam #1 (floors 4 - 6)

Beam Material Properties

$f_{c'} := 45MPa = 6.527 \cdot ksi$

$f_{yw} := 345MPa = 50 \cdot ksi$

$f_{yf} := 345MPa = 50 \cdot ksi$

$E_s := 200GPa = 2.901 \times 10^{4} \cdot ksi$

Beam Geometric Properties

$L_b := 98.425in$

Design Forces

$V_{u1} := 244\ kip$

$M_{u1} := \frac{V_{u1} \cdot L_b}{2} = 1000.654 \cdot kip \cdot ft$

Flextural Strength (M_n)

$M_u \le \phi_b \cdot M_n$

$\phi_b := 0.9$

$M_n = M_p \le 1.5\ M_y$

$M_{p1} = f_{yf}\ Z_{x1}$ $\quad$ $M_{p1} = (50\ ksi)\ Z_{x1}$

$M_{y1} = f_{yf}\ S_{x1}$ $\quad$ $M_{y1} = (50\ ksi)\ S_{x1}$

Let the $\phi M_{n1} = \phi M_{p1} = M_{u1} = 1.001 \times 10^{3} \cdot kip \cdot ft$

$Z_{x\_req1} := \frac{M_{u1}}{\phi_b \cdot (f_{yf})} = 266.638 \cdot in^3$

Shear Strength (V_n)

$V_u1 \le \phi_v \cdot V_{n1}$

$\phi_v := 1.0$

$V_p = 0.6\, f_{yw}\, A_w$

$V_{p1} = A_{w1}\ 0.6 \cdot f_{yw} = 3.002 \times 10^4\ \text{psi}\ \ h_1\ t_{w1}$

Let the $\phi V_n = \phi V_p = V_u$

$$V_{p1} := \frac{V_{u1}}{\phi_v} = 2.44 \times 10^5\ \text{lbf} \qquad V_{p1} = 244 \cdot \text{kip}$$

Try section W14x159

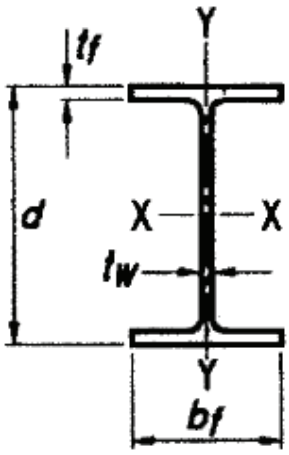

Cross section properties:

$A_{sec1} := 46.7\text{in}^2$

$d_1 := 15.0\text{in}$

$t_{w1} := 0.745\text{in}$

$b_{fl} := 15.60\text{in}$

$t_{fl} := 1.19\text{in}$

$I_1 := 1900\text{in}^4$

$S_{x1} := 254\text{in}^3$

$Z_{x1} := 287\text{in}^3$

$\phi_{vVn1} := 335\text{kip}$

$\phi_{bMpx1} := 1080\text{kip} \cdot \text{ft}$

$\text{Result}_1 := \text{"Check is OK"}$

$\text{Result}_2 := \text{"Check is NOT OK"}$

$\text{section}_1 := \text{"W14x159"}$

Check strengths

a) shear strength

$V_{u1} = 244 \cdot \text{kip}$

$\text{Shear\_Strength} := \text{if}\left(\phi_{vVn1} > V_{u1}, \text{Result}_1, \text{Result}_2\right) = \text{"Check is OK"}$

b) flextural strength

$M_{u1} = 1.001 \times 10^3 \cdot \text{kip} \cdot \text{ft}$

$\text{Moment\_Strength} := \text{if}\left(\phi_{bMpx1} > M_{u1}, \text{Result}_1, \text{Result}_2\right) = \text{"Check is OK"}$

$Z_{x\_req1} = 266.638 \cdot in^3 \qquad Z_{x1} = 287 \cdot in^3$

$\text{Plastic\_Modulus} := \text{if}\left(Z_{x1} > Z_{x\_req1}, \text{Result}_1, \text{Result}_2\right) = \text{"Check is OK"}$

Check local buckling due to flextural

1-Web Local Buckling (WLB)

$$\frac{d}{t_w} \le \alpha \cdot \sqrt{\frac{E_s}{f_{yw}}}$$

$\alpha := 3.05$ (AISC Table: C-B5.1)

$\frac{d_1}{t_{w1}} = 20.134 \qquad \alpha \cdot \sqrt{\frac{E_s}{f_{yw}}} = 73.435$

$$\text{Web\_Buckling1} := \text{if}\left(\frac{d_1}{t_{w1}} \le \alpha \cdot \sqrt{\frac{E_s}{f_{yw}}}, \text{Result}_1, \text{Result}_2\right) = \text{"Check is OK"}$$

2-Flange Local Buckling (FLB)

$$\frac{b_f}{t_f} \le \beta \cdot \sqrt{\frac{E_s}{f_{yf}}}$$

$\beta := 0.38$ (AISC Table: C-B5.1)

$\frac{b_{f1}}{2t_{f1}} = 6.555 \qquad \beta \cdot \sqrt{\frac{E_s}{f_{yf}}} = 9.149$

$$\text{Flange\_Buckling} := \text{if}\left(\frac{b_{f1}}{2t_{f1}} \le \beta \cdot \sqrt{\frac{E_s}{f_{yf}}}, \text{Result}_1, \text{Result}_2\right) = \text{"Check is OK"}$$

Check web stability due to shear

For $V_n = 0.6\, f_{yw}\, A_w$

The web stability check is

$\frac{d}{t_w} \le 2.45 \cdot \sqrt{\frac{E_s}{f_{yw}}} \qquad \frac{d_1}{t_{w1}} = 20.134 \qquad 2.45 \cdot \sqrt{\frac{E_s}{f_{yw}}} = 58.989$

$$\text{Web\_Buckling2} := \text{if}\left(\frac{d_1}{t_{w1}} \le 2.45 \cdot \sqrt{\frac{E_s}{f_{yw}}}, \text{Result}_1, \text{Result}_2\right) = \text{"Check is OK"}$$

Embedment length

$$V_u = 0.9 f_b \beta_1 b_f l_e \left[\frac{(0.58 - 0.22\beta_1)}{\left(0.88 + \frac{(L_b/2)}{l_e}\right)} \right] \qquad f_b = 54.0\sqrt{f_c'}\left(\frac{t_{wall}}{b_f}\right)^{0.66}$$

Guess: $l_{e1} := 3.28\,ft$

Given

$$V_{u1} = 0.9 \cdot 54 \cdot \sqrt{\frac{f_{c'}}{psi}} \cdot psi \cdot \left(\frac{t_{wall}}{b_{f1}}\right)^{0.66} \cdot \beta_1 \cdot b_{f1} \cdot l_{e1} \cdot \frac{(0.58 - 0.22 \cdot \beta_1)}{\left(0.88 + \frac{L_b}{2 \cdot l_{e1}}\right)}$$

$EL(t_{wall}, b_{f1}, \beta_1) := Find(l_{e1})$

$\beta_1 := 0.8$

$t_{wall} := 1.148\,ft$

$$Embedment\_Length_1 := Ceil\left(\frac{EL(t_{wall}, b_{f1}, \beta_1)}{in}, 3.937\right) \cdot in = 35.433\,in$$

Coupling Beam #1 Design Summary

A	d	t_w	b_f	t_f	I	S_x	Z_x	$\varphi_v V_n$	$\varphi_b M_p$	Emb. Length
in^2	in	in	in	in	in^4	in^3	in^3	kips	kip-ft	in
46.70	15.0	0.75	15.60	1.19	1900	254	287	335	1080	35.43

BIBLIOGRAPHY

ACI Committee 318, 2011. *ACI 318-08 Building Code Requirements for Reinforced Concrete* and *Commentary*, American Concrete Institute. Farmington Hills MI.

AISC, 2005. *ANSI/AISC 341-05- Seismic provisions for structural steel buildings*, American Institute of Steel Construction, Chicago.

AISC, 2011. *ANSI/AISC 325-11- Steel Construction Manual*, American Institute of Steel Construction, Chicago.

Aksogan, O. Bikce, M. and Resatoglu, R., 2002. *Free Vibration Analysis of Multi-bay Coupled Shear Walls*, Cukurova University, Adana 01330, Turkey.

Aktan, A. E. and Bertero, V. V., 1984. *Seismic Response of R/C Frame-Wall Structures*, ASCE Journal of the Structural Division, Vol. 110, No. ST 8, pp 1803-1821.

Aristizabal-Ochoa, J.D., Shiu, K.N. and Corley, W.G., 1979. *Effects of Beam Strength and Stiffness on Coupled Wall Behavior*, Proceedings of the Second US National Conference on Earthquake Engineering, pp 323-332.

Aristizabal-Ochoa, J.D. and Sozen, M.A. 1976. *Behavior of Ten-storey Reinforced Concrete Walls Subject to Earthquake Motions*, University of Illinois Report SRS No. 431.

ASCE, 2010. *ASCE 7-10 Minimum Design Loads for Buildings and Other Structures*, American Society of Civil Engineers, Reston VA.

Bertero, V.V., Anderson, J.C., Krawinkler, H., Miranda, E. and the CUREE and Kajima Research Teams, 1991. *Design Guidelines for Ductility and Drift Limits*, Report No. UCB/EERC-91/15 Earthquake Engineering Research Center, University of California Berkeley, CA.

Black, C. J., Makris, N., and Aiken, I. D., 2002. *Component Testing, Stability Analysis and Characterization of Buckling-Restrained Unbonded Braces*. Report No. PEER 2002/08, Univ. of California, Berkeley, CA.

Boivin, Y., 2006. *Assessment of the Seismic Performance of a 12-Storey Ductile Concrete Shear Wall System Designed According to the NBCC 2005 and CSA A23.3 2004 Standards*. Ph.D. Dissertation, University of Sherbrooke, pp 221.

Bozdogan, K. B. and Öztürk, D., 2007. *An Approximate Method for Free Vibration Analysis of Multi-Bay Coupled Shear Walls*, Mathematical and Computational Applications, Vol. 12, No. 1, pp 41-50.

Buckle, I. G. and Mayes, R.L., *Seismic Isolation History, Application, and Performance*-World View, Earthquake Spectra, Vol. 6, No. 2, pp 161-201.

Carr, A.J., 2008. *RUAUMOKO - Inelastic Dynamic Analysis Computer Program*, University of Canterbury.

Chai, Y. H. and Chen, Y., 2009. *Reexamination of the Vibrational Period of Coupled Shear Walls by Differential Transformation*, Journal of Structural Engineering, Vol. 135, No. 11, pp 1330-1339.

Chopra, A.K., 2006. *Dynamics of Structures – Theory and Applications to Earthquake Engineering*, Prentice Hall, 3rd edition, 912 pp.

Chopra, A.K. and Goel, R.K. 2002. *A modal pushover analysis procedure for estimating seismic demands for buildings*, Earthquake Engineering and Structural Dynamics Vol. 31, No. 3, pp 561-582.

Coull, A. and El Hag, A.A., 1975. *Effective coupling of shear walls by floor slabs, ACI Journal Proceedings*, Vol. 72, No. 8, pp 429-431.

Coull, A. and Mukherjee, P. R., 1973. *Approximate Analysis of natural Vibrations of Coupled Shear Walls*, Earthquake Engineering and Structural Dynamics, Vol. 2, pp 171-183.

CSA, 2004. *A23.3-04 Design of concrete structures*, Canadian Standards Association, Rexdale, Canada.

Dusicka, P., Itani, A.M. and Buckle, I. G., 2002. *Cyclic Behavior of Shear Links and Tower Shaft Assembly of San Francisco-Oakland Bay Bridge Tower*, Report No. CCEER 02-06, Center for Civil Engineering Earthquake Research, University of Nevada, Reno, NV.

El-Tawil, S., Fortney, P., Harries, K.A., Shahrooz, B.M., Kurama, Y., Hassan, M. and Tong, X., 2009. *Recommendations for Seismic Design of Hybrid Coupled Wall Systems*, ASCE/SEI, 80 pp.

El-Tawil, S. and Kuenzli, C. M., 2002b. *Pushover of Hybrid Coupled Walls. Part II: Analysis and Behavior*. ASCE Journal of Structural Engineering, Vol. 128, No. 10, pp 1282-1289.

FEMA. 2000a. *FEMA 350 Recommended Seismic Design Criteria for New Steel Moment Frame Buildings*. Federal Emergency Management Agency, Washington, DC.

FEMA, 2000b. *FEMA 356 Prestandard and Commentary for the Seismic Rehabilitation of Buildings*, Federal Emergency Management Agency, Washington DC.

FEMA, 2000c. *FEMA 349 Action Plan for Performance Based Seismic Design*, Federal Emergency Management Agency, Washington DC.

FEMA, 1998. *FEMA 306 Evaluation of Earthquake Damaged Concrete and Masonry Wall Buildings*, Federal Emergency Management Agency, Washington DC.

Fortney P.J., Shahrooz B.M., and Rassati G.A., 2004. *The Next Generation of Composite Coupling Beams*, Proceedings of the 5th International Conference on Composite Construction, South Africa.

Gong B., and Shahrooz B. M., 1998. S*eismic behavior and design of composite coupled wall systems*, Report No. UC-CII 98/01, Cincinnati Infrastructure Institute, Cincinnati, OH.

Gudimetla, P. S., Adibi-Asl, R., and Seshadri, R., 2010. *Incorporation of Strain Hardening Effect into Simplified Limit Analysis*, Journal of Pressure Vessel Technology, Vol. 132.

Harries, K.A., 2001. *Ductility and Deformability of Coupling Beams in Reinforced Concrete Coupled Walls*, Earthquake Spectra, Vol. 17, No. 3, pp 457-478.

Harries, K.A. and McNeice, D.S., 2006. *Performance-Based Design of High-Rise Coupled Wall Systems*, The Structural Design of Tall and Special Structures, Vol. 15, No. 3, pp 289-306.

Harries, K.A., and Shahrooz, B., 2005. *Hybrid Coupled Wall Systems*, Concrete International. Vol. 27, No. 5, pp 45-51.

Harries, K.A., Fortney, P., Shahrooz, B.M. and Brienen, P., 2005. *Design of Practical Diagonally Reinforced Concrete Coupling Beams* – A Critical Review of ACI 318 Requirements, ACI Structures Journal. Vol. 102, No. 6, pp 876-882.

Harries, K.A., Moulton, D. and Clemson, R., 2004a. *Parametric Study of Coupled Wall Behavior – Implications for the Design of Coupling Beams*. ASCE Journal of Structural Engineering Vol. 130, No. 3, pp 480-488.

Harries, K.A., Shahrooz, B.M., Brienen, P. and Fortney, P. 2004b. *Performance Based Design of Coupled Walls*. Proceedings of the 5th International Conference on Composite Construction, South Africa.

Harries, K.A., Mitchell, D., Redwood, R.G. and Cook, W.D., 1997. *Seismic Design of Coupling Beams - A Case for Mixed Construction*, Canadian Journal of Civil Engineering, Vol. 24, No. 3, pp 448-459.

Harries, K.A., Mitchell, D., Cook, W.D. and Redwood, R.G., 1992. *Seismic response of steel beams coupling reinforced concrete walls*, ASCE Journal of the Structural Division, Vol. 119, No. 12, pp 3611-3629.

Hassan, M., 2004. *Inelastic dynamic behavior and design of hybrid coupled wall systems*, Ph.D. Dissertation, University of Central Florida, 321 pp.

Hull, D., 2006. *On the Application of Fixed Point Theory to the Design of Coupled Core Walls*, MSCE Thesis, Department of Civil and Environmental Engineering, University of Pittsburgh.

Hull, D., Harries, K.A., 2008. *On the Application of Fixed Point Theory to the Design of Coupled Core Walls*, International Journal of Structural Stability and Dynamics, Vol. 8, No. 1, pp 161-186.

Imbsen Software Systems, 2007. *XTRACT – cross sectional X structural Analysis of Components v3.0.9*. Computer Program.

Irwin, A. W., 1984. *Design of Shear Wall Buildings*. Report No. CIRIA 102, Construction Industry Research and Information Association, London, England.

Iwanami, K., Suzuki, K., and Seto, K., 1996. *Vibration Control Method for Parallel Structures Connected by Damper and Spring*, JSME International Journal, Vol. 39, No. 4, pp 714-720.

Kelly, J.M., 1982. *Aseismic base isolation*, Shock and Vibration Digest, Vol. 14, pp 17-25.

Khan, M.J. 1996. *Nonlinear Response of Reinforced Concrete Coupling Members in Earthquake Resisting Shear Wall Structures*, MEng Thesis, McGill University, 164 pp.

Lee, H. J., Kuchma, D. A., Baker, W., and Novak, L. C., 2008. *Design and Analysis of Heavily Loaded Reinforced Concrete Link Beams for Burj Dubai*, ACI Structural Journal, Vol. 105, No. 4, pp 451-459.

Lybas, J.M. and Sozen, M.A. 1977. *Effect of Beam Strength and Stiffness on Dynamic Behavior of Reinforced Concrete Coupled Walls*, University of Illinois Report SRS No. 444.

Manatakos, C.K. and Mirza, M.S., 1999. *Analysis and Design of Concrete Coupled Core Substructures Subject to Gravity and Lateral Loads*, Innovation in concrete structures: design and construction, pp 425-435.

Mander, J.B., Preistley, M.J.N. and Park, R., 1988. *Theoretical Stress-Strain Model for Confined Concrete*, ASCE Journal of Structural Engineering, Vol. 114, No. 8, pp 1804-1826.

McNeice, D., 2004. *Performance-Based design of a 30-Storey Coupled Wall Structure*, MSCE. Thesis, Department of Civil and Environmental Engineering, University of South Carolina.

Minami, S., Yamazaki, S., Toyama, K., and Tahara, K., 2004. *Experimental Study on Coupled Vibration Control Structures*, 13th World Conference on Earthquake Engineering, Vancouver, paper # 2351.

Mirza, M.S. and Lim, A.K.W., 1990. *Behaviour and design of coupled slab–structural wall systems*, Canadian Journal of Civil Engineering, Vol. 17, No. 5, pp 705-723.

NBCC 1990. National Building Code of Canada. National Research Council of Canada, Ottawa, ON.

Nilson, A., Darwin, D., and Dolan, C., 2003. *Design of Concrete Structures*, McGraw Hill, 13th edition, 779 pp.

NZS, 2006. *NZS 3101.1&2-06 Concrete Structures Standard*, New Zealand Standards Association, Wellington, New Zealand.

Paulay, T., 2002. *A Displacement-focused seismic design of mixed building systems*, Earthquake Spectra. Vol 18, No. 4, pp 689- 718.

Paulay, T. and Santhakumar, A. R., 1976. *Ductile behavior of coupled shear walls*. ASCE Journal of the Structural Division, Vol. 102(ST1) pp 93-108.

Qadeer, A. and Stafford Smith, B., 1969. *The bending stiffness of slabs connecting shear walls*, ACI Journal Proceedings, Vol. 66, No. 6, pp 464-473.

Richardson, A., 2003. *Vibration Control of Multiple Structures – Theory and Application*, Ph.D. Dissertation, Florida A&M University, 286 pp.

Rutenberg, A., 1975. *Approximate Natural Frequencies for Coupled Shear Walls*, Earthquake Engineering and Structural Dynamics, Vol. 4, pp 95-100.

Saiidi, M., 1979. *Simple and complex models for nonlinear seismic response of reinforced concrete structures*, University of Illinois. Urbana, Illinois.

Santhakumar, A.R., 1974. *Ductility of Coupled Shear Walls*, Ph.D. Dissertation, University of Canterbury NZ.

Satyarno, I., Carr, A.J. and Restrepo, J., 1998. *Refined Pushover Analysis for the Assessment of Older Reinforced Concrete Buildings*, Proc. NZ Nat. Soc. For Earthquake Engg, Tech Conf. Wairakei, pp 75-82.

Schwaighofer, J. and Collins, M.P., 1977. *Experimental study of the behaviour of reinforced concrete coupling slabs*, ACI Journal Proceedings, Vol. 74, No. 3, pp 123-127.

SEAOC, 1995. *Vision 2000 a Framework for Performance-Based Engineering*, Structural Engineers Association of California, Sacramento, CA.

Seto, K., Ookuma, M., Yamashita, S., and Nagamatsu, A., 1987. *Method of Estimating Equivalent Mass of Multi-Degree-of-Freedom System*, JSME International Journal, Vol. 30, No. 268, pp 1638-1644.

Shahrooz, B.S., Deason, J.T. and Tunc. G., 2004a. *Outrigger Beam-Wall Connections. I: Component Testing and Development of Design Model*, ASCE Journal of Structural Engineering. Vol. 130, No. 2, pp 253-261.

Shahrooz, B.S., Tunc, G. and Deason, J.T., 2004b. *Outrigger Beam-Wall Connections. II: Subassembly Testing and Further Modeling Enhancements*, ASCE Journal of Structural Engineering. Vol. 130, No. 2, pp 262-270.

Smyrou, E., Sullivan, T.J., Preistley, M.J.N. and Calvi, G.M., 2008. *Study of the Behaviour of Slab-Coupled T-Shaped RC Walls*, Proceedings of the 14th World Conference on Earthquake Engineering, Beijing, China.

Stafford-Smith, B. and Coull, A., 1991. *Tall Building Structures – Analysis and Design*, Wiley-Interscience, 1st edition, 537 pp.

Taranath, B., 2009. *Reinforced Concrete Design of Tall Buildings*, CRC Press, 1st edition, 989 pp.

Teshigawara, M., Sugaya, K., Kato, M. and Matsushima, Y., 1998. Seismic Test on 12-storey Coupled Shear Wall with Flange Walls, reprinted in *List of Technical Papers written in English authored by Japan-side Researchers*, US-Japan Cooperative Earthquake Research Program on Composite and Hybrid Structures.

Wallace, J. W. and Moehle, J. P., 1992. *Ductility and Detailing Requirements of Bearing Wall Buildings*, Journal of Structural Engineering, Vol. 118, No. 6, pp 1625-1644.

Wang, Q. and Wang, L. Y., 2005. *Estimating Periods of Vibration of Buildings with Coupled Shear Walls*, Journal of Structural Engineering, Vol. 131, No. 12, pp 1931-1935.

Watanabe, A., Hitomoi, Y., Saeki, E., Wada, A., and M. Fujimoto., 1988. *Properties of braces encased in buckling-restraining concrete and steel tube*. Proceedings of the 9th World Conference on Earthquake Engineering, Vol. IV, Tokyo-Kyoto, Japan, pp 719-724.

Wu, J.R. and Li, Q.S., 2003. *Structural performance of multi-outrigger-braced tall buildings*, The Structural Design of Tall and Special Buildings, Vol. 12, No. 2, pp 155–176.

Xuan G., Shahrooz B.M., Harries K.A., and Rassati G.A., 2008. *A Performance-Based Design Approach for Coupled Core Wall Systems with Diagonally Reinforced Concrete Coupling Beams*. *Advances in Structural Engineering*, Vol. 11, No. 3, pp 265-280.